Wave-to-wire Modelling of Wave Energy Converters

Wave-to-wire Modelling of Wave Energy Converters

Critical Assessment, Developments and Applicability for Economical Optimisation

Revised Version

PhD Thesis
Defended in public at Aalborg University
(19 September 2014)

Francesco Ferri

Department of Civil Engineering,
The Faculty of Engineering and Science,
Aalborg University, Aalborg, Denmark

River Publishers

ISBN 978-87-93237-24-7 (e-book)

Published, sold and distributed by:
River Publishers
Niels Jernes Vej 10
9220 Aalborg Ø
Denmark

Tel.: +45369953197
www.riverpublishers.com

Recent publications in the DCE Thesis Series

ISSN 1901-7294
DCE Thesis No. 60

Contents

0.1 Acknowledgements

The research presented in this thesis was financially supported by the Danish Council for Strategic Research under the Programme Commission on Sustainable Energy and Environment (Contract 09-067257, Structural Design of Wave Energy Devices).

Most of all, I would like to thank Jens Peter and Aurélien. Jens Peter and his wise point of view, guided me during the whole PhD period, smoothing my rough edges off and helping me whenever it was needed. Aurélien is an example to me in both pedagogical and technical aspects. I believe that sharing one's wisdom is the best, but most difficult, thing to do, and Aurélien can do it so naturally.

I would like to acknowledge all the colleagues at the Department of Civil Engineering; a special thanks goes to Peter Frigaard, for his way to be a manager, to Vivi Søndergaard, for her valuable corrections, and to Helle Schrøder Hansen, Pernille Bisgaard Pedersen, for their help with any bureaucratic matters, which are still obscure to me.

I would like to thank Niels Drustrup and Nikolaj Holk for their support in the laboratory work. The Wave Energy Research Group, me included, would be in panic without them.

I would like to broadly thank every single person I have been working with: both lucky and unlucky collaborations do exist, and they always teach you something new. A special thank goes to Vittoria University Institute for Integrated Energy System, to Fraunhofer Institute for Wind Energy and Energy System Technology (IWES), to Bologna University, to Chalmers University and to École Central de Nantes.

Thank you to my old and new family.

0.2 English Summary

The wild development of the world from the 1769, years in which James Watt patented his steam engine, brought utterly to the actual, real or assumed, economical, political, environmental and energetic crisis. The answer to the question “how to solve these problems?" is a tangled unsolved discussion, but talking about renewable energy partially ravels the problem out. Wave energy is a large, mostly untapped, renewable energy resource. It has the potential to contribute significantly to the future energy mix, but the sector has not yet rolled off into the market in consequence of a number of technical and non-technical issues. These can be efficiently summarised in the cost of the energy produced by the various wave energy converters: If compared with other renewable energy technologies the cost of energy from the ocean waves is still significantly higher. Holding the comparison it also important to notice that there is not a clear front runner in the wave energy sector, which fades effort and funding over a too broad frame.

In order to assist efficient development and analysis of wave energy converters and therefore to accelerate the sector progression towards commercialisation, a generally applicable, efficient and reliable wave-to-wire model tool is needed. A wave-to-wire model identifies the relation from the source of energy of a particular location to the expected device productivity. The latter being expressed in terms of electricity fed into the grid. The model needs to output a coarse picture of the actual status of the different devices and their power productivity, which is used afterwards to sieve promising concepts out.

In a macro-scale the work can be divided into two main contributions

First, highlight the complementarity between numerical simulation and laboratory experience, in what can be efficiently summarised as: *reliable model*. Numerical models are per se meaningless, but easy to manipulate, fast and relatively cheap. Physical models are complex, slow and expensive but realistic if adequately implemented. Since there is no real need of “new", but more of “how can we get the best of what we have", the numerical model used is entirely based on well established methods. The experimental data is used as a check point to verify the direction of the numerical path.

Second, shed light on what should be the objective of the sector: minimisation of the cost of energy. Two different techniques to reduce the cost of energy are compared: the former maximises the system revenue (income) by acting on the control logic, while the second extends the first methods adding a penalty term due to the effect of the control logic on the structural design. Once more, both methods are based on well established or standard techniques.

0.3 Dansk Resumé

Med den industrielle udvikling efter 1769, tidspunktet hvor James Watt tog patent på dampmaskinen, er der opstå et økonomisk, politisk, miljømæssig og energimæssig krise – hvad enten man anser denne for antagelig eller reel. Svaret på spørgsmålet ”hvordan løser man disse problemer?” er en kompliceret og ufuldendt diskussion, men med introduktionen af vedvarende energiproduktion, er der givet et bud på, hvordan man til dels kan løse disse problemer. Bølgeenergi er en uudnyttet vedvarende energikilde, som har potentiale til at bidrage betydeligt til fremtidens blandede energiforsyning. Dog har bølgeenergisektoren endnu ikke udbudt denne mulighed på markedet grundet en række tekniske og ikke-tekniske årsager. Disse kan mest effektivt opsummeres ved at på pege produktionsudgifterne som opstår ved brug af de forskellige energitransformatorer: Sammenlignet med andre vedvarende energiteknologier, er produktionsudgifterne stadigt betydeligt højere, når man udnytter energi fra havets bølger. Hvis man bliver ved denne sammenligning, er det også vigtigt at være opmærksom på, at der ikke er en klar frontløber i bølgeenergisektoren, hvilket gør at indsats og finansering spredes over et bredt felt.

For at kunne bidrage til en effektiv udvikling og analyse af bølgeenergikoncepter og dermed bidrage til en acceleration af hele sektorens fremgang mod kommercialisering, er det nødvendigt med et effektivt og på lideligt wave-to-wire værktøj, som er generelt anvendeligt. En wave-to-wire model identificerer relationen mellem en energikilde på et bestemt sted og enhedens forventede produktion. Sidstnævnte er udtrykt i form af elektricitet, der leveres til elnettet. Modellen skal kunne give et groft billede af den faktiske status af sektoren og dens potentiale, og senere bruges til at finde frem til de mest lovende koncepter.

På et makroniveau kan arbejdet fordeles på to hovedindsatser.

Først skal komplementaritet mellem numerisk simulation og eksperimentel erfaring fremhæves, hvilket mest effektivt kan opsummeres som: Pålidelig model. Numeriske modeller er i sig selv meningsløse men lette at manipulere, hurtige og relativt billige, hvor fysiske modeller er komplekse, langsomme og dyre, men realistiske hvis implementeret i tilstrækkelig grad. Siden der ikke er et faktisk behov for ”noget nyt” men snarere ”at få det bedste ud af hvad vi har”, er den anvendte numeriske model udelukkende baseret på veletablerede metoder. Eksperimentel data bliver anvendt som verifikation til at styre retningen af den numeriske udvikling.

Dernæst, kaste lys på hvad der bør være målet for sektoren: Minimering af de samlede energiomkostninger. To forskellige teknikker til at reducere omkostningerne er sammenlignet: Den første maksimerer systemomsætning (indkomst) ved at ændre på kontrolstrategien, mens den anden udvider de første metoder ved at tilføje et straf baseret på kontrolstrategiens indflydelse på det strukturelle design. Begge modeller er igen baseret på veletablerede eller standardiserede teknikker.

0.4 List of Publication

The thesis is presented as a collection of the following eight papers, given in Appx. A.

Paper 1: Ferri, F; Sichani, M T; Frigaard, P B. A case study of short-term wave forecasting based on FIR filter:optimisation of the power production for the Wavestar device. Proceeding of the 22^{nd} International Ocean and Polar Engineering Conference, Rhodos, Greece, 2012.

Paper 2: Ferri, F; Kramer, M M; Pecher, A. Validation of a wave-body interaction model by experimental tests. Proceeding of the 23^{rd} International Ocean and Polar Engineering Conference, Anchorage, Alaska, 2013.

Paper 3: Wehmeyer, C; Ferri, F; Skourup, J; Frigaard, P B. Experimental Study of an Offshore Wind Turbine TLP in ULS Conditions. Proceeding of the 23^{rd} International Ocean and Polar Engineering Conference, Anchorage, Alaska, USA, 2013.

Paper 4: Zurkinden, A S; Ferri, F; Beatty, S; Kofoed, J P; Kramer, M M. Non-Linear Numerical Modeling and Experimental Testing of a Point Absorber Wave Energy Converter. Ocean Engineering, pp. 11-21, vol. 78, 2014.

Paper 5: Ferri, F; Ambühl, S; Fischer, B; Kofoed, J P. Balancing power output and structural fatigue of wave energy converters by means of control strategies. Energies, March 2013.

Paper 6: Wehmeyer, C; Ferri, F; Andersen, M T; Pedersen, R R. Validated state space model of a TLP including a flexible topside in non-linear regular waves. Submitted to Energies, April 2014.

Paper 7: Angelelli, E; Zanuttigh, B; Ferri, F; Kofoed, J P. Experimental assessment of the mooring influence on the power output of a Wave Activated Body floating WEC. Proceeding of the 10^{th} European Wave and Tidal Energy Conference, Aalborg, Denmark, 2013.

Paper 8: Ferri, F; Andreoni, G; Perisic, N; Lavelle, J; Kofoed, J P. Cable-free Floating Object Tracking Using an Image Processing Approach. Proceeding of the 10^{th} European Wave and Tidal Energy Conference, Aalborg, Denmark, 2013.

This thesis has been submitted for assessment in partial fulfillment of the PhD degree. The thesis is based on the submitted or published scientific papers which are listed above. Parts of the papers are used directly or indirectly in the extended summary of the thesis. As part of the assessment, co-author statements have been made available to the assessment committee and are also available at the Faculty. The thesis is not in its present form acceptable for open publication but only in limited and closed circulation as copyright may not be ensured.

Other relevant publications from the author, not appended to this document, are listed hereafter.
List of submitted publications:

Markus, D; Ferri, F; Wuchner, R; Frigaard, P B; Bletzinger, K U. Complementary numerical-experimental benchmarking for shape optimization and validation in waves and currents. Submitted to Computer & Fluid. 2014.

List of published publications:

Ferri, F; Kracht, P. Implementation of a Hydraulic Power Take-Off for wave energy application: deliverable D4.7. Department of Civil Engineering, Aalborg University, Aalborg. DCE Technical Reports, nr. 157, 2013.

Ferri, F; Kramer, M. Laboratory experiments on Wavestar device: Definition and comparison of hydrodynamic coefficients: deliverable D4.1-3. Department of Civil Engineering, Aalborg University, Aalborg. DCE Technical Reports, nr. 158, 2013.

Angelelli, E; Zanuttigh, B; Martinelli, L; Ferri, F. Physical and numerical modelling of mooring forces and displacements of a wave Activated Body Energy converter. Proceeding of the 33rd International Conference on Ocean, Offshore and Arctic Engineering, San Francisco, California, USA, 2014.

0.5 Nomenclature

Symbols and Acronyms	Description
ACRONYMS	
A-WEC	Attenuator WEC
AEP	Annual Energy Production
BEM	Boundary Element Method
BIEM	Boundary Integral Equation Method
CAPEX	Capital Expenditure
CCC	Complex Conjugate Control
CF	Cost Factor
CFD	Computational Fluid Dynamic
CIES	Control, Instrumentation and Electrical System
CoE	Cost of Energy
CoG	Centre of Gravity
CW	Capture Width
DNS	Direct Numerical Simulation
DoF	Degree of Freedom
E	Turnover or Revenue
EoM	Equation of Motion
FFT	Fast Fourier Transform
FIR	Finite Impulse Response
FLS	Fatigue Limit State
FOWT	Floating Offshore Wind Turbine
FRF	Frequency Response Function
fWEC	floating WEC
GHG	Green House Gasses
HS	Hydrodynamic Sub-system
HSS	Hosting Structure System
IFFT	Inverse Fast Fourier Transform
IMU	Inertial Motion Unit
IRF	Impulse Response Function
KC	Keulegan-Carpenter Number
LES	Large Edge Simulation
LUCF	Land use change and forestry
MPC	Model Predictive Control
MS	Main Structure
O&M	Operation and Maintenance
OFS	Onshore Facility System
OPEX	Operational Expenditure
OT	Over Topping
OWC	Oscillating Water Column
P	Proportional Control
PA-WEC	Point Absorber WEC
PAC	Phase and Amplitude Control
PaM	Panel Method
PCS	Power Connection System

Continued on next page...

...continued from previous page

Symbols and Acronyms	Description
PD	Proportional Derivative Control
PI	Proportional Integral Control
PID	Proportional Integral Derivative Control
PIDc	Proportional Integral Derivative Control with compensation of the radiation term
PSD	Power Spectral Density
PTO	Power Take-Off
RANSE	Reynold-averaged Navier-Stokes Equation
RS	Reaction System
SDWED	Structural Design of Wave Energy Devices
SKS	Station Keeping System
SN	Stress Number of Cycles Curve
SPH	Smoothed Particle Hydrodynamics
T-WEC	Terminator WEC
TLP	Tension Leg Platform
ULS	Ultimate Limit State
WEC	Wave Energy Converter
WAB	Wave Activated Body
SYMBOLS	
A	Wave Amplitude
$A(i)$	Cross-sectional area of the critical structural detail for the i-th control strategies
A_p	Body Projected Area
$C_1(i)$	Fraction of the Total Investment Cost over the WEC Lifetime Dependent on the Control Strategy
C_2	Fraction of the Total Investment Cost over the WEC Lifetime Independent on the Control Strategy
$\mathbf{CA}$	Radiation Damping Coefficient Matrix
C_c	Damping Control Coefficient
C_D	Viscous Drag Coefficient
C_D^*	Linearised Viscous Drag Coefficient
$\mathbf{CM}$	Added Mass Coefficient Matrix
$\mathbf{CM}_\infty$	Limit of the Added Mass Coefficient Matrix for $\omega \rightsquigarrow \infty$
CO_2	Carbon Dioxide
C_{tot}	Total investment cost over the WEC lifetime
D	Characteristic Length of the Body
D_{PTO}	Constant PTO Force Level
dt	Time Discretisation Step
f	Wave Frequency
f_D	Viscous Drag Force, Time Domain
F_D	Viscous Drag Force, Frequency Domain
$\overline{f}_{ex}$	Wave Excitation Force Vector, Time Domain
$\overline{F}_{ex}$	Wave Excitation Force Vector, Frequency Domain

Continued on next page...

...continued from previous page

Symbols and Acronyms	Description
$\overline{F}_{ex}^{0}$	Wave Excitation Force Frequency Coefficient Vector
$\overline{f_i}$	External Force Vector acting on the i-th Body, Time Domain
$\overline{F}_m$	Mooring Force Vector, Frequency Domain
f_{max}	Maximum Control Load
f_p	Wave Peak Frequency
f_{PTO}	PTO Force Acting on the Body, Time Domain
F_{PTO}	PTO Force Acting on the Body, Frequency Domain
f_{PTO}^{*}	Constrained PTO Force, Time Domain
F_{PTO}^{th}	Theoretical Commanded PTO Force by the Main Logic Controller, Frequency Domain
$\overline{f}_{rad}$	Radiation Force Vector, Time Domain
$\overline{F}_{rad}$	Radiation Force Vector, Frequency Domain
$\overline{F}_T$	Resultant Force Vector, Frequency Domain
f_u	Control Load, Time Domain - Equivalent to f_PTO
$G(s)$	Generic Linear Time Invariant Transfer Function
h	Time Discretisation Step
H	Wave Height
$\mathbf{H}(\overline{p})$	Transformation Matrix associated to the vector $\overline{p}$
He	Hessian Matrix of the MPC
h_{ex}	Impulse Response Function from the Surface Elevation to the Excitation Force
H_{ex}	Transfer Function from the Surface Elevation to the Excitation Force
h_{η}^{v}	Impulse Response Function from the Surface Elevation to the Reference Velocity
H_{η}^{v}	Transfer Function from the Surface Elevation to the Reference Velocity
H_{m0}	Spectral Estimation of the Significant Wave Height
h_{opt}	Impulse Response Function from the Excitation Force to the Reference Velocity
H_{opt}	Transfer Function from the Excitation Force to the Reference Velocity
h_{RAD}	Impulse Response Function of the Radiation Force
$\mathbf{I_c}$	Inertia Matrix of the Rigid Body around CoG
j	Current Time Instant
J	Cost Function
k	Wave Number
K_c	Stiffness Control Coefficient
k_e	Rate of Discount
$\mathbf{K_m}$	Linearised Mooring Stiffness Matrix
k_{pto}	Stiffness of the PTO system
L	Lagrangian
m	Mass of the Rigid Body
$\mathbf{M}$	Mass Matrix of the Body

Continued on next page...

...continued from previous page

Symbols and Acronyms	Description
M_c	Mass Term of the Feed-Back Controller
M_{pto}	Mass of the PTO system
n	Number of Generalised DoFs
N_{IRF}	Order of the IRF
Np	Number of Panels
N_p	Number of Steps in the Prediction Horizon
ODE	Ordinary Differential Equations
p	Percentage of the Total Investment Costs Affected by the Control Strategy
$\mathbf{P}$	Matrix to Map the MPC State Vector Increment in the Output Space
P_i	Potential Energy of i-th Body
pr	Probability of Occurrence
$\mathbf{Q}$	Weight Matrix in the MPC formulation
$\overline{q}$	Body Displacement Vector in the Generalised DoFs Time Domain
$\dot{\overline{q}}$	Body Velocity Vector in the Generalised DoFs Time Domain
$\ddot{\overline{q}}$	Body Acceleration Vector in the Generalised DoFs Time Domain
q_i	i-th Generalised DoF
$\mathbf{S}^T(\overline{p})$	Skew Symmetric Matrix of the Vector $\overline{p}$
$S_j(\omega)$	Wave Spectrum
T	Wave Period
T_f	Upper Bound of the Time Integration
$\mathbf{T_D}$	Input Matrix for the Viscous Drag Force
T_i	Kinetic Energy of i-th Body
T_p	Wave Peak Period
$\mathbf{T_{PTO}}$	Input Matrix for the PTO Force
$u[j \dots j + N_p - 1]$	Optimal MPC Trajectory
$\overline{v}$	Body Velocity Vector Time Domain
$\overline{V}$	Body Velocity Vector Frequency Domain
$\dot{\overline{v}}$	Body Acceleration Vector Time Domain
$\dot{\overline{V}}$	Body Acceleration Vector Frequency Domain
v_A and v_B	state of the PTO interconnection points
x	x-axis direction or heading direction
$\mathbf{x}$	State Vector in the MPC Formulation
y	y-axis direction or sideway direction
z	z-axis direction or vertical direction
SUBSCIPTS	
ref	The subscript identify the reference control strategy
GREEK LETTERS	
α	Spectral Intensity Factor

Continued on next page...

...continued from previous page

Symbols and Acronyms	Description
γ	Peak Enhancement Factor
$\mathbf{\Delta}\nu$	Increment of the Wave Excitation Force
$\mathbf{\Delta u}$	Increment of the MPC Control Variable
ζ_{pto}	Critical Damping Ratio of the PTO system
η	Surface Elevation
λ	Wave Length
$\overline{\xi}$	Body Displacement Vector Time Domain
$\overline{\overline{\Xi}}$	Body Displacement Vector Frequency Domain
ρ	Water Density
ς	Fluid Particle Velocity
τ_ν	Matrix to Map the MPC Disturbance Increment in the Output Space
$\tau_{\mathbf{u}}$	Matrix to Map the MPC Control Increment in the Output Space
τ	Time Constant of the PTO system
ω	Angular Frequency
ω_{pto}	Natural Frequency of the PTO system

List of Figures

List of Tables

Introduction

1

As presented in the title, the thesis analyses technical matters related to one important and untapped renewable energy source. More specifically, the implementation and analysis of wave energy conversion system models and their utilisation are the primary points. The word "Wave-to-wire" defines inputs and outputs of the sought model, the former being the source of energy (ocean waves) and the latter being the usable absorbed energy feed into the electrical grid (wire). The reason for needing to talk about renewable energy is a matter of finding the right motivations. In his book, MacKay (2008) found three objective catalysts to lead the debate (paraphrasing the text):
1 - Even though the scenario is rather uncertain, measurements and indications say that using fossil fuels is changing the climate (Cubasch et al., 2013). Climate change is correlated to the greenhouse effect, which in turn is driven by the modified rate of production/absorption of the so called greenhouse gases. This unbalance or transient scenario is blamed on several human activities, which often regress to fossil fuels combustion.
2 - Fossil fuels as oil, gas and coal are a nonrenewable resource, thus it seems reasonable to imagine that their cheap supply will run out within a “short" timeframe. Production of such resources must inevitably reach a maximum, or “peak”, but the discussion about “how to locate the Oil Peak" is scattered and subjective. According to IEA (2013) based on the actual knowledge, the oil production will peak around 2020, but as argued in (BP, 2013), this information is misleading due to the technical evolution. It does not really matter when, the point is the presence of a production limit. Alternative energy sources are thus needed. Furthermore, instead of setting a valuable raw material (fossil fuels) on fire, it could be wise to use it to produce high quality goods.
3 - The stability and security of the energy supply is not of secondary importance. Assuming that fossil fuels are available, they are oddly distributed in few countries of the world, and ruled by even fewer companies. In this scenario, there is a real risk of making the economy of a whole state vulnerable to the whims of that restricted group of people. Thus the independency on those energy sources is a valuable option.

On top of these motivations, two others, but non only, can be added to the discussion:
4 - The environmental aspects should never be forgotten. An undesired by-product of the fossil fuel activities is the environmental pollution. The consequence of accidental pollution of the water, soil and air has been made evident once more with the Deepwater Horizon accident (BP, 2010), while the estimation of the operational pollution rate of fossil fuels is still somewhat unclear. The environment pollution matters greatly because it has direct and indirect consequences on the human wellness, especially in future generations.

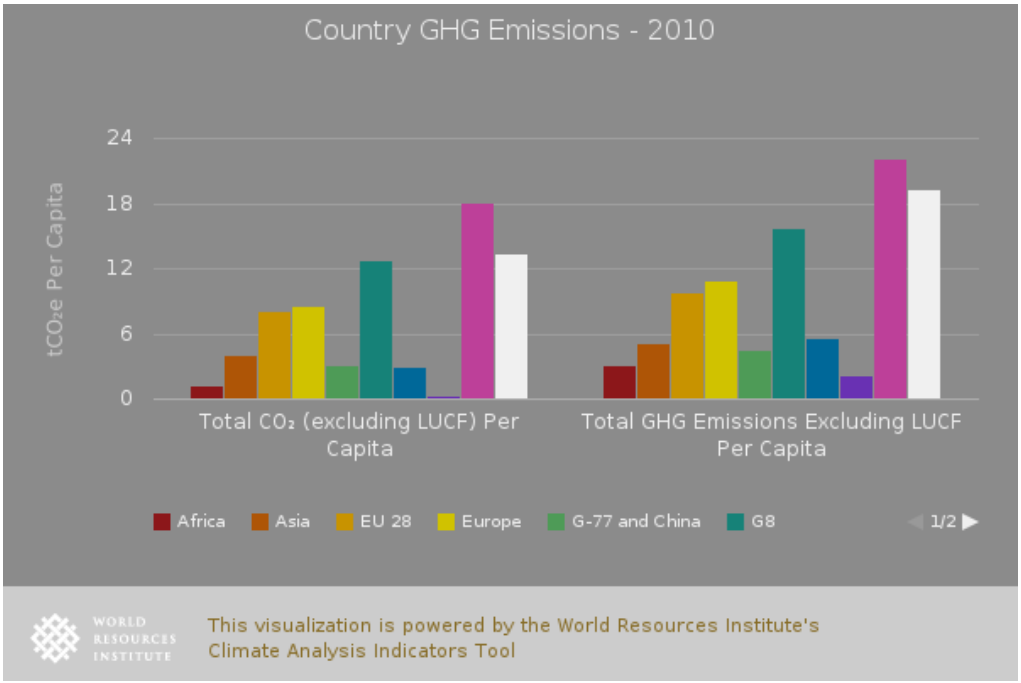

Fig. 1.1. Green House Gas (GHG) and Carbon Dioxide (CO_2) pro capita emission, (World Resource Institute, 2010). The data excluded the contribution from the land use change and forestry (LUCF).

5 - The growth of a new sector brings new job opportunities in both research and industrial corporations. In 2012, 5.7 million people have been estimated to be employed directly and indirectly in the renewable energy sector (Ferroukhi et al., 2013), mostly in solar and biofuels. But estimation says that the number can triple in accordance with the actual development planes.

Each of the above motivations get even more important when looking at the prospected trends of development of different countries.

As shown in Fig. 1.1, the pro capital pollution rate of emerging countries like China and India are well below the actual rate of developed countries like USA, Australia, Canada and Europe. The pro capita pollution rate is expressed in ton of carbon dioxide (CO_2) and green house gasses (GHG) emission per person, excluding the contribution from the land use change and forestry (LUCF). If the living standard of these countries are exported to or imported by the emerging ones, there is a real risk of a sharp increase in the climate change rate, a short-term depletion of fossil fuels and a general shortage of electricity supply.

Regardless of the chosen motivation, the need for alternative sources of energy is evident.

1.1 Renewable Energy

Even if the renewable energy sources are considered to be unlimited, it is possible to generally define a resource as "$renewable$" when its production/consumption rate is balanced in a human timeframe. In addition, in order to be sustainable its utilisation should result in an environmental benefit. The latter point excludes nuclear, coal and

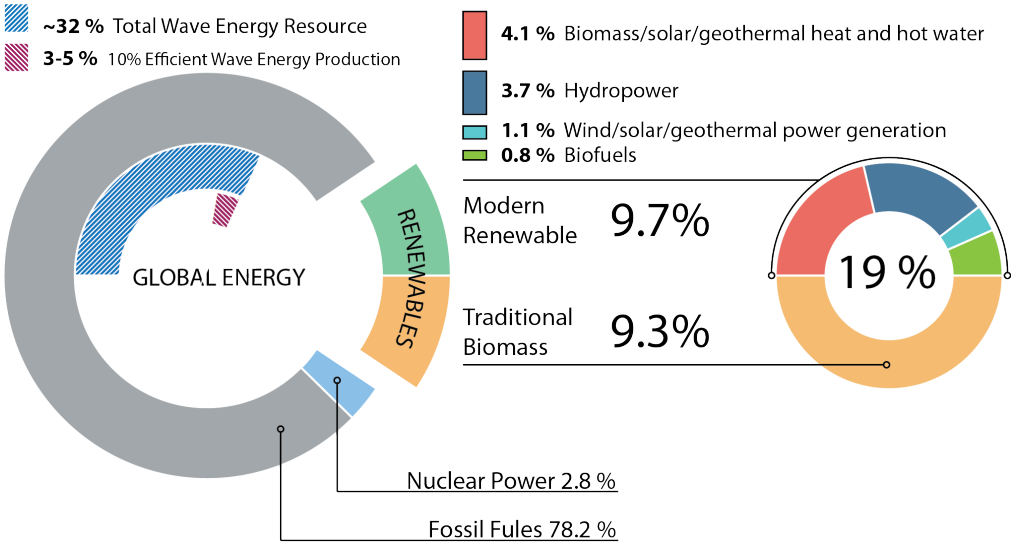

Fig. 1.2. Worldwide distribution of the global energy consumption, (Mcginn et al., 2013).

Oil & Gas resources from the list because their exhaustion time frame is still somehow unclear de facto. Since renewable energies are often less concentrated, widely distributed, unstable, etc., their exploitation needs to be a summation of small contributions. In a global frame, renewable energy accounts for 19 % of the total consumed energy (Mcginn et al., 2013). As shown in Fig. 1.2, this fraction is equally shared between traditional biomass – mainly wood - used to cook or heat, and modern renewables. In this subset, we account for hydropower, biomass, solar PV and thermal, geothermal, wind and biofuels.

The worldwide electrical energy consumption is around 13 % of the global energy consumption and almost 22 % is provided by renewable sources, Fig. 1.3. Among them, the hydropower has the larger share, around 77 % of the electrical energy from renewables.

1.1.1 Wave Energy

The wave energy sector is currently not a noticeable contributor but it has a high potential to play a significant part to the world energy mix in the future. The practically exploitable wave power potential has been assessed to be up to 3-3.7 TW, (Mørk et al., 2010), which is about a fourth of the global demand and roughly the double of the global electrical consumption. As shown in Fig. 1.3, if an overall efficiency of 10 % could be achieved, the energy produced from ocean waves may cover 20-30 % of the global electrical consumption. The wave energy resource is well distributed in temperate and subtropical zones of both hemispheres. Further, the wave energy resource eases the energy supply process, being close to the highly dense populated zones (coastlines). Compared with oil and gas offshore structures, wave energy converters are associate with a smaller environmental risk, while sharing a low visual impact that makes the resource well accepted by the community, (Chozas, 2013).

Waves occur in all sizes and forms owing to the magnitude of the force acting on the water. Small objects impacting the water surface will generate short waves, while the gravitational attraction of the moon and sun will generate long waves (tides). The

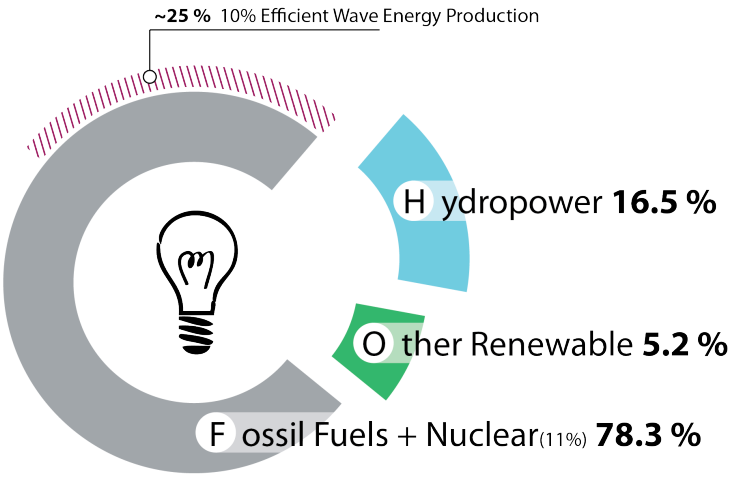

Fig. 1.3. Worldwide distribution of the electrical energy consumption, (Mcginn et al., 2013). The class "Other renewable" includes wind, solar, geothermal and biofuels used to generate electricity.

wave energy converter (WEC) mainly interacts with wind generated waves that are the consequence of the odd dynamic pressure distribution of the air phase (wind) exerted on the water surface. As a result of the distance between generation point and closest shoreline in the downstream direction (fetch), as well as the strength of the blowing wind and water depth, the waves will reshape toward the least dissipative form, i.e. gravitational waves. Gravitational waves can travel long distance with negligible energy dissipation, as long as the associate dynamic pressure field does not interact with the seabed. Thus, the energy content is reduced in the near-shore zone either in friction or breaking wave phenomenas. Since the waves are wind driven, and the wind is a result of the uneven distribution of the irradiated energy by the sun over the earth surface, it follows that waves are just a second derivative of the solar energy.

The advantages of the wave energy resource is given by its predictability (Chozas, 2013) and the higher energy density if compared with wind and solar. On the contrary, higher density means higher ratio between extreme and operational energy, which entails higher structural costs. Thus the source variability over seasons becomes a critical point. Unlucky, as shown in Fig. 1.4, the lower variability can be found in low density inhabited areas of the southern hemisphere, away from the energy request. Another interesting point is the complementarity between wind and wave source, (Chozas, 2013), which well matches with the concepts of renewable energy mix.

Even if rooted back at the beginning of the twentieth century, the modern wave energy sector first rose in the seventies together with the oil crises when Masuda (1971) created the first navigation buoy driven by an oscillating water column WEC. From those years in which the basement of the sector had been developed, according to Nielsen (2012) and Gadonneix et al. (2010), hundreds of patents have been released even if the sector went through different phases of interest.

Nowadays, sevral converters (Fig. 1.5) have reached the pre-commercial stage; this shows that the embedded energy potential has been considered enough to attract both stakeholders and developers.

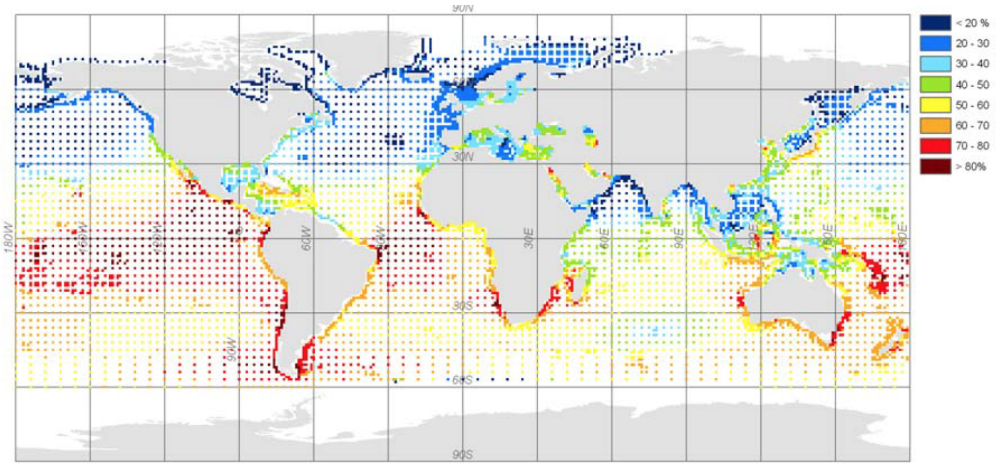

Fig. 1.4. Map of the wave energy resource variability from season to season (Cruz, 2007)

Fig. 1.5. Pre-commercial WECs listed in (Gadonneix et al., 2010), from left to right and from top to bottom: McCable Wave Pump, WavePlane, OceanLinx, Oyster, WaveGen Limpet, OPT Ocean Power Technology, Wavestar, IPS OWEC, SEABASED, Pelamis, SEEWEC, AWS Ocean Energy, Poseidon, OE Ocean Energy, Pico OWC. Only WECs developed in physical models are shown.

All the proposed concepts conceived so far can be grouped in three macro-systems, classified by the working principle of the primary energy capture:

- Oscillating Water Column (OWC)
- Overtopping (OT)
- Wave Activated Body (WAB)

The proposed classification is based on (Drew et al., 2009; Falcão, 2010). Others possible subdivisions are based on, for example, the distance from shore, the power take off chain mechanism, the orientation to the wave front, etc. For further details about classification and working principle see (Clement et al., 2002; Drew et al., 2009; Brooke, 2003; Falcão, 2010; Nielsen, 2012). The WAB class can be subdivided in three group based on the dimension and orientation of the body: point absorbers (PA-WEC) - small body compared with the wave length, attenuator (A-WEC) aligned with the wave propagation direction and terminator (T-WEC) perpendicular to the wave propagation direction.

Until the last decade, in absence of a standardised procedure, the development of different concepts went in random directions leading to various issues. The most relevant ones are the credibility gap between stakeholder, community and developers as well as the investment losses. In order to contain and manage the growing sector, standard protocols have been defined in the EquiMar project, (Ingram et al., 2011). Its aim is to give a generalised step by step method to guide developers from the paper sketch to the commercial device, while encouraging the use of small-scale physical tests, together with numerical simulations. Another important contribution to the sector was recently introduced by Weber (2012), with the concept of performance and readiness indexes matrix, Fig. 1.6. The methodology presents the optimal path with balanced indexes, aiming for the minimal cost of energy (CoE), while minimising the overall investment cost in the development stage. In order to achieve this goal, the variation of the performance index should be steep in the starting phase with small scale while flattening when a satisfactory performance is conceived; the other index should follow the complementary path - green line in Fig. 1.6. According to the author, the analysis of the best pre-commercial WECs shows an overly high readiness index for the corresponding performance index - yellow line and blue dots in Fig. 1.6 - leading to a prospected CoE too high if compared with other renewable resources.

Various limiting parameters do exist for the sector to be able to become a viable solution in a short time frame. The predominant one is the (levelised) CoE: too high if compared with other sources of energy. For WEC, but more generally for off-shore structures, the overall lifetime cost is driven by structural costs, which are ascribable to extreme and fatigue loads (design loads, (Carbon Trust and DNV, 2005)). As presented by Fitzgerald (2009) and Previsic and Shoele (2013), the WEC cost breakdown reveals that bottle-necks are located mainly in structural costs and later in the mooring and PTO costs. But in a case with a large number of small units, i.e. for a PA-WECs farm the operation and maintenance (O & M) procedures will have an important share too.

Another important parameter is the number of different WEC concepts, too large to make possible to focus the research effort on a few promising devices. This large distribution of “feasible" solutions is tailored by the uncertainties of the performance capability, evaluated in model tests.

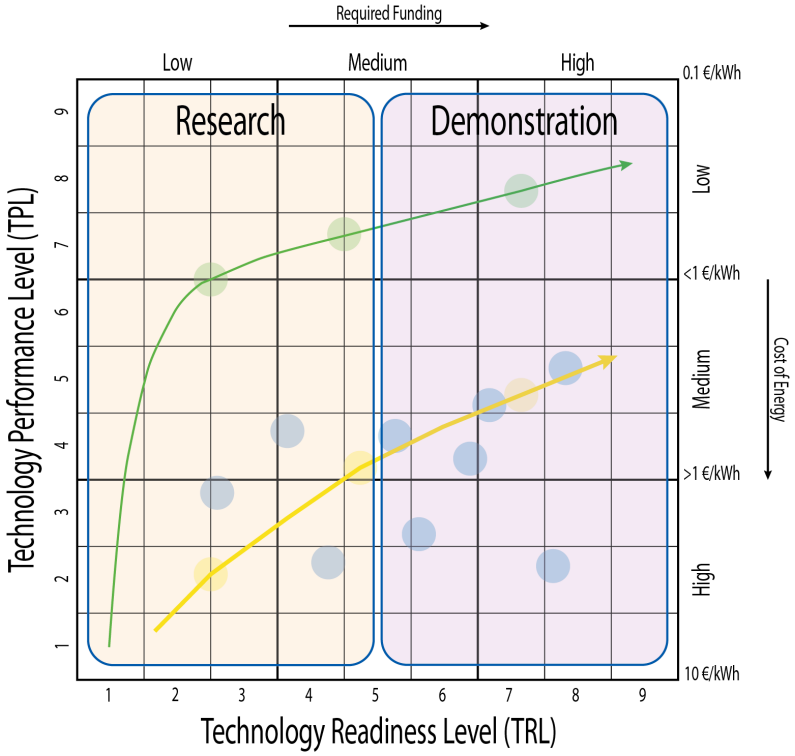

Fig. 1.6. Performance and readiness index matrix (Weber, 2012). The blue dots represent some of the patented WECs, and the yellow line represents the actual prospective of the sector. The green line represents a viable solution to reduce the cost of energy (CoE) of WECs.

Both, numerical and physical models have been used to analyse and compare different concepts, and together with the progress in computer science, the focus moved from laboratory based analysis towards a numerical/physical integrated analysis. Nowadays, numerical wave-to-wire models of WECs are a well-known methodology of analysis of WECs, and they cover a large part of the available literature of the sector. Most of the works presented are based on the linearised Diffraction/Radiation theory inherited from the Oil & Gas and naval sectors, (Hansen et al., 2012; Abraham and Kerrigan, 2013; Babarit and Clement, 2006; Fusco and Ringwood, 2013; Beatty et al., 2008; Costello et al., 2011) etc., though in the last years more and more focus has been given to the extension of the linear problem with non-linear contributions, (Sclavounos, 2012; Guerinel et al., 2013; Bhinder et al., 2011). The need of non-linear terms in the numerical model formulation is tailored by the violation of the assumptions of the underlined linearised theory. The latter is based on small waves and body motion where the body wetted surface does not change significantly in time and viscous effects are negligible due to the small velocities. In contrast, a WEC is requested to move as much as achievable in specific degree of freedoms (DoFs), which bring to the afore mentioned violations. So far, the most comprehensive analysis of WECs based on a weakly non-linear wave-to-wire model is presented in (Babarit et al., 2012). Different WEC systems at different locations are compared in terms of power performance, while highlighting the level of uncertainty of the results.

In addition to the large utilisation and development of wave-to-wire models, the computational power growth brought at the top the WECs optimisation matter. Optimisation or efficiency maximisation of WEC is a hot topic of research which can be easily and cheaply achieved with numerical models. So far, mainly two techniques have been used:

hydrodynamic optimisation based on the shape optimisation (Alves et al., 2007; Gilloteaux and Ringwood, 2010) and efficiency maximisation through control schemes. The energy maximisation of wave energy converter by mean of control strategy is a vast topic of research. The close form solution of the maximisation problem is one of the earliest finding of the sector, and in the last decades the interest moved toward real-time implementation of the control strategy, (Hals, 2010; Fusco and Ringwood, 2013; Babarit et al., 2009; Cretel et al., 2011a; Hals et al., 2011a; Price, 2009; Fusco and Ringwood, 2010a; Nielsen et al., 2013). However, the recent works presented by Borgarino et al. (2012) and by Zurkinden et al. (2013) highlighted the importance of the structural design in the global optimisation of WECs.

In contrast to this large number of works in the numerical environment, the literature regarding the validation of numerical results based on physical model tests is somehow loose, (Durand et al., 2007; Lopes et al., 2009; Paredes et al., 2013), and mostly based on simple geometries.

1.2 Objectives

In order to cope with the need for renewable and complementary energy plans, the wave energy sector offers an important research field due to the high embedded potential. But the cost of the produced energy causes the resource to be largely untapped.

With the aim of assisting efficient development and analysing WECs and thereby accelerating the sector progression towards commercialisation, a generally applicable, efficient and reliable wave-to-wire model tool is needed.

As a consequence of the large number of different WEC concepts, the model is seldomly generally applicable, and focus has been given to the WECs of the wave activated body (WAB) type. The efficiency and reliability of the model are defined once the overall objective is stated. Within the framework of the Structural Design of Wave Energy Devices (SDWED), which granted this work to a great extent, the word “efficient" means low computational cost and “reliable" means an uncertainty level as small as attainable.

Three different WECs defines the base of analysis, namely Wavestar (2014), Dexawave (2014) and Weptos (2014). They are listed in increasing order of complexity from a model point of view, and presented in Fig. 1.7.

Among the other before-mentioned issues, four points are considered critical in the implementation of a wave-to-wire model and they define the objective of the thesis.

- Identification of the critical sub-systems for a general WAB WEC. Albeit similar to a large extent, WECs of the OT and OWC types are not considered as a part of this work. The selection of the key sub-systems is led by the analysis of predominant loads acting on the WEC.
- Analysis of the available model for the selected sub-systems and identification of the best cost-effective solutions. The definition of “best" is defined as a trade-off between computational time, accuracy and precision, being the last one related to the actual stage of the wave energy sector. Entailed by the large number of concepts, what is needed is mostly a rough sieving of the available devices rather than a detailed

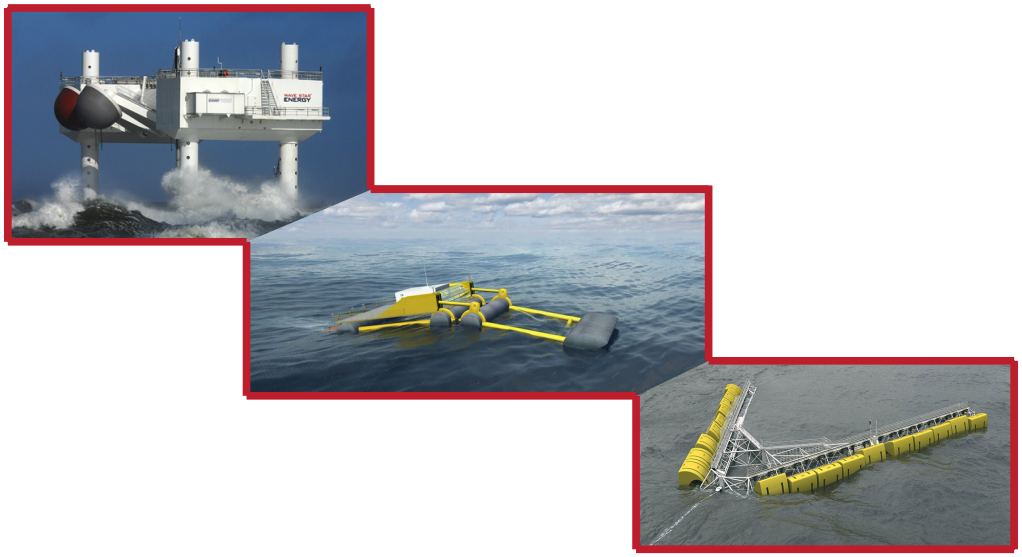

Fig. 1.7. From left to right: Wavestar WEC, Dexa wave WEC and Weptos WEC. The photograph of the Wavestar shows the large-scale prototype tested in Hanstholm, DK, while the other two are graphical representations.

analysis of them. Therefore, the best model will have a rather coarse precision keeping the computational time to the lower achievable level and the accuracy at the highest possible level.

- Validation of the numerical models by means of physical tests. In order to quantify/reduce the uncertainty of the numerical results. These steps are indispensable to create a fair comparison without exception, or reducing the gap, between numerical and physical results.

- Economical optimisation of WECs. The first step will be the increment of the WEC absorbed energy by means of advanced control strategies, which will be then balanced by structural fatigue analysis. The main attempt is dual: implementation of widely known control strategies into a WEC physical model in order to understand the real applicability of those techniques and to apply well established fatigue analysis procedures in order to introduce a structural variable into the economical optimisation of the WEC.

A corollary objective of the thesis, tailored by a specific need found in the physical tests, is the implementation of a non-contact position and orientation tracking system.

1.3 Thesis Outline

The thesis is organised in a collection of papers including a thorough introduction to the work. The general and specific problems are stated in the introduction, while the detailed analysis of the issues is given in Appx. A which collects all the papers. Two other appendixes are included, Appx. B and Appx. C, which give details about the Wavestar WEC physical model and the Weptos WEC numerical model. The latter describes the first set of interim results obtained for the Weptos WEC, but due to large range of uncertainty

expected in function of the approximation used the model has not been incorporated in the thesis as such. The introduction is divided in five chapters as indicated in Fig. 1.8.

In Ch. 1, the general leading motivation is given together with the previous and current status of the wave energy sector. The chapter attempts to shed light on the current issues faced by the sector which are limiting the exploitation of the wave energy resource, seeding the objectives of the work in those elements which have been considered key points.

In Ch. 2, the system breakdown and qualitative analysis of a generic WEC of the WAB type are given. The result of the quantitative analysis is the definition of critical sub-components from a model point of view. For each of the subsystems, the actual status of development is analysed to identify the key points, which are then addressed in detail in Chaps. 3 and 4. Also, the relevant literature is listed.

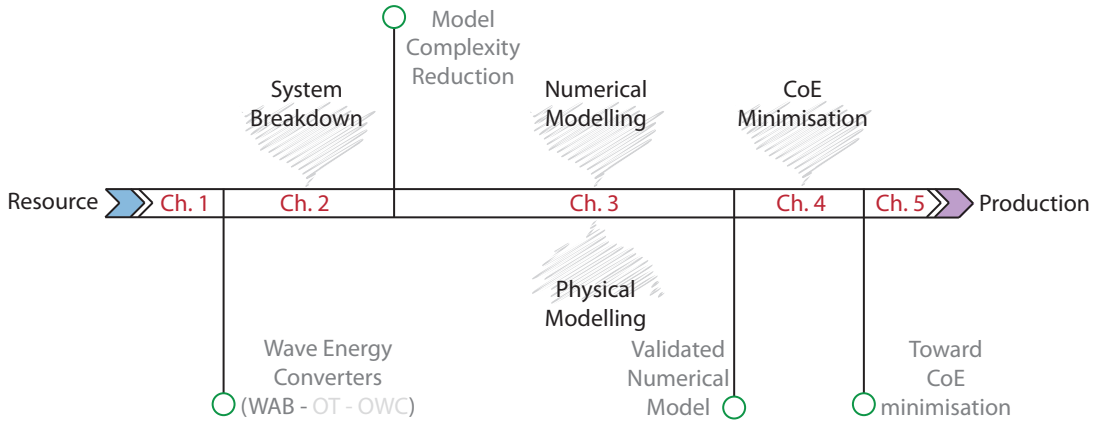

Fig. 1.8. Thesis outline diagram.

Ch. 3 is divided in two main sections. Sec. 3.1 lists the available numerical models for each of the selected sub-systems, whilst the ones considered relevant are further detailed. As already introduced in the context of this work, “relevant", previously “best", is selected in agreement with the relatively low level of precision required in the analysis. Therefore, low computational cost methods with the highest - achievable - precision will be preferred. The second part of the chapter, Sec. 3.2, describes the physical models used and the validation of the numerical results, giving a critical discussion over the limitation of the proposed methodologies. The resultant model is subsequently used as a base for the optimisation of the WECs discussed in Ch. 4.

Similar to the previous chapter, 4 is divided in two main sections. Sec. 4.1 briefly describes five well know control techniques. Also, their implementation is described, highlighting the main difficulties and deviations from the reading theory. In the second part of the chapter, Sec. 4.2, the control laws introduced are used together with standard structural fatigue methods to find a balanced optimal economical design. In the last section the focus will stay put on a simplified version of the Wavestar WEC, reducing the system to a single degree of freedom to ease the analysis of the system.

Ch. 5 summarises the main outcome of the work presented in the thesis, together with the prospected future works.

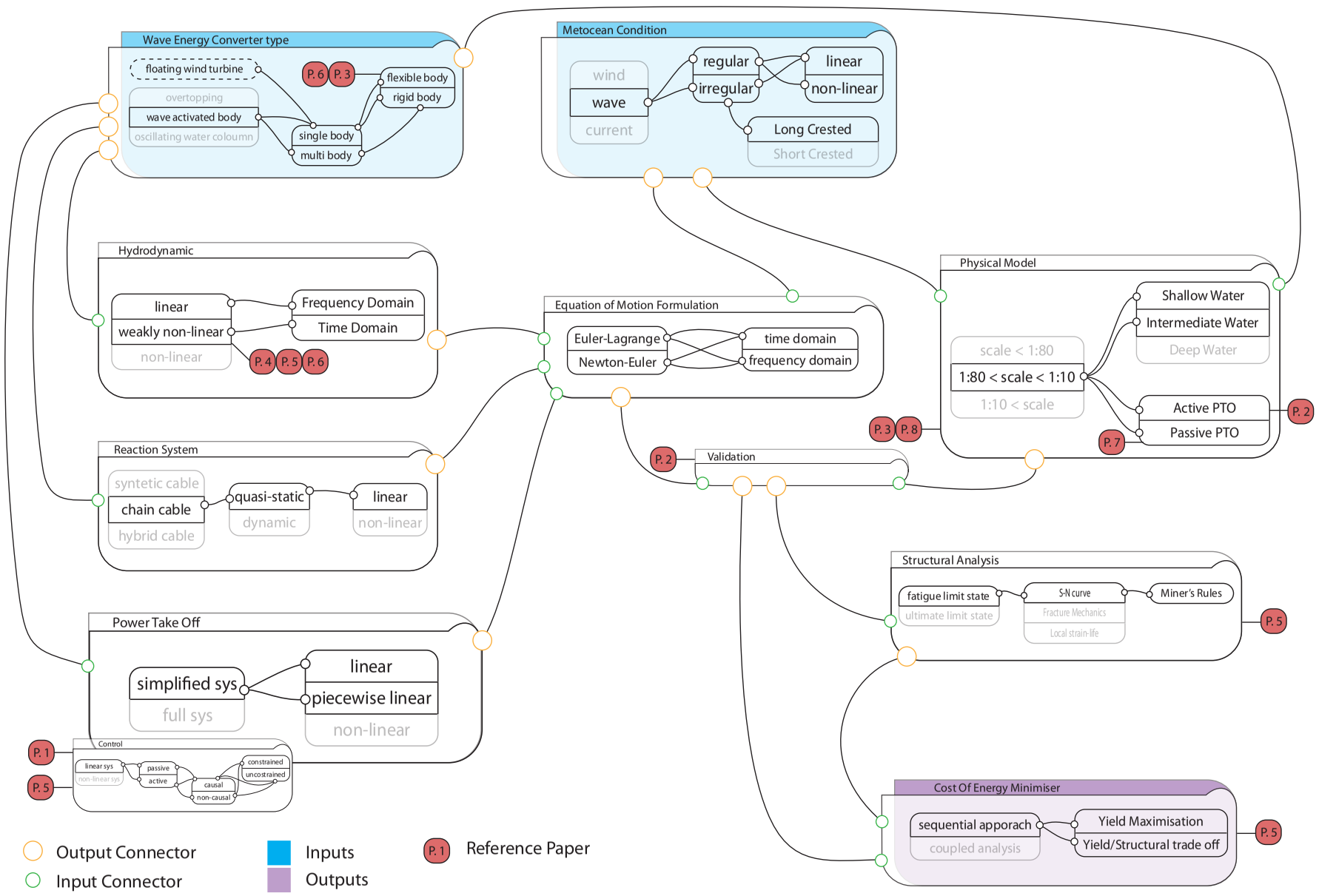

Fig. 1.9. Objective of the thesis and interconnection between sub-modules. The colour legend is located at the left-bottom of the figure. Greyed texts and boxes represent alternative solution and methodologies not used in this thesis. The figure is inspired by (Taghipour, 2008)

2 WEC system breakdown and relevant literature

A wave energy converter (WEC) can be defined as a dynamic system with one or more degree of freedoms (DoFs), used to transform the wave energy content into “useful” — typically electrical — energy. The definition infers the wave as the input, and the “useful” energy as the output of the system. The term useful has been highlighted because along with the electrical power production, a WEC can have other uses, for example potable water production (Nolan and Ringwood, 2006). In the following, as already introduced previously, only WECs of the WAB type are considered.

On a macro scale, the device breakdown shows six main subsystems, listed below and exemplified in Fig. 2.1 with relative interconnection:

- Main Structure (MS) - Hydrodynamic System (HS) plus Hosting Structure System (HSS)
- Power Take Off (PTO) System
- Reaction System (RS) or Station Keeping System (SKS)
- Control, Instrumentation and Electrical System (CIES)
- Power Connection System (PCS)
- Onshore Facility System (OFS)

Even though each of these elements is indispensable for the system to work, only the first four element of the list will be further discussed hereafter. The choice can be justified by the objective of the work presented in the thesis: the definition of global and steady state parameters, rather than transient and specific ones. Further, the PTO and the CIES systems will be discussed together since they are tightly linked. The nomenclature has been chosen in agreement with (Hamedni et al., 2014), developed during the SDWED project.

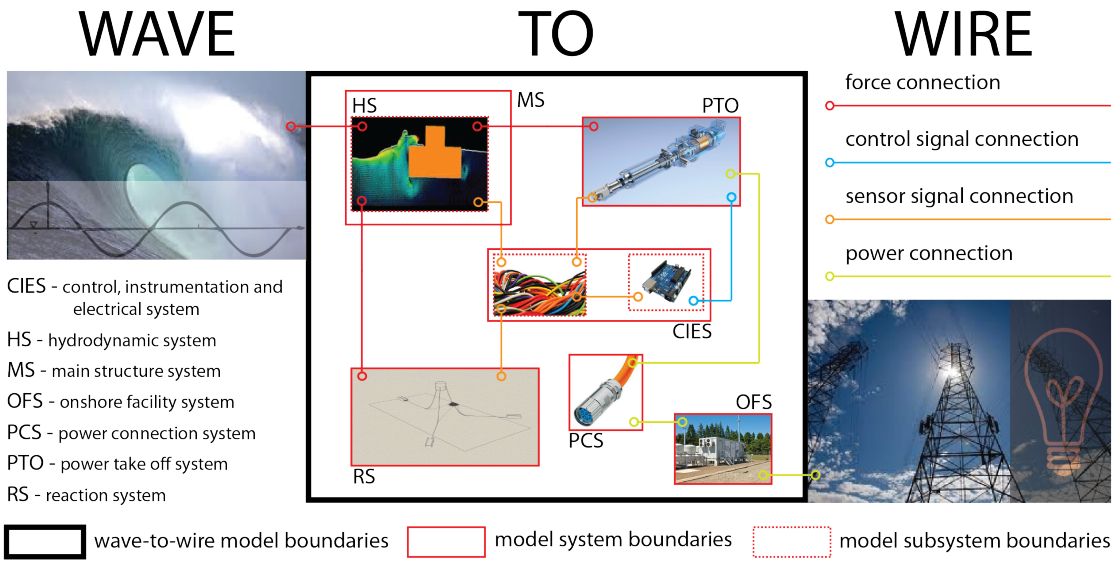

Fig. 2.1. Wave-to-wire model definition and WEC system breakdown.

2.1 Main Structure

The main structure of a WEC is a polymorph element that changes from device to device; Fig. 1.5 gives some examples of devices. It is unrealistic to define a general shape, but from a mechanical point of view the system can be seen, to a great extent, either as a single rigid body or a multi body system. Deviations from this assumption may be given by the Anaconda WEC or similar types, (Chaplin et al., 2007), although they can be considered as a multi-body system once the single body size is properly defined based on structural eigenmode analysis. The main structure either holds, or is, the hydrodynamic subsystem (HS) of the WEC. The HS is defined as the element through which the device interacts with the energy source; thus it is the place where the energy conversion starts. For WECs with a large emerged, or non interacting with waves, volume, the main structure will be composed by the HS and the Hosting Structure System (HSS), the latter being the house of the CIES. Besides converting the wave energy content into mechanical energy at the HS, the MS is required to last extreme loads, prevent the contact between water moisture and electrical part, withstand corrosion, as well as ease and reduce the cost of operational and maintenance (O&M) procedures. The MS placement is as such a key point. As introduced in Ch. 1, the CoE is the limiting factor for most WECs conceived so far. The power absorbed in operational sea states and the related turnover (income associated with the energy production) is too small if compared with the total cost of the system over its lifetime. The cost of the system is made by capital expenditure ($CAPEX$) and operational expenditure ($OPEX$) in first approximation.

In many cases, the total cost is driven by structural capital costs. It is important to highlight that for point absorber WECs installed in large numbers the O&M could become as important as the structural cost. But the matter is not further described in the thesis.

When the structural cost is the bottleneck, both the ultimate limit state (ULS) and the fatigue limit state (FLS) design parameters should be considered in the first stage of analysis (Veritas, 2013; DNV, 2010).
The ULS corresponds to the maximum load-carrying resistance caused by extreme events.

The latter is defined for WECs as sea states associated with high energy density and small likelihood, i.e. one event over ten, fifty, hundred years. As a consequence to most of the wave energy content being concentrated near the free surface, a body placed closer to the water surface will access a larger pool of energy. While this is convenient in operational sea states, it turns harmful in extreme conditions. The power per unit width of wave front associated with operational and extreme sea-states can be 5-50 and >2000 kW/m respectively. The WEC needs a survivability strategy in order to reduce the magnitude of the design loads associated to extreme sea states and thereby reduce the capital cost. Different survivability scenarios have been proposed like submergences, shape-variation, control, etc. (Folley and Chaplin, 1998).
On the other hand, the device can be placed somewhere away from the high energetic zone, which reduces the extreme/operational loads ratio and the convertible energy too. From another perspective, the choice of the design standard is also a fundamental element. In contrast to the Oil & Gas industry where stringent rules or guidelines need to be applied as a consequence of the high magnitude associated with the system breakdown, for the wave energy sector the risk associated with the system failure can be lowered to the same level as in the offshore wind sector. Briefly, the magnitude of the failure is mainly the cost of the device without any major implication for human life risk, environmental risk, etc. Although specific standards have been proposed in recent years (Carbon Trust and DNV, 2005), so far the wave energy sector needs to refer to the wind sector, whose standardisation is more mature (Veritas, 2013).
The other structural design parameter cited is the FLS. In spite of the large number of load cycles that the WEC will withstand through its expected lifetime, fatigue is generally considered to have a smaller impact on the design of the system. This assumption can be shared to a great extent for WECs with a resistive controller, but when an active control strategy is used the conclusion is not so trivial; for the definition of the controller types see Ch. 4. In fact, when an active control strategy is adopted, the amplitude of the PTO duty cycle will undergo a large increase if compared with a resistive controller. The load amplification causes a greater stress accumulation on the structure and a subsequent growth of capital cost.

Besides the CoE, as already introduced in the previous chapter, the large number of WEC concepts is also partially liable of the slow development rate of the sector. Among the patented concepts — more than hundred (Gadonneix et al., 2010) — only few of them have reached the pre-commercial stage, whilst the majority is still in conceptual/small-scale test. This large variability is imputable directly to the MS, since both PTO and reaction systems rely on more mature and standardised technologies.

A vast case history — mostly based on numerical methods — describes the functionality of the different concepts (Chaplin et al., 2007; Hansen et al., 2012; Pecher et al., 2012b; Silva et al., 2013; Mackay et al., 2012; Seidel et al., 2012; Beatty et al., 2008; Babarit et al., 2012) in operational conditions. Despite their importance, extreme events are rarely considered from a numerical point of view (Palm et al., 2013a) and more present in the literature concerned with physical modelling (Zanuttigh et al., 2013). On the contrary, the dissemination of results of large scale prototypes is loose, (Marquis et al., 2010; Pecher et al., 2012a). To a great extent the numerical analysis is based on the linearised hydrodynamic problem solution (see Ch. 3), inherited from Oil & Gas and the naval industry. But if a prediction of the economical effect of extreme loads needs to be endorsed, then non-linear waves are the base for the design (Carbon Trust and DNV, 2005). Regrettably, only few examples of utilisation of fully non-linear solvers are available

(Yu and Li, 2011; Palm et al., 2013a; Westphalen et al., 2009) due to their considerable computational cost. Similar to the lack of research in extreme sea-states, the literature about the influence of the control strategy into the fatigue design of the WEC is also limited (Borgarino et al., 2012; Zurkinden et al., 2013).

2.1.1 MS system key points

From what has been previously introduced, two issues are considered for further analysis in the next chapters.
First, the definition of a fast numerical methodology able to output reliable results in different control scenarios in operational sea states. The term “results" accounts for the calculation of absorbed power and loads. Although the wave structure interaction can be evaluated with different levels of accuracy, only the methods which infer a small computational time can be used to compare a large number of different systems. The validation procedure is needed to estimate the level of uncertainties expected in the results. The topic is further covered in Ch. 3, and it is based on the implementation of standard numerical methods and their analysis in physical models. In addition, as discussed in Ch. 4, the numerical model is used as a base of optimisation of the given WEC, not only from an energy perspective but also from an economical one, pushing toward a minimisation of the actual CoE. At this stage, FLS will be used in the model too.
Second, the predictability of ULS or other extreme loads using a simple and low computational cost model. The topic is further covered in Appx. A.3 and Appx. A.6, and it is based on the implementation of standard numerical methods and their analysis in physical models. Although the model describes a floating offshore wind turbine (FOWT), similarities with large WECs could allow a partial extension of the methods to the wave energy sector.

Due to the large variability of WEC concepts, exceptions from what stated above are likely to exist. For example, whenever the HS is also hosting the CIES, insulation and maintenance may become important elements too, meaning that their influence should not be disregarded even in the first stage of analysis.

2.2 Power Take Off System

A PTO system is defined as the chain of processes which transforms the available energy at the HS, i.e. activated body, reservoir, chamber, etc., into electricity to be delivered to the grid. The definition infers the encompassment of a control law (CIES system) into the PTO system.

The PTO system is the key element of a WEC, first of all because it is the distinguishing element between a floating body and an energy converter. The dynamic response of a WEC is highly correlated to both the PTO type and the control law. The PTO exerts time varying loads on the HS, and widely on the MS, which affect the absorption capability of the system. The absorption capability of a WEC are commonly quantified in term of the capture width (CW), defined as the ratio between absorbed energy and incoming energy per meter of wave front. Although each WEC developer/company has the tendency to develop its own PTO system, few main different classes of the PTO type are widely used into the wave energy sector. In particular for WECs of the WAB type — the focus of this thesis — two main system are adopted:

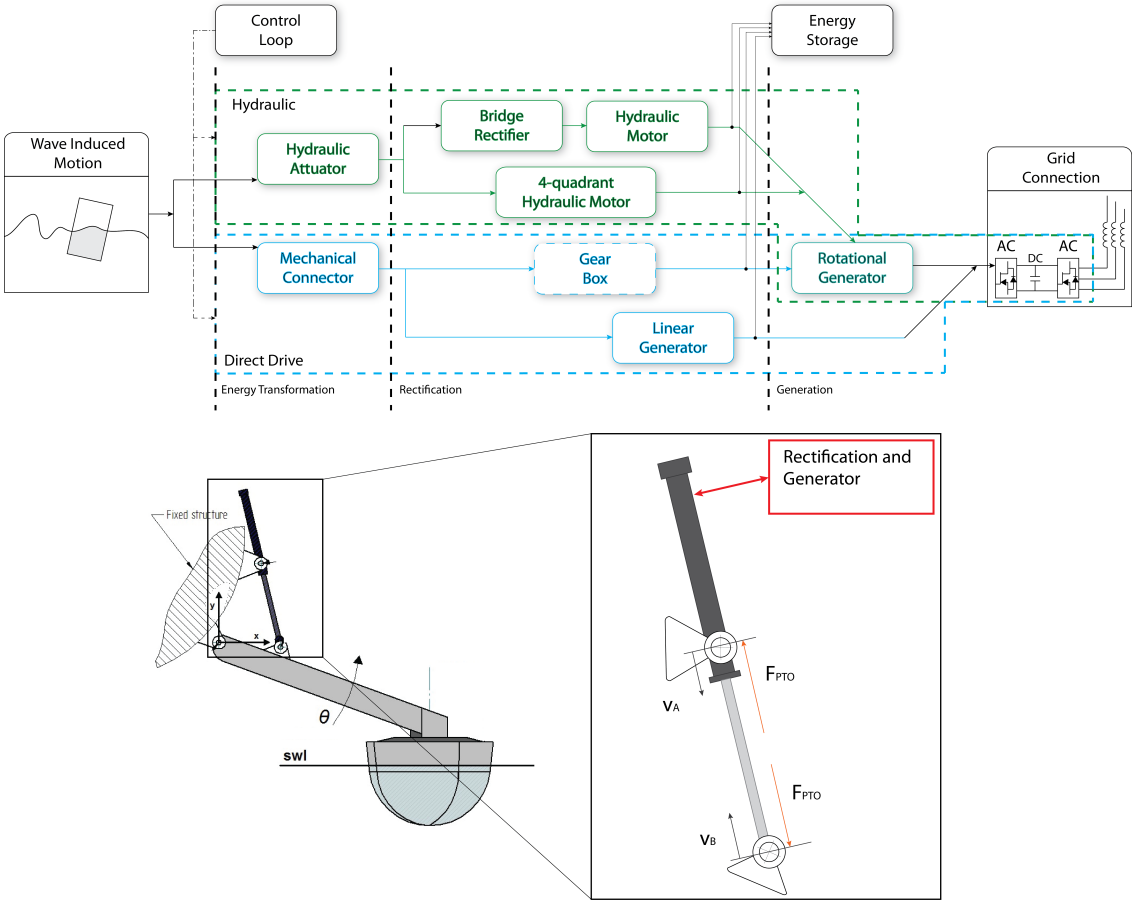

Fig. 2.2. Top: general PTO scheme for WEC of the WAB type. Green and cyan colours are used to distinguish between hydraulic and direct drive systems respectively. Bottom: sketch of the interconnection for a PTO system with the Wavestar WEC.

- Mechanical direct driven system
- Hydraulic system

For the sake of simplicity in this thesis, the direct drive class also includes those PTO systems where the connection between the HS and the generator is obtained by means of mechanical elements but excluding any fluid. For example, PTO with gear boxes is considered a direct driven system. Further, along with the hydraulic systems, the air compressed systems are also a possible solution, but their utilisation is bounded by the limited overall efficiency (Lemofouet and Rufer, 2005).

The PTO system receives high harmonic forces (up to MN) with long oscillation periods (from 1-20 s), and it needs to fulfil the required grid specification. Furthermore, it is important to bear in mind the aggressive environmental conditions where the device is situated (i.e. high salinity, distance from land, high load in storm condition, water spray, slamming load, etc.).

It is possible to draft a common scheme for the two PTO classes, see Fig. 2.2, where the available energy, either kinetic or potential, is transferred from the HS into the generator, in parallel with a control scheme, and a storage system (if needed); the transformation can be either single or multistage.

2.2.1 Mechanical direct driven system

This is the simpler PTO type among the two, which makes it the first studied solution in the early research years in the sector: a reduced number of components is a basic request especially in offshore matters. The generator, either linear or rotative, and the HS are directly linked via mechanical connectors, such as mooring line, gearbox, pulley or belt. The main cons were inefficiency, high cost and weight of the overall system, but in recent years, technical improvements led by the wind sector have made this type of PTO a viable solution for a small size WEC. The design airgap velocity have been reduced from 60 m/s to 0.5 m/s fitting with PA-WEC (Mueller, 2002; Mueller and Baker, 2002; Shek et al., 2008; Binh et al., 2012; Ivanova et al., 2005; Polinder et al., 2005; Polinder et al., 2007; Eriksson et al., 2005). In addition, enhancements in power electronics (Brooking et al., 2002), together with advances in the sector of battery and ultra capacitor, have also meant an improvement on the quality of the energy fed into the grid, which means a possible match between the produced electricity quality and the grid code. Common examples of PA-WEC using linear mechanical direct driver are Archimede Wave Swing, Uppsala Point Absorber and the "L10" Buoy.

Even though linear generators are commonly used in direct drive WEC, rotating generators can also be adopted. For example, the Weptos WEC, (Pecher et al., 2012b), adopts a rotating generator driven by a cluster of activated bodies mounted in a single large structure. The main disadvantage of rotating generator is the minimum angular velocity required by the generator to work properly, which forces the utilisation of a gearbox with related challenges.

2.2.2 Hydraulic System

In this class of PTO, a fluid flux generated by a hydraulic piston (actuator) connected to the HS impels the motion of a motor that is coupled to a rotating generator. The fluid can be both water and oil, even though the utilisation of the latter allows a better control on performance and durability of the system. Although hydraulic PTO systems are robust and designed to work with large forces and small velocities, which coincide with the characteristic framework of WECs, the complexity of the system is a limiting factor in off-shore applications. They do normally adopt accumulators even though the utilisation of a power electronic unit can replace this need, i.e. Wavestar WEC (2014). According to Kamizuru et al. (2012) and Costello et al. (2011), the hydraulic circuit can either use or not use a bridge rectifier at the output of the actuator. The rectified solution is simpler but less efficient and controllable, but in both cases the system is far more complex compared to the direct drive option. Results of both numerical, (Costello et al., 2011; Hansen et al., 2012; Falcão, 2007; Zhang et al., 2012) and physical, (Marquis et al., 2010; Henderson, 2006; Lasa et al., 2012) WEC models with hydraulic PTO systems have been extensively reported in recent years. A diverse model has been recently presented by Hansen et al. (2013), where a multi-chamber hydraulic PTO system has been used as a simulation base and built in full scale too.

Common examples of WECs with hydraulic PTO system are: Wavestar, CPT, AquaBUOY, OPT, Wavebob for the PA-WEC type, Pelamis, Dexadevice for the A-WEC type and Oyster for the T-WEC type.

2.2.3 CIES system

The control logic is normally included in the definition of the PTO system due to their strong bound. The control system defines how the PTO system works, and in turn affects the operation of the WEC. The modification of the control logic is the most straightforward way to modify the efficiency of the WEC and therefore to modify its revenue. A robust literature about the implementation and optimisation of the control logic within the wave sector is available. Some examples are:Hansen et al. (2013); Fusco and Ringwood (2013); Cretel et al. (2011a); Babarit and Clement (2006); Binh et al. (2012); Falcão (2007); Fossen (2011); Falnes (2002); Hals (2010); Abraham and Kerrigan (2013), but more details are given in Ch. 4. But most of the example available are based on numerical simulation and only few example of implementation of advance control strategies in physical models are available.

2.2.4 PTO system key points

From the previously introduced issues, two are considered for further analysis in the next chapters.

First, due to the need of a fast numerical method, it is of primary interest to solve the implementation of a PTO model problem by simplified transfer function and lumped models. In those models, only the eigenfrequency of the PTO within the wave/WEC frequency range is then needed. The topic is further covered in Ch. 3 where examples of simplified PTO models are given for both numerical and physical cases.

Second, a critical point in the PTO/control system is the implementation of advanced control strategies, and the evaluation of their true capability, in physical models. Due to the bad scalability of PTO systems, the implementation of advanced control schemes in laboratory tests is often unfeasible. The topic is further covered in Ch. 3 where two examples oh the implementation of PTO in physical models is given.

2.3 Reaction System - Station Keeping System

Besides from the first order motion induced by linear waves, offshore structures are subject to forces, such as wave, current and wind, that are causing a drift in the mean position. Reaction or station keeping systems are adopted in every WEC to achieve the following tasks:

- Maintain the floating structure on station, plus/minus a certain tolerance, under operational and extreme condition.
- Reduce/remove load on the electrical connection.
- Ensure alignment of directional WEC.
- Avoid impact with other structures (ships, WECs, etc.).

Nevertheless, reaction systems should not wrongly affect the power production of WECs, have low cost, high reliability level, low environmental impact and require little inspection and maintenance. As shown in Fitzgerald (2009), the RS has a large share in the overall

lifetime cost of the converter, thus its cost optimisation goes along with the economical optimisation of the energy produced by a WEC. Similar to the main structure, the station keeping system shall be designed to last extreme events, whose loads can exceed operation loads by a decade or more. Further, the variability of WEC design does not allow an a priori best configuration, which instead needs to match the WEC and location characteristics. But based on simple considerations, it is possible to identify two different classes:

1. Mooring system for large WEC with self-referencing body, i.e. FO^3, Weptos, Wave Dragon.

2. Mooring system for activated body WEC without referencing body or small size self-referencing WEC.

On the one hand, in class 1 the reaction system does not influence the dynamic behaviour of the HS to a great extent, i.e. only the long period motion of the referencing body is modified. On the other hand, in class 2, while the reaction system needs to be still in compliance with the stationkeeping requirement, the WEC will undergo a modification of the overall body response in both static and dynamic ranges. For this class, disregarding the mooring model— either the full description or a linearised version— will increase the uncertainties of the predicted power performance of the device heavily. A first example of the direct implementation of the mooring system into the power absorption maximisation of a PA-WEC is presented in (Richter et al., 2013). The design of reaction systems for a WEC is a difficult task, mainly because the technical design needs to be balanced by fundamental non-technical matters.
First in place comes the risk based design for off-shore renewable converters, (IEC/TC, 2013). In order to reduce cost of energy of WEC systems, the mooring system should be designed with a lower risk level than an Oil & Gas offshore platform. The utilisation of a recent standard from the offshore wind sector (Veritas, 2013) will lead to a cost reduction of the mooring system in consequence of the reduction of the amount of material employed. In light of the weight of the reaction system in the overall lifecycle cost of the WEC — ca 20 % (Fitzgerald, 2009), its cost reduction is an important matter.
But a large number of failures of WECs at real sea deployments — directly related to a failure of the stationkeeping system — has caused a lack of faith in the public opinion toward the wave energy sector. Paraphrasing Gadonneix et al. (2013), the sector underestimates the embedded technical difficulties, increasing the discontent of observers, stakeholders and community. So, the mooring system needs to increase the associated level of reliability to be accepted, which is the diametrically opposite of what has been shortly stated.

Specific design rules have been inherited from the offshore industry, i.e. naval and Oil & Gas , but a WEC differs from those applications by the dynamic response. Ships and platforms are meant to reject the wave disturbance while WECs are tuned to be in resonance with it. The velocity associated with the stationkeeping of a WEC is larger than the one of ships and platforms, therefore non linear processes as internal viscous damping need to be accounted with a dynamic cable model, (Johanning et al., 2007). Several works addressed this issue with both experimental and numerical analysis, i.e. (Dubuque, 2011; Ruiz-Minguela et al., 2008; Rhinefrank et al., 2010; Zanuttigh et al., 2013; Parmeggiani et al., 2013; Palm et al., 2013a; Paredes et al., 2013). The above mentioned numerical examples are all based on a fully dynamic model of the mooring cable. The main drawback of these methods is the high computational time, which mostly limits their utilisation in optimisation or fatigue assessment routines. These types of analysis are commonly

conducted with a quasi-static approach, (Vicente et al., 2011; Richter et al., 2013). While waiting for the computation time of dynamic model to drastically drop, an alternative approach has been proposed by Fitzgerald and Bergdahl (2008) where the fully dynamic model is used to tune the frequency response of the mooring system including both stiffness and damping terms.

2.3.1 Reaction system key points

Based on the needs of the analysis presented in this thesis, a linear approach with constant parameter is used. However, dynamic simulation or physical model test of the station keeping system are then used to calibrate the linear parameter of one of those models.

The mooring analysis is restricted to the only case of spread mooring systems, where each of the mooring cable is constituted by a simple suspended chain, without intermediate bodies. The influence of the full reaction system into the power capability of a floating WEC is further analysed in Appx. A.7 with experimental tests.

Modelling and Validation

3

As suggested by the EquiMar protocol, the performance index method and others, the feasibility of the WEC concepts and its potential performance should be evaluated and optimised as early as possible in the development process. The utilisation of models, numerical or physical, is a necessary step therefore. In the modelling phase, different sources of errors are expected to deviate the model output from the unknown truth. A general overview of the problem is described in Fig. 3.1 which is based on the analysis presented in (ASME, 2009). The methodology (validation and verification) estimates the accuracy of a numerical simulation in two steps. The verification step establishes the accuracy of the code based on a benchmark with available analytical solutions. The validation step estimates the simulation modelling error range based on a comparison with appropriate experimental results. The errors which lie between the truth and model output are measurement (physical), algorithm (numerical) and structural (physical and numerical). A brief description of the errors is given in the following. Measurement errors are the easiest to identify and quantify. They are related to the instrumentation accuracy and precision, to the error introduced by the physical environment i.e. wave basin reflection, and to the operation of the experiments i.e. wave generation technique, consistency on the procedures, etc. Algorithm errors are defined by the solver error i.e. truncation errors, discretisation, etc., and by the parametric errors i.e. model inputs and sensitivity of the model to their variation. Structural errors are related to model inadequacy and simplification. For a physical model, one possible source of structural error is the scaling law used. For example, the underestimation of the scale effect can lead to a modification of the ratio between predominant forces. For a numerical model, one possible source of structural error is the model approximation and its underlying theory, for example using a potential solver for a viscous dominated flow. The following sections provide further details.

3.1 Numerical Modelling

Simulation are mainly helpful in earning insight to the dynamic behaviours and interactions that are often not promptly evident from theory. Even though simulations are often

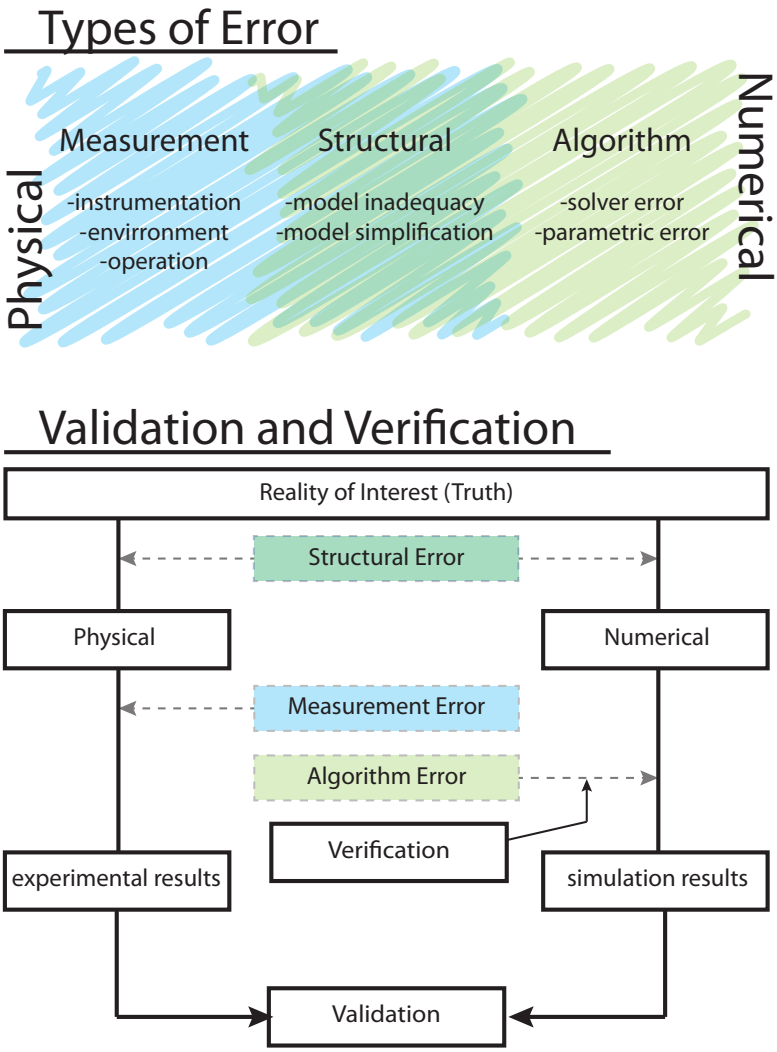

Fig. 3.1. Types of error and framework of validation and verification of numerical models. Figure inspired by (ASME, 2009).

chosen to study transient dynamics, compare conceptual designs, risk assessment, etc. They are merely a representation of a theory that is abstracted from observation of the physical process. Numerical models need to be realistic, simple and easy to manipulate; these are conflicting requirements. Realistic models are seldom simple, and simple models are seldom realistic. Thus, the definition of what is considered relevant infers features and behaviours that are pertinent and those can not be neglected in the model. From the key elements listed in the previous chapter, steady state and global parameters are considered pertinent features in the model selection. In point of fact, the different methodologies applied to calculated power performances and structural fatigue damages of WECs (Ch. 2) are based on long simulations, thus the computational cost of the models needs to be considered. This requirement is in accordance with the aims of the SDWED project, which is partially funding the work presented in this document. The main project objective is the definition of a generally applicable, efficient and reliable wave-to-wire model tool, used to assist an efficient development and analysis of WECs.

For each of the elements discussed in Ch. 2, the available models are listed and the ones considered relevant in the framework of this thesis will be further discussed.

3.1.1 Hydrodynamic System / Wave Structure Interaction

The combination of hydrostatic and hydrodynamic pressure fields exerts variable loads on any floating structure exposed to the wave structure. There are several models with different levels of accuracy to solve the time varying loads on the structure, where the common ones are:

- Morison's Equation - Semi empirical non-linear model
- PaM - Panel Method (also known as Boundary Element Model (BEM), Boundary Integral Equation Method (BIEM) and Diffraction/Radiation problem)
- CFD/(u)RANSE - (unsteady) Reynold-averaged Navier-Stokes Equation
- SPH - Smoothed Particle Hydrodynamics
- CFD/LES - Large Edge Simulation
- CFD/DNS - Direct Numerical Simulation

The different model types are listed in ascending order of required computational time/cost and model complexity. The DNS method is considered not usable for any practical application for the time being due to the excessive required computational time.

Simulations of WECs based on CFD methods are possible (Yu and Li, 2011; Palm et al., 2013a), but their utilisation is limited to short-time simulations in consequence of their large computational cost, i.e. extreme condition assessment. Mostly the (u)RANSE turbulence method is used, while LES is still too heavy from a computational point of view to be widely used in practical applications. So far, the Morison and PaM models are the common adopted methodology when a fast analysis needs to be carried out. An example is the assessment of time average parameters such as annual energy production (AEP) and capture width (CW) of the WECs. The relevant bibliography includes a broad spectrum of case studies, which was efficiently summarised in the work presented by Babarit et al. (2011); Babarit et al. (2012). The studies show, based on a hybrid model, the power performances of the predominant WECs at different European locations on the Atlantic coast. In this context, the term "hybrid", or weakly non-linear model (3.18), infers a combination of the linear Diffraction/Radiation (PaM) solution and simplified non-linear contributions, such as the viscous drag term from the Morison's equation or non-linear hydrostatic models. The verification of the PaM solution is presented in (Sarpkaya, 2010; Hulme, 1982) for two geometries: a cylinder and a hemisphere respectively. The verification of the Morison's equation is presented in (Morison et al., 1950) for a cylinder.

The choice of a hybrid model is inherited from the analysis of predominant forces acting on the structure, which can be conducted using non-dimensional parameters. Using a non-dimensional analysis brings a reduction of the structural error on the numerical model Fig. 3.1, increasing the adequacy of the model for the specific case. For bluff bodies (Faltinsen, 1993) subject to oscillatory flows, one can refer to the Keulegan-Carpenter (KC) number in first approximation. The KC number describes the relative importance of viscous over inertial forces in oscillatory flows, and it is defined as:

$$KC = \frac{V_{max} * T}{D} \tag{3.1}$$

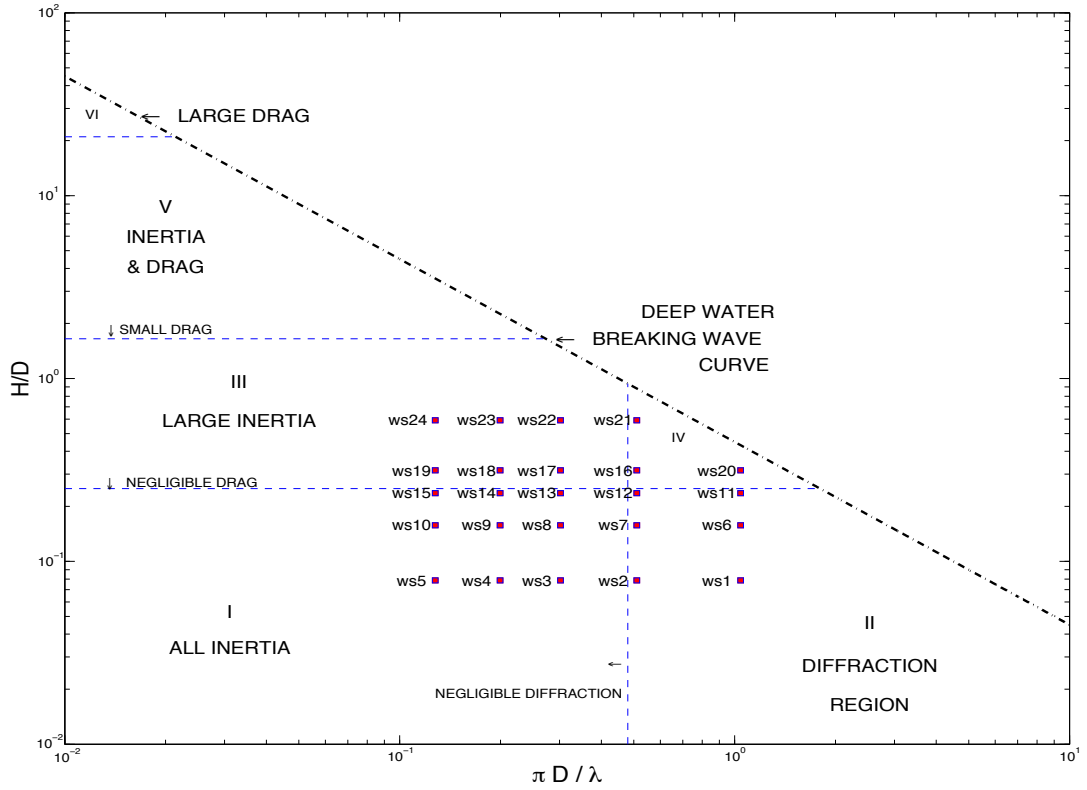

Fig. 3.2. Different wave excitation force regimes for a matrix of wave states, in agreement with Chakrabarti (1987). H: wave height, D: characteristic length of the object, λ: wave length. Each red dots represents a different wave period (T) and H duo. The numbering is rising in T first and later in H.

V_{max} is the maximum velocity, T is the period of oscillation and D is the characteristic length of the object. Three flow regime regions can be drafted:

- KC<2 - inviscid, irrotational flow: inertia dominated model (Radiation/Diffraction model)
- 10>KC>2 - transient region: drag and inertia model (Hybrid model)
- KC>10 - turbulent flow: drag dominated model (Morison eq.)

PA-WECs are assumably nested in the intermediate set, while the A-WEC types are likely to be inertia dominated. For the case of the T-WECs type, the model depends on the size of the system. A comprehensive discussion over the topic can be found in (Faltinsen, 1993; Chakrabarti, 1987). The non-dimensional analysis of a single floater of the Wavestar WEC is summarised in Fig. 3.2. The plot shows the different excitation force regimes as presented in (Chakrabarti, 1987) in function of the $KC = H/D$ number (deep water approximation) and the diffraction parameter $\pi D/\lambda$ for different wave states (red dots). Here, H is the wave height and λ is the wave length. The concepts of wave excitation force will be discussed later on. As seen in Fig. 3.2 the viscous drag loads will have a negligible weight in the excitation force exerted by the wave on the Wavestar WEC floater. This approach has been used as a base study for the work developed in both Appx. A.4 and Appx. A.6, respectively for the Wavestar WEC and a FOWT of the tension leg platform (TLP) type. Even though FOWTs are not specifically included in title of the thesis, their

analysis has been part of the work due to their partial similarity with large size floating WECs with self reference structure, e.g. Weptos WEC, FO^3 WEC.

Panel Method

The method solves the Laplace equation for an inviscid, incompressible, irrotational fluid, also called ideal fluid. The 3D problem is mapped into a surface problem (panel methods) and the velocity potential in the fluid domain is solved from the given boundary condition. The first level of analysis is coupled with a linearised kinematic and dynamic free-surface boundary condition that is valid for small waves ($H/\lambda \ll 1$), i.e. the limit of linear wave in which the wavy surface can be approximated by the water shape at rest, thus applying first order Taylor expansion. This assumption greatly simplifies the problem because the free surface is known before-hand and is not part of the problem to be solved. In the limit of small body motion and small waves, the loads acting on the structure can be approximated by a linear function of the surface elevation. Further, if steady state conditions are sought, the loads have the same frequency as the waves that are causing them. In this framework, the hydrodynamic problem can be separated in two problems, called the radiation and excitation problems.

The excitation problem defines the loads exerted by the passing waves on the structure held at the equilibrium position. Due to the linearisation of the free surface boundary condition, the wetted surface is constant. The excitation problem is further divided in two contributions, called diffraction and Froude-Krylov. The diffraction problem is valid when $D \geq \lambda$, thus the wave field near the body is affected by the stationary body, so that there is no flux on the body surface.
The Froude-Krylov problem is valid when $D \ll \lambda$, thus the wave field is not affected by the presence of the body, and the velocity potential on the wetted surface equals the incident (wave) potential. When the first order approximation does not hold the modification of the Froude-Krylov contribution with the instantaneous wetted surface integration is the most straightforward alternative to the linearised problem (Guerinel et al., 2013).
The excitation force vector ($\overline{F}_{ex}$) is calculated as a summation of both diffraction and Froude-Krylov contributions. The excitation loads are proportional to the incident waves, for each of the DoFs of the body. A single rigid body can be described by six DoFs, these are commonly defined in the offshore sector as surge (translation in the x axis), sway (translation in the y axis), heave (translation in the z axis, vertical direction), roll (rotation about the x axis), pitch (rotation about the y axis) and yaw (rotation about the z axis). Therefore, a general force vector is composed by three forces and three moments. The relation between the excitation force and the incident wave is a function of the wave frequency, and it can be defined in the frequency domain as:

$$\overline{F}_{ex}(\omega) = \overline{F}^{0}_{ex}(\omega) \cdot A(\omega, kx) \tag{3.2}$$

$\overline{F}^{0}_{ex}$ is the complex excitation force coefficients vector, $A(\omega, kx)$ is the wave amplitude function of the wave frequency (ω), wave number (k) and spatial coordinate (x).

The radiation problem defines the loads exerted by the body motion induced waves on the body itself in otherwise still water. In the absence of constraints, a single rigid body freely moves in six modes, which have been defined above. Each elements of the radiation force vector ($\overline{F}_{rad}$) has a term proportional to the body acceleration (Added Mass) and a

term proportional to the body velocity (Radiation Damping). The coefficients are function of the body's motion frequency. The radiation force vector is defined in the frequency domain as:

$$\begin{aligned}\overline{F}_{rad}(\omega) &= \mathbf{CM}(\omega)\dot{\overline{V}}(\omega) + \mathbf{CA}(\omega)\overline{V}(\omega) \\ &= \left(-\omega^2\mathbf{CM}(\omega) + i\omega\mathbf{CA}(\omega)\right)\overline{\Xi}(\omega)\end{aligned} \tag{3.3}$$

Here, $\mathbf{CM}(\omega)$ and $\mathbf{CA}(\omega)$ are the added mass and radiation damping matrix respectively, $\dot{\overline{V}}$, $\overline{V}$ and $\overline{\Xi}$ are the body acceleration, body velocity and body displacement vectors defined in the frequency domain, and i is the complex operator. Both $\mathbf{CM}(\omega)$ and $\mathbf{CA}(\omega)$ are square matrixes of dimension $nDoF \times nDoF$, being $nDoF$ the number of DoF of the structure.

Softwares like WAMIT (WAMIT, 2014), ANSYS AQWA (ANSYS, 2014) and Nemoh (open-source) (LHEEA-ECN, 2014) solve the diffraction/radiation problem by using the panel method in frequency domain.

The results of the frequency domain representation is influenced by the quality of the surface discretisation. In order to reduce/quantify this source of error, a sensitivity study of the result variation in function of the number of discretisation points is needed.

Fig. 3.3 shows the results of the sensitivity analysis for a cylindrical floater with diameter of 10 m and draft of 10 m. The number of panel (Np) is varied from 56 to 2136, the latter being the reference solution.

Morison Equation

The Morison equation (Morison et al., 1950) is a semi-empirical equation which encompasses both inertia and viscous loads. In the context of this work, the focus will stay on the viscous contribution only. The importance of this contribution for a WEC ought to be deducted from its working principle. Contrary to Oil & Gas and FOWT structures, which are designed to avoid resonance phenomena, WECs are especially tuned to have at least one eigenfrequency in the wave frequency range. A direct consequence of this condition is the non-negligible influence of viscous drag loads on the motion of the structure caused by the amplified body velocity. The resonance condition is not only obtained in the design phase, but also with application of advance control strategies as explained in Sec. 4.1. In such conditions, the assumption of irrotationality of the flow is broken and flow separation may occur, resulting in a reduced motion amplitude. The viscous drag contribution (f_D) is implemented as a quadratic term in function of the relative velocity between body (v) and fluid particles (ς). f_D can be defined in the time domain as:

$$f_D = \frac{1}{2}\rho A_p C_D (v(t) - \varsigma(t))|v(t) - \varsigma(t)| \tag{3.4}$$

Here, ρ is the water density, A_p is the body surface projection in the plane perpendicular to the axis of application of the force and C_D is the drag coefficients. Due to the quadratic term, f_D cannot be defined in the frequency domain as such. The frequency domain force (F_D) can be obtained from a linearisation of the above equation, as:

$$F_D(\omega) = C_D^* \left(V(\omega) - \varsigma(\omega)\right) \tag{3.5}$$

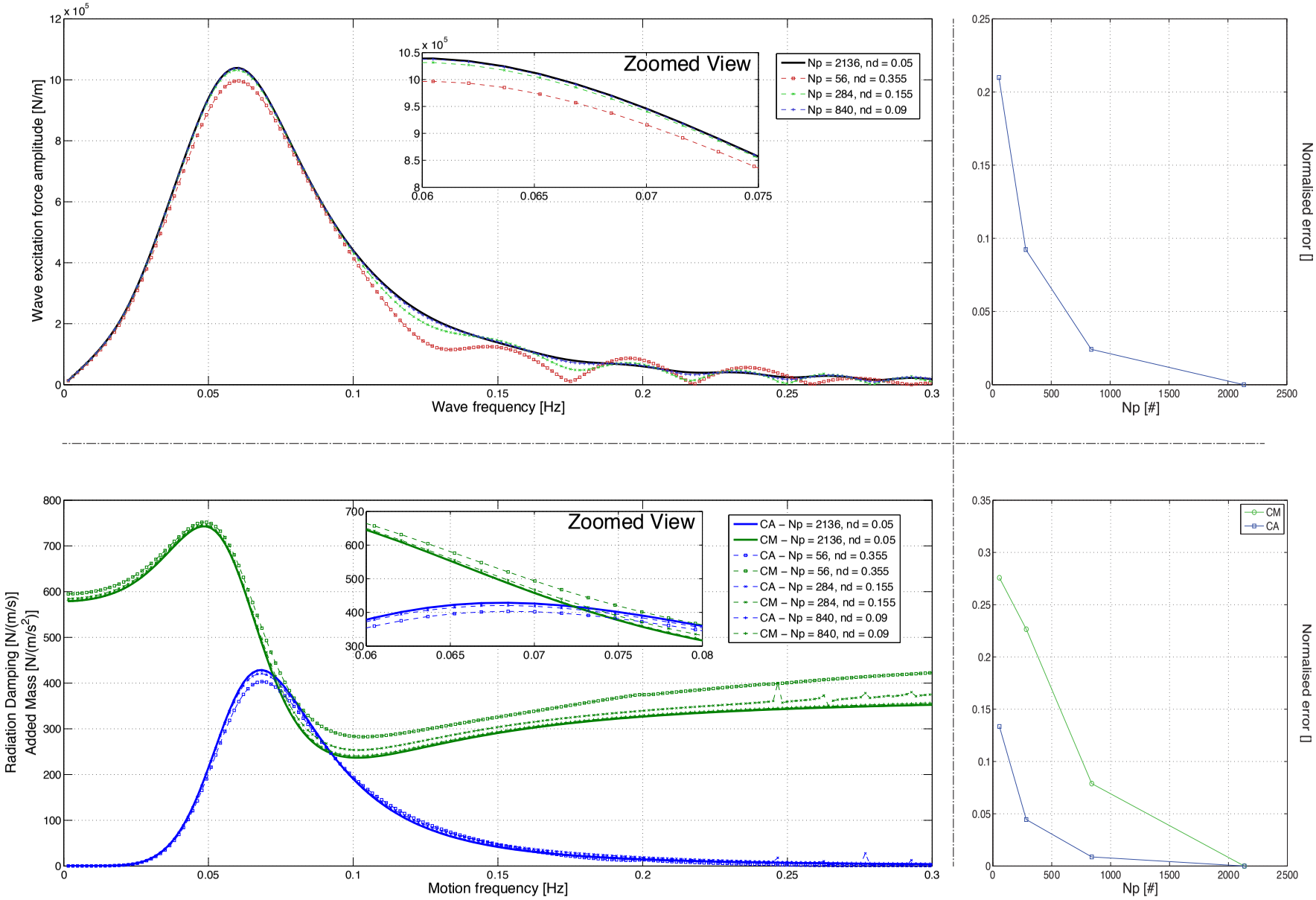

Fig. 3.3. Mesh convergency study for a cylinder (diameter=10 m and draft=10 m). Np is the number of panels and nd is the smaller panel dimension divided by the cylinder diameter. Top left: Wave excitation force amplitude coefficients per unit of wave amplitude in function of the wave frequency. Top right: Evolution of the normalised error of the wave excitation problem in function of Np, with respect to the case $Np = 2136$. Bottom left: Radiation damping (CA) and added mass (CM) coefficients per unit of body velocity and acceleration respectively in function of the body motion frequency. Bottom right: Evolution of the normalised error of the radiation problem in function of Np, with respect to the case $Np = 2136$.

where C_D^* is the linearised viscous drag coefficients. Here, $V(\omega)$ and $\varsigma(\omega)$ are the frequency domain pairs of the respective time domain variable presented in (3.4). A commonly adopted linearisation technique is based on the energy conservation approach as described in (Sarpkaya, 2010).

Through the thesis, the frequency/time domain pairs of a quantity are represented with upper and lower case letters respectively.

Appx. A.4, Appx. A.5 and Appx. A.6 address the influence of the drag contribution for the Wavestar WEC floater and for a FOWT. In agreement with the non-dimensional analysis shown in Fig. 3.2, the viscous drag contributions are negligible for a passive controlled WEC — not in resonance — while in case of an active/advanced control strategy the viscous drag term can have an impact in the overall force summation. For example, for the Wavestar the viscous drag contribution is as high as 20 % as shown in Appx. A.5. In the case of the FOWT, the viscous drag contribution is high for two reasons: a relatively small characteristic length of the body close to the water surface and a flat bottom with sharp edges. One of the critical points in the present viscous drag formulation is the definition of the point where the force is evaluated. As suggested by Faltinsen (1993), the right position needs to be empirically estimated, though 25 % of the wave height from the still water level in the downward direction could be a first guess.

The other critical point is the definition of the C_D coefficients in waves. As presented in Appx. A.4, an experimental approach can be used, but due to the small contribution of the viscous drag loads, the calculated coefficients could be affected by a high level of uncertainty. An alternative and promising approach presented by Bhinder et al. (2011) is an iterative fitting procedure based on CFD results which has been used to evaluate the C_D coefficient for a cylinder in harmonic waves. In this way, the experimental noise issues are solved, but the definition of a proper turbulent model becomes a key parameter though.

Another approach can be seen inAppx. A.6 where the structure has been decomposed in simple subelements, and the contribution from each of them included in the formulation of the full structure. The advantage is the ease in the definition of the drag coefficient for each sub elements as described in (Faltinsen, 1993).

Hydrostatic Force

Besides the hydrodynamic loads, the other important contribution to the wave structure interaction is given by the hydrostatic force. The hydrostatic force vector ($\overline{F}_{hy}$) is the results of the combined action of loads — gravitational and buoyancy — acting on the body in still water. In the limit of the small body motion the hydrostatic force vector is proportional to the displacement of the body, and it can be defined in the frequency domain as:

$$\overline{F}_{hy}(\omega) = \mathbf{K_{hy}}\overline{\Xi}(\omega) \tag{3.6}$$

$\mathbf{K_{hy}}$ is the linear hydrostatic stiffness matrix.

When the small body approximation is not valid, the integration of the hydrostatic pressure over the instantaneous wetted surface could be used to account for the linearisation error. This non-linear contribution need to be coupled with the non-linear Froude-Krylov contribution, which is also calculated on the instantaneous wetted surface. Even though

these non-linear contributions can be of high relevance for the numerical models of the WECs they have been considered out of the scope of the thesis.

The hydrostatic stiffness matrix is obtained from the PaM softwares cited above.

3.1.2 PTO system

The PTO system with embedded controller is of paramount importance for the dynamic behaviour of the WEC. Fig. 2.2 shows the schematics of the two PTO systems mostly used with a WEC of the activated body type: hydraulic and direct drive. As input the PTO model receives the state (position,velocity, acceleration) of the interconnection points (v_A and v_B), and it outputs the force (F_{PTO}) acting on the MS and RS plus the energy absorbed by the system.

Based on the controllability of the PTO force, two main model sets can be identified for the systems shown in Fig. 2.2. For the case of good controllability, i.e. direct drive or hydraulic PTO with variable pressure (4-quadrant motor branch), the PTO loads will be governed by the chosen control law. Therefore, the loads commanded by the controller (F^{th}_{PTO}) will be modified by the response of the PTO.
This approximation is based on the following assumption. In order to ensure controllability of the PTO, the characteristic time scale of the low level controller - i.e. magnetic flux and pressure signals - is designed to be much smaller in magnitude than the time scale of the controlled load. Therefore the PTO response can be approximated with only a linear time invariant transfer function ($G(s)$).

For a less controllable system, i.e. constant pressure hydraulic PTO, the description of the full model can be simplified with a piecewise linear function, such as a Coulomb damper. It is important to notice that the discontinuity of the Coulomb damper is often replaced by a linear transition region around the zero velocity point, in order to avoid stiffness and instability in the numerical model (Babarit et al., 2012). This equals the adoption of a check valve dynamic in the full description of the hydraulic PTO. As shown in Appx. A.7 the Coulomb model also fits well in a friction dominated PTO system, often applied in small-scale laboratory systems.

The code-to-code verification of the approximated systems, for the case of direct drive PTO (controllable) and constant pressure hydraulic PTO (less controllable) is given in Fig. 3.4. In both cases, the benchmark is the full numerical model of the PTO system.

On top of the former motivation leading to a model simplification, it is also necessary to point out the need of consistency in the wave-to-wire model. Indeed, the overall accuracy of the wave-to-wire model will be determined by the part of the system with lower accuracy, in this case the hydrodynamic model. Therefore, an over-complex PTO model will not increase the overall accuracy of the wave-to-wire model.

In general, the force exerted by the PTO system can be described by one of the following simplified models:

$$F_{PTO} = \begin{cases} G(s) * F^{th}_{PTO} & \text{for a direct drive or variable pressure hydraulic PTO;} \\ F_{PTO}(v) & \text{for a constant pressure hydraulic or friction dominated PTO.} \end{cases} \tag{3.7}$$

The transfer function ($G(s)$) and the Coulomb damper model can be represented as:

$$G(s) = \begin{cases} 1 & \text{for an ideal PTO with unitary transfer function;} \\ \frac{1}{M_{pto}s^2} & \text{for a mass system;} \\ \frac{1/M_{pto}}{s+\omega_{n}{}^2_{pto}} & \text{for a mass-spring system;} \\ \frac{1/k_{pto}}{\tau_{pto}s+1} & \text{for a damper-spring system;} \\ \frac{1/k_{pto}}{\tau_{pto}^2 s^2+2\zeta_{pto}\tau_{pto}s+1} & \text{for a mass-spring-damper system.} \end{cases} \tag{3.8}$$

$$F_{PTO}(v) = \begin{cases} D_{PTO} \cdot sign(v) & \text{if } |v| > |v_L|; \\ D_{PTO} \cdot \frac{v}{|v_L|} & \text{if } |v| \leq |v_L|. \end{cases} \tag{3.9}$$

M_{pto}, k_{pto}, ω_{npto}, τ_{pto} and ζ_{pto} are respectively the characteristic mass, stiffness, natural frequency, time constant and critical damping ratio of the system, and D_{PTO} is the constant PTO force, v is the relative boundaries velocity and v_L is the limit velocity of the linear range. For a pure Coulomb damper, the latter variable becomes zero.

So far, the domain identity of F_{PTO} has not been explicitly specified, but in order to avoid inconsistency in the definition of the equation of motion, the proper domain needs to be tagged. A linear commanded load can be expressed in both the time ($f_{PTO}(t)$) and the frequency ($F_{PTO}(\omega)$) domains by applying forward or inverse Fourier transform. On the other hand, for non-linear models the force exerted by the PTO can be defined in time domain only. The time domain formulation is also used when $f_{PTO}(t)$ is constrained. The application of constraint is often needed in order to bound the results of the linear model when excessively large motion or loads are obtained. For example, the application of an advance control strategy to tune the WEC into resonance, see Appx. A.5, will lead to a displacement response operator per unit of incident wave height tending to infinity, which infers infinite velocity and power too. These conditions are physically unrealistic and either a displacement or a velocity or a PTO load constraint is required. The constrained PTO force f^*_{PTO} can be obtained by:

$$f^*_{PTO}(t) = g(v_A, v_B, f(PTO)) \cdot f_{PTO}(t) \tag{3.10}$$

where $g(v_A, v_B, f(PTO))$ is a general non-linear function of the boundary state and PTO type.

Theoretical Commanded Loads

The loads commanded by the controller (F^{th}_{PTO}) has a major influence on the power performances and dynamic response of the WEC. It is a common technique to define

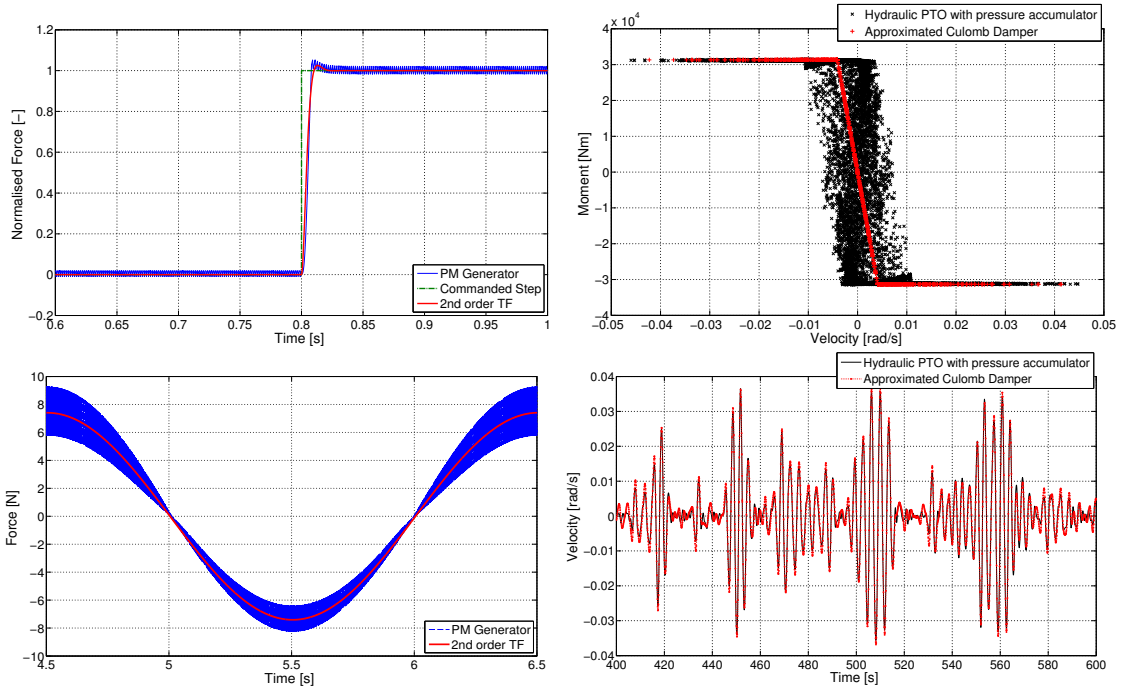

Fig. 3.4. Code-to-code verification of PTO models. Left side: Direct drive permanent magnet generator (PMG) with torque control response (blue line) vs second order transfer function response (red line); responses for unitary step and sinusoidal excitation. Right side: Constant pressure hydraulic PTO response (black line) vs approximated Coulomb damper response (red line); velocity-force curve and responses for irregular wave excitation.

a control law linear to the WEC velocity (V) and displacement (Ξ) in the first stage of analysis — proportional-integral (PI) control.

$$F_{PTO}^{th}(\omega) = C_c V(\omega) + K_c \Xi(\omega) \tag{3.11}$$

C_c and K_c are the controller damping and stiffness coefficients. For $K_c = 0$ the controller reverts to a simple resistive or passive controller - proportional (P) control. The bandwidth of the controller is relatively narrow, and the energy extraction is only significant in the close neighbourhood of the resonance frequency of the oscillator (WEC). For $K_c \neq 0$ the controller is called active PI controller. The compensation of the intrinsic stiffness of the WEC causes the system to be in resonance with the wave frequency over a broader range, inferring a larger absorbed power. Further details about advanced control laws are given in Ch. 4.

3.1.3 Reaction System - Station Keeping System

Besides the heavy economical weight of reaction systems in the overall cost of the WEC, their influence on the dynamic behaviour of the WEC is in many cases strongly correlated to the system type. For example, bottom fixed reaction systems, e.g. Wavestar support structure, are assumed to be infinitely rigid and they will not be considered in the numerical model. For mooring systems associable to class 1 (Ch. 2) in operational sea states, the numerical model can be reverted to a simple stiffness coefficient, obtained from the force/displacement curve of the complete reaction system set-up. The force displacement curve can be obtained either from quasi-static or dynamic numerical models

or from experimental tests. For this type of system, the expected motion is relatively small in consequence of the large ratio between structure dimension and wave length in operational sea states. Therefore, both velocity and acceleration of the fairleads tend to be at zero, which means convergency between dynamic and quasi-static model of the reaction system. For mooring system associable to class 2, the numerical modelling needs to describe both conservative and non conservative loads. The term conservative is used as a synonym for no energy dissipation. In this case, the utilisation of linear stiffness coefficients as well as a quasi-static description will only partially describe the reaction system loads. In order to solve this problem, a dynamic model of the mooring cable needs to be used. In the framework of the SDWED project, the implementation of the dynamic reaction system models in the equation of motion of WECs has been pursued. The dynamic model of the reaction system (MOODY (Palm et al., 2013b)) developed by Chalmer University uses the finite element method with high-order polynomial basis function and discontinuous elements. The spatial discretisation is based on the local discontinuous Galerkin method (Fitzgerald and Bergdahl, 2008). Although the dynamical model of the reaction system needs to be applied to fully define the impact of the mooring system in the overall body motion, the actual computational cost of the integrated model is currently too high to simulate a full set of sea states. This high computational cost is partially related to the fact that the software is implemented in Matlab, thus a sharp drop of the computational cost is expected if the software will be implemented in other languages. For the time being, one of the available solutions found is the one proposed by Fitzgerald and Bergdahl (2008). However, this method has not been tested in the timeframe of the work described in this thesis. The general mooring force vector ($\overline{F}_m$) is expressed in the frequency domain as:

$$\overline{F}_m(\omega) = \mathbf{K_m}\overline{\Xi}(\omega) \tag{3.12}$$

where $\mathbf{K_m}$ is the linearised mooring stiffness matrix.

3.1.4 Wave model

For all the cases presented in this thesis except for the FOWT work, the waves are modelled using the linear potential theory. The model is once more based on the assumption of unviscid, irrotational, incompressible fluid, and small waves (H/λ). Two types of waves are used through the work: regular (monochromatic) and irregular (multichromatic). Further, only 2D long-crested waves are adopted. Even though most of the real sea waves are irregular, the utilisation of regular waves is often used as a first stage of analysis due to implicit simplification of the problem. For a pure harmonic wave excitation force, the WEC model simplifies to a mass-spring-damper system with constant coefficient. Moreover, the usage of regular wave quickly induces a steady state behaviour of the WEC response, which entails a reduction of the time needed to reach steadiness of parameters like absorbed power, maximum load, etc. Few wave periods are enough to quantify the problem. Of course regular waves do not reproduce the natural variability of the energy source and cannot be used to estimate the behaviour of the WEC in a real location. So, irregular sea states are used, which can be modelled by a simple superposition of independent regular waves under the assumption of linear theory. It is important to notice that in case of irregular sea states the simulation time needed to be long enough to reach steadiness of the sough parameters. As suggested in the Equimar project, after 500-1000 waves the steady state is reached (Ingram et al., 2011, pg. 197). The wave model is described in frequency domain by a standard spectrum ($S_j(\omega)$), which defines the distribution of the wave power spectral density (PSD) across the frequency range. For a regular wave the

spectrum reverts to a simple impulse, while for irregular sea states one of the commonly used model is the parametrised JONSWAP spectrum. Different types of parametrisation are possible and hereafter the one described in (Frigaard and Andersen, 2010) is presented:

$$S_j(\omega) = \alpha \frac{f_p^4}{f^5} H_{m0}^2 \gamma^\beta e^{\left[-\frac{5}{4}\left(\frac{f_p}{f}\right)^4\right]} \tag{3.13}$$

$$\alpha = \frac{0.0624}{0.230 + 0.0336\gamma - \frac{0.185}{1.9+\gamma}}; \quad \beta = e^{\left[-\frac{(f-f_p)^2}{2\sigma^2 f_p^2}\right]}; \quad \sigma = \begin{cases} 0.07 & \text{if } f \leq f_p \\ 0.09 & \text{if } f > f_p \end{cases}$$

where f is the wave frequency, f_p is the peak wave frequency defined as $1/T_p$ where T_p is the wave peak period, α is the spectral intensity and γ is the peak enhancement factor. The sea state is fully defined by three parameters only, H_{m0}, T_p and γ. Large values of γ (>3.3) identify a narrower distribution of the energy about the peak wave period, while when γ become one, the JONSWAP spectrum coincides with the Pierson-Moskowitz spectrum, which describes a fully-developed sea state.

The generation of a time domain signal from the PSD has been realised using two different generation methods in this work: random phase and white noise filtering. The random phase is a deterministic method, which maps exactly the discretised target PSD function into a finite time series by the means of inverse Fourier transform (IFFT). The single harmonic components are combined with random phases. The white noise filtering is a probabilistic method, where the discretised target spectrum is firstly converted in a time domain filter, and then applied to a white noise time series (input stochastic process). The resultant stochastic process is coloured as defined in the target PSD distribution. The method is probabilistic because the PSD of the output matches the target PSD only in a probabilistic sense: only if the length of the time series go to infinity do the two PSDs coincide. The time domain filter is obtained with the same methodology described in Appx. A.1, once the target PSD is formulated accordingly.

Different assumptions are used for the FOWT case where the analysis is focused on ULS conditions. According to (Veritas, 2013), the ULS are described by non-linear wave models, the non-linearity order being function of the water depth. For the tested conditions, the stream function wave theory developed by Dean and Dalrymple (1991) minimised the error with the measured surface elevation in experimental tests, and it has been used as input for the model thus. It is important to bear in mind that using a non-linear wave model involves a consistent growth of complexity in case of irregular sea-states, which often results in a reduction of the order of the non-linear model toward a second-order Stoke wave.

3.1.5 Equation of Motion

The main loads acting on the WEC, and described so far, are assembled in the equation of motion of the WEC using the Newton-Euler formulation. The nomenclature used from now onwards is consistent with the one adopted in the Nemoh PaM software, being the source of the hydrodynamic model. For a single body WEC, the equation of motion (EoM) about its centre of gravity (CoG) is defined in the frequency domain as:

$$\overline{F}_T(\omega) = \mathbf{M}\dot{\overline{V}}(\omega) \tag{3.14}$$

$\overline{F}_T$ is the total force vector acting on the body and $\mathbf{M}$ is the mass matrix of the body - including both mass (diagonal) and inertia matrix. Using the forces defined above (3.14) becomes:

$$\begin{aligned} \overline{F}_{ex} &= \mathbf{M}\dot{\overline{V}}(\omega) + \overline{F}_{rad} + \overline{F}_{hy} + \overline{F}_{m} + \mathbf{T_{PTO}}F_{PTO} + \mathbf{T_D}F_D \\ &= \left[-\omega^2\left(\mathbf{M}+\mathbf{CM}\right) + i\omega\left(\mathbf{T_{PTO}}C_c + \mathbf{T_D}F_D + \mathbf{CA}\right) + \mathbf{T_{PTO}}K_c + \mathbf{K_{hy}} + \mathbf{K_m}\right]\Xi \end{aligned} \tag{3.15}$$

Here, $\mathbf{T_{PTO}}$ and $\mathbf{T_D}$ are input matrixes used to map the PTO and linearised viscous drag forces into the body DoFs. The dependency of the variables to ω is not represented for compactness.

The EoM can be described at any point, once the kinematic of the system is defined. Kinematic describes the motion of objects without considering the cause for the motion. In particular, the EoM around a generic point CO can be defined as:

$$\mathbf{H}^T(\overline{p})\overline{F}_T = \mathbf{H}^T(\overline{p})\mathbf{M}\mathbf{H}(\overline{p})\dot{\overline{V}}(\omega) \tag{3.16}$$

$\mathbf{H}(\overline{p})$ is the transformation matrix associated to the position vector $\overline{p}$ from CoG to CO defined as:

$$\mathbf{H}(\overline{p}) = \begin{bmatrix} \mathbf{I} & \mathbf{S}^T(\overline{p}) \\ \mathbf{0} & \mathbf{I} \end{bmatrix} \tag{3.17}$$

where $\mathbf{I}$ and $\mathbf{0}$ are identity and zero matrix of appropriate dimension and $\mathbf{S}^T(\overline{p})$ is the skew symmetric matrix associated with the cross product between the position vector and the angular acceleration. For a comprehensive discussion over the topic see (Fossen, 2011)

When F_D and F_{PTO} become non-linear the frequency domain formulation of the EoM cannot be used. By taking the inverse Fourier transform, (3.15) is mapped into the time-domain, leading to a system of integro-differential equations; Cummins' equation (Cummins, 1962):

$$\begin{aligned} \left(\mathbf{M}_j + \mathbf{CM}_{j,\infty}\right)\dot{\overline{v}}(t) + \sum_{k=1}^{N_{dof}} \int_{-\infty}^{t} h_{RAD,jk}(t-\tau)v_k(\tau)d\tau \\ + \mathbf{T_{D,j}}f_D + \left(\mathbf{K_{hy,j}} + \mathbf{K_{m,j}}\right)\overline{\xi} = f_{ex} + f_{PTO} \end{aligned} \tag{3.18}$$

Here, j identifies each of the N_{dof} equations, being N_{dof} the number of DoFs of the body, $\mathbf{CM}_{j,\infty}$ represents the limit of the added mass coefficient for $\omega \rightsquigarrow \infty$, h_{RAD} is the impulse response function (IRF) of the radiation force, $\dot{\overline{v}}$, $\overline{v}$ and $\overline{\xi}$ are the body acceleration, body velocity and body displacement vectors defined in the time domain, and the lower case f is used for the time domain pair of the respective frequency domain force, i.e. f_{ex} is the wave excitation force in the time domain and F_{ex} is the wave excitation force in the frequency domain. The IRF can be obtained using a frequency sampling method from the frequency response function (FRF) (Parks and Burrus, 1987). h_{RAD} vanish for $t < 0$ and it is called causal IRF (not anticipative system). The integral term in (3.18) is a convolution integral.

f_{ex} can be obtained using either a time or a frequency domain method. The frequency domain method is similar to the random noise method (Sec. 3.1.4). The wave spectrum is multiplied by the wave excitation FRF, and the phase of the resultant FRF is summed to a

random phase and mapped in the time domain by taking the inverse Fourier transform. The time domain method is based on the convolution of the wave excitation IRF (h_{ex}) with the time series of the surface elevation (η). h_{ex} is non-causal (anticipative system) and the outputs of the system depends on past, current and future inputs. The result of the convolution between h_{ex} and η is delayed in time by a factor $N_{IRF}/2 * dt$ where N_{IRF} is the order of the IRF and dt is the time distance from one sample to the other. From a simulation view point the non-causality of the wave excitation force is not of particular interest since η is know from the beginning to the end, but this issue matters greatly for the controllability of the WEC in real-time applications. Indeed, in order to evaluate f_{ex} at the current time a short-time prediction of the surface elevation is needed, causing a growth of the model uncertainty. The topic will be further discussed in Ch. 4.

For an array of Nb bodies, the equation of motion does not change in shape, if the bodies are mechanically uncoupled, i.e. an array of PA-WECs, or connected to a common fixed reference frame, i.e. the Wavestar WEC (multi-body system with fixed reference frame). In this last case, the motion of each floater is mechanically decoupled from each other under the assumption of infinitely rigid reference frame. Whilst for a multi-body system with moving reference, the EoM needs to be adapted to the specific case. On the one hand, the formulation of the problem in the multi-body frame eases its definition, but on the other hands if the number of bodies is large, the dimension of the problem can result in a large demand in terms of computational power. A good alternative to solve the issue is the usage of generalised DoF. In this framework, the standard six DoFs of a rigid body are extended with extra DoFs, which describe alternative modes of motion of the structure. The Weptos WEC is an example of a multi-body WEC. The system described by Pecher et al. (2012b) is composed by 40 floaters, therefore the number of DoF of the whole system is 246. If a generalised approach is used instead, the system dimension reduces to 46. The definition of generalised DoF is a built-in functionality in WAMIT and Nemoh. While WAMIT outputs also the hydrostatic and mass matrix for the generalised problem, Nemoh does not. Since part of the work conducted in this thesis is based on Nemoh results, once the hydrodynamic problem is defined in terms of generalised DOFs, all the others contributions need to be defined accordingly. The formulation of the mass matrix for the system can become a non-trivial task if both translation and rotation of coordinate systems need to be endorsed in the Newton-Euler method. In order to reduce the risk of error in the mass matrix formulation, an energy based approach (Euler-Lagrange) is used in the following. The Euler-Lagrange formulation is commonly used in multi-body solvers from robotic application, and it seems to be a growing topic of research in the wave energy sector too, (Ó'Catháin et al., 2008; Mccomb et al., 2013). In general for a multi-body system with n generalised DoFs (q_i with i ranging form 1 to n), the Euler-Lagrange equations can be written as:

$$\frac{d}{dt}\frac{\partial L}{\partial \dot{q}_i} - \frac{\partial L}{\partial q_i} = \overline{f_i} \tag{3.19}$$

where $\overline{f_i}$ is the external force vector acting on the i-th body and L is the Lagrangian, defined from the kinetic energy (T_i) and the potential energy (P_i) of each element of the system as:

$$L = \sum_i T_i(\dot{q}_i, q_i) - \sum_i P_i(q_i) = \frac{1}{2}\dot{\overline{q}}^T \mathbf{M}(\overline{q})\dot{\overline{q}} - \sum_i P_i(q_i) \tag{3.20}$$

where $\mathbf{M}$ is the mass matrix of the system in terms of generalised DoF, obtained from the application of constraints in the multi-body system, see Appx. C for further details. $\overline{q}$ and $\dot{\overline{q}}$ are the vectors of the body displacement and velocity in the generalised DOFs.

In the first stage of analysis, the mass matrix can be linearised, therefore the EoM can be formulated using the Newton-Euler as:

$$\mathbf{Tr}\left[\overline{f_1}\dots\overline{f_n}\right]^T = \mathbf{M}(\overline{q})\ddot{\overline{q}} \sim \mathbf{M}\ddot{\overline{q}} \tag{3.21}$$

where $\mathbf{M}(\overline{q})$ and $\mathbf{M}$ are the mass matrix and its linearised version respectively, $\mathbf{Tr}$ is the summation matrix used to sum up the different contributions for each body acting on the same DoF and the vector of forces and moment is obtained from the force summation. $\ddot{\overline{q}}$ is the vectors of the body acceleration in the generalised DOFs.

3.1.6 Simulations

The objective of the simulations is the definition of time averaged parameters as the annual energy production (AEP) or the capture width (CW) and the estimation of loads time series of a given WEC in a given location.

The AEP is the two dimensions' sum of the matrix obtained by multiplying the scatter diagram (SD) and the power matrix of the specific WEC at the given location.

The SD defines the wave climate at the specific location using a 2D histogram where the probability of occurrence (pr) of each sea states is given in function of H_{m0} and T_p. The base wave model is the JONSWAP, and the parameter (γ) is assumed fixed for each location, although it is a function of the . Two different SDs have been used in the simulations, both related to Danish locations and summarised in Tab. 3.1 and Tab. 3.2. For the Danish section of the North Sea, the γ parameter is set to 3.3.

The power matrix is defined from the mean power associated at each sea state of the SD. The mean power is estimated using the wave-to-wire model of the given WEC. The procedure to calculate the AEP is exemplified in Fig. 3.5.

The system of ordinary differential equations (ODE) was solved in Matlab and Simulink using the built-in ode-solvers (Murphy, 2011; MATLAB, 2013). Due to the simplification used in the sub-models, the system of ODE is often non-stiff, and to a large extent an explicit Runge-Kutta scheme of order 2 or 4 guarantees a truncation error small enough for the accuracy of the model. A system of ODEs is defined non-stiff when every eigenfrequency of the system lays in a similar frequency range. The truncation error of a solver is defined as the difference between the true solution and the approximated one. The truncation error is defined from the order of the solver. For the Runge-Kutta scheme of order 4, the local truncation error is $O(h^5)$ while the global truncation error is $O(h^4)$. Local refers to the instantaneous error and global to the accumulated error. h is the time discretisation.

3.2 Physical Modelling and Numerical Modelling Validation

A physical model reproduces a real life process on a different scale. The main benefit in physical modelling is the incorporation of all contributions, and if a proper physical set-up is used, a physical model gives trustable results. But the main deficiencies of physical modelling are the relatively large cost and amount of time required compared with some

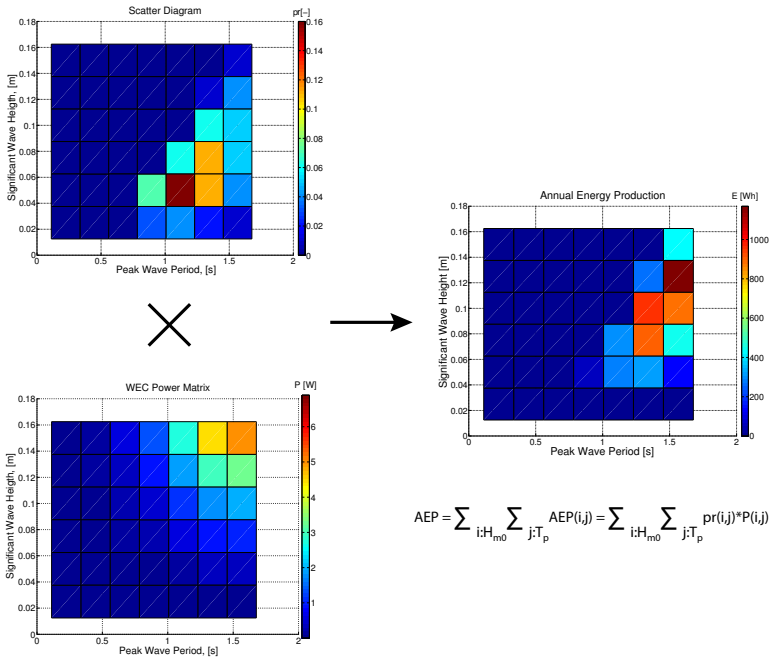

Fig. 3.5. Assessment of the AEP from the location SD and WEC power matrix.

Tab. 3.1. Relative occurrence of different wave states (pr) from six years, buoy measurements located at 6332100N, 474700E, water depth: 17 m ($[H_{m0}]$ = m, $[T_P]$ = s). Both parameters defines the mean value over an interval. The adopted discretisation is 1 s in T_p and 0.5 m in H_{m0}.

H_{m0}/T_P	0.5	1.5	2.5	3.5	4.5	5.5	6.5	7.5
0.25	-	-	-	0.04	0.04	0.02	0.01	-
0.75	-	-	-	0.07	0.17	0.11	0.05	0.01
1.25	-	-	-	-	0.06	0.11	0.05	0.01
1.75	-	-	-	-	-	0.06	0.05	0.02
2.25	-	-	-	-	-	0.01	0.05	0.02
2.75	-	-	-	-	-	-	0.01	0.02
3.25	-	-	-	-	-	-	-	0.01

Tab. 3.2. Operational sea states parameters for the Danish North Sea

Wave State #		1	2	3	4	5
H_{m0}	[m]	1.1	2.0	3.0	4.0	5.0
T_p	[s]	6.1	7.4	8.7	9.8	10.7
pr	[-]	0.448	0.225	0.108	0.051	0.024

numerical tools, and the presence of unavoidable errors, see Fig. 3.1. Physical models should be seen mostly as a design and model validation tool, more than a design tool itself, especially in light of the large growth of computational power in recent years.

3.2.1 Sources of Uncertainty

As discussed in the chapter preamble, different sources of uncertainty are ascribable to the experimental results, mainly grouped in structural and measurement. The structural errors are mainly linked to the scaling law used to define the physical set-up. Given

that it would be optimal to maintain the mutual interactions between dominating loads unaltered, it is not possible to simultaneously scale gravitational, inertial and viscous forces, unless modification of the so-called constant parameter is endorsed, i.e. gravitational acceleration, medium viscosity, etc. In marine applications, the commonly used scaling laws are Froude and Reynolds. Generally, the physical analysis of steady state parameters of large bodies is carried out using Froude scaling law (bulk properties), while both fast transient phenomena localised at the boundary of the volume and small body dynamics are ascribable to the Reynolds scaling law. As shown in Fig. 3.2, the scaling law should be decided based on the results of non-dimensional analysis of the flow regimes. For the specific case of the Wavestar presented in the figure, the complete dynamic similarity using Froude scaling law will not be achieved, because viscous drag loads will not be scaled correctly. However, as presented in Appx. A.4 the relative weight of viscous loads is less than 5 % for a passive controller set-up, thus the viscous scaling error is considered of small impact in the overall summation. The quality of the results is directly related to the scaling factor: the larger it is, the smaller the scale induced errors are. A commonly adopted scale frame for experimental wave energy converter models is between 1:50 and 1:10, being first a proof of concepts and second a design and feasibility study. For extreme cases, e.g. FOWT in ULS, a scale ratio as low as 1:100 is still considered in the correct range, (Ingram et al., 2011). Larger scales are considered to be beyond the scope of this work.

Another important source of structural error is related to the implementation of a PTO system in the physical model. This is most probably the critical component in the physical model definition. PTO systems generally do not scale with Froude scaling law, besides there are manufacture limitations lead by electrical component efficiency, material strength, which retain the scaling of full-size PTOs. The most important consideration to bear in mind when reproducing a scaled PTO system is to keep the reaction force at the interface between the PTO system and moving body similar to the target system. An example of PTO model scalability can be found in Appx. A.7. Although it could be possible to scale a linear electrical actuator or a hydraulic PTO to match the required load range in the experiments, the weight of the system would restrain its applicability. The choice has been directed towards a linear air piston, whose force/velocity response resembles to a great extent an approximated Coulomb damper model, Fig. 3.6. The variation of the constant loads, used for example to optimise the mean absorbed power for the given scatter diagram, was achieved by modification of the PTO lever arm. This makes the pair with the modification of the constant pressure level for a hydraulic PTO. It should be noted that although the air piston is quite small, its weight is already at the edge of the weight reserved for the PTO system.

Besides structural errors, measurement errors need to be identified, quantified and mitigated if possible. The instrumentation errors are often considered of less importance ($\leq 1\%$) once the instrument range and measured range are consistently chosen. The main environmental error for a wave energy application is the index of wave reflection characteristic of the wave basin. This source of uncertainties can be quantified with a 3D analysis of the wave field, with and without the structure in water. A standard index of reflection for mild slope beach is below 10 % in terms of wave amplitude. The operation errors are often subjective and more difficult to estimate. One source of operational error is the modification of the system response induced by a measurement system. Of particular interest is the case of the slack moored floating WEC (fWEC). The assessment of the position and orientation in the 3D space is fundamental to quantify power performance

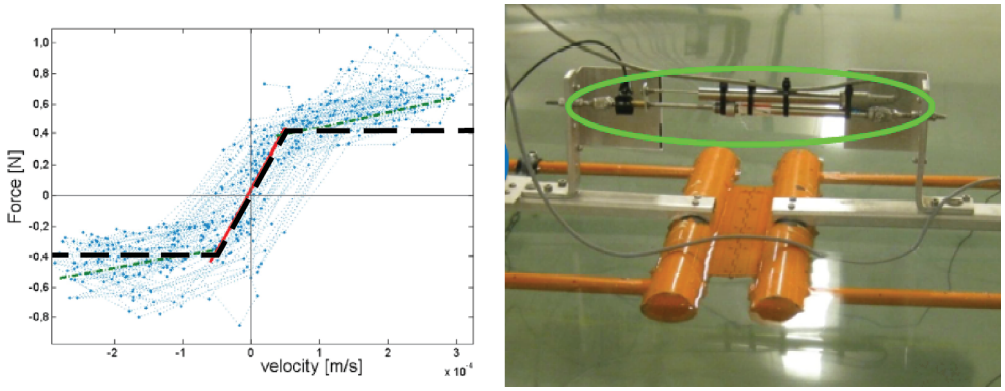

Fig. 3.6. Scale PTO force/velocity characterisation compared with an ideal approximated Coulomb damper model. On the right side the physical PTO model is shown in the final configuration.

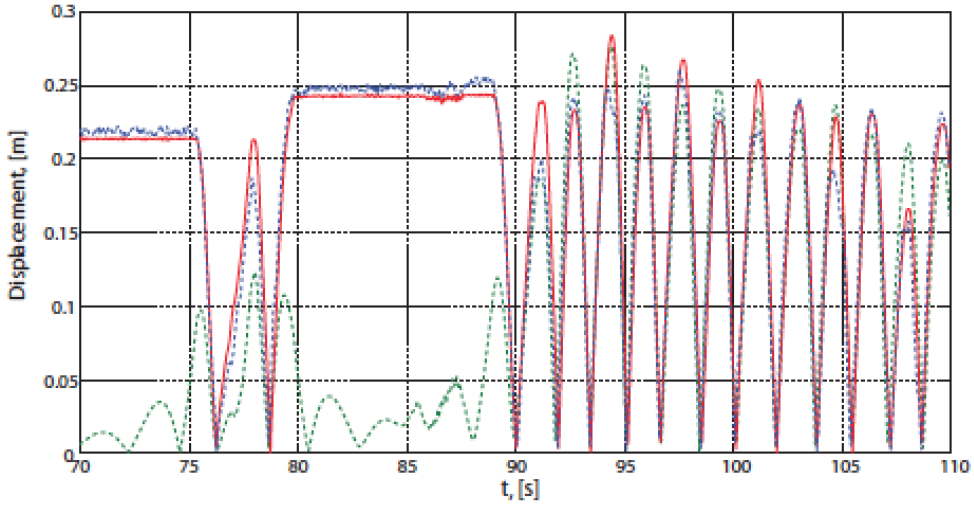

Fig. 3.7. Measured displacement time series. Colour map: red - reference signal, blue - optical signal and green - accelerometer integrated signal.

as well as the response operator of the structure. The measurement system should not interfere with the system dynamics, meaning no additional weight or loads should be ascribable to its presence. An interesting approach to solve the problem is shown in Appx. A.8, where a video based methodology inherited from the augmented reality sector has been presented. Fig. 3.7 summarises the comparison of experimental results between the presented methodology and other two measuring devices: a potentiometer based system and an inertial measurement unit (IMU) system. The potentiometer based system is the reference signal (red line), but its utilisation in a fWEC is limited due to the presence of a spring to tightly wind up the connecting thread. IMU (green line) is accurate and precise with respect to the structure orientation, but since they measure accelerations they suffer of error accumulation in the double integration which cause the signal to drift. In order to avoid this drift, the raw signal needs to be filtered with a high pass filter ending in a poor accuracy of the system in case of slow motion of the fWEC. The video based (blue line) system shows a good agreement in all the tested frequency ranges. It is important to highlight the main limitation of the video based system: the presence of a singularity in the tracking algorithm that induces discontinuities in the results.

For a general description of the laboratory testing procedures and issues, see (Ingram et al., 2011).

3.2.2 Validation of Numerical Models

Due to the strong assumptions adopted, e.g. ideal fluid, in the numerical model definition, the validation step is a crucial point.

In this section, the comparison between experiment and numerical data is briefly summarised, the detailed description is presented in Appxs. A.2, A.4, A.7, A.3, A.6. The comparison between experiments and numerical results traces the structure of Sec. 3.1.

Hydrodynamic System / Wave-Structure Interaction

For the Wavestar single floater described in Appx. B, the wave body interaction is decomposed in three terms: hydrostatic, radiation and wave excitation force. All three sets of test are run in a condition where the other forces are zero or known: the hydrostatic tests are run in the limit of zero velocity and acceleration without waves, the radiation tests are run from the knowledge of the hydrostatic force and without waves, the wave excitation tests are run with standstill floater and waves acting on it. In order to simplify the analysis, only one harmonic per test is used, and in order to check the model linearity the response to different input amplitudes is analysed. The frequency domain coefficients are obtained by minimisation of the error between models and measured loads in the least square sense. As presented in Appx. A.2, the agreement between numerical and experimental results is sometimes counterintuitive at first glance. Especially for the small amplitude waves and motions, where the higher accuracy of the reading theory is expected, the measurement uncertainties become as important as the measured value itself leading to erroneous results. The data presented in Appx. A.2 for the wave excitation force was biased by an offset in the calibration function. The correct frequency domain response is re-presented in Appx. A.4.

PTO system

Approximated models similar to the ones presented in Fig. 3.4 can be used and compared against experimental test data. The results for the linear electrical motor used in the Wavestar set-up are presented in Fig. 3.8. Two simplified transfer function models are used with order one (blue dots) and two (red dots). As highlighted in the frequency domain plot (right side in Fig. 3.8), the second-order model represents the main dynamics in the frequency range of interest, the latter being $0.5 - 2[Hz]$. Moreover, the first-order model does not fit the “truth" in the high frequency range, underestimating the response of the actuator.

Reaction System - Station Keeping System

As introduced above, the simplified description of the mooring force (3.12) of mooring system of class 2 is somehow underestimating the energy dissipation, which occurs in the

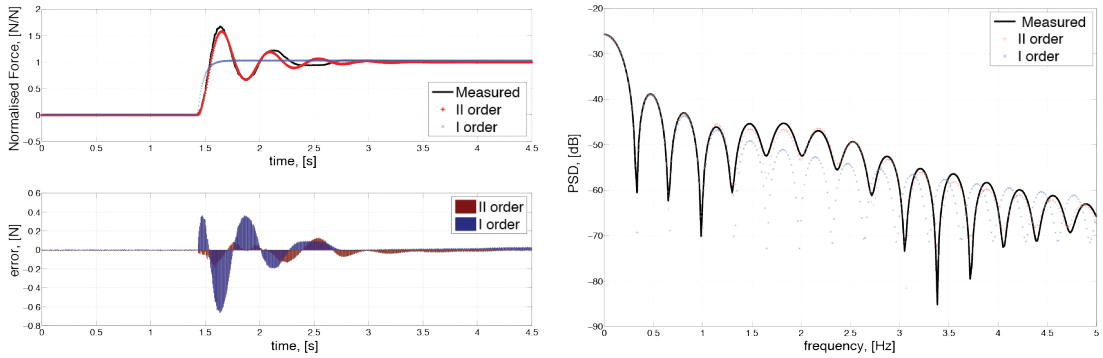

Fig. 3.8. Validation of PTO models. Left side: Time domain comparison between measured (black), first-order transfer function (blue) and second-order transfer function (red) responses to a step in the commanded force, normalised with the end force. On the bottom side the discrepancy time series between models and measurement is plotter. Right side: Power spectral density of the measured and modelled data.

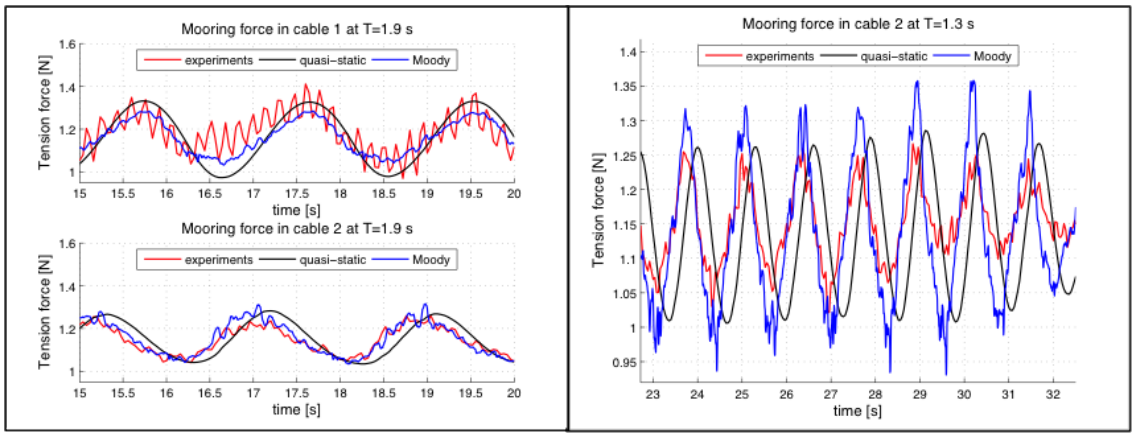

Fig. 3.9. Validation of mooring models. Time domain comparison between measured (red), quasi-static model (black) and dynamic model (blue) responses to a sinusoidal motion of the fairlead. Left side: Period of oscillation 1.9. Right side: Period of oscillation 1.3. The periods are normalised by the natural period of the floater in heave.

mooring cable. As presented in Fig. 3.9, for a long period of oscillation (left side) the quasi-static, measured and dynamic mooring tension responses have similar magnitude and a small phase shift. But for shorter waves, the quasi-static approximation fails to describe the energy dissipation process, highlighted in the phase shift with respect to the measurement data and dynamical solution too.

Equation of Motion

The comparison between the EoM (3.15,3.18) and the measured data is the last step in the model validation. The Wavestar single floater is used once more as example due to its intrinsic simplicity. In addition for this case study it is possible to estimate the variation of the model error in function of control strategy. This point is particularly important because by applying an advanced control strategy the linear potential theory is likely to be violated in consequence of the amplitude amplification induced by the resonance condition. The

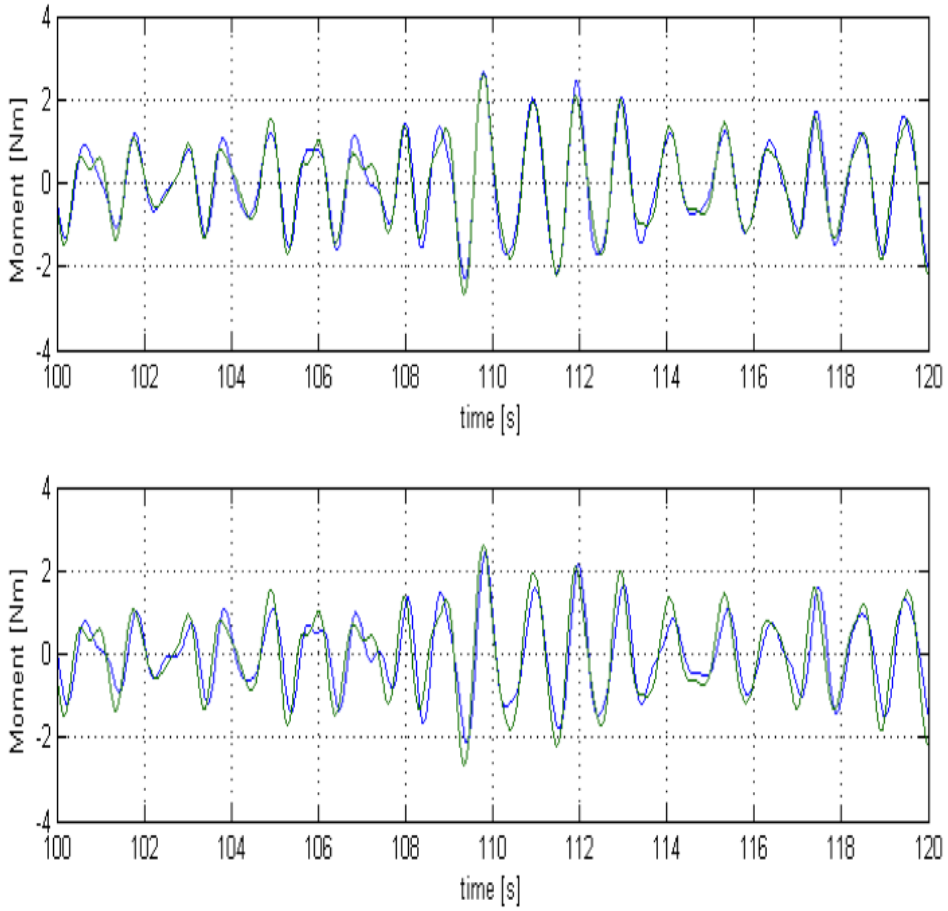

Fig. 3.10. Time series comparison between simulated and measured force acting on the Wavestar WEC single floater for two control configurations: P (upper plot) and PI (lower plot). Colour map: measured data (green line) and simulated data (blue line).

estimation of the uncertainties in function of the control strategy is fundamental to balance the results of the control optimisation presented in Ch. 4. Fig. 3.10 shows the time series of measured (green) and simulated (blue) force acting on the PTO connection points for the two control strategy presented in (3.11). The normalised mean square error for the P control case (upper plot) is 92 % while for the PI control case (lower plot) is 81 % as expected.

WEC Optimisation

4

As stated in the introduction of the thesis, Sec. 1.1.1, the current CoE of WECs is, in general, still significantly higher than other more mature renewable energy technologies, thus the sector has not yet reached a competitive economical level to roll off into the market. The WECs tested and studied so far have a relative small turnover compared to the high capital cost, which to a large extent is driven by the structural loads in extreme conditions. The turnover is defined as the income associated with the energy production. On the one hand, the simplest approach to increase the economic viability of WECs is to increase their turnover by means of improved control strategies. The first part of the chapter deals with the brief introduction of the different control approaches used to maximise the energy absorbed by the WEC and related issues. On the other hand, whether this method defines a CoE minimiser for WECs is not obvious. An advance controller infers larger turnover but also larger design loads, the latter being related to the structural cost of the WEC. In Sec. 4.2 the focus will stay put on assembling a simple methodology toward a more balanced optimisation of WECs from an economic prospective. The results are extrapolated from simulation of the numerical model, whose validation was presented in Ch. 3.

4.1 Control

A controller identifies a set of processes which monitor, and alter if needed, the state of a dynamic system by manipulating its inputs. In WAB WECs, one of the primary objectives of the controller is to modify the absorbed power — either mechanical or electrical — by manipulating the force exerted by the PTO on the HS. A high absorbed power level entails correct and higher velocity, high machinery force and correct phase (timing). The concept of maximum energy absorption has been independently realised by Evans (1981) and Falnes (2002), back in the 1970s. Named complex conjugate control (CCC) and phase and amplitude control (PAC) by the authors, they provide an upper bound for the WAB WEC capability. In recent years, though, more and more studies have been presented on the topic, mostly dealing with approximation of the afore mentioned “best“ solution. Besides the control law proposed in (3.11), other alternatives are possible, commonly classified in two groups: passive and active. In this context, the term “passive“ infers a purely resistive control strategy characterised by an unidirectional energy flux, i.e. the linear passive damper control (P) presented in (3.11) for $K_c = 0$. The term “active“ refers

to those control strategies where in order to enlarge the absorbed power some energy is fed back into the HS during a part of the wave cycle using a bidirectional energy flux.

In the “passive“ class, besides the P controller, the latching and declutching strategies are worth mentioning. Latching and declutching controllers were first studied by Budal et al. (1982), and later applied to complex system. Several authors focused on the implementation of latching and declutching controller for a floating WEC, in both physical and numerical models, i.e. (Babarit and Clement, 2006; Durand et al., 2007; Lopes et al., 2009; Ringwood and Butler, 2004; Babarit et al., 2009). However, their implementation remain marginal due to the embedded limitations, such as non-causality of the control scheme, performance losses in multi DoFs systems and abrupt loads variation; as recently pointed out by Cretel et al. (2011b). On the contrary, the P controller is often identified as a lower power performance bound for WECs due to the simple applicability. An example of its implementation on physical and numerical models can be found in (Hansen et al., 2012; Marquis et al., 2010).

The “active“ group includes a broad range of controllers, appealing for the substantial theoretical increment of the power performance if compared with the P controller. Two main controller sub-classes exist: non-causal and causal. The former relies on the prediction of either the body velocity or the excitation loads to define the maximum absorption trajectory, while the latter approximates the non-causal model with a causal one in order to remove the uncertainties related with the prediction, Perdigão and Sarmento (1989). Examples of non-causal controllers are both CCC and PAC, while by far the most known causalised controller are the feed-back ones (Hansen et al., 2012; Nielsen et al., 2013). The PI controller presented in (3.11) identifies one possible configuration. It should be noted that every causalised controller is intrinsically sub-optimal in multi-frequency sea-states.

Recently, the optimal control theory within the framework of model predictive control (MPC) has been introduced, addressing the problem of constraint control. The most relevant examples of MPC implementation are given in (Hals et al., 2011b; Richter et al., 2013; Brekken, 2011; Cretel et al., 2011a; Abraham and Kerrigan, 2013). MPC defines a stand-alone class, which spans in both active and passive controller sets, in function of the defined constrained problem (Cretel et al., 2011a). Further, the MPC includes both causal and non-causal controllers, given that the model disturbance — the wave induced load — can be either defined from causal and non-causal excitation force model.

For a comprehensive description of viable control solutions see, (Price, 2009; Hals et al., 2011a).

4.1.1 Maximising the Absorbed Energy

The following discussion is valid for a single degree of freedom WAB WEC, but similar conclusions can be sketched for multi-DoF systems whenever the presence of cross-coupling terms is included in the formulation. As described in Falnes, 2002, Ch.6, for a single DoF WEC of the WAB type the maximum energy absorption happens when the incident wave frequency matches the body natural frequency, i.e. resonance condition. CCC and PAC define two alternative closed form solutions for the maximum energy absorption control trajectory. On the one hand, as analysed in (Korde, 2000; Hals et al., 2011a) the complex conjugate approach is anti-causal and its implementation requires forecast of the body velocity. Since the system is highly damped the auto-correlation length of the body velocity

is relatively short and its prediction, based on past observation, becomes uncertain (Nielsen, 2012); since the prediction of the velocity is not reliable, the controller is not practically feasible. On the other hand, the phase and amplitude approach relies on the prediction of the surface elevation. For a relative narrow-band wave spectrum the prediction of the surface elevation is considered more reliable than the body velocity as shown in (Fischer and Kracht, 2012; Fusco and Ringwood, 2010b) and Appx. A.1.

The PAC is further discussed and its block diagram exemplified in Fig. 4.1. The general scheme used for the controller is a velocity tracking, whose reference signal is the optimal body velocity at the actual instant of time $t = k$ ($v[k]$). The reference signal is calculated either from (4.1) or (4.2), based on the information of the excitation force, which is in turn calculated from the surface elevation (η).

$$v[k] = h_{opt} * f_{ex}[k, k-1, ...] = h_{opt} * h_{ex} * \eta[k, k-1, ...] = h_{\eta,v} * \eta[k, k-1, ...] \quad (4.1)$$

$$V(\omega) = \frac{F_{ex}(\omega)}{2CA(\omega)} = H_{opt}(\omega)F_{ex}(\omega) = H_{opt}(\omega)H_{ex}(\omega)\eta(\omega) = H^{v}_{\eta}(\omega)\eta(\omega) \quad (4.2)$$

Equations (4.1) and (4.2) are time/frequency domain Fourier transform (FFT) pairs, where capital letters are used for the frequency domain variables. H_{opt} in the transfer function from the excitation force to the reference velocity, H_{ex} is the transfer function from the surface elevation to the excitation force and H^{v}_{η} is the transfer function from the surface elevation to the reference velocity.

If $\eta(t)$ is known a priori, the velocity can be obtained from (4.2) by forward and inverse FFT application. The real time implementation of the controller is somewhat non-trivial. The whole process can be divided in three steps.

- Short-term prediction of the surface elevation in order to complete the non-causal part of H_{ex};
- Evaluation of the optimal velocity at the actual instance of time from the actual and past value of $f_{ex}[k, k-1, ...]$;
- Minimisation of the error between reference and true signals.

The first step in the controller definition is addressed in Appx. A.1. The wave excitation force is predicted in the short-time using a deterministic method, which is implemented by finite impulse response (FIR) filters. The FIR filter technique has been selected for its simple implementation and phase linearity, but other approaches are possible, i.e. infinite impulse response filter and neural network (Schoen et al., 2008; Schoen et al., 2011; Fischer and Kracht, 2012; Fusco and Ringwood, 2010a; Fusco and Ringwood, 2008). The FIR filter is implemented by using the frequency sampling design methods (Parks and Burrus, 1987). The reference velocity is obtained from the predicted excitation force by using a state observer, commonly in the form of Hilbert transform or Kalman filters (Fagley, 2012; Fusco and Ringwood, 2010a). The observer defines the frequency and amplitude of the excitation force. The former output is used to assess the actual transfer function H_{opt}, which is then multiplied by the excitation force amplitude to give the reference velocity. As an alternative, the first two steps can be joined using a FIR mapping from the surface elevation — measured some distance in the up-wave direction — directly into the optimal velocity. The filter is designed as per the excitation force prediction, but the fitted transfer function is now H^{v}_{η} rather than H_{ex}. Fig. 4.2 shows the comparison between measured

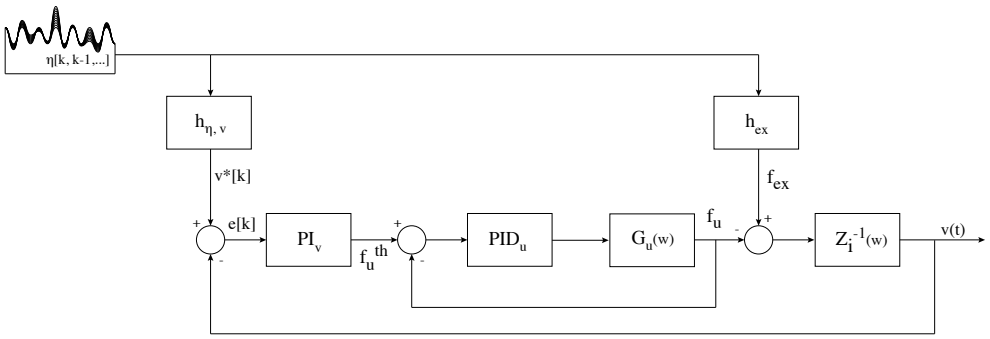

Fig. 4.1. General layout of the time domain controller implemented with the PAC scheme.

and estimated wave excitation force and optimal velocity trajectory, together with the position/velocity diagram.

The error between reference and actual velocity ($e[k]$) is the input for velocity controller. Different formulations of the latter have been tested, i.e. resonant controller (Zmood and Holmes, 2003), internal model controller (Francis and Wonham, 1976), lead-lag compensator (Bakshi, 2009), but the best tracking quality (phase and amplitude) and disturbance rejection was obtained with a simple PI controller.

The signal presented in Fig. 4.2 (right hand side) for the Wavestar WEC single floater already highlights one of the major limitation of the method. The large amplitude of the commanded optimal trajectory can easily become un-realistic. For the presented case in the optimal trajectory the floater is required to be completely submerged (lower condition) and out of the water (upper condition) for a large part of the time series, being the upper and lower conditions sketched in dotted black lines. This large non-linearity already happens for relative small waves, i.e. in Fig. 4.2 the used sea state has $H_{m0} = 0.02m$ and $T_p = 1.2s$, model scale 1:20 and floater diameter 0.25 m. The sketched boundaries are a function of the floater displacement as well as the available emerged volume due to the non-symmetry in the horizontal plane.

The other important limitation of the PAC is the inability to handle constraints. Both position and velocity constraints can be handled by defining feasible and not-feasible set for the optimal solution (Hals et al., 2011a; Fusco and Ringwood, 2013), although the controller will present abrupt variation of velocity and position which could undermine its robustness. On the contrary, the application of PTO constraint is not easily implementable. The control law required the utilisation of large amount of reactive power, which often overcomes the PTO limits, and as shown in Appx. A.5 the saturation of the PTO load invalidate the performance of the controller to a great extend.

Implementation of the PAC has been attempted in a physical model of the Wavestar WEC, for further information see Appx. B. The study has seen physical tests issues like wave directionality, presence of an interaction between the body motion and the measured surface elevation up-wave, performance degradation induced by noise and PTO delay in the velocity tracker and brought the physical implementation of the controller to an end. Although each of these issues could ideally be solved (Fusco and Ringwood, 2010a; Frigaard and Brorsen, 1995), the growing implementation complexity is not balanced by

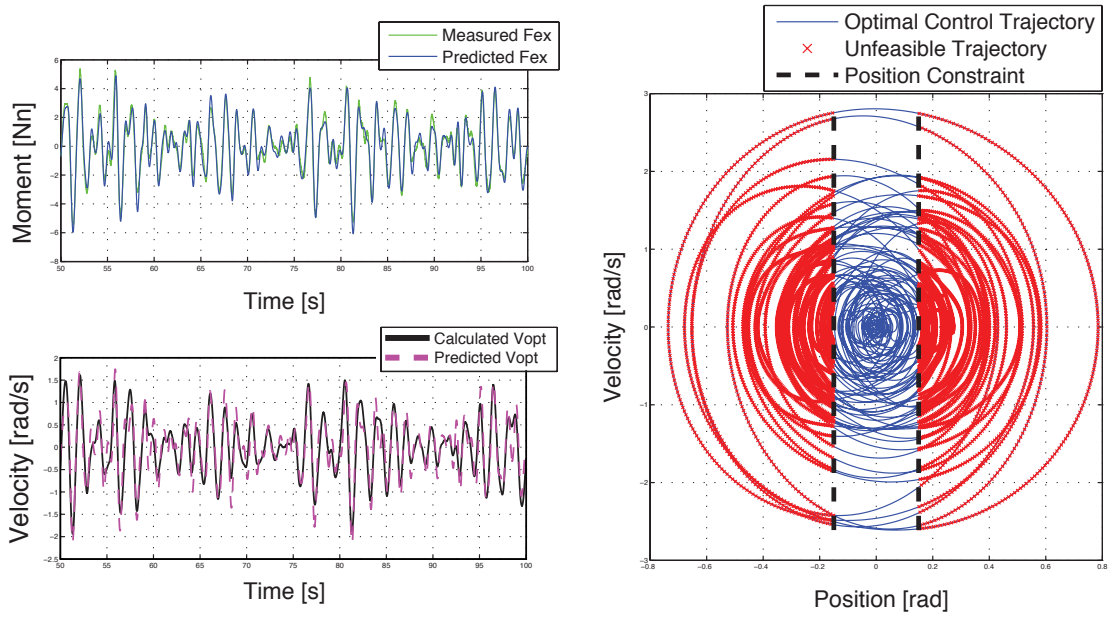

Fig. 4.2. Optimal control prediction stage. From top to bottom and from left to right: Time series comparison between measured (green) and estimated (blue) wave excitation force. Time series of the calculated (black) and estimated (magenta) optimal velocity trajectory. Optimal feasible (blue) and unfeasible (red) position and velocity trajectories. The set of feasible position is delimited by black dotted lines.

the growth of power performance numerically estimated if compared with a simple PI controller in realistic (constraint) cases, see Appx. A.5.

4.1.2 Other Controllers

Practical alternatives to the PAC are feed-back and MPC. Generally, latching and declutching schemes present theoretical and practical implementing limitations which have reduced their importance. Among the others, the one important limitation is related to the effect of the abrupt control loads variation commanded by the controllers. The application of non-smooth PTO loads will induce vibration on the structural and mechanical components, which can revert in larger need of O&M procedures. The effect cannot be grasped in a fully rigid numerical model of WEC, though a hydro-elastic model should be used in the analysis. The implementation of latching and declutching is not further considered, due to the excessive model complexity.

The full feed-back controller law (Nielsen et al., 2013) can be formulated in time domain as:

$$f_u(t) = C_c v(t) + K_c \xi(t) + M_c \dot{v}(t) + \int_{-\infty}^{t} h_{RAD}(t-\tau) v(\tau) d\tau \tag{4.3}$$

where f_u is the commanded loads, C_c, K_c and M_c are the damping, stiffness and mass control coefficients, t is the actual instant of time and h_{RAD} is the IRF of the frequency radiation function. The last term of the right hand side of (4.3) defines the causalised compensation of the radiated energy. The controller can handle both velocity/position and force constraints. Velocity and position constraints can be implemented by adding a load that penalises the constraint violation. The PTO constraints can be solved using

an anti-windup procedure, which resets the error accumulation in the integral term of the controller (Åström and Hägglund, 2005). The results from the simulations presented in Appx. A.5, and reported in Fig. 4.4, summarise the theoretical difference between the three of the of the five different configurations derived from (4.3) listed below:

- P controller $C_c \neq 0,\ K_c = M_c = 0,\ Tf = -\infty$
- PI controller $C_c,\ K_c \neq 0,\ M_c = 0,\ Tf = -\infty$
- PD controller $C_c,\ M_c \neq 0,\ K_c = 0,\ Tf = -\infty$
- PID controller $C_c,\ K_c,\ M_c \neq 0,\ Tf = -\infty$
- PIDc controller $C_c,\ K_c,\ M_c \neq 0,\ Tf \neq -\infty$

where the acronyms P, I, D and c stand for proportional, integral, derivative and convolution compensation respectively. As presented in (Hansen et al., 2012) the bandwidth of the PI, the PD and the PID controllers does not differ significantly, therefore only the PI controller was used in the analysis. All of them can tune the natural frequency of the system to the one of the incoming wave. On the contrary, the P controller cannot match the incoming wave frequency, therefore the performance will diminish as the wave frequency gets away from the natural frequency of the oscillator. A direct aftereffect is a larger step of efficiency between P and PI/PD controllers, while the efficiency variation between the other cases is rather flat.

It is important to bear in mind that besides the growth of the power performance, the utilisation of advance control strategy will also induce a growth of the model uncertainties, as introduced in Fig. 3.10 for the P and PI controllers. This behaviour further reduces the true difference between the different controllers, especially in the active controller cases. K_c, M_c and C_c coefficients are obtained by matching the impedance of the specific WEC; the last coefficient can be obtained from a stochastic analysis of the input process (Nielsen et al., 2013) also. The capability of tuning the controller coefficients is a great advantage for its implementation in physical models. In fact, even if the calculated coefficients from the solution of the linear PaM problem are accurate, they will be different from the real system ones for the summation of structural model errors in both numerical and physical models, Fig. 3.1. This fact together with an efficiency similar to the one of PI scheme bounds the applicability of the PID and PIDc controller in physical models. The larger number of parameters and induced complexity is not compensated by the increased power performance. The PI and PD have similar characteristics but the latter is affected negatively by the higher noise level of the acceleration measurement than the position measurement.

MPC defines together with the PAC the upper limit for the power capability of the WEC in unconstrained cases. Indeed, the two controllers revert to the same “optimal" solution when the PTO is ideal. On the contrary, when the PTO presents limitations, the constraints (position, velocity, PTO loads and PTO loads variation) are directly included in the cost function formulation (J) for the MPC, leading to a theoretical “optimal" constraint solution.

The term “optimal" means maximisation of the mean absorbed power. The cost function J is obtained from the discretisation of the average absorbed power over a time period T.

$$J[j] = \sum_{i=j}^{j+N_p} f_u[i]v[i] = \frac{1}{2}\mathbf{\Delta u}^T {\tau_\mathbf{u}}^T \mathbf{Q}\, \tau_\mathbf{u}\mathbf{\Delta u} + \mathbf{\Delta u}^T {\tau_\mathbf{u}}^T \mathbf{Q}\,(\mathbf{Px} + \tau_\nu \mathbf{\Delta}\nu) \tag{4.4}$$

where $j \in \mathbb{Z}$ denotes the current time instant, f_u is the control load, N_p is the number of time steps of the prediction horizon, $\mathbf{Q}$ is the weight matrix, $\mathbf{\Delta u}$ is the increment of the control variable and $\mathbf{\Delta}\nu$ is the increment vector of the wave excitation force. The matrices $\mathbf{P}$, $\tau_\mathbf{u}$ and τ_ν map the state vector as well as the control and the disturbance increment sequences into the output space. The product ${\tau_\mathbf{u}}^T \mathbf{Q}\, \tau_\mathbf{u}$ represents the Hessian matrix (He). The problem is convex with unique solution when $He \succ 0$. The overall optimisation problem with the constraint on the control force (f_{max}) can be written as:

$$\underset{f_u[i]}{max} J[j] \quad \text{such that} \quad |f_u[i]| \leq f_{max}, \qquad i = j, ...j + N_p \tag{4.5}$$

The working principle of the MPC is shown in Fig. 4.3. At each time step (j) the optimal trajectory ($u[j \ldots j + N_p - 1]$) which maximises J — the absorbed power — is calculated for the given feasible sets. Although the optimal control trajectory is defined in the whole prediction horizon, applying the receding horizon principle (Kwon et al., 2005), only the first sample ($u[k]$) of the sequence is used, allowing the controller to react to any unpredicted future disturbance.

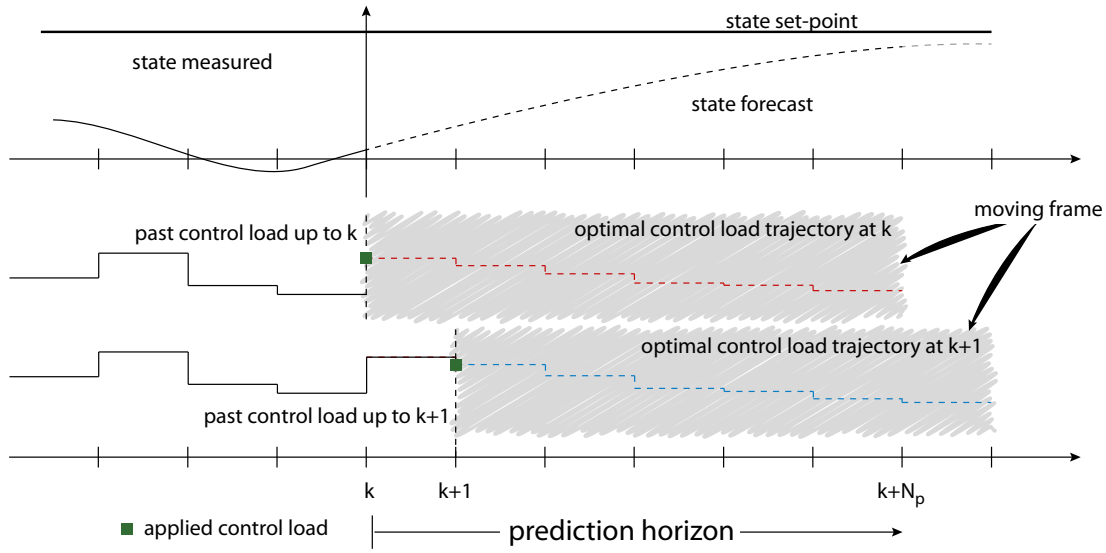

Fig. 4.3. MPC with receding horizon control principle. The blue dots represent the first sample of the optimal control trajectory used at each time sample. Based on (Li et al., 2012).

The performance of the MPC leans to the ones of the phase and amplitude controller when N_p approaches infinity. But practically, N_p is a trade-off between computational cost and accuracy. The computational time of the quadratic problem is cubic in N_p. A prediction horizon equal to the period of one full wave is a good first guess (Soltani and Sichani, 2013; Cretel et al., 2011b).

The performance of the MPC is also affected by the uncertainty of the system disturbance prediction (wave excitation force) over the control horizon. The results presented in Appx. A.5 do not account for this source of error, so they define an upper limit for the MPC formulation. For the Wavestar WEC single floater applied to the Hanstholm scatter diagram in presence of active constraints, and in case of a perfect prediction of the excitation force, the MPC is capable to extract roughly 25 % more energy per year if compared with the active feed-back scheme. It is important to bear in mind that due to the absence of the disturbance prediction error, the results from the MPC should be regarded only as a upper limit of the controller capability. If the prediction error is included, the gap between the MPC results and the feed-back control results is reduced, but the quantification of this effect is not publicly available yet.

Practical implementations of MPC are not available in literature. Among the others, two of the major issues are the computational cost of the method when constraints are active and the reduced capacity of the controller to be tuned to the true physical environment.

Fig. 4.4 summarises the application of the above mentioned control strategies for the Wavestar WEC single floater for the Hanstholm scatter diagram Tab. 3.1.

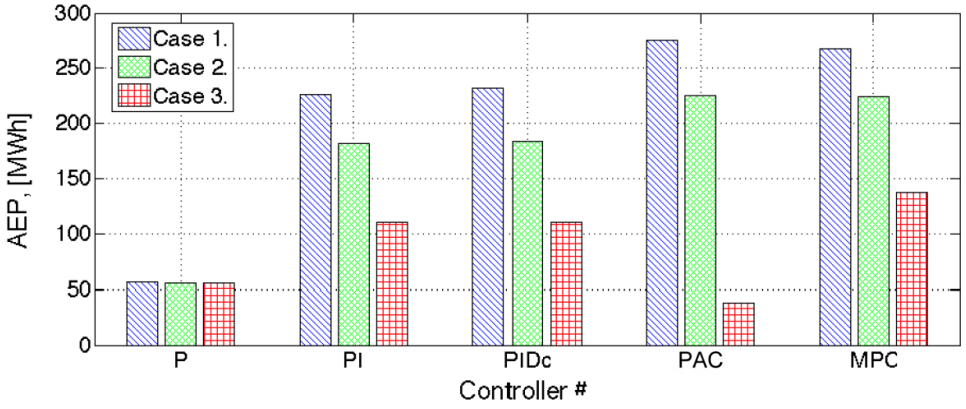

Fig. 4.4. Comparison of the AEP for the Wavestar WEC for the Hanstholm SD with different control scheme and cases. Cases: 1 - Unconstrained linear model; 2 - Unconstrained weakly non-linear model; 3 - Constrained weakly non-linear model.

4.2 Structural Optimisation

As presented so far, minimising the CoE by means of control can generally be defined as a 1D optimisation problem. Indeed only the AEP was considered. On the one hand, this methodology will reduce the CoE by varying the turnover of the WEC, but on the other hand, the larger loads compared to a P control exerted by the PTO on the structure will induce a different load scenario on the structural elements. Following, different load scenarios will (probably) modify the design specification leading to different CAPEX and OPEX values for the structure. Since the structural-related costs cover a large share of the overall lifetime cost of WECs, then the CoE will be affected too.

Due to the fact that the control law will be suppressed — or modified — in extreme sea states, it is possible to foresee only a modification of the cyclical loads acting on the structure, and accordingly its fatigue design. Standards for oil and gas (see e.g. (ISO,

2007)) as well as offshore wind turbines (IEC, 2005; Veritas, 2013; GmbH, 2005) and (offshore) steel structures (DNV, 2010; CEN, 2005) recommend the use of SN curves for fatigue analyses of structural designs. The SN curve characterises the material performance concerning fatigue and shows the relation between the number of load cycles at a given stress amplitude leading to fatigue failure.

Although fatigue response and control law are interdependent, the implementation of a fully coupled system is restrained by the complexity of the methodology used to quantify the fatigue behaviour. Nevertheless, at the first stage of analysis one could focus on the implementation of a sequential approach instead. The sequential methodology presented in Appx. A.5 combines power performances and fatigue analysis results of a WEC into a cost factor (CF), which eases the selection of an economically best control law. Fig. 4.5 sketches the flow diagram of the proposed method, going from the WEC and location definitions, down to the identification of the minimum CF. The definition of the AEP

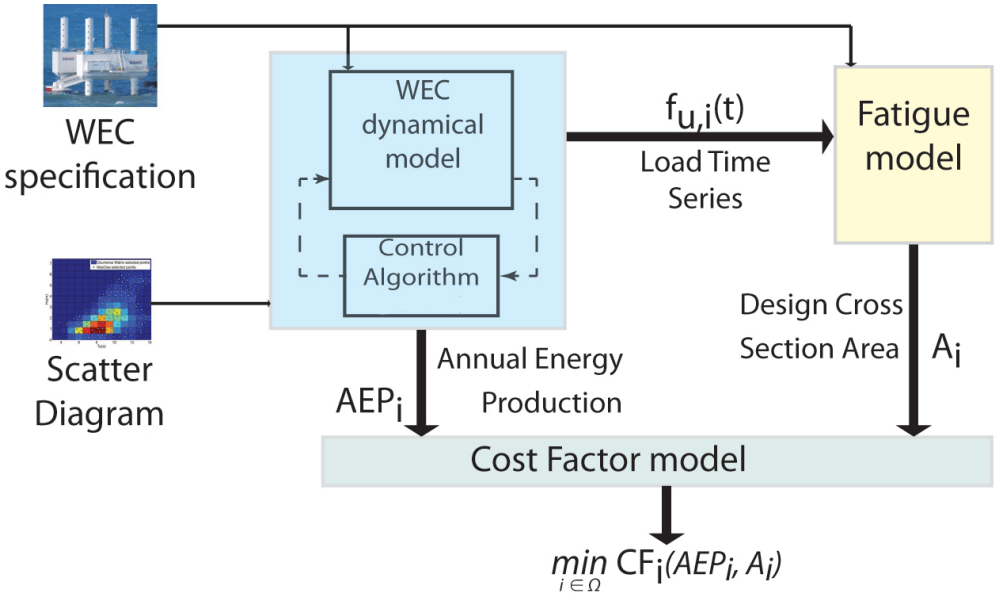

Fig. 4.5. Flow diagram of the combined control and fatigue analysis methodology. Model inputs: WEC specification and SD. Model output: minimal cost function.

assessment is given in Fig. 3.5 while literature and definitions related to the fatigue model are given in Appx. A.5. Indeed, the fatigue analysis is not part of the work conducted in this thesis, but results of a collaborative task, and specifications on the fatigue model are not given hereafter.

The derivation of the cost factor model is described in the following. Excluding the dependency on the discount rate, the CoE for a specific WEC is calculated as the ratio between total investment cost (C_{tot}) and turnover (E) through the project lifetime (Davey et al., 2009). C_{tot} is defined as the summation of capital expenditures (CAPEX) and operational expenditures (OPEX) over the design lifetime, while E can be considered in first approximation proportional to the AEP of the device, by the constant parameter k_e (rate of discount).

$$CoE(i) = \frac{C_{tot}(i)}{E(i)} = \frac{CAPEX(i) + OPEX(i)}{k_e AEP(i)} \tag{4.6}$$

Because both investment cost and turnover are affected by the control strategy adopted, a dependency on the i-th control strategy (Sec. 4.1) is introduced using the term (i). Moreover C_{tot} can be divided in two contributions: one proportional to the control strategy ($C_1(i)$) and another independent of it (C_2).

$$C_{tot} = C_1(i) + C_2 = f(i)pC_{tot} + (1-p)C_{tot} \tag{4.7}$$

Here, p represents the percentage of the total investment costs affected by the control strategy. For example, in the case of the Wavestar WEC single floater, $C_1(i)$ includes the CAPEX of the arm structure as well as the CAPEX of the PTO system mainly, but also any expected variation of the cost of O&M cost ascribable to the control law. Similarly, C_2 includes the CAPEX of the full structure, PTO and arm excluded, as well as commissioning/decommissioning costs, electricity connection and O&M costs not related to the control strategy.

Assuming a linear relation between cost and structural dimension (cross-sectional area) and defining a certain controller, i.e. the P controller, as a base of comparison, the association between the CoE and the above mentioned CF can be defined as:

$$CoE(i) = \frac{p\frac{A(i)}{A_{ref}} + (1-p)}{AEP(i)} \frac{C_{tot,ref}}{k_e} = CF(i)\frac{C_{tot,ref}}{k_e} \tag{4.8}$$

$$CF(i) = \frac{p\frac{A(i)}{A_{ref}} + (1-p)}{AEP(i)} \tag{4.9}$$

$A(i)$ and A_{ref} are respectively the cross-sectional area of the critical structural detail for the i-th and the reference control strategies, determined in the fatigue model, and $C_{tot,ref}$ is the total investment cost over the device lifetime for the reference control strategy. The linear relation between cost and structural dimension (cross-sectional area) assumes a fixed length of the detail in the analysis. Under this assumption the cost is directly proportional with the cross-sectional area of the structural detail. A different control strategy entails a modification of the AEP, but also a variation of the design cross-sectional area of the selected structural detail, reflected in the CF.

The model relies on the definition of the parameter p, which is WEC specific and in general rather uncertain. In order to study the influence of p on the overall results a sensitivity analysis needs to be carried out.

In Appx. A.5, the whole algorithm is applied to the Wavestar WEC single floater case, subject to the Hanstholm SD, with the P controller as reference case. The main result is reported in Fig. 4.6 where the CF is graphed in function of the adopted control strategy and in function of the p parameter. It should be noted that for the case $p = 0$ the optimisation problem reverts to a simple control optimisation problem. The p parameter is varied within the range $0 - 20\%$, chosen in agreement with the wind turbine sector due to the absence of specific data. In the offshore wind sector the capital expenditure varies between 50-70 % of the overall lifecycle costs of an offshore wind turbine (Berkhout et al., 2012). The costs of the turbine itself make about one third of it (Blanco, 2009). That is, the value of p is very likely to lie well below 20 %.

For the specific test case, two main conclusion can be drawn. First, the derivative of the output variation in the parameter space is small, so the propagation of the uncertainty on the p parameter in the overall model is rather limited. Second, the MPC is the CF minimiser,

but due to the assumption of perfect knowledge of the future in the actual implementation, the comparison results are positively biased. As cited before, the prediction error, which is the base of the MPC, is not implemented in the present formulation and the quantification of its effect is still unclear. Based on the actual stage of development and if the judgment is balanced by implementation simplicity, tunability, etc., the cost-effective solution is the PI controller. In any case, it seems clear that the implementation of an active control strategy reduces the CF by a factor two in the best scenario if compared with a standard passive controller technique.

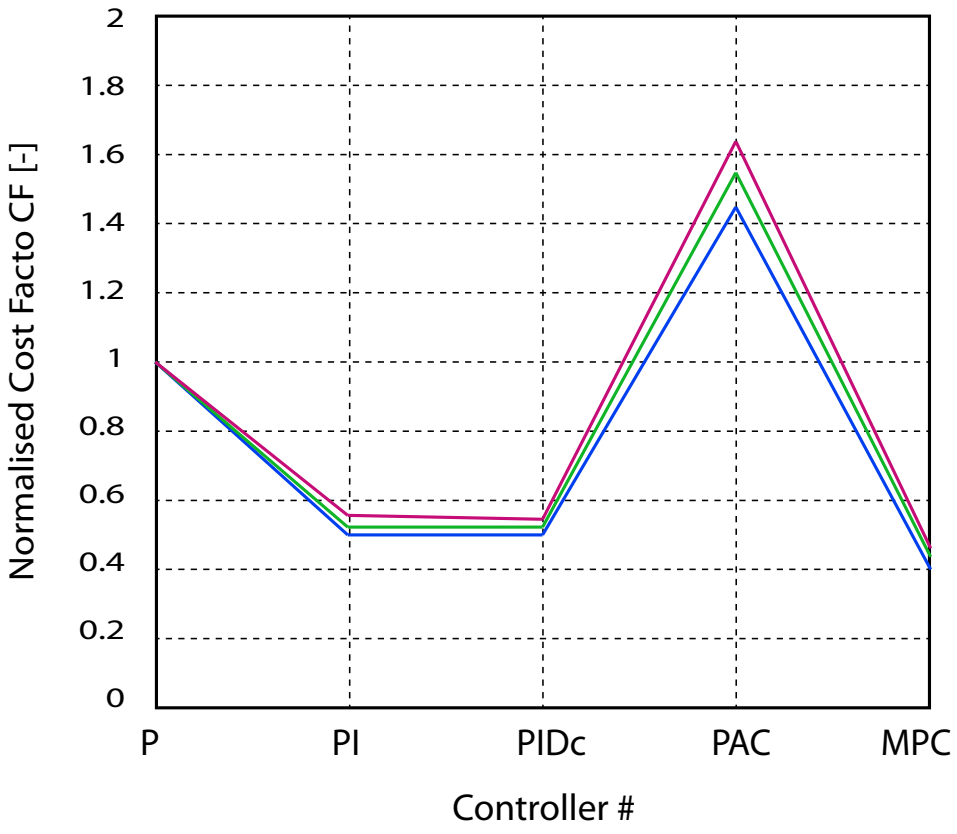

Fig. 4.6. Comparison of CF for different p values and different control strategies. Colour map: p=0% (blue), p=10% (green), p=20% (magenta).

Even though the main assumption adopted — linear relation between WECs cost and structural dimensions — is rather stringent, the CF still gives a valuable tool to gain insight into the economic potential of a WEC in function of the applied control strategy.

Summary and Conclusions

5

The risk of a future energy crisis and environmental deterioration is real if political and economical plans are not considered by now. In order to keep the growth of average world temperature below $2\ ^oC$ (Birol et al., 2013, [450 scenario]) a sharp and utter change of the overall pollution rate is needed and the change needs to happen in this period of time.

Wave energy is a large — mostly untapped — energy resource. It can contribute to the future energy mix if a number of initially underestimated issues are solved within a short period of time. As introduced in Ch. 1, the most important limitation of the sector to roll-off into the market is the actual or estimated CoE, which is affected by technical and non-technical matters. To further complicate the problem, the large number of patented devices hinders the concentration of the development effort over the few promising concepts, if any. In agreement with the objective of the SDWED project, which partially funded this work, the definition of a general applicable and reliable numerical model of WECs (wave-to-wire model) is paramount for the sector.

The model should be used to compare different WECs technologies and output a reduced range of candidates to be further developed and/or optimised. Time average parameters are used as the base of comparison, the most important being the AEP of WECs at specific locations. The assessment of the AEP relies on relatively long time simulations that together with the large number of WECs and suitable locations shed light on the need for a computationally fast wave-to-wire model. Due to the large number of WEC types only WAB WECs are considered in the analysis.

Numerical wave-to-wire modelling of WECs is not a novel topic: in literature hundreds of example can be found for several WEC types. But two main problems of the proposed solution are found and addressed in this work. On the one hand, the numerical model needs to be compared with experimental data in order to validate the reading theory and the embedded approximations. The comparison between numerical and physical models is presented in Ch. 3. Most of the examples are related to the Wavestar WEC, due to the concept's simplicity, which eases the analysis. On the other hand, the main limitation of the analysis based on numerical simulation presented so far is the obstinate maximisation of the energy produced by the WEC, which only addresses part of the CoE

minimisation problem. The classical energy maximisation approach and the proposed CoE minimisation approach are both presented in Ch. 4. The base of the CoE minimisation approach is the following: the maximisation of the energy absorbed by the WEC is obtained via modification of the control logic, which entails a modification of the loads exerted by the PTO on the structure. Therefore, the control strategy will have a (quantifiable) influence in both capital and operational costs related to the structural and lately in the CoE of the WEC. The overall approach can be classified in three sequential steps.

1 - In Ch. 2, a general WAB WEC system breakdown is presented, highlighting the predominant and representative components. The breakdown tool is the first step of analysis where the definition of what is considered relevant defines features that will be, or will not be, included in the model in a macro scale. As concluded in Ch. 2, three main subcomponents are considered fundamental for the wave-to-wire model: hydrodynamic subsystem, power take off subsystem with annex control logic and reaction subsystem. For each of those, a set of issues based of the following study is listed. Their importance lies ether in the active contribution on the main dynamic of the WEC or in the economical share or most likely on both.

2 - In Ch. 3, the available numerical and physical modelling techniques are presented and skimmed on the basis of the set of problems highlighted in the breakdown procedure. This part represents the stage two of the analysis: the numerical model is further refined based on the required objective, and all subcomponents and overall system need to be compared with experimental data sets. The need of a fast wave-to-wire model excludes linear and non-linear models based on the volume discretisation, such as CFD and SPH methods. Waiting for the computational power of computers to drastically increase, they can be used to assess fast transient phenomenas more than time average parameters. Solution of the Diffraction/Radiation problems based on panel methods and Morison's equation are two viable solutions. The free software Nemoh is a promising solution (free of charge and solution in line with the other competitors) but the computational time appears to be a bottleneck. For the case of the Weptos WEC Appx. C a convergency study has not been run for time issues. But the Nemoh code is expected to be further developed at the end of the code competition proposed by NREL (Open-WARP).

Due to the high velocity expected for the converter, if compared with Oil & Gas or FOWT structures, a hybrid or weakly non-linear model is the correct solution based on the non-dimensional analysis. The comparison between numerical hydrodynamic model and experimental data can be summarised in two points: first, the uncertainties of the experimental data need to be quantified in order not to bias the comparison, and second the larger the motion of the system the large the numerical error is, due to uncontemplated contributions, i.e. slamming, overtopping, etc.

PTO systems and their control logic differentiate a WEC from a traditional floating structure. The two common types of PTO deployed in WAB WECs are direct drive and hydraulic. Although their full numerical models are still affordable from a computational cost view point, they can be efficiently substituted by a simplified model reducing the computational time by a factor 2-10. This change is mainly ascribable to the removal of the higher harmonics, which stiffen the system of ODE. The model can be found by an interpolation of the characteristic PTO curves, similar to a principal component analysis of the numerical system. The comparison with experimental data shows a good general agreement for different cases.

The reaction systems are fundamental for the position compliance of floating WAB WECs. Although their implementation in the wave-to-wire model is based on a simple stiffness matrix, results shows that, in operational conditions, a large dissipation of energy happens around the cable. The general solution would require the application of dynamic solvers based on multi-body or FE methods, but their computational cost is still far too high. The implementation of a linear stiffness-damping reaction system model based on experimental or dynamic solvers data appears the cost-effect solution, but its implementation is reserved for future analysis.

One of the most important points achieved in this work is presented in the effect of the control strategy in the overall error of the wave-to-wire model. The application of an advanced control strategy does have an influence in the model prediction uncertainty, which needs to be used carefully when different control strategies are compared to each other.

3 - In Ch. 4, the two different optimisation methodologies are presented: the first is a 1-D optimisation based on the modification of the control strategy, and the second is a 2-D optimisation based on the control strategy and its effect on the structural design. In the context of this thesis, "optimisation" is considered a synonym for CoE minimisation.

The application of advanced control strategies is the simplest way to modify the economical viability of a WEC. Several standard techniques are presented in literature and five of them have been compared. The energy absorbed, response in a constraint scenario, tunability and implementation simplicity are the criteria used to select among the different control logics. The PI controller seems to be superior to all the others as a trade off between selection criterion. Although MPC shows better results, the judgment is weighted by its ideal implementation: the results are a function of the prediction of the future forces, and perfect knowledge of the future has been assumed in the implementation.

Since the load exerted by the PTO on the structure is a function of the control strategy, the latter is likely to induce a modification of the fatigue behaviour of the structure. The quantification of these effects is the based of the 2-D optimisation of the WEC. Although the best solution should be a fully coupled numerical model, the complexity of the fatigue analysis restrained its implementation. Therefore, a sequential approach has been used. The CF is introduced to analyse the effect of the control strategy on the COE with respect to a reference scenario, in this case P control. The results for the Wavestar WEC are in line with the 1-D optimisation. The PI controller can reduce the CF by a factor 1.5-2 in realistic constraint scenarios, which is second only to the MPC reduction. Same as before, the MPC cannot really be considered in the selection due to its idealised implementation.

5.1 Future Work

The definition of a general and reliable wave-to-wire model and the implementation of a 2-D optimisation methodology are, among others, two important steps for the quantification of the true potential of the wave energy sector.

In continuation of the work presented in this thesis, the most straightforward future step is the validation of the wave-to-wire model for different test cases, and possibly the extension of the model for the other two types of WEC. Although the first set of interim results for the Weptos WEC are promising the number of approximations used does not

allow to draw any major conclusion on the model validity. In order to obtain a general wave-to-wire model, the formulation of the equation of motion needs to be automatised and the Lagrangian approach seems to be one of the possible candidates.

Once the extended validation of the wave-to-wire model is achieved, the procedure presented in the 2-D CoE minimisation needs to be applied too.

The 2-D CoE analysis presented in this thesis is only a “toward" steps. Its importance lies in shedding light on the true problem of the CoE minimisation more than the brutal energy maximisation. But its implementation is only in an embryonic form. First of all, the result of the model should be validated by FE structural analysis, and secondly the fatigue model should be implemented in the control algorithm ending in a fully coupled system. The natural framework of this global optimisation problem is the MPC scheme.

In this frame of research, the appraisal of the unbiased capability of the MPC including the uncertainty of the disturbance prediction is a relevant topic and it is expected to be analysed in the upcoming future. In addition the implementation of the MPC in physical models and the quantification of the uncertainties of the numerical model when MPC is considered are two other topics for future development of the MPC framework.

Personally I think that in order to facilitate the development of a generally applicable and reliable wave-to-wire model, we need to create a free flux of information between research centres in terms of numerical knowledge and experimental data sets.

Bibliography

Abraham, E. and Kerrigan, E. C. (2013). „Optimal Active Control and Optimization of a Wave Energy Converter“. In: 4.2 (2013), pp. 324–332 (cit. on pp. 7, 19, 46).

Alves, M, Traylor, H, and Sarmento, A (2007). „Hydrodynamic Optimisation of a Wave Energy Converter Using a Heave Motion Buoy“. In: *Proceeding of European Wave and Tidal Energy Conference, EWTEC*. Porto, Portugal, 2007, pp. 1–8 (cit. on p. 8).

ASME (2009). *Standard for Verification and Validation in Computational Fluid Dynamics and Heat Transfer: ASME V&V 20-2009*. Tech. rep. New York, NY, USA, 2009 (cit. on pp. 23, 24).

Babarit, A. and Clement, A. (2006). „Optimal latching control of a wave energy device in regular and irregular waves“. In: *Applied Ocean Research* 28.2 (Apr. 2006), pp. 77–91 (cit. on pp. 7, 19, 46).

Babarit, A., Guglielmi, M., and Clément, A. H. (2009). „Declutching control of a wave energy converter“. In: *Ocean Engineering* 36.12-13 (Sept. 2009), pp. 1015–1024 (cit. on pp. 8, 46).

Babarit, A., Hals, J., and Krokstad, J. (2011). „Power Absorption measures and Comparisons of Selected Wave Energy Converters“. In: *Proceeding of International Conference on Ocean, Offshore and Artic Engineering OMAE*. 2011, pp. 1–10 (cit. on p. 25).

Babarit, A., Hals, J., Muliawan, M., Kurniawan, A., Moan, T., and Krokstad, J. (2012). „Numerical benchmarking study of a selection of wave energy converters“. In: *Renewable Energy* 41 (May 2012), pp. 44–63 (cit. on pp. 7, 15, 25, 31).

Bakshi, V. (2009). *Control Systems*. Technical Publications, 2009 (cit. on p. 48).

Beatty, S., Buckham, B. J., and Wild, P. (2008). „Frequency Response Tuning for a Two-Body Heaving Wave Energy Converter“. In: *Proceeding of International Offshore and Polar Engineering Conference, ISOPE*. Vol. i. Vanciuver, Canada, 2008, pp. 342–349 (cit. on pp. 7, 15).

Berkhout, V., Faulstich Stefan; Gorg, P., Kühn, P., Linke, K., Lyding, P., Pfaffel, S., Rafik, K., Rohrig, K., Rothkegel, R., Stark, E., and Witte, J. (2012). *Wind Energy Report Germany 2012*. Tech. rep. 2012 (cit. on p. 54).

Bhinder, M. A., Babarit, A., Gentaz, L., and Ferrant, P. (2011). „Assessment of Viscous Damping via 3D-CFD Modelling of a Floating Wave Energy Device“. In: *Proceeding of European Wave and Tidal Energy Conference, EWTEC*. Southampton, 2011, pp. 1–6 (cit. on pp. 7, 30).

Binh, P. C., Truong, D. Q., and Ahn, K. K. (2012). „A Study on Wave Energy Conversion Using Direct Linear Generator“. In: *Proceeding of International Conference on Control, Automation and Systems*. Jeju Island. Korea, 2012, pp. 64–69 (cit. on pp. 18, 19).

Birol, F., Cozzi, L., Gul, T., Dorner, D., Baroni, M., Besson, C., Hood, C., Kesicki, F, Olejarnik, P., Trueby, J., Noort, K. van, Wanner, B., and Wilkinson, D. (2013). *Redrawing the energy-climate map*. Tech. rep. Paris, France: IEA - International Energy Agency, 2013, pp. 1–134 (cit. on p. 57).

Blanco, M. (2009). „The economics of wind energy". In: *Renewable and Sustainable Energy Reviews* 13.6-7 (Aug. 2009), pp. 1372–1382 (cit. on p. 54).

Borgarino, B, Babarit, A, Singh, J., and Kramer, M. M. (2012). „Assessing the structural forces in the Wavestar wave energy converter , using a coupled hydro-elastic methodology". In: *Proceeding of International Conference on Ocean Energy - ICOE*. Dublin, Ireland, 2012, pp. 1–6 (cit. on pp. 8, 16).

BP (2013). *Energy Outlook 2030*. Tech. rep. London, UK: BP - British Petroleum, 2013 (cit. on p. 1).

Brekken, T. K. A. (2011). „On Model Predictive Control for a point absorber Wave Energy Converter". In: *Proceeding of PowerTech - IEEE*. Trondheim, Norway, 2011, pp. 1–8 (cit. on p. 46).

Brooke, J. (2003). *Wave Energy Conversion*. Elsevier Ocean Engineering Series. Elsevier Science, 2003 (cit. on p. 6).

Brooking, P., Mueller, M., Baker, N., Haydock, L., and Brown, N. (2002). „Power conversion in a low speed reciprocating electrical generator". In: *Proceeding of International Conference of Electrical Machines*. 2002 (cit. on p. 18).

Budal, K., Falnes, J., Iversen, L. C., Lillebekken, P. M., Oltedal, G., Hals, T., Onshus, T., and Høy, A. (1982). *The Norwegian wave-power buoy project*. 1982 (cit. on p. 46).

Carbon Trust and DNV (2005). *Guidelines on design and operation of wave energy converters*. Tech. rep. May. 2005 (cit. on pp. 6, 15).

CEN (2005). *Eurocode 3: Design of Steel Structures—Part 1-9: Fatigue EN 1993-1-9*. Tech. rep. Brussels, Belgium, 2005 (cit. on p. 53).

Chakrabarti, S. (1987). *Hydrodynamics of offshore structures*. Computational Mechanics, 1987 (cit. on p. 26).

Chaplin, J. R., Farley, F. J. M., Prentice, M. E., Rainey, R. C. T., Rimmer, S. J., and Roach, A. T. (2007). „Development of the ANACONDA all-rubber WEC". In: *Proceeding of European Wave and Tidal Energy Conference, EWTEC*. Porto, Portugal, 2007 (cit. on pp. 14, 15).

Chozas, J. (2013). *Technical and Non-Technical Issues Towards the Commercialisation of Wave Energy Converters*. DCE Thesis. Department of Civil Engineering, Aalborg University, 2013 (cit. on pp. 3, 4).

Clement, A., Mccullen, P., Falcão, A. F. O., Fiorentino, A., Gardner, F., Hammarlund, K., Lemonis, G., Lewis, T., Nielsen, K., Petrocini, S., Pontes, M. T., Schild, P., Sjostrom, B. O., Sorensen, H. C., and Thorpe, T. (2002). „Wave energy in Europe : current status and perspectives". In: *Renewable and Sustainable Energy Reviews* 6 (2002), pp. 405–431 (cit. on p. 6).

Costello, R., Ringwood, J. V., and Weber, J. (2011). „Comparison of Two Alternative Hydraulic PTO Concepts for Wave Energy Conversion". In: *Proceeding of European Wave and Tidal Energy Conference, EWTEC*. 1. Southampton, 2011 (cit. on pp. 7, 18).

Cretel, J. A. M., Lightbody, G, Thomas, G. P., and Lewis, A. W. (2011a). „Maximisation of Energy Capture by a Wave-Energy Point Absorber using Model Predictive Control". In: *Proceeding of International Federation of Automatic Control - IFAC*. 2002. 2011, pp. 3714–3721 (cit. on pp. 8, 19, 46).

Cretel, J. A. M., Lewis, A. W., Thomas, G. P., and Lightbody, G. (2011b). „A Critical Assessment of Latching as Control Strategy for Wave-Energy Point Absorbers“. In: *Proceeding of International Offshore and Polar Engineering Conference, ISOPE*. Vol. 8. 2011, pp. 680–686 (cit. on pp. 46, 51).

Cruz, J. (2007). *Ocean Wave Energy: Current Status and Future Prespectives*. Green Energy and Technology. Springer, 2007 (cit. on p. 5).

Cubasch, U., Wuebbles, D., D., C., Facchini, M., Frame, D., Mahowald, N., and Winther, J. (2013). *Introduction in: Climate Change 2013: The Physical Science Basis.* Tech. rep. Cambridge, UK and New York, NY, USA: IPCC - Intergovernmental Panel on Climate Change, 2013 (cit. on p. 1).

Cummins, W (1962). *The impulse response function and ship motion*. Tech. rep. 1962 (cit. on p. 36).

Davey, T., Harrison, G. P., and Stallard, T. (2009). *Procedures for Economic Evaluation - Deliverable D7.2.1*. Tech. rep. EQUIMAR - Equitable Testing, Evaluation of Marine Energy Extraction Devices in terms of Performance, Cost, and Environmental Impact, 2009, pp. 1–15 (cit. on p. 53).

Dean, R. and Dalrymple, R. (1991). *Water Wave Mechanics for Engineers and Scientists*. Advanced series on ocean engineering. World Scientific, 1991 (cit. on p. 35).

DNV (2010). *Fatigue Design of Offshore Steel Structures: DNV-RP-C203*. Tech. rep. Høvik, Norway, 2010 (cit. on pp. 14, 53).

Drew, B, Plummer, a. R., and Sahinkaya, M. N. (2009). „A review of wave energy converter technology“. In: *Institution of Mechanical Engineers, Part A: Journal of Power and Energy* 223.8 (Dec. 2009), pp. 887–902 (cit. on p. 6).

Dubuque, G. (2011). „A Lumped Parameter Equilibrium Model of a Submerged Body with Mooring Lines“. PhD thesis. University of Washington, 2011 (cit. on p. 20).

Durand, M, Babarit, A, Pettinotti, B, Quillard, O, Toularastel, J. L., and Clément, A. H. (2007). „Experimental validation of the performances of the SEAREV Wave Energy Converter with real time latching control“. In: *Proceeding of European Wave and Tidal Energy Conference, EWTEC*. 1. 2007 (cit. on pp. 8, 46).

Eriksson, M, Isberg, J, and Leijon, M (2005). „Hydrodynamic modelling of a direct drive wave energy converter“. In: *International Journal of Engineering Science* 43.17-18 (Nov. 2005), pp. 1377–1387 (cit. on p. 18).

Evans, D. V. (1981). „Power from water waves“. In: *Annual Review of Fluid Mechanics* 13 (1981), pp. 157–187 (cit. on p. 45).

Fagley, C. P. (2012). „Computational Investigation of Irregular Wave Cancellation Using a Cycloidal Wave Energy Converter“. In: *Proceeding of International Conference on Ocean, Offshore and Artic Engineering OMAE*. Rio de Janeiro, Brazil, 2012, pp. 1–8 (cit. on p. 47).

Falcão, A. (2010). „Wave energy utilization: A review of the technologies“. In: *Renewable and Sustainable Energy Reviews* 14.3 (Apr. 2010), pp. 899–918 (cit. on p. 6).

Falcão, A. F. D. O. (2007). „Modelling and control of oscillating-body wave energy converters with hydraulic power take-off and gas accumulator“. In: *Ocean Engineering* 34.14-15 (Oct. 2007), pp. 2021–2032 (cit. on pp. 18, 19).

Falnes, J. (2002). *Ocean Waves and Oscillating Systems*. Cambridge University Press, 2002 (cit. on pp. 19, 45, 46).

Faltinsen, O. (1993). *Sea Loads on Ships and Offshore Structures*. Cambridge Ocean Technology Series. Cambridge University Press, 1993 (cit. on pp. 25, 26, 30).

Ferroukhi, R., Lucas, H., Renner, M., Lehr, U., Breitschopf, B., Lallement, D., and Petrick, K. (2013). *Renewable Energy and Jobs*. Tech. rep. volume of December. Abu Dhabi, United Arab Emirates: IRENA - International Renewable Energy Agency, 2013, pp. 1–144 (cit. on p. 2).

Fischer, B and Kracht, P (2012). „Online-Algorithm using Adaptive Filters for Short-Term Wave Prediction and its Implementation". In: *Proceeding of International Conference on Ocean Energy, ICOE*. Dublin, Ireland, 2012, pp. 1–6 (cit. on p. 47).

Fitzgerald, J and Bergdahl, L (2008). „Including moorings in the assessment of a generic offshore wave energy converter: A frequency domain approach". In: *Marine Structures* 21.1 (Jan. 2008), pp. 23–46 (cit. on pp. 21, 34).

Fitzgerald, J. (2009). *Position Mooring of Wave Energy Converters - An engineering study into the mooring of structures in a highly exposed shallow ocean regime, within the context of the economics of renewable energy conversion*. Chalmers University of Technology, 2009 (cit. on pp. 6, 19, 20).

Folley, M. and Chaplin, R. (1998). „An Investigation into the effect of extreme waves and the design of wave energy converters". In: 1998, pp. 1–1 (cit. on p. 15).

Fossen, T. (2011). *Handbook of Marine Craft Hydrodynamics and Motion Control*. Wiley, 2011 (cit. on pp. 19, 36).

Francis, B. and Wonham, W. (1976). „The Internal Model Principle of Control Theory". In: *Automatica* 12.5 (1976), pp. 457–465 (cit. on p. 48).

Frigaard, P. and Brorsen, M. (1995). „A time-domain method for separating incident and reflected irregular waves". In: *Coastal Engineering* 24.3-4 (Mar. 1995), pp. 205–215 (cit. on p. 48).

Frigaard, P. and Andersen, T. (2010). *Technical Background Material for the Wave Generation Software AwaSys 5*. DCE Technical Reports. Department of Civil Engineering, Aalborg University, 2010 (cit. on p. 35).

Fusco, F and Ringwood, J (2008). „A Study on Short-Term Sea Profile Prediction for Wave Energy Applications". In: *Proceeding of European Wave and Tidal Energy Conference, EWTEC*. Uppsala, Sweden, 2008 (cit. on p. 47).

Fusco, F. and Ringwood, J. V. (2010a). „Short-Term Wave Forecasting for Real-Time Control of Wave Energy Converters". In: *IEEE Transactions on Sustainable Energy* 1.2 (July 2010), pp. 99–106 (cit. on pp. 8, 47, 48).

Fusco, F. and Ringwood, J. V. (2010b). „Short-term wave forecasting with AR models in real-time optimal control of wave energy converters". In: *IEEE International Symposium on Industrial Electronics* (July 2010), pp. 2475–2480 (cit. on p. 47).

Fusco, F. and Ringwood, J. V. (2013). „A Simple and Effective Real-Time Controller for Wave Energy Converters". In: *IEEE Transactions on Sustainable Energy* 4.1 (2013), pp. 21–30 (cit. on pp. 7, 8, 19, 48).

Gadonneix, P., Castro, F. B. de, Medeiros, N. F. de, Drouin, R., Jain, C. P., Kim, Y. D., Ferioli, J., Nadeau, M.-J., Sambo, A., Teyssen, J., Naqi, A. A., Ward, G., Guobao, Z., and Frei, C. (2010). *2010 Survey of Energy Resources*. Tech. rep. World Energy Council - For suistainable energy, 2010, pp. 1–618 (cit. on pp. 4, 5, 15).

Gadonneix, P., Kim, Y. D., Meyers, K., Ward, G., and Frei, C. (2013). *World Energy Resources: 2013 survey*. Tech. rep. World Energy Council, 2013, pp. 1–468 (cit. on p. 20).

Gilloteaux, J. C. and Ringwood, J (2010). „Control-Informed Geometric Optimisation of Wave Energy Converters“. In: *Proceeding of International Federation of Automatic Control - IFAC*. 2010, pp. 1–8 (cit. on p. 8).

GmbH (2005). *Guideline for the Certification of Offshore Wind Turbines*. Tech. rep. Hamburg, Germany, 2005 (cit. on p. 53).

Guerinel, M., Zurkinden, A. S., Alves, M., and Sarmento, J. N. A. (2013). „Validation of a Partially Nonlinear Time Domain Model using instantaneous Froude-Krylov and Hydrostatic Forces“. In: *Proceeding of European Wave and Tidal Energy Conference, EWTEC*. Aalborg, 2013 (cit. on pp. 7, 27).

Hals, J. r. (2010). „Modelling and phase control of wave-energy converters“. PhD thesis. Norwegian University of Science and Technology, 2010, pp. 1–257 (cit. on pp. 8, 19).

Hals, J., Falnes, J., and Moan, T. (2011a). „A Comparison of Selected Strategies for Adaptive Control of Wave Energy Converters“. In: *Journal of Offshore Mechanics and Arctic Engineering* 133.3 (Mar. 2011), pp. 031101–031101 (cit. on pp. 8, 46, 48).

Hals, J., Falnes, J., and Moan, T. (2011b). „Constrained optimal control of a heaving buoy wave-energy converter“. In: *Journal of Offshore Mechanics and Arctic Engineering* 133.1 (2011), p. 011401 (cit. on p. 46).

Hamedni, B., Mathieu, C., and Ferreira, C. B. (2014). *Generic WEC System Breakdown: D5.1 SDWED*. Tech. rep. 2014, pp. 1–40 (cit. on p. 13).

Hansen, R., Kramer, M., and Vidal, E. (2013). „Discrete Displacement Hydraulic Power Take-Off System for the Wavestar Wave Energy Converter“. In: *Energies* 6.8 (Aug. 2013), pp. 4001–4044 (cit. on pp. 18, 19).

Hansen, R. H., Kramer, M. M., and All, P. (2012). „Modelling and Control of the Wavestar Prototype“. In: *Proceeding of European Wave and Tidal Energy Conference, EWTEC*. 2012, pp. 1–10 (cit. on pp. 7, 15, 18, 46, 50).

Henderson, R. (2006). „Design, simulation, and testing of a novel hydraulic power take-off system for the Pelamis wave energy converter“. In: *Renewable Energy* 31.2 (Feb. 2006), pp. 271–283 (cit. on p. 18).

Hulme, A. (1982). „The wave forces acting on a floating hemisphere undergoing forced periodic oscillations“. In: *Journal of Fluid Mechanics* 121 (Aug. 1982), pp. 443–463 (cit. on p. 25).

IEA (2013). *World energy outlook*. Tech. rep. Paris, France: IEA - International Energy Agency, 2013 (cit. on p. 1).

IEC (2005). *Wind Turbines—Part 1: Design Requirements IEC 61400-1*. Tech. rep. Geneva, Switzerland, 2005 (cit. on p. 53).

IEC/TC (2013). *IEC 62600-10 TS: Marine energy - Wave, tidal and other water current converters - Part 10: Assessment of mooring system for Marine Energy Converters (MECs)*. Tech. rep. Cd. 2013 (cit. on p. 20).

Ingram, D., Smith, G., Bittencourt-Ferreira, C., and Smith, H. (2011). *EquiMar: Protocols for the Equitable Assessment of Marine Energy Converters*. Tech. rep. 213380. Edinborough, 2011, pp. 1–280 (cit. on pp. 6, 34, 40, 42).

ISO (2007). *Petroleum and Gas Industries—Fixed Steel Offshore Structures: ISO 19902*. Tech. rep. Geneva, Switzerland, 2007 (cit. on p. 52).

Ivanova, I. A., Agren, O., Bernhoff, H., and Leijon, M. (2005). „Simulation of Wave-Energy Converter With Octagonal Linear Generator“. In: *IEEE Journal of Ocean Engineering* 30.3 (2005), pp. 619–629 (cit. on p. 18).

Johanning, L., Smith, G. H., and Wolfram, J. (2007). „Measurements of static and dynamic mooring line damping and their importance for floating WEC devices“. In: *Ocean Engineering* 34.14-15 (Oct. 2007), pp. 1918–1934 (cit. on p. 20).

Kamizuru, Y, Verdegem, L, Erhart, P, Langenstein, C, Andren, L, Lenß en, M, and Ag, B. R. (2012). „Efficient Power Take-Offs for Ocean Energy Conversion“. In: *Proceeding of International Conference on Ocean Energy, ICOE*. Dublin, 2012, pp. 1–8 (cit. on p. 18).

Korde, U. (2000). „Control System Applications In Wave Energy Conversion“. In: *Proceeding of OCEANS 200 MTS/IEEE conference*. 2000, pp. 1817–1824 (cit. on p. 46).

Kwon, W., Han, S., and Han, S. (2005). *Receding Horizon Control: Model Predictive Control for State Models*. Advanced Textbooks in Control and Signal Processing. Springer, 2005 (cit. on p. 51).

Lagarias, J. C., Reeds, J. A., Wright, M. H., and Wright, P. E. (1998). „Convergence Properties of the Nelder-Mead Simplex Method in Low Dimensions“. In: *SIAM Journal of Optimization* 9 (1998), pp. 112–147 (cit. on p. 157).

Lasa, J., Antolin, J. C., Angulo, C., Estensoro, P., Santos, M., and Ricci, P. (2012). „Design, Construction and Testing of a Hydraulic Power Take-Off for Wave Energy Converters“. In: *Energies* 5.12 (June 2012), pp. 2030–2052 (cit. on p. 18).

Lemofouet, S and Rufer, A (2005). „Hybrid Energy Storage Systems based on Compressed Air and Supercapacitors with Maximum Efficiency Point Tracking“. In: *Proceeding of European Conference on Power Electronics and Apllications, EPE*. Dresden, 2005, pp. 1–10 (cit. on p. 17).

Lopes, M., Hals, J., Gomes, R., Moan, T., Gato, L., and Falcão, A. O. (2009). „Experimental and numerical investigation of non-predictive phase-control strategies for a point-absorbing wave energy converter“. In: *Ocean Engineering* 36.5 (Apr. 2009), pp. 386–402 (cit. on pp. 8, 46).

MacKay, D. (2008). *Sustainable Energy – without the hot air*. UIT Cambridge, 2008 (cit. on p. 1).

Mackay, E., Cruz, J., Retzler, C., Arnold, P., Bannon, E., and Pascal, R. (2012). „Validation of a new wave energy converter design tool with large scale single machine experiments“. In: *Proceeding of Asian Wave and Tidal Conference Series*. Korea, 2012 (cit. on p. 15).

Marquis, L, Kramer, M, and Frigaard, P (2010). „First Power Production figures from the Wave Star Roshage Wave Energy Converter“. In: *Proceeding of International Conference on Ocean Energy, ICOE*. 2010, pp. 1–5 (cit. on pp. 15, 18, 46).

Masuda, Y. (1971). „Wave-activated generator“. In: *Proceeding of International Exposition Oceans, France*. 1971 (cit. on p. 4).

MATLAB (2013). *version 8.1.0.604 (R2013a)*. Natick, Massachusetts: The MathWorks Inc., 2013 (cit. on p. 38).

Mccomb, C., Lawson, M., and Yu, Y.-H. (2013). „Combining Multi-Body dynamics and potential flow simulation methods to model a wave energy converter“. In: *Proceeding of Marine Energy Technology Symposium, METS*. Washington D.C., 2013, pp. 1–8 (cit. on p. 37).

Mcginn, D., Green, D., Hinrichs-rahlwes, R., Sawyer, S., Sander, M., Taylor, R., Giner-reichl, I., Teske, S., Lehmann, H., and Hales, D. (2013). *Renewables 2013 Global Status Report 2013*. Tech. rep. Pairs, 2013, p. 178 (cit. on pp. 3, 4).

Morison, J. R., Johnson, J. W., and Schaaf, S. A. (1950). „The Force Exerted by Surface Waves on Piles“. In: *Journal of Petroleum Technology* 2 (1950), pp. 149–154 (cit. on pp. 25, 28).

Mørk, G., Barstow, S., Kabuth, A., and Pontes, M. T. (2010). „Assessing the global wave energy potential“. In: *Proceeding of International Conference on Ocean, Offshore and Arctic Engineering, OMAE*. 2008. Shanghai, China, 2010, pp. 1–8 (cit. on p. 3).

Mueller, M. (2002). „Electrical generators for direct drive wave energy converters“. In: *IEE Proceedings - Generation, Transmission and Distribution* 149.4 (2002), p. 446 (cit. on p. 18).

Mueller, M. and Baker, N. (2002). „A low speed reciprocating permanent magnet generator for direct drive wave energy converters.“ In: *Proceeding of Power Electronics, Machine and Drivers, IET*. 7. 2002, pp. 468–473 (cit. on p. 18).

Murphy, G. (2011). *Ordinary Differential Equations and Their Solutions*. Dover books on mathematics. Dover Publications, 2011 (cit. on p. 38).

Nielsen, K. (2012). *Ocean Energy Technology Study*. Tech. rep. May. Danish Wave Energy Center (DanWEC), 2012, pp. 1–63 (cit. on pp. 4, 6, 47).

Nielsen, S. R., Zhou, Q., Kramer, M. M., Basu, B., and Zhang, Z. (2013). „Optimal control of nonlinear wave energy point converters“. In: *Ocean Engineering* 72 (Nov. 2013), pp. 176–187 (cit. on pp. 8, 46, 49, 50).

Nolan, G. and Ringwood, J. (2006). „Control of a heaving buoy wave energy converter for potable water production“. In: *Proceeding of IET Irish Signals and Systems Conference ISSC*. 2006, pp. 421–426 (cit. on p. 13).

Ó'Catháin, M., Leira, B. J., Ringwood, J. V., and Gilloteaux, J.-C. (2008). „A modelling methodology for multi-body systems with application to wave-energy devices“. In: *Ocean Engineering* 35.13 (Sept. 2008), pp. 1381–1387 (cit. on pp. 37, 154).

Palm, J., Eskilsson, C., Paredes, G. M., and Bergdahl, L. (2013a). „CFD Simulation of a Moored Floating Wave Energy Converter“. In: *Proceeding of European Wave and Tidal Energy Conference, EWTEC*. Aalborg, 2013 (cit. on pp. 15, 16, 20, 25).

Palm, J., Paredes, G. M., Pinto, F. T., and Bergdahl, L. (2013b). „Simulation of Mooring Cable Dynamics Using a Discontinuous Galerkin Method“. In: *Proceeding of International Conference on Computational Methods in Marine Engineering - MARINE*. Hamburg, 2013, pp. 1–12 (cit. on p. 34).

Paredes, G. M., Eskilsson, C., Palm, J., Bergdahl, L., Leite, L. M., and Taveira-pinto, F. (2013). „Experimental and Numerical Modelling of a Moored , Generic Floating Wave Energy Converter“. In: *Proceeding of European Wave and Tidal Energy Conference, EWTEC*. Aalborg, 2013 (cit. on pp. 8, 20).

Parks, T. and Burrus, C. (1987). *Digital filter design*. Topics in digital signal processing. Wiley, 1987 (cit. on pp. 36, 47).

Parmeggiani, S., Kofoed, J., and Friis-Madsen, E. (2013). „Experimental Study Related to the Mooring Design for the 1.5 MW Wave Dragon WEC Demonstrator at DanWEC“. In: *Energies* 6.4 (Apr. 2013), pp. 1863–1886 (cit. on p. 20).

Pecher, A, Kofoed, J. P., Larsen, T, and Marchalot, T (2012a). „Experimental Study of the Weptos Wave Energy Converter“. In: *Proceeding of International Conference on Ocean, Offshore and Artic Engineering - OMAE*. Rio de Janeiro, Brasil, 2012, pp. 1–8 (cit. on p. 15).

Pecher, A., Kofoed, J. P., and Larsen, T. (2012b). „Experimental study of the Weptos wave energy converter“. In: *Proceeding of International Conference on Ocean, Offshore and Arctic Engineering, OMAE*. Rio de Janeiro, Brazil, 2012, pp. 1–11 (cit. on pp. 15, 18, 37, 154, 157, 158).

Perdigão, J. N. B. A. and Sarmento, A. J. N. A. (1989). „A phase control strategy for OWC devices in irregular seas“. In: *Proceeding of International Workshop of Water Wave and Floating Body - iwwwfb*. 1989, pp. 205–209 (cit. on p. 46).

Polinder, H., Mecrow, B., Jack, A., Dickinson, P., and Mueller, M. (2005). „Conventional and TFPM Linear Generators for Direct-Drive Wave Energy Conversion“. In: *IEEE Transactions on Energy Conversion* 20.2 (June 2005), pp. 260–267 (cit. on p. 18).

Polinder, H, Mueller, M. A., Scuotto, M, and Prado, M. G. D. S. (2007). „Linear generator systems for wave energy conversion“. In: *Proceeding of European Wave and Tidal Energy Conference, EWTEC*. Porto, Portugal, 2007, pp. 1–8 (cit. on p. 18).

Previsic, M. and Shoele, K. (2013). „Cost Reduction Pathways for Wave Energy“. In: *Proceeding of European Wave and Tidal Energy Conference, EWTEC*. Aalborg, Denmark, 2013, pp. 1–8 (cit. on p. 6).

Price, A. A. E. (2009). „New Perspectives on Wave Energy Converter Control“. PhD thesis. University of Edinburgh, 2009, pp. 1–319 (cit. on pp. 8, 46).

Åström, K. and Hägglund, T (2005). *Advanced PID Control*. The Instrumentation, Systems, and Automation Society (ISA), 2005 (cit. on p. 50).

Rhinefrank, K., Schacher, A., Prudell, J., Stillinger, C., Naviaux, D., Brekken, T., Jouanne, A. V., Newborn, D., Yim, S., and Cox, D. (2010). „NUMERICAL and EXPERIMENTAL ANALYSIS of a NOVEL WAVE ENERGY CONVERTER“. In: *Proceeding of International Conference on Ocean, Offshore and Artic Engineering OMAE*. 2010 (cit. on p. 20).

Richter, M., Magaña, M., Sawodny, O., and Brekken, T. K. A. (2013). „Nonlinear Model Predictive Control of a Point Absorber Wave Energy Converter“. In: 4.1 (2013), pp. 118–126 (cit. on pp. 20, 21, 46).

Ringwood, J. and Butler, S. (2004). „Optimisation of a wave energy converter“. In: *Proceeding of International Federation of Automatic Control - IFAC - CAMS 2004*. 2004, pp. 155–160 (cit. on p. 46).

Ruehl, K, Michelen, C, Kanner, S, Lawson, M, and Yu, Y. H. (2014). „Preliminary Verification and Validation of WEC-Sim , an Open-Source Wave Energy Converter Design Tool Preprint“. In: *Proceeding of International Conference on Ocean, Offshore and Arctic Engineering - OMAE*. March. San Francisco, California, USA, 2014, pp. 1–8 (cit. on p. 154).

Ruiz-Minguela, J., Prieto, A., Marón, M., Rodríguez, R., Ricci, P., Fernández, D., and Taboada, M. (2008). „Design and Testing of the Mooring System for a New Offshore Wave Energy Converter“. In: *Proceeding of International Conference on Ocean Energy, ICOE*. Brest, 2008, pp. 1–9 (cit. on p. 20).

Salter, S. H. (1974). „Wave power“. In: *Nature* 249 (June 1974), pp. 720–724 (cit. on p. 153).

Sarpkaya, T. (2010). *Wave Forces on Offshore Structures*. Wave Forces on Offshore Structures. Cambridge University Press, 2010 (cit. on pp. 25, 30).

Schoen, M. P., Hals, J., and Moan, T. (2008). „Robust control of heaving wave energy devices in irregular waves“. In: *Proceeding of Mediterranean Conference on Control and Automation*. 1. Ajaccio, France: Ieee, June 2008, pp. 779–784 (cit. on p. 47).

Schoen, M. P., Hals, J. r., and Moan, T. (2011). „Wave Prediction and Robust Control of Heaving Wave Energy Devices for Irregular Waves“. In: *IEEE Transactions on Energy Conversion* 26.2 (2011), pp. 627–638 (cit. on p. 47).

Sclavounos, P. D. (2012). „Nonlinear impulse of ocean waves on floating bodies“. In: *Journal of Fluid Mechanics* 697 (2012), pp. 316–335 (cit. on p. 7).

Seidel, J., Fagley, C., and Siegel, S. (2012). „Numerical Simulations of a Cycloidal Wave Energy Converter“. In: *Proceeding of Asian Wave and Tidal Conference Series*. Korea, 2012, pp. 1–6 (cit. on p. 15).

Shek, J. K. H., Macpherson, D. E., and Mueller, M. A. (2008). „Phase and Amplitude Control of a Linear Generator“. In: *Proceeding of Power Electronics, Machine and Drivers, IET*. York, 2008, pp. 66–70 (cit. on p. 18).

Silva, D., Rusu, E., and Soares, C. (2013). „Evaluation of Various Technologies for Wave Energy Conversion in the Portuguese Nearshore“. In: *Energies* 6.3 (Mar. 2013), pp. 1344–1364 (cit. on p. 15).

Soltani, M. and Sichani, M. (2013). „Model Predictive Control of Buoy Type Wave Energy Converter“. In: *Proceeding of International Federation of Automatic Control - IFAC*. Cape Town, 2013, pp. 1–7 (cit. on p. 51).

Taghipour, R. (2008). „Efficient Prediction of Dynamic Response for Flexible and Multi- Body Marine Structures“. PhD thesis. Norwegian University of Science and Technology, 2008, pp. 1–178 (cit. on pp. 11, 154).

Veritas, D. N. (2013). *DNV-OS-J103 Design of Floating Wind Turbine Structures*. Tech. rep. June. 2013 (cit. on pp. 14, 15, 20, 35, 53).

Vicente, P. C., Falcão, A. F. D. O., and Justino, P. A. P. (2011). „Optimization of Mooring Configuration Parameters of Floating Wave Energy Converters“. In: *Proceeding of International Conference on Ocean, Offshore and Arctic Engineering, OMAE*. Rotterdam: Asme, 2011, pp. 759–765 (cit. on p. 21).

Weber, J (2012). „WEC Technology Readiness and Performance Matrix – finding the best research technology development trajectory“. In: *Proceeding of International Conference on Ocean Energy, ICOE*. Dublin, 2012, pp. 1–10 (cit. on pp. 6, 7).

Westphalen, J, Greaves, D. M., Williams, C. K., Taylor, P. H., Causon, D. M., Mingham, C. G., Hu, Z. Z., Stansby, P. K., Rogers, B. D., and Omidvar, P (2009). „Extreme Wave Loading on Offshore Wave Energy Devices using CFD : a Hierarchical Team Approach“. In: *Proceeding of European Wave and Tidal Energy Conference, EWTEC*. Uppsala, 2009, pp. 500–508 (cit. on p. 16).

Yu, Y and Li, Y (2011). „A RANS Simulation of the Heave Response of a Two-Body Floating Point Wave Absorber Preprint“. In: *Proceeding of International Offshore and Polar Engineering Conference, ISOPE*. Maui, Hawaii, 2011 (cit. on pp. 16, 25).

Zanuttigh, B., Angelelli, E., and Kofoed, J. P. (2013). „Effects of mooring systems on the performance of a wave activated body energy converter“. In: *Renewable Energy* 57 (Sept. 2013), pp. 422–431 (cit. on pp. 15, 20).

Zhang, D., Li, W., Lin, Y., and Bao, J. (2012). „An overview of hydraulic systems in wave energy application in China“. In: *Renewable and Sustainable Energy Reviews* 16.7 (Sept. 2012), pp. 4522–4526 (cit. on p. 18).

Zmood, D. N. and Holmes, D. G. (2003). „Stationary Frame Current Regulation of PWM Inverters With Zero Steady-State Error“. In: *IEEE Transaction on Power Electronics* 18.3 (2003), pp. 814–822 (cit. on p. 48).

Zurkinden, A. S., Lambertsen, S. r. H., Damkilde, L., Gao, Z., and Moan, T. (2013). „Fatigue analysis of a wave energy converter taking into account different control strategies“. In: *Proceeding of International Conference on Ocean, Offshore and Artic Engineering - OMAE*. Rio de Janeiro, Brazil, 2013, pp. 1–8 (cit. on pp. 8, 16).

Online Resources

ANSYS (2014). *ANSYS Aqwa*. 2014. Available at: `http://www.ansys.com/Products/Other+Products/ANSYS+AQWA`, visited on June 25, 2014 (cit. on p. 28).

BP (2010). *Deepwater Horizon accident and response*. 2010. Available at: `http://www.bp.com/en/global/corporate/gulf-of-mexico-restoration/deepwater-horizon-accident-and-response.html`, visited on Apr. 21, 2014 (cit. on p. 1).

Dexawave (2014). *Blue ocean energy*. 2014. Available at: `http://www.dexawave.com/`, visited on June 27, 2014 (cit. on p. 8).

LHEEA-ECN (2014). *Nemoh*. 2014. Available at: `http://lheea.ec-nantes.fr/doku.php/emo/nemoh/start`, visited on June 25, 2014 (cit. on p. 28).

Li, D., Yuanqing, X., Mengyin, F., and Magdi, S. M. (2012). *Discrete-Time Model Predictive Control, Advances in Discrete Time Systems*. 2012. Available at: `http://www.intechopen.com/books/advances-in-discrete-time-systems/discrete-time-model-predictive-control`, visited on June 1, 2014 (cit. on p. 51).

WAMIT (2014). *The state of the art in wave interaction analysis*. 2014. Available at: `http://www.wamit.com/index.htm`, visited on June 25, 2014 (cit. on p. 28).

Wavestar (2014). *Unlimited clean energy*. 2014. Available at: `http://wavestarenergy.com/`, visited on June 12, 2014 (cit. on pp. 8, 18, 147).

Weptos (2014). *Innovating in wave energy*. 2014. Available at: `http://www.weptos.com/da` (cit. on pp. 8, 153).

World Resource Institute, i. (2010). *Climate Analysis Indicators Tool - CAIT 2.0*. 2010. Available at: `http://cait2.wri.org/`, visited on Feb. 7, 2014 (cit. on p. 2).

Papers' Collection

A

A case study of short-term wave forecasting based on FIR filter: optimisation of the power production for the Wavestar device.

Ferri F.[a], **Sichani M.T.**[a] **and Frigaard P.B.**[a]

[a] Department of Civil Engineering, Aalborg University, Aalborg, Denmark.

In Proceeding of the 22nd International Offshore and Polar Engineering Conference (ISOPE), Rodhos, Greece, 2012.

ABSTRACT:
Short-term wave forecasting plays a crucial role for the control of a wave energy converter (WEC), in order to increase the energy harvest from the waves, as well as to increase its life time. In the paper it is shown how the surface elevation of the waves and the force acting on the WEC can be predicted using FIR filter. The predictors have been validated in laboratory with unidirectional regular and irregular waves. Here a single point absorber, (1:20) scale of the Wavestar device, is used. The results show that it is possible to predict wave and forces acting on the device using a properly designed FIR filter

KEY WORDS: FIR FILTER; NUMERICAL MODEL; ACAUSAL FUNCTION; WEC.

A case study of short-term wave forecasting based on FIR filter: optimization of the power production for the Wavestar device.

Francesco Ferri, Mahdi T. Sichani and Peter Frigaard
Department of Civil Engineering, AAU
Aalborg, Denmark

ABSTRACT Short-term wave forecasting plays a crucial role for the control of a wave energy converter (WEC), in order to increase the energy harvest from the waves, as well as to increase its life time. In the paper it is shown how the surface elevation of the waves and the force acting on the WEC can be predicted using FIR filter. The predictors have been validated in laboratory with unidirectional regular and irregular waves. Here a single point absorber, (1:20) scale of the Wavestar device, is used. The results show that it is possible to predict wave and forces acting on the device using a properly designed FIR filter

KEY WORDS: FIR filter; Numerical model; acausal function; WEC.

INTRODUCTION

The Most of the natural system has a control strategy ¨partially based on the prediction of the following steps; this give the chance to modify the undertaken path in order to follow the incoming input. The wave energy converters (WECs) do not distinguish themself for this basic idea, they need the knowledge of a portion of future in order to get the maximum output, (Falnes, 2002). If we glance at the underneath theory there are two main reasons related to the forecast request. The first is the presence of non-causal function in the model which simulates the dynamic of a WEC, while the second reason is the delay imposed by the controller and by the system to adjust themself at the new conditions. The system studied to obtain the forecast is a linear time invariant system with a finite length impulse response (FIR) based on the Airy's wave theory or linear theory; as the class name suggests this filter is based on a linear approximation. Although real systems are rather different form linear ones, using the superposition property it is possible to reach a good system identification as well as a good description of real sea states. Another good reason to choose a linear system as a forecast tool lives in the description of the conditions in which a WEC produces energy and where the WEC hydrodynamics parameter are evaluated: basically a low ratio between waves amplitude and significant body length. This leads to the description of the fluid-body interactions by the linear potential theory, where the pressure field can be solved by the well know boundary element method (BEM). Linear approximation means seeking the solution for small oscillation around the mean value; therefore this condition become consistent with the zone where the WEC can work. The output from a BEM software is then used to evaluate the velocity of the body excited by a given wave load, and that velocity can be used in an optimal control algorithm, (Korde, 2000). The waves have been predicted in the laboratory at a distance 5 and 10 times the floater diameter. These values have been chosen in order to fulfill the non-causal request of the system and the system delay as above mentioned, (Falnes, 2001). The WEC under investigation is a point absorber converter, with a hemispherical floater and a constrained motion: 1 degree of freedom (dof). The prediction system has been tested in regular and irregular 2D waves. It is important to underline the frame of reference, since from one measurement point no cross spectrum can be detected. In order to extend the concept in 3D waves then a cluster of filter is request, in order to separate the different wave components.

WEC MODELLING

The dynamic of a WEC is analyzed through the application of the Newton's second law. In this particular case the system under investigation is a single degree of freedom system, free to rotate in the pitch direction with small amplitude displacement. Holding this case the system can be approximate as a linear system by Eq. 1

$$m\ddot{x} = f_{hy}(t) + f_{PTO}(t) + f_{others}(t) \qquad 1$$

where m is the mass of the system $\ddot{x}$ is the acceleration of the system f_{hy} is the force acting on the system due to hydrodynamic interactions between the device and the water f_{PTO} is the force induced by the power take off (PTO) system integrated on the device f_{others} is the contribution of other force like mooring force or second order forces like friction, drift etc. The contribution of the second order forces is neglected, while the mooring force disappears since in this case study the buoy is hinged on a rigid structure. The hydrodynamic force can be decomposed into

Validation of a wave-body interaction model by experimental tests.

Ferri F.[a], **Kramer M.M.**[a] **and Pecher A.F.**[a]

[a] Department of Civil Engineering, Aalborg University, Aalborg, Denmark.

In Proceeding of the 23rd International Offshore and Polar Engineering Conference (ISOPE), Anchorage, Alaska, USA, 2013.

ABSTRACT:
Within the wave energy field, numerical simulation has recently acquired a world-wide consent as being a useful tool, besides physical model testing. The main goal of this work is the validation of a numerical model by experimental results. The numerical model is based on a linear wave-body interaction theory, applied for a point absorber wave energy converter. The results show that the ratio floater size/wave amplitude is a key parameter for the validity of the applied theory.

KEY WORDS: WAVE ENERGY CONVERTERS; PHYSICAL MODEL TESTING; NUMERICAL MODEL VALIDATION; HYDRODYNAMIC COEFFICIENTS.

Validation of a wave-body interaction model by experimental tests

Francesco Ferri, Morten Mejlhede Kramer, Arthur Pecher
Department of Civil Engineering, Aalborg University
Aalborg, Denmark

ABSTRACT

Within the wave energy field, numerical simulation has recently acquired a worldwide consent as being a useful tool, besides physical model testing. The main goal of this work is the validation of a numerical model by experimental results. The numerical model is based on a linear wave-body interaction theory, applied for a point absorber wave energy converter. The results show that the ratio floater size/wave amplitude is a key parameter for the validity of the applied theory.

KEY WORDS: Wave energy converters; physical model testing; numerical model validation; hydrodynamic coefficients.

INTRODUCTION

Nowadays, due to growth in theoretical knowledge and computational power, it has become easier to develop numerical tools that are capable of predicting the dynamical behavior of floating objects. Wave energy converters (WEC) are a relative new application in the marine environment, as their development first started in the seventies and after a period of stall, raised again in the latest part of the twentieth-century (Falnes, 2007). The main interest in this renewable resource is due to its intrinsic energy potential, the high energy density and the relatively long term predictability of the incoming sea state. The raw wave energy potential has been assessed in the order of 3.7 TW, which is slightly below the actual world power consumption (Mork et al., 2010). A leading or commercial technology is still not available and this can be addressed to various reasons. Among others WEC needs to withstand extreme loads resulting from storms, i.e. the ratio between operational and extreme loads on components of the device can exceed a ratio of 10, and severe environmental condition, i.e. salty water, and to produce electricity in agreement with different tight grid codes, i.e. requiring a satisfactory stable and smooth power production. In the last 40 years, more than hundred patents have been released, which differ in geometry, power extraction technology, working principle, etc. Drew et al. (2009) gave a general overview of the actual available technologies and strategies to increment the energy extraction capability. The latest point is dealing with control algorithms and it has been extensively studied in the last years, since a controller appears to be able to increase the energy extraction efficiency and keep unchanged the global cost. The basic idea for all the available solution is to cancel the intrinsic body reactance controlling the load reactance, as explained by Falnes (2002), or in other words to tune the system to be in resonance with the approaching wave, e.g. Babarit and Clement (2006) Brekken (2011), Falcao et al. (2008), Candido and Justino (2011) and Fusco and Ringwood (2012) are some of the available works. However, none of the proposed solutions seem to be without technical challenges, as a consequence of the system complexity. All the above cited works make use of the linear wave-body interaction theory, which has been inherited from the naval and off-shore oil and gas sectors. In those fields, the theory shows reliable result in relatively calm sea state, as they have been validate through many years of research and experience. In wave energy, the linear model is used also to evaluate global performance of a WEC. Thereby, the performance index can be used as basis for comparison of different technologies and to optimize the geometry of a specific technology. Generally speaking, the main weakness of this type of model is related with some of the assumptions behind the theory. For instance, WECs of the wave activated body type could develop significant viscous forces in certain operational conditions, which are neglected into the linear model formulation. Therefore, the numerical model can lead to a general performance overestimation. The general aim of the work carried out is to validate the wave-body interaction linear model for the Wavestar WEC by experimental tests and to evaluate a possible adimentional range of work for the model. The main outline of the article is briefly presented. Section: METHODS describes the general working principle of the selected device, together with a description of its general purpose and what will be compared, section: MODELS IMPLEMENTATION gives a more exhaustive description of its numerical and physical implementation and how the results have been assessed, section: RESULTS AND DISCUSSIONS compares and discusses the main outcomes from both the numerical and physical model, and finally section: CONCLUSIONS recapitulates and gives

Experimental Study of an Offshore Wind Turbine TLP in ULS Conditions

Wehmeyer C.[a], **Ferri F.**[b], **Skourup J.**[c] **and Frigaard P.B.**[b]

[a] Rambøll Offshore Wind, Esbjerg, Denmark;

[b] Department of Civil Engineering, Aalborg University, Aalborg, Denmark;

[c] Rambøll Port and Geostructures, Esbjerg, Denmark.

In Proceeding of the 23rd International Offshore and Polar Engineering Conference (ISOPE), Anchorage, Alaska, USA, 2013.

ABSTRACT:
An extensive model test program has been carried out in order to assess the behavior of a tension leg moored substructure as support of a Floating Offshore Wind Turbine (FOWT). The floater was inspired by an industrial design. The tests focused on the ultimate limit state (ULS) behavior, therefore no aerodynamic or gyroscopic effects were included, i.e. the turbine hub was represented by a lumped mass, and focus given to wave forces and dynamic behavior. The model tests have been conducted in the 3D deep water basin of the Hydraulics and Coastal Engineering Laboratory at the University of Aalborg at a scale of 1:80. The model tests were made with a range of monochromatic, bichromatic and irregular waves. All waves are modeled long crested and were run with and without sub and super harmonics. Three different structure layouts were tested, i.e. the tests were run with substructure only, with a rigid tower representation and with a flexible tower representation. Three submerged load cells measured the response of the tendons, and two accelerometers measured the response the total structure, being located at the substructure – tower interface and in the nacelle. The paper describes the setup of the test and a first set of interim results.

KEY WORDS: Floating Offshore Wind Turbine; Physical Model Test; Tension Leg Platform.

Experimental Study of an Offshore Wind Turbine TLP in ULS Conditions

Christof Wehmeyer
Rambøll Offshore Wind
Esbjerg, Denmark

Francesco Ferri
Hydraulics and Coastal Engineering Laboratory, Department of Civil Engineering, AAU
Aalborg, Denmark

Jesper Skourup
Rambøll Ports & Geostructures
Copenhagen, Denmark

Peter Bak Frigaard
Hydraulics and Coastal Engineering Laboratory, Department of Civil Engineering, AAU
Aalborg, Denmark

ABSTRACT

An extensive model test program has been carried out in order to assess the behavior of a tension leg moored substructure as support of a Floating Offshore Wind Turbine (FOWT). The floater was inspired by an industrial design. The tests focused on the ultimate limit state (ULS) behavior, therefore no aerodynamic or gyroscopic effects were included, i.e. the turbine hub was represented by a lumped mass, and focus given to wave forces and dynamic behavior. The model tests have been conducted in the 3D deep water basin of the Hydraulics and Coastal Engineering Laboratory at the University of Aalborg at a scale of 1:80. The model tests were made with a range of monochromatic, bichromatic and irregular waves. All waves are modeled long crested and were run with and without sub and super harmonics. Three different structure layouts were tested, i.e. the tests were run with substructure only, with a rigid tower representation and with a flexible tower representation. Three submerged load cells measured the response of the tendons, and two accelerometers measured the response the total structure, being located at the substructure – tower interface and in the nacelle. The paper describes the setup of the test and a first set of interim results.

KEY WORDS: Floating Offshore Wind Turbine, Physical Model Test, Tension Leg Platform

INTRODUCTION

A major difference between Offshore Oil & Gas structures and Offshore Wind structures is the applications of floating units in terms of water depth. The Offshore Wind Industry considers floating structures at much lower water depth, i.e. > 60 meter. In these waters the influence of non-linear irregular waves has a higher significance than in deep waters, especially in design conditions, see Fig. 1. As Offshore Wind Turbines are dynamically sensitive structures, it seems sensible to assume that the surface elevation history influences the structures behavior. Even though the floating part can be assumed more or less rigid, the slender tower supporting a heavy nacelle rotor assembly influences the structures response significantly, due to its flexibility. The presented test setup focused on the response of a Floating Offshore Wind Turbine Tension Leg Platform in design environmental conditions, i.e. the interaction of linear and non-linear extreme sea states and the corresponding motion response. Of interest are high frequency transient effects triggered by steep waves, known as ringing. These cause accelerations, which are prone to define the design level of turbine components. The afore mentioned steep waves cause as well slack line events, which if included in the design can be assumed design driving for anchors, tendons and connectors. The floater design was an industry inspired three armed structure.

Seen from a response point of view, Matha (2009), through numerical model studies, has firstly pointed out the important relationship between the FOWT pitch response and the tower flexibility. The pitch natural frequency of the total FOWT structure decreases with increasing tower flexibility. The finding was supported by further studies from e.g. Bachysnki et al (2012) and Bae et al. (2012). Seen from a loading point of view, Gurley et al (1998) have shown the importance of correct wave modeling in terms of high frequency pitch response. They found that second order irregular wave fields are much more prone to initiate ringing response, than first order irregular waves. Such ringing responses may be induced by steep sided waves and as well by, but not exclusively, as a consequence of slack line events, Kimball (2012). Goupee et al (2012) found that the TLP responses in

Non-linear numerical modeling and experimental testing of a point absorber wave energy converter.

Zurkinden A.S.[a], **Ferri F.**[a], **Beatty S.**[b], **Kofoed J.P.**[a] **and Kramer M.M.**[a]

[a] Department of Civil Engineering, Aalborg University, Aalborg, Denmark;

[b] Department of Mechanical Engineering, University of Victoria, Victoria, Canada.

In Ocean Engineering, vol. 78, pp. 11-21, 2014.

ABSTRACT:
A time domain model is applied to a three-dimensional point absorber wave energy converter. The dynamical properties of a semi-submerged hemisphere oscillating around a pivot point where the vertical height of this point is above the mean water level are investigated. The numerical model includes the calculation of the non-linear hydrostatic restoring moment by a cubic polynomial function fit to laboratory test results. Moreover, moments due to viscous drag are evaluated on the oscillating hemisphere considering the horizontal and vertical drag force components. The influence on the motions of this non-linear effect is investigated by a simplified formulation proportional to the quadratic velocity. Results from experiments are shown in order to validate the numerical calculations. All the experimental results are in good agreement with the linear potential theory as long as the waves are sufficiently mild i.e. $H/\lambda \leq 0.02$*. For steep waves,* $H/\lambda \geq 0.02$ *however, the relative velocities between the body and the waves increase thus requiring inclusion of the non-linear hydrostatic restoring moment to effectively predict the dynamics of the wave energy converter. For operation of the device with a passively damping power take-off the moment due to viscous drag is found to be negligible.*

KEY WORDS: WAVE ENERGY CONVERTER; POINT ABSORBER; NON-LINEAR HYDROSTATIC MOMENT; NON-LINEAR DRAG MOMENT; LINEAR POTENTIAL THEORY.

Ocean Engineering 78 (2014) 11–21

Contents lists available at ScienceDirect

Ocean Engineering

journal homepage: www.elsevier.com/locate/oceaneng

Non-linear numerical modeling and experimental testing of a point absorber wave energy converter

A.S. Zurkinden [a,*], F. Ferri [a], S. Beatty [b], J.P. Kofoed [a], M.M. Kramer [a]

[a] Department of Civil Engineering, Aalborg University, 9000 Aalborg, Denmark
[b] Department of Mechanical Engineering, University of Victoria, P.O. Box 1700 Victoria, BC, Canada

ARTICLE INFO

Article history:
Received 29 April 2013
Accepted 14 December 2013
Available online 17 January 2014

Keywords:
Wave energy converter
Point absorber
Non-linear hydrostatic moment
Non-linear drag moment
Linear potential theory

ABSTRACT

A time domain model is applied to a three-dimensional point absorber wave energy converter. The dynamical properties of a semi-submerged hemisphere oscillating around a pivot point where the vertical height of this point is above the mean water level are investigated. The numerical model includes the calculation of the non-linear hydrostatic restoring moment by a cubic polynomial function fit to laboratory test results. Moreover, moments due to viscous drag are evaluated on the oscillating hemisphere considering the horizontal and vertical drag force components. The influence on the motions of this non-linear effect is investigated by a simplified formulation proportional to the quadratic velocity. Results from experiments are shown in order to validate the numerical calculations. All the experimental results are in good agreement with the linear potential theory as long as the waves are sufficiently mild i.e. $H/\lambda \leq 0.02$. For steep waves, $H/\lambda \geq 0.04$ however, the relative velocities between the body and the waves increase thus requiring inclusion of the non-linear hydrostatic restoring moment to effectively predict the dynamics of the wave energy converter. For operation of the device with a passively damping power take-off the moment due to viscous drag is found to be negligible.

1. Introduction

The dynamical behavior of wave energy converters (WEC's) has been extensively investigated during the past years by means of analytical and numerical studies, including testing at laboratory scale and under real-sea conditions. Many concepts have been suggested namely the oscillating water-column principle, overtopping wave energy converters, point-absorber concepts and floating pitching devices. A comprehensive review of WEC systems can be found in Falnes (2007), Clement et al. (2002), and Falcao (2010). Examples of the state-of-the-art devices are provided in Neumann et al. (2008), http://www.wavedragon.net, http://www.wavestarenergy.com, http://www.weptos.com/. Point absorbers (PA) constitute an important class of wave energy converters particularly with regard to the relative simplicity of offshore deployments. This paper presents the results of a numerical and experimental study of a single Wavestar buoy (http://www.wavestarenergy.com).

For a single body device, maximum power capture in regular waves is known to occur when the PA is in a resonance condition (Falnes, 2002). The theoretical maximum power capture of an axisymmetric point absorber is reported in Budal and Falnes (1975), Evans (1976, 1981), and Mei (1976). Oscillating in resonance with the wave frequency will result in large motion amplitudes compared to the dimensions of the device. Advanced control strategies such as optimal phase or amplitude control (Falnes, 2002) are done to maximize power capture by encouraging resonance behavior. As a result, numerical models of WEC's under advanced control must account for non-linear effects such as non-linear hydrodynamic forces that occur at large motion amplitudes.

Numerical models of WEC dynamics, which assume inviscid, irrotational and incompressible flow, normally use Boundary Element Methods (BEM) to estimate the frequency dependent hydrodynamic loads. Such models often exhibit high inaccuracy in high wave steepness. The effects of nonlinearities induced by viscous drag, kinematics or control strategies are typically assessed by corresponding time domain models. The present study is tied up to the development of such a technique which is also referred to as hybrid frequency–time domain modeling. The successful implementation of such models is reported in Taghipour et al. (2008), Kristiansen et al. (2005), Barbarit and Clement (2006), Backer (2008), and Alves (2011). Recently, Guerinel et al. (2011, 2013) presented a model for a cone and a hemispherical shaped WEC geometry which takes into account the hydrostatic and Froude–Krylov nonlinear effects by an integration over the

* Corresponding author. Tel.: +45 9940 8570; fax: +45 9814 8243.
E-mail address: az@civil.aau.dk (A.S. Zurkinden).

0029-8018/$ - see front matter © 2013 Elsevier Ltd. All rights reserved.
http://dx.doi.org/10.1016/j.oceaneng.2013.12.009

Balancing Power Output and Structural Fatigue of Wave Energy Converters by Means of Control Strategies.

Ferri F.[a], **Ambühl S.**[a], **Fischer B.**[b] **and Kofoed J.P.**[a]

[a] Department of Civil Engineering, Aalborg University, Aalborg, Denmark;

[b] Division Control Engineering and Energy Storages, Fraunhofer Institute for Wind Energy and Energy System Technology, Kassel, Germany.

In Energies, vol. 7, pp. 2246-2273, 2014.

ABSTRACT:
In order to reduce the cost of electricity produced by wave energy converters (WECs), the benefit of selling electricity as well as the investment costs of the structure has to be considered. This paper presents a methodology for assessing the control strategy for a WEC with respect to both energy output and structural fatigue loads. Different active and passive control strategies are implemented (proportional (P) controller, proportional-integral (PI) controller, proportional-integral-derivative with memory compensation (PID) controller, model predictive control (MPC) and maximum energy controller (MEC)), and load time-series resulting from numerical simulations are used to design structural parts based on fatigue analysis using rain-flow counting, Stress-Number (SN) curves and Miner's rule. The objective of the methodology is to obtain a cost-effective WEC with a more comprehensive analysis of a WEC based on a combination of well known control strategies and standardised fatigue methods. The presented method is then applied to a particular case study, the Wavestar WEC, for a specific location in the North Sea. Results, which are based on numerical simulations, show the importance of balancing the gained power against structural fatigue. Based on a simple cost model, the PI controller is shown as a viable solution.

KEY WORDS: PASSIVE CONTROL; ACTIVE CONTROL; MODEL PREDICTIVE CONTROL (MPC); FATIGUE ANALYSIS; WAVE ENERGY CONVERTER (WEC); WAVESTAR.

Energies **2014**, *7*, 2246-2273; doi:10.3390/en7042246

OPEN ACCESS

energies

ISSN 1996-1073

www.mdpi.com/journal/energies

Article

Balancing Power Output and Structural Fatigue of Wave Energy Converters by Means of Control Strategies

Francesco Ferri [1,*], Simon Ambühl [1], Boris Fischer [2] and Jens Peter Kofoed [1]

[1] Department of Civil Engineering, Aalborg University, Sohngaardsholmsvej 57, Aalborg, Denmark; E-Mails: sia@civil.aau.dk (S.A.); jpk@civil.aau.dk (J.P.K.)

[2] Division Control Engineering and Energy Storages, Fraunhofer Institute for Wind Energy and Energy System Technology (IWES), Koenigstor 59, Kassel, Germany; E-Mail: boris.fischer@iwes.fraunhofer.de

* Author to whom correspondence should be addressed; E-Mail: ff@civil.aau.dk; Tel.: +45-9940-8574; Fax: +45-9940-8552.

Received: 25 December 2013; in revised form: 11 March 2014 / Accepted: 19 March 2014 / Published: 9 April 2014

Abstract: In order to reduce the cost of electricity produced by wave energy converters (WECs), the benefit of selling electricity as well as the investment costs of the structure has to be considered. This paper presents a methodology for assessing the control strategy for a WEC with respect to both energy output and structural fatigue loads. Different active and passive control strategies are implemented (proportional (P) controller, proportional-integral (PI) controller, proportional-integral-derivative with memory compensation (PID) controller, model predictive control (MPC) and maximum energy controller (MEC)), and load time-series resulting from numerical simulations are used to design structural parts based on fatigue analysis using rain-flow counting, Stress-Number (SN) curves and Miner's rule. The objective of the methodology is to obtain a cost-effective WEC with a more comprehensive analysis of a WEC based on a combination of well known control strategies and standardised fatigue methods. The presented method is then applied to a particular case study, the Wavestar WEC, for a specific location in the North Sea. Results, which are based on numerical simulations, show the importance of balancing the gained power against structural fatigue. Based on a simple cost model, the PI controller is shown as a viable solution.

Keywords: passive control; active control; model predictive control (MPC); fatigue analysis; wave energy converter (WEC); wavestar

---

1. Introduction

Wave energy converters (WECs) have a high potential to contribute significantly to the world energy mix in the future. The practically exploitable wave power potential has been assessed to be up to 3.7 TW, which is about a fourth of the global demand and roughly a double of the global electrical consumption [1]. The global power consumption is ∼15 TW of which 10% is electrical power. A diverse spectrum of WEC prototypes has been realised, and further investigations on control strategies for electricity harvesting (see e.g., [2]) and structural design (see e.g., [3]) are ongoing.

In terms of maximum absorbed power namely reactive controller or maximum energy controller (MEC), the condition for optimality was firstly derived in the 1970s [4]. In recent years, the focus has moved to a more realistic implementation of the proposed controller, using both passive and active controllers. In the context of wave energy, the term "passive controller" refers to a purely resistive control strategy such as proportional (P) controller, latching control, *etc*. The implementation of this type of control has been proved to work both in numerical and physical models [5–10]. On the other hand, the term "active controller" refers to those control strategies that imply energy feedback to the converter in order to increase the overall absorption. This class includes proportional-integral (PI) controller [10], suboptimal (PIDc) controller [11,12], MEC [13] and others. Recently, the optimal control theory within the framework of model predictive control (MPC) has been introduced in order to incorporate constraints in the control problem [14–17]. The MPC groups both passive and active controllers together in function of the applied constraints as shown in [17]. The advantage of using MPC is that it overcomes both the unrealistic amplitude of motion predicted by the theory and the inability to handle constraints in theoretical formulations.

Overall, much effort has been put into finding the optimal control strategies where the main focus is the maximisation of the gained mechanical or electrical energy. Albeit maximising the absorbed energy is an important task, it has not been proven whether this is also optimal from an overall cost point of view. Since the global aim of the sector is the commercialisation of WECs, the economic quota needs to be considered too. For offshore structure, due to the high ratio between extreme and operational loads, the structural cost is expected to lie in the range 30%–50% of the capital cost [18,19]. This entails that the economic quota can be related to the structural dimension in the first approximation. When designing a WEC, besides the static load, the structure also needs to account for cyclic loads (fatigue) in the prospected lifetime. While the static loads are uncoupled to the chosen control algorithm, the fatigue behaviour of the WEC is coupled to the control strategy. Standards for oil and gas (see e.g., [20]) as well as offshore wind turbines [21–23] and (offshore) steel structures [24,25] recommend the use of Stress-Number (SN) curves for fatigue analyses of structural designs. The SN curve characterises the material performance concerning fatigue and shows the relation between the number of load cycles at a given stress amplitude leading to fatigue failure.

The work shown in [26] defines a first attempt to combine control and fatigue analysis, but only a simple passive control strategy is considered. In addition, neither constraints nor controller phase delay have been addressed.

The present article shows a simple non-recursive methodology to select the best control strategy for a given WEC where both energy absorption and structural design are considered. The methodology

flowchart is presented in Figure 1. The dynamical model of the WEC is modified by a certain control strategy; five different strategies are used in the case study below. The WEC model receives the array of sea states as input, which defines the given location, and generates the annual energy production (AEP) for a given control strategy plus the time series of loads at the specific point selected for the fatigue assessment. The fatigue assessment is the second step of the algorithm, which receives as input the load time-series at a given location for a certain control strategy. Based on rain-flow counting [27] and offshore standards [22,24], the needed design cross section area for the given lifetime is evaluated. Derived from a simple parameterised, cost model the output from step one (AEP) and step two (material needed) can be combined. The control strategy leading to the lowest overall estimated cost could be chosen. The presented methodology is then applied to the Wavestar WEC [28] which is located at Danish Wave Energy Center (DanWEC) in Hanstholm (Denmark).

Figure 1. Work flow diagram of the proposed methodology. Subscript "i" refers to the i-th-control strategy and Ω defines the set of the selected control strategies. WEC: wave energy converter; and AEP: annual energy production.

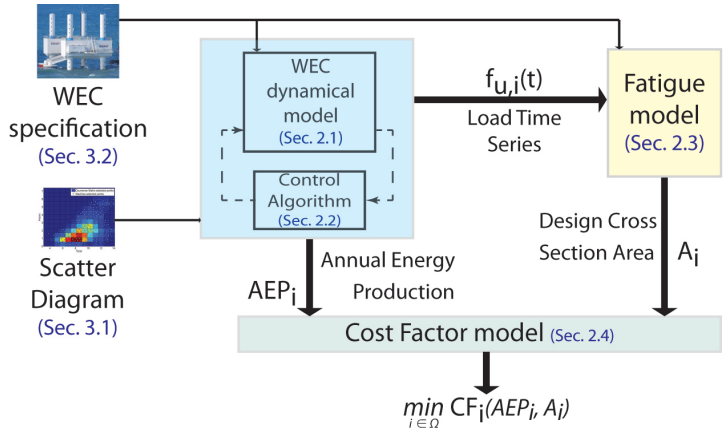

The paper is organised in five sections: Section 1 introduces the problem, together with the previous and proposed solution; Section 2 gives a general introduction of the different models used, namely WEC modelling, control problem and fatigue assessment; Section 3 specifies the equations presented in Section 2 for a particular WEC in a definite location; Section 4 contains a detailed discussion around the take-home messages embedded in the results; and Section 5 gives a brief recap of the work done besides the main outcome of the article.

2. Theoretical Background

A numerical model is used to describe the dynamical behaviour of a given WEC due to its flexibility. Despite the fact that numerical models are only an approximate representation of the corresponding physical models, once their accuracy is proven they represent a cheap and a fast tool for analysing a WEC, compared to physical modelling. In particular, numerical models based on linear potential

theory coefficients require low computation cost whilst outputting accurate results if the motion of the WEC is kept bounded around the linearisation point [29,30].

It is important to bear in mind that the proposed numerical model is specified for WECs of the point absorber type due to the problem formulation simplicity, but the same approach can be used for a generic WEC of the activated body type after providing a representative model for the wave-body interaction. In the following, the definition of the used numerical model, control strategies and fatigue model composing the main algorithm are presented. The equations are expressed in the international system of units (SI) system of measurement and each parameter is expressed in accordance with the SI base.

2.1. Numerical Model

A WEC can be defined as a dynamic system with one or more degrees of freedom, used to transform the wave energy content into useful—typically electrical—energy. In this work, only the absorbed mechanical power will be considered. The transfer from mechanical to electrical power is not taken into account. A point absorber is a particular type of WEC where the characteristic length of the device is small compared with the wavelength. A single body floating system, like a point absorber WEC, presents a resonant-like behaviour similar to a mechanical oscillator. The dynamical model of system can be obtained using the Newton-Euler equation. If the system has only one degree of freedom, then the Newton-Euler equation is simplified to [13]:

$$\sum_i F_i = M\ddot{x} \tag{1}$$

where F_i represents a generic force/moment acting on the rigid body; M represents the mass/inertia of the body; and $\ddot{x}$ represents the body linear/angular acceleration. The wave-body interaction can be linearised around the equilibrium point by assuming small body motions (that is when the motion's amplitude is much smaller than the wave length) and by considering steady state conditions. According to the diffraction/radiation theory, the hydrodynamic problem can be dealt with as two subproblems. A third contribution in the force summation of Equation (1) comes in place from the linearised hydrostatic problem [13]:

$$F_{ex} + F_{RAD} + F_{hy} + \sum_i F_i = M\ddot{x} \tag{2}$$

where F_{ex} is the wave excitation force; F_{RAD} is the radiation force; and F_{hy} is the hydrostatic restoring force.

The wave excitation force is defined as an external force acting on the fixed structure subjected to a wave field and is defined by a complex function associated with the frequency of the incoming wave. It accounts for two distinct contributions namely the diffraction force plus the first order Froude-Krylov force evaluated for fixed wetted surface. The radiation force describes the loads acting on the structure due to its motion in still water and is defined as [13]:

$$F_{RAD}(\omega) = V(\omega)\left[j\omega\left(A(\omega) - a_\infty\right) + B(\omega)\right] = j\omega X(\omega) H_{RAD}(\omega) \tag{3}$$

where $V(\omega)$ is the Fourier transform of the velocity of the system; $A(\omega)$ is the added mass coefficient; a_∞ represents the limit value of the added mass when the frequency tends to infinity; $B(\omega)$ is the

radiation damping coefficient; and $H_{RAD}(\omega)$ is the frequency response function of the radiation force per unit of body velocity. The hydrostatic restoring force, F_{hy}, describes the difference between gravitational force and the buoyancy force due to the submerged volume. F_{hy} is proportional to the body displacement, where the hydrostatic stiffness coefficient K_{hy} is the proportionality factor.

Equation (2) can be recast into Equation (4) by including the wave-body interaction [13]:

$$\left[j\omega(M + A(\omega) - a_\infty) + B(\omega) + B_i + \frac{1}{j\omega}K_{hy}\right] V(\omega) = F_{ex}(\omega) + F_u(\omega) \tag{4}$$

where B_i represents any additional source of damping; and the summation of the external forces has been replaced by the control force (F_u). The control force represents the force imposed by the WEC's power take off (PTO) system, *i.e.*, electrical generator. The effect of the controllable load into the body dynamic will be discussed in the next section. By taking the inverse Fourier transform, Equation (4) is mapped into the time-domain, leading to an integro-differential equation, commonly known as the Cummins equation [31]:

$$(M + a_\infty)\ddot{x}(t) + \int_{-\infty}^{t} h_{RAD}(t - \tau)\dot{x}(\tau)d\tau + B_i\dot{x}(t) + K_{hy}x(t) = f_{ex}(t) + f_u(t) \tag{5}$$

where $\ddot{x}(t)$ is the body acceleration; $\dot{x}(t)$ is the body velocity; $x(t)$ is the body displacement; h_{RAD} is the impulse response function of the radiation force; $f_u(t)$ is the control force; and $f_{ex}(t)$ is the wave excitation force. For a simple system such as a point absorber, the convolution integral can be efficiently substituted by a state-space model [32,33]. Even if the two formulations are both an approximation of the frequency response function, the state space model formulation is adopted when the model predictive controller is conceived, because the model of the WEC is built in a state-space form.

2.2. WEC Control Strategies

The average mechanical power ($\bar{P}$) absorbed by a generic WEC over a time period (T) is the mean value of the product of the control load, $f_u(t)$, and the body velocity in the used degree of freedom, $\dot{x}(t)$ [13]:

$$\bar{P} = \frac{1}{T}\int_0^T f_u(t)\dot{x}(t)dt \tag{6}$$

The absorbed mean power is often used as a performance indicator for a generic WEC. The dynamic response of a WEC, and its production capabilities, is affected by the applied control scheme. Because the scope of the work is the balanced power optimisation of a WEC against structural fatigue, it is important to define both non-aggressive and aggressive controllers. In the context of this work, the term "aggressiveness of a controller" is meant in a qualitative sense. It refers to the actuator duty cycle.

Five different control strategies will be introduced and used in the case study. Three of them, P, PI and PIDc, are applied for the true comparison while the other two controllers (MEC and MPC) are employed as benchmarks. The P, PI and PIDc controllers have been chosen for their implementation simplicity and efficacy. They are listed in increasing aggressiveness order. The power performance of the three controllers will be compared with the maximum achievable mean power. The theoretical superior limit

of $\bar{P}$ depends on the model set-up; the simulation parameters are defined in Section 3.1. If the PTO is ideal, the MEC will define the WEC performance upper bound. On the other hand, if the PTO is not ideal, the MPC will be considered to be the optimal controller due to the inability of the MEC to handle physical constraints.

2.2.1. MEC

For a simple oscillator, the optimal energy transfer between external source and the moving body happens when the system is in resonance with the input's frequency. The analytical solution of the maximum absorbed power problem is [13]:

$$V(\omega) = \frac{F_{ex}(\omega)}{2(B(\omega) + B_i)} \tag{7a}$$

$$F_u(\omega) = -Z_i^*(\omega)V(\omega) \tag{7b}$$

where $Z_i^*(\omega)$ is the complex conjugate of the intrinsic mechanical impedance of the oscillator [13]:

$$Z_i(\omega) = j\omega(M + A(\omega) - a_\infty) + B(\omega) + B_i + \frac{1}{j\omega}K_{hy} \tag{8}$$

Some considerations can be drawn from Equation (7):

- Since $B(\omega)$ is a real function, the resonance condition is achieved when the body velocity is in-phase with the wave excitation force (Equation (7a)).
- The power maximisation is an impedance matching problem [34]. Therefore, the control load needs to counteract the reactance of the oscillator (Equation (7b)).
- Some energy needs to be fed back to the floater during a wave cycle. Therefore, the actuator needs to be reversible, and the instantaneous power will be both positive and negative at different positions of the wave cycle.
- The actuator is considered ideal, *i.e.*, there is no limitation on the force amplitude together with an unitary transfer function (no phase delay).

In addition to the inability to handle physical constraints and the unrealistic large amplitude of motion, the practical implementation of this type of controller is crippled by the non-causality of the control law. The definitions introduced in Equation (7) require information about the future incoming wave [13] and body velocity [35], which needs to be predicted. Given that the system is highly damped, the body velocity is a broad-band process, and its prediction cannot be reliable. On the other hand, under the assumption that the wave spectrum is a relative narrow-band process, its prediction can be considered reliable. Several works have addressed the issue of forecasting the incoming wave in the short range [36–38] for a real-time application of the controller. It is important to bear in mind that for a numerical simulation the input time series is known a priori, so there is no need to forecast the future waves since they are already available.

Among the two methods introduced in Equation (7), the reference velocity method (Equation (7a)) is adopted. In order to implement this type of controller, a low level velocity tracking system needs to be implemented; a PI controller has been chosen as a low-level logic.

Another issue arises when the reference velocity needs to be evaluated: the transfer function (TF) between the excitation force and the optimal reference is frequency dependent. This type of problem can be solved using an observer of the excitation force state, in the form of an Extended Kalman Filter [38] or a Hilbert Transform [39].

2.2.2. Model Predictive Controller

MPC refers to an advanced, digital control technique. Its basic principle is to calculate optimal values for the control signals over a certain time horizon in the future. To this end, it uses a dynamic model of the plant, current measurements to update the dynamic states of this model, and the future course of external inputs; the latter being the wave excitation force and the control force in this paper. Given that the dynamic model sufficiently represents the real system and that measurements for updating the states and a prediction of the future wave excitation force are available, the WEC's behaviour over the time horizon can be calculated depending on the control force. This is used to determine the optimal trajectory of the control force by solving a possibly constrained optimisation problem. This optimisation problem includes a cost function that reflects the control objectives. The optimal control force is then applied to the point absorber until the new measurement and predictions samples are available. After that, the whole procedure is repeated in order to account for unforeseen disturbances. The ability of directly incorporating constraints in the optimisation problem makes MPC a straightforward choice for control problems with constraints on the control input or the plant states.

Several applications of MPC for the control of WEC are reported in the literature. Some of them directly incorporate the objective of maximum average power into the cost function [14–17]. For this work, the variant presented in [17] was chosen. It uses a non-standard method for deriving the time discrete model from the time continuous model in Equation (5). The resulting control algorithm allows for relatively large sample periods without degrading the accuracy. Large sample periods are generally desirable because the computational effort in solving the optimisation problem at every time step is large.

The general formulation of the applied cost function J is the time discrete version of Equation (6), that is [17]:

$$J[k] = \sum_{i=k}^{k+N_p} f_u[i]\dot{x}[i] \tag{9}$$

where $k \in \mathbb{Z}$ denotes the current time instant; and N_p is the number of time steps of the prediction horizon. The overall optimisation problem with the constraint on the control force can be written as [17]:

$$\underset{f_u[i]}{max} J[k] \quad \text{such that} \quad |f_u[i]| \leq f_{max}, \qquad i = k, ...k + N_p \tag{10}$$

If feasible, the solution of this problem yields an optimal control sequence over the prediction horizon. Using the receding horizon control principle, only the current sample f_u[k] is applied to the WEC, leading to the ability of the controller to react to unforeseen disturbances. The whole problem formulation can be found in [17]. Here, it should only be noted that for using computationally efficient algorithms to solve Equation (10), the defined optimisation problem has to be convex. Reference [17] shows that the cost function (Equation (9)) leads to a quadratic program, *i.e.*, linearly constrained

optimisation problem with a quadratic objective function. Although no universal proof of its convexity is given, this property can be ensured by a numerical check after the design of the controller.

2.2.3. P Controller—Passive Controller

When the WEC actuator only works in an unidirectional mode, no energy can be fed back to the oscillator. This type of controller commonly known as passive damper has the great advantage of requiring simple machinery and having a smaller ratio between peak average power. Otherwise, since the body reactance will not be compensated, the WEC will mainly work in a tight range around the natural frequency of the oscillator, limiting the overall system efficiency. The general form of the control force is as follows [10]:

$$f_u(t) = c_c \dot{x}(t) \tag{11}$$

where c_c is the damping coefficient of the control force.

2.2.4. PI Controller—Spring-Damper Controller

The PI controller is also denoted as spring-damper controller because an additional term proportional to the body displacement is used to compensate the intrinsic reactance of the body. In theory, the PD controller can also achieve similar results, but as shown in [10] it presents a narrower frequency band, which leads to a lower overall efficiency. These type of controllers are optimal controllers in the case of regular waves, but they become non-optimal for irregular waves. The downgrade is related to the lack of compensation of the memory term of the fluid. In fact, the optimal control law needs to include the convolution term related to the fluid memory, as can be derived from the application of the Pontryagin's maximum principle [12]. The general form of the PI control force is as follows [10]:

$$f_u(t) = c_c \dot{x}(t) + k_c x(t) \tag{12}$$

where k_c is the stiffness coefficient of the control force.

2.2.5. PID Controller with Memory Compensation—Sub-Optimal Controller

The PID controller is a mass-spring-damper controller with the introduction of an additional convolution term. The general form of the controller is as follows [12]:

$$f_u(t) = c_c \dot{x}(t) + k_c x(t) + m_c \ddot{x}(t) + \int_{-\infty}^{t} h_{RAD}(t-\tau)\dot{x}(\tau)d\tau \tag{13}$$

where m_c is the mass coefficient of the control force. The convolution integral of Equation (13) represents the compensation of the memory term of the fluid (*i.e.*, radiation force). This type of controller is a sub-optimal controller because it approximates the optimal non-causal solution with a causal one [12,35]. In order to avoid the uncertainties related to the body velocity prediction, see Section 2.2.1., the integral term concerning the time interval from $t + \delta t$ to ∞ is neglected.

2.3. Fatigue Assessments

Fatigue failure is an important failure mode of offshore structures and expectably even more for WECs where the resonance condition is sought. For estimating the fatigue of a structural part, the Stress-Number (SN) of cycles curve together with Miner's rule [40] is used here. SN curves for offshore applications can be found in [24]. Miner's rule uses sequence independent linearised damage accumulation and assumes that fatigue failure occurs when [40]:

$$\sum_{i=1}^{N_i} \frac{n_i}{N_i} = 1 \tag{14}$$

where N_i is the total number of cycles of a given stress range leading to fatigue failure; and n_i the expected number of cycles at the same stress range during the life-time of the WEC. The SN curve shows the number of cycles leading to fatigue failure of a given stress amplitude. When using the SN approach, a linear or bilinear formulation, where plastic deformation is allowed, can be implemented. Rain-flow counting (see [27]) can be used to discretise the load time series into groups/intervals of load amplitudes. A certain interval i has n_i cycles per year of a certain load range ΔQ_i (e.g., normal force). It is assumed that the stress range $\Delta\sigma_i$ can be expressed by a design parameter z (e.g., cross section area) and the corresponding load range ΔQ_i:

$$\Delta\sigma_i = \frac{\Delta Q_i}{z} \tag{15}$$

The bilinear SN curve has a slope change at $\Delta\sigma_D$ where the number of cycles to failure N_D is equal to 1×10^6:

$$\begin{aligned} N &= K_1 S^{-m_1} \quad \text{for} \quad S \geq \Delta\sigma_D \\ N &= K_2 S^{-m_2} \quad \text{for} \quad S < \Delta\sigma_D \end{aligned} \tag{16}$$

where $K_{1,2}$ are the stress intensity factors; and $m_{1,2}$ are the crack growth parameters. A design equation can be used to calculate the design equation parameter z and can be written for a bilinear approach using the Miner's rule as, see e.g., [41]:

$$1 - \underbrace{\sum_i \sum_j \sum_{k_1} \frac{T_{FAT} n_{ijk_1}}{K_1^c} s_{ijk_1}^{m_1} P(H_{m0_i}, T_{P_j})}_{S \geq \Delta\sigma_D} - \underbrace{\sum_i \sum_j \sum_{k_2} \frac{T_{FAT} n_{ijk_2}}{K_2^c} s_{ijk_2}^{m_2} P(H_{m0_i}, T_{P_j})}_{S < \Delta\sigma_D} = 0 \tag{17}$$

where $\log(K^c)$ is the characteristic value of $\log(K)$; n_{ijk} is the number of stress ranges per year given the significant wave height H_{m0_i} and the wave peak period T_{P_j}; $s_{ijk} = \Delta Q_{ijk}/z$ is the stress range ijk given H_{m0_i} and T_{P_j}. The fatigue design life T_{FAT} is equal to $FDF \cdot T_L$ with fatigue design factor (FDF) and design life time T_L. The joint probability of H_{m0_i} and T_{P_j} is equal to $P(H_{m0_i}, T_{P_j}) = P(H_{m0_i})P(T_{P_j}|H_{m0_i})$ and indicates the probability of occurrence of a certain sea state.

2.4. Cost Factor

This section focuses on bringing together the influence of a certain control strategy on harvested energy, which will define the income during lifetime, and the resulting structural design which drives the investment costs. In order to compare different control strategies, a simple economical model is used.

From a certain structural detail, one can hardly comment on the control strategy's overall cost impact. But one can, based on some simple assumptions get an idea of the relative impact of the different control strategies on the overall cost.

It is assumed that the total lifetime costs consists of one part, which is dependent on the control strategy (called C_1, mainly cost for PTO and structure of PTO arm) and other investment costs (called C_2, e.g., platform, or electricity connection to shore), which are assumed to be constant for all control strategies. The control dependent costs are assumed to be proportional to the cross sectional area of a certain critical structural component. The cost factor CF_c, which shows the ratio between total investment costs and the absorbed energy (AEP_c), for a given control strategy c can be written as:

$$CF_c = \frac{C_1 + C_2}{E_c} = \frac{p \cdot C_{ref,tot} \frac{A_c}{A_{ref}} + (1-p) \cdot C_{ref,tot}}{AEP_c} \tag{18}$$

where $C_{ref,tot}$ is the total lifetime cost of a certain design with a reference control strategy; A_{ref} is the cross sectional area of a critical structural component for the reference control strategy; A_c is the resulting cross sectional area of control strategy c; and p represents the percentage of the total lifetime costs, which are dependent on the control strategy. Even though the main assumption adopted—linear relation between WECs cost and structural dimensions—is rather stringent, the cost factor can still give a valuable tool to gain insight into the economic potential of a WEC and afterwards ease the comparison between proposed concepts.

3. Case Study Results

This section presents a case study focused on the Wavestar WEC. The particular WEC has been chosen mainly because its numerical model already has been compared with experimental data from a scaled physical model of the device [29,30]. The effect of different control strategies and constraints on the power output as well as the fatigue of different subcomponents are assessed. The Wavestar device is located at DanWEC (Danish North Sea coast) near Hanstholm. This prototype (see Figure 2) consists of four piles and two floaters as well as a platform where the mechanical and electrical devices are stored. The floaters which are excited by the passing waves drive a hydraulic system which impels a turbine and a generator. The Wavestar device was installed in 2009 and fed electricity into the grid until it was moved to the harbour for reconfiguration in September 2013.

3.1. Site Assessement

Sea state measurements over a period of six years are provided by [42], based on recordings from a buoy (6332100N, 474700E, water depth: 17 m) located near the Wavestar device. The dataset contains the frequency domain wave parameters, significant wave height (H_{m0}) as well as the peak period (T_P), measured with a time interval of 3 h. The resulting probability of occurrence of different wave states are shown in Table 1 and are used in this case study.

The incoming wave direction is not considered in this case study and is assumed to be of minor importance for the load and power output assessment, as a consequence of the symmetry of the system.

Figure 2. (**A**) Wavestar prototype at Hanstholm (Denmark); and (**B**) sketch of floater details with main components and coordinate system.

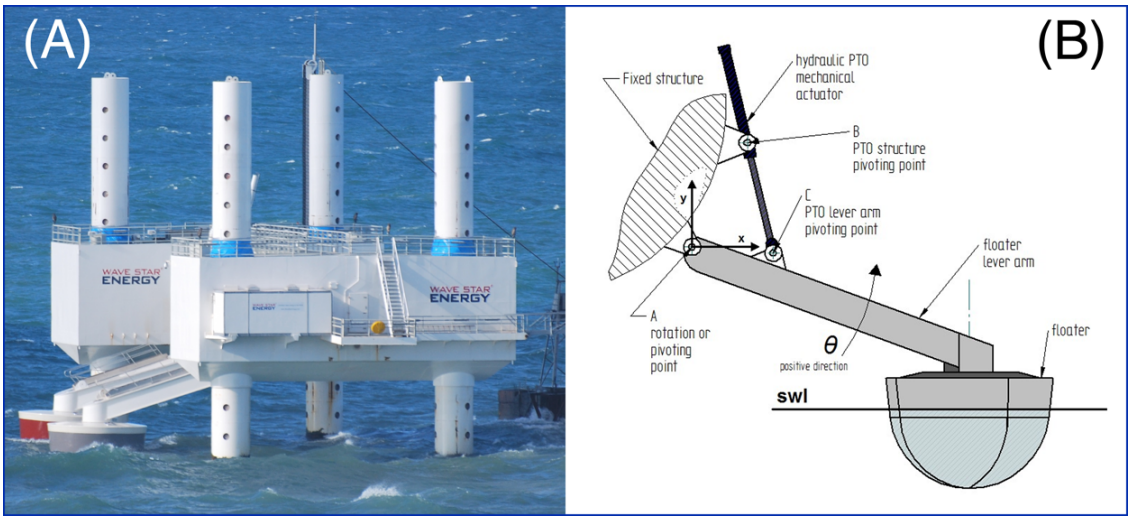

Table 1. Relative occurrence of different wave states from six years, buoy measurements ($[H_{m0}]$ = m, $[T_P]$ = s). Both parameters defines the mean value over an interval. The adopted discretisation is 1 s in T_p and 0.5 m in H_{m0}.

H_{m0}/T_P	0.5	1.5	2.5	3.5	4.5	5.5	6.5	7.5
0.25	-	-	-	0.04	0.04	0.02	0.01	-
0.75	-	-	-	0.07	0.17	0.11	0.05	0.01
1.25	-	-	-	-	0.06	0.11	0.05	0.01
1.75	-	-	-	-	-	0.06	0.05	0.02
2.25	-	-	-	-	-	0.01	0.05	0.02
2.75	-	-	-	-	-	-	0.01	0.02
3.25	-	-	-	-	-	-	-	0.01

3.2. Numerical Model of the Wavestar WEC

Since the Wavestar machine belongs to the point absorber WEC class, the model introduced in Equation (5) can be used to describe the dynamic response of the system. Table 2 and Figure 3 summarise the model parameters used in this case study.

For each sea state described in Table 1, a surface elevation time series of 30 h is fed into the numerical model. The time series' length is determined by the need to minimise the statistical uncertainty of the model input, related to the irregularity of the wave. The White Noise filtering technique is adopted to generate the surface elevation time series, using Wavelab [43]. The filter uses a JONSWAP spectral model [44] with peak enhancement factor (γ) equal to 3.3 and a sample frequency equal to 20 Hz.

The linear hydrodynamic coefficients as well as the hydrostatic stiffness coefficients have been evaluated using a commercial Boundary Element Method (BEM) solver [45]. The radiation frequency

functions plotted in Figure 3 have been interpolated with a rational polynomial approximation, whose order is reduced using the Hankel singular value [32]. The resultant second order TF is listed in Table 2. Order reduction is an important topic mostly in the MPC formulation because of computational time, but for consistency the minimum order model has been adopted throughout the work.

Figure 3. Hydrodynamic frequency response functions for the Wavestar model: (**A**) bi-axis plot of the wave excitation moment magnitude coefficients (solid line) and phase coefficients (dotted line); and (**B**) plot of the radiation moment damping coefficients (solid line) and added mass coefficients (dotted line).

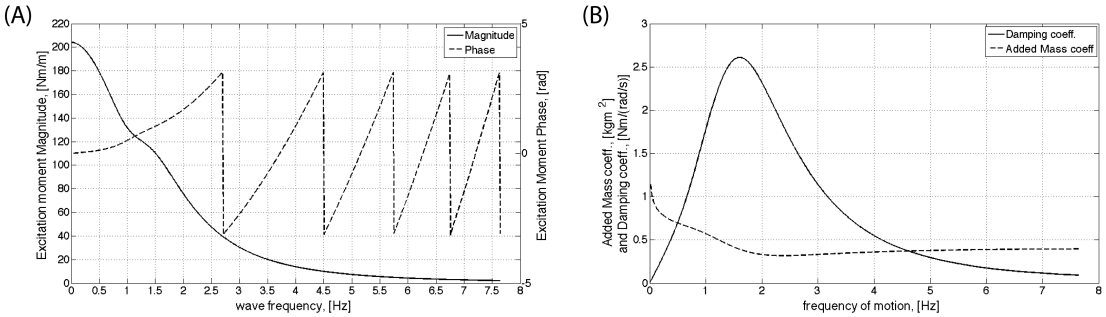

Table 2. Model parameters for the Wavestar WEC [10,30,45]. TF: transfer function.

Hydrostatic and structural parameters			
Moment of Inertia	J_{st}	2.45×10^6	kg·m^2
Hydrostatic Stiffness	K_{hy}	14.0×10^6	N·m/rad
Maximum exerted moment	M_{max}	1.0×10^6	N·m
Drag Coefficient	C_D	0.25	-
PTO stroke	S_{PTO}	2.0	m
Natural Period in Pitch	T_n	~3.5	s
Hydrodynamic model parameters			
Added mass at infinity frequency	a_∞	1.32×10^6	kg·m^2
Radiation Moment TF numerator	a_{RAD}	$[\,4.93\,,\,1.08\,] \times 10^6$	-
Radiation Moment TF denominator	b_{RAD}	$[\,1\,,\,2.56\,,\,5.16\,]$	-
Excitation Moment TF numerator	a_{EX}	$[\,5.4 \times 10^{10}\,,\,2.7 \times 10^{12}\,]$	-
Excitation Moment TF denominator	b_{EX}	$[\,3.6 \times 10^4\,,\,3.9 \times 10^5\,,\,1.5 \times 10^6\,,\,2.6 \times 10^6\,,\,1.6 \times 10^6\,]$	-

The power performance of the WEC is evaluated for the unconstrained model and for two other cases, all defined in Equation (5):

- Case 1—Unconstrained case. Neither the saturation of the maximum PTO force, nor the maximum allowed PTO stroke, nor the additional damping is included.
- Case 2—Unconstrained case with linearised viscous drag moment implemented as additional damping. Neither the saturation of the maximum PTO force, nor the maximum allowed PTO stroke is included.

- Case 3—PTO constraint and linearised viscous drag moment implemented as additional damping. The PTO constraint is implemented as a saturation function of the full control force.

Hereafter, the rationale behind these choices is briefly given. The linearised viscous drag moment has been inserted in the WEC model in order to account for a viscous dissipative effect. This type of effect is normally negligible when the system operates in a non-resonant condition due to the relative low body velocity. On the other hand, when the resonance condition is achieved, a significant part of the energy is dissipated in turbulence [46]. Given that the main focus of the work is on the implementation of optimal control strategies, the viscous drag moment is likely to play an important role in the assessment of the absorbed power. The viscous drag coefficient reported in Table 2 has been obtained from laboratory tests [30].

The PTO constraint is introduced to simulate a model as close as possible to the device deployed at DanWEC in Hanstholm (Denmark). This type of constraint reflects a realistic feature of many types of actuators, to be used in a WEC, and it is worth investigating its effect in both power and fatigue assessment. The PTO constraint is taken from [10]. All the parameters presented are summarised in Table 2. The simulations were carried out using the Simulink/Matlab environment.

In order to simulate a realistic PTO system, two other parameters were identified besides the saturation function applied in Case 3:

- Case 4—End-Stop of the PTO actuator. Another external force is added in the force summation in the right hand side of Equation (5). The force is proportional to both the penetration of the piston into the end-stop system and the penetration velocity.
- Case 5—PTO delay [10]. In this case, a second order TF is applied to the theoretical control force $f_u^*(t)$ in order to obtain the true control force $f_u(t)$.

In both cases, the PTO was saturated as in Case 3. The sensitivity analysis of the WEC model response with respect to these two additional cases shows that the PTO constraint is the most critical parameter. In fact, in Case 4, the End-Stop system is rarely exerted as a result of the non-optimality of the controller induced by the limited PTO capacity. Further, in Case 5, the PTO delay is small compared with the system dynamic. Therefore, the induced phase shift accounts for only a small reduction of the power performances. Since the contribution of Cases 4 and 5 is below 1% in both AEP and cross section area, these cases will be omitted in the following.

3.3. Control Strategies of the Wavestar Device

The controller schemes presented in Section 2.2 have been introduced into the WEC model in order to estimate its average power performances. As shown in Figure 1, the implementation of the dynamical response of the WEC is uncoupled with the structural fatigue assessment:

- P—proportional or passive controller (Section 2.2.3.);
- PI—proportional-integral or spring-damper controller (Section 2.2.4.);
- PIDc—proportional-integral-derivative with memory compensation or sub-optimal controller (Section 2.2.5.);
- MEC—maximum energy controller (Section 2.2.1.);

- MPC—model predictive controller (Section 2.2.2.).

The MEC is considered a benchmark for Cases 1 and 2 since it defines the theoretical upper bound of the absorbed energy. For Case 3, the MPC will be considered as reference point; the MEC is indeed unable to deal with constraints. The remaining controllers are then used to assess the effect of control aggressiveness into the absorbed power.

The MPC cannot be considered an applicable controller in the present formulation, because in the simulations the control algorithm was assumed to have perfect knowledge of the future excitation moment over the full prediction horizon. Therefore, uncertainties related to the excitation moment prediction are discarded with a reasonable increment of the power performance. Furthermore, the current state of the plant is assumed to be perfectly known. Hence, the MPC results are considered an upper bound in terms of the objective function rather than a practicable solution in the present formulation. The implementation of the different controllers is described in detail in the following.

The MEC is implemented using the velocity tracking logic where the velocity signal is generated in two steps: first, the actual wave frequency and amplitude are observed using the Hilbert transform [39] and, second, the observed frequency and amplitude are used in a look-up table to recover the reference velocity at the actual sample time. The general control layout traces out the implementation presented in [47]. The Ziegler-Nichols closed-loop tuning method was used to tune the PI low-level velocity controller [48].

The MPC model is based on the state-space approximation of the WEC model summarised in Table 2. The sample time employed in the MPC is 0.05 s. The other important parameter used to tune the performances of the MPC is the length of the prediction horizon, N_p. At each time sample, the optimiser searches the optimal trajectory over the prediction horizon using the Hildreth's quadratic programming algorithm [49]. The computational cost of this method is a cubic function in the N_p variable. Recalling that the simulation time length is 30 h, it is clear how the definition of N_p becomes a crucial point. The best compromise between MPC performance and computational time was found to be N_p = 120, with negligible degradation of the power performances if compared to the MEC in the unconstrained case. Using this set of parameters, the MPC roughly foresees one full wave ahead. The MPC predicts the same AEP of the maximum energy controller in Cases 1 and 2, as will be presented in Figure 4. The difference between the two controllers grows as the wave period increases, because the prediction horizon becomes too short. In the considered case study, the probability of occurrence of the long period sea state is relative low, which reduces the global influence of the actual MPC set up error. Depending on the specific scatter diagram, N_p needs to be adapted to the current sea state. The adjustment will be based on the results of a sensitive analysis on the power performance of the WEC in function of N_p.

Controllers P, PI and PIDc have already been defined up to the establishment of the control parameters (c_c, k_c, m_c). They have been assessed using a global maximisation routine, whose objective function is the mean absorbed power. The global maximum point is obtained using a local maximisation algorithm (Nelder-Mead method [50]) with randomly seeded starting points (scattered search [51]). The algorithm is repeated for each sea state, each controller and each case.

A special attention needs to be given to the PI and PIDc controllers when the PTO moment is constrained. In order to reduce the error accumulated in the integrator introduced by the abrupt

saturation, an integral windup with back-calculation scheme was used [52]. The main improvement given by the windup scheme is a reduction of controller overshooting.

Figure 4. AEP of the WEC as a function of the applied controller for each simulated case. Control type proportional (P) controller, proportional-integral (PI) controller, proportional-integral-derivative with memory compensation (PID) controller, maximum energy controller (MEC) and model predictive control (MPC).

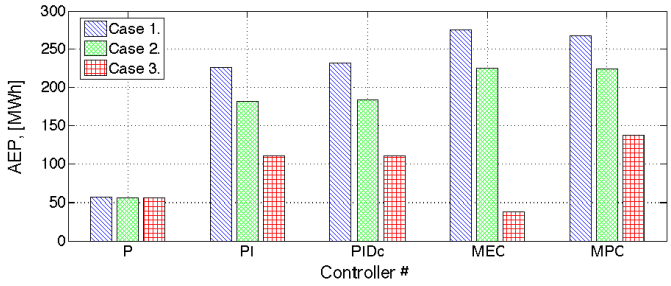

The absolute performance of the different controllers is quantified using the power matrix, which defines the average power production for each simulated sea-state. Figures 5 and 6 report the power matrix of P and PI controller, for the unconstrained (Case 1) and PTO constrained cases (Case 3), normalised by the benchmark controller power matrix. As introduced in Section 2.2.3., the passive control strategy is unable to tune the response of the oscillator to the incoming wave frequency. Therefore, only sea-states with T_p close to the natural period T_n of the system will have a power production equal to the reference point. The performances of the P controller reduce quickly as T_p moves away from T_n (Figure 5A); the natural period of the floater is $\sim$3.5 s. On the other hand, since the PI controller can extend the bandwidth of the oscillator, it will result in a power performance similar to the benchmarks (MEC), which is shown in Figure 5B.

Moreover, when the PTO moment is bounded, most of the energy in the high energetic sea-states cannot be absorbed (Figure 6A), leading to a better relative performance of the P controller relative to both the benchmark (MPC) and PI controller. As introduced in Section 2.2, the benchmark changes as the considered case changes. It is important to notice that the power performance of the MPC worsens when the PTO saturation is included, while the P controller does not undergo significant performances variations. This fact is in connection to the relatively smaller control moments commanded by the P controller, relative to the other controllers. Figure 6B shows that the PI controller can handle PTO constraints almost without losing performance when compared with the MPC. A direct consequence of this lies in the practical applicability of the controller. Taking into account the implementation simplicity of the PI controller and its negligible power performance reduction in the constraint case, this method becomes much more attractive than the MPC, provided an effective sea state adaptation of the PI controller parameters is available.

Figure 5. Comparison of P and PI controller power performance normalised by the MEC results, for unconstrained case (Case 1): (**A**)—P controller power matrix for Case 1; and (**B**)—PI controller power matrix for Case 1.

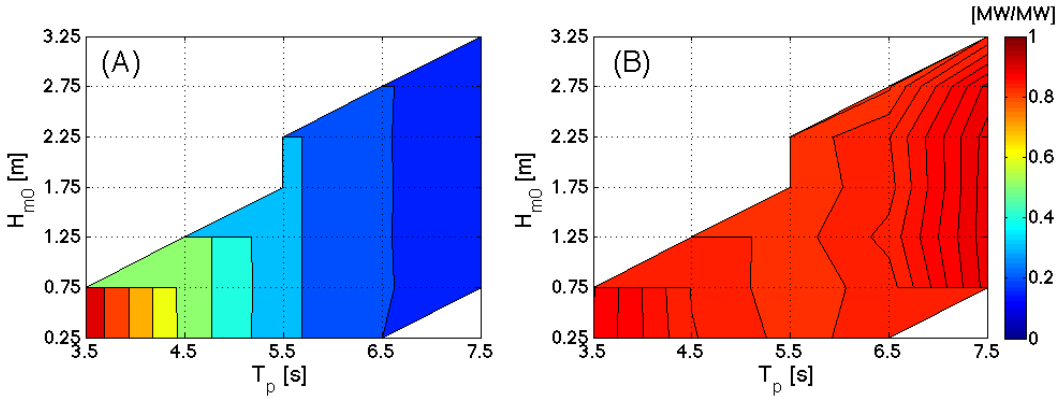

Figure 6. Comparison of P and PI controller power performance normalised by the MPC results, for constrained case (Case 3): (**A**)—P controller power matrix Case 3; (**B**)—PI controller power matrix Case 3.

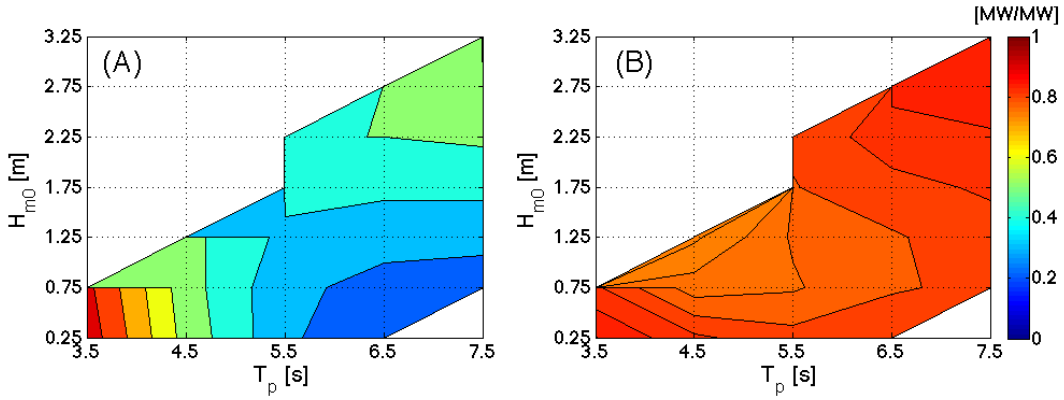

Using the power results of the Wavestar WEC and the scatter diagram shown in Table 1, the AEP can be evaluated. Unlike the power matrix, the AEP should be regarded as the global relative energy performance indicator of the particular WEC at the specific location. In Figure 4, the AEP of the Wavestar WEC at the Hanstholm location is given for each case and controller.

The energy performance of the P controller can be increased reasonably by a factor of two when an active controller is adopted into the WEC model. The five-fold increase of the unconstrained case is mainly linked to the unrealistic motion amplitude achieved in the high-energetic sea states. In those conditions, the linear theory assumptions are heavily violated, and the simulation results become unreliable. The viscous dissipative term accounts for a global performance reduction of up to 15% if an active controller is used. For the passive controller, the small body velocity induced by the non-resonant WEC makes the turbulence effect negligible [30].

Both active controllers used (PI and PIDc) show similar results. In addition, their operation is close to the benchmark capability. Given that the performance gap does not seem to be a function of the applied constraint, it is reasonable to assume that both PI and PIDc controllers have a flat power performance compared with the optimal controller. This trend is also visualised in Figures 5 and 6B.

3.4. Fatigue Assessment

For the fatigue assessment, the focus is put on different components of the floater arm. Due to the fact that the floater can be taken out of the water during storm events, extreme events are of minor importance for the structural design of the floaters. Critical subcomponents whose failure may lead to an overall breakdown are bolted as well as welded connections. Therefore, the focus here is on the two welded details and one bolted connection shown in Figure 7. Failure of one of these would lead to structural failure of the arm due to inability of controlling the motion of the arm. Time-series of loads of 30 h are compiled for different control strategies and each wave state shown in Table 1.

Figure 7. Position of the two welded details as well as the bolted connection between the arm and the power take off (PTO) of the Wavestar device.

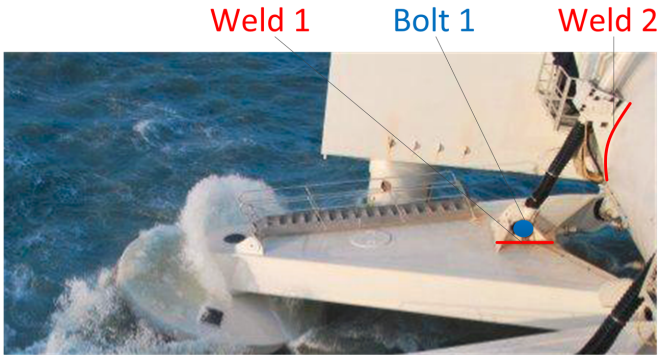

Table 3 and Figure 8 show the two SN curves, taken from [24], used in this case study. Weld 1 is located at at a cruciform joint, and Weld 2 is placed parallel to the direction of applied stress. Fatigue behaviour of both welds can be explained considering the SN curve of a so-called "F" detail [24]. Here it is assumed that cathodic protection is used. The bolted connection between the arm and the PTO is in double shear. According to [24] for bolts in shear a linear SN curve should be done. The SN curve is defined by the parameters m_1 and m_2, which are equal to the negative inverse slope of the SN curves and $\log(K_1)$ as well as $\log(K_2)$, which show the intercept of $\log(N)$ axis.

Table 3. Parameters of Stress-Number (SN) curves shown in Figure 8 for the three different considered connections at the Wavestar WEC. The parameters are taken from [24].

	m_1 (-)	$\log(K_1)$ (-)	m_2 (-)	$\log(K_2)$ (-)
Weld 1	3	11.455	5	15.091
Weld 2	3	11.455	5	15.091
Bolt 1	5	16.301	-	-

Figure 8. Considered SN curves for the Wavestar case study. The SN curves are taken from [24] and the parameters m_1, m_2, K_1 and K_2 (see Equation (17)) are shown in Table 3.

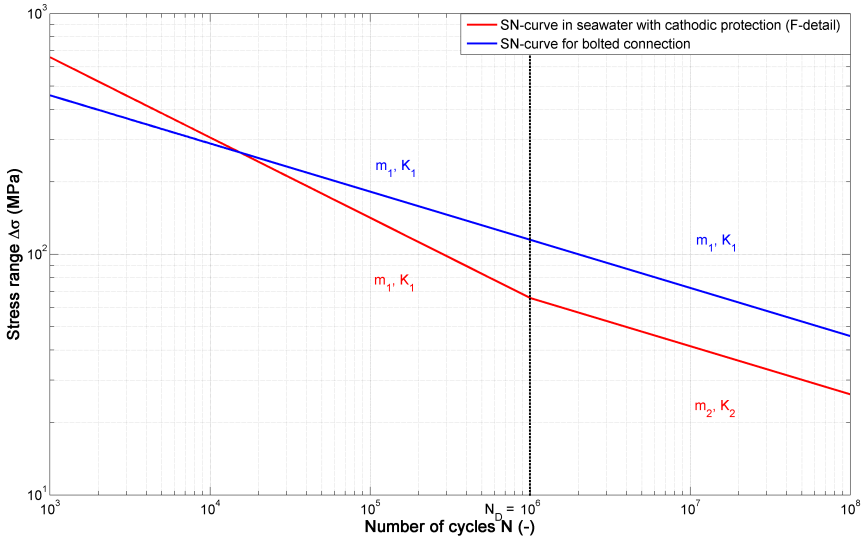

The life time T_L of the Wavestar power plant is assumed to be 20 years, and no maintenance actions are considered here. The fatigue design is performed with a FDF of 3, which is in accordance with [22] for details which are not inspected.

Figure 9 shows the design cross section area of the three different connections defined in Figure 7 for different control strategies as well as different cases. The design cross section area is meant to be the cross section area resulting from the design. In general, different control strategies as well as different cases lead to different cross section areas. The simplest control strategy leads to the smallest fatigue loads onto the structure and, therefore, to the smallest cross section area. For this control strategy, the impact of different cases is negligible. For all other controllers, the unconstraint case (Case 1) gives the largest cross section areas. When viscous drag effects on the floater are included (Case 2), the loads onto the structure are decreased compared with Case 1 and, therefore, the needed cross section is reduced. The smallest cross section areas are reached in Case 3 where the PTO maximum deliverable moment is included in the simulations.

Figure 10 shows the number of expected cycles during 20 years for Weld 1 using MPC with different cases. Figure 10A shows the expected number of cycles, $n_{1,i}$, during one life-time of 20 years for a given load range ΔQ_i in the unconstraint Case 1 whereas Figure 10B shows the number of expected cycles, $n_{2,i}$, for MPC given constraint Case 3. Part C in Figure 10 shows the difference between the number of expected cycles during one life-time for a given load range. The constraint leads to more cycles with small and load amplitudes equal to the constraint whereas the unconstraint case leads to a small number of loads with large amplitude. Cycles with large load amplitudes have a large impact on fatigue due to the fact that the number of cycles up to failure for a given load range relates exponentially to the load range (see Equation (16)). This small number of large loads are the reason why the design cross section area is increased for Case 1 (unconstraint) by a factor of 5 (see Figure 9) compared with Case 3 (constraint).

Figure 9. Design cross section areas for the three different connections defined in Figure 7 for different control strategies as well as different implementation forms (Cases).

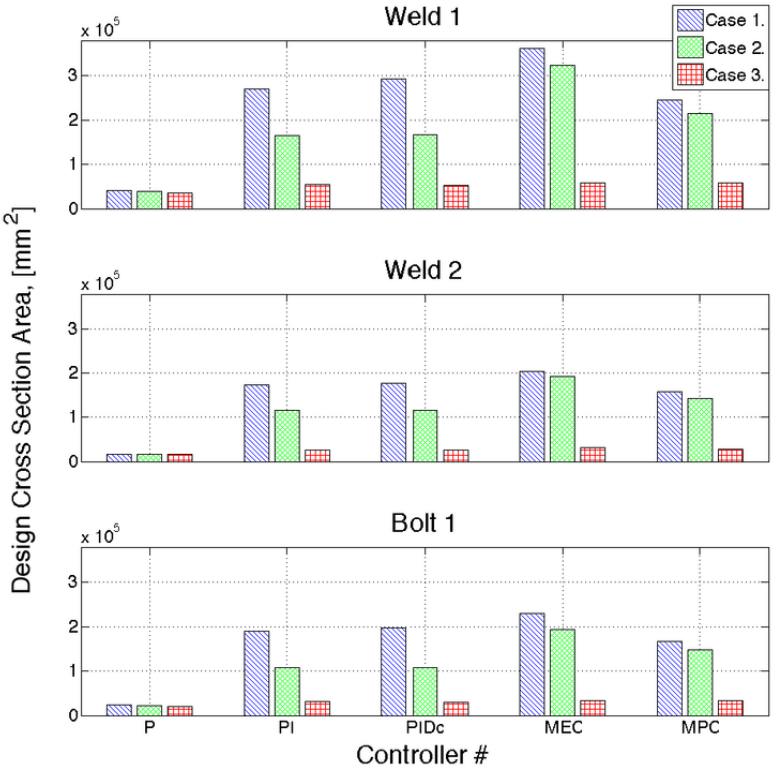

Figure 10. Expected number of cycles for a given load range during life-time of 20 years: (**A**) expected number of cycles for a given load range at Weld 1, using MPC and Case 1 (unconstraint); (**B**) expected number of cycles at Weld 1, using MPC and Case 3 (constraint); and (**C**) difference of number of cycles between **A** and **B**.

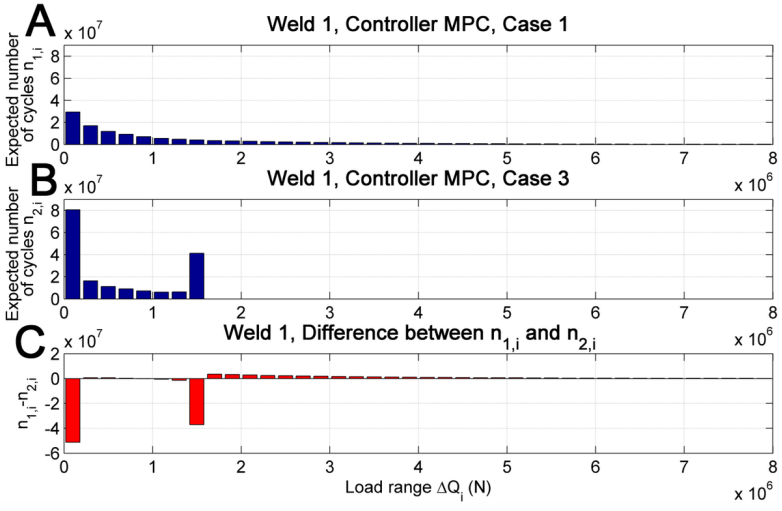

4. Discussion

In the following, the discussion of the results for the specific case study elaborated in Section 3 is given. It is important to bear in mind that whilst the proposed method can be extended, prior to modification, to other WECs of the activated body type, any extrapolation of the results of Section 3, for any other device, should be considered inaccurate. Different conclusion should also be expected if different connection points are chosen for a given WEC.

Figure 11 shows the comparison between the AEP and the cross section area of Weld 1 for Case 1 (A-Unconstrained case) and Case 3 (B-PTO constrained case) in function of the applied control strategy. The data is normalised by the results of Case 1, MEC. The PTO constraint induces a two-fold reduction of the AEP of the WEC, but it also drives a similar mitigation of the structural fatigue of Weld 1. The same conclusion can be drawn for the other connections. The usage of the PI controller leads to a two-fold growth of the AEP of the WEC, keeping the increment of the required cross section area to 1.5-fold. The AEP defined so far is related to the absorbed energy. If a PTO efficiency of 70% between the absorbed energy and the electrical energy produced is adopted, the AEP will vary. The AEP of the P controller will be reduced by 30% while the AEP of the PI controller will suffer a larger reduction, due to the doubling of losses exerted in the bidirectional process, [53]. In addition, when an active controller is used, the system complexity will increase with respect to a simple passive controller, which might induce a reduction in availability of the WEC.

Figure 11. Comparison of AEP (blue) and Cross Section Area (green) between different control strategies, for (**A**) Case 1 and (**B**) Case 3. The data is normalised by the AEP and Cross Section Area of MEC Case 1. The Cross Section Area data refers to the Weld 1 detail.

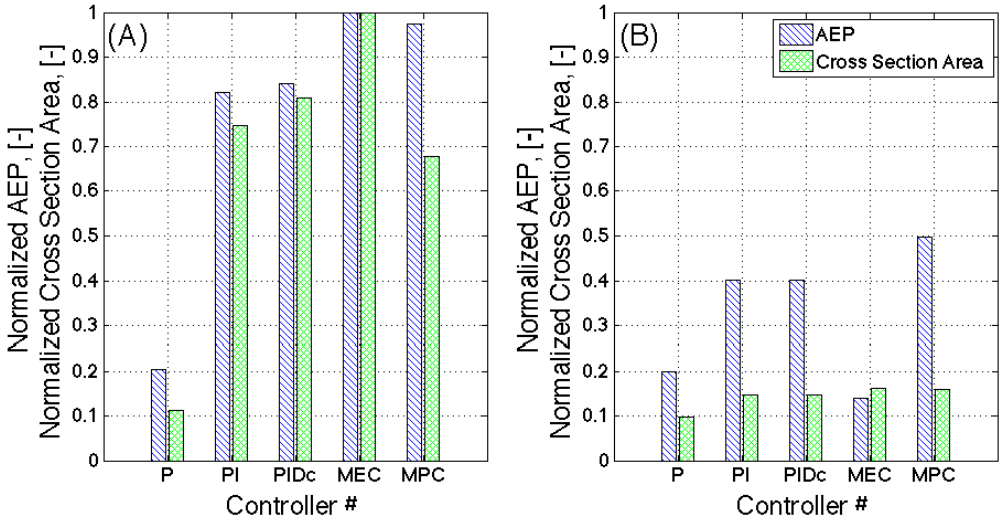

Based on the cost factor, CF (see Equation (18)), different control systems can be compared on an economical level. It is assumed that the critical structural component, whose cross section area is used for calculating the cost factor, is Weld 1. Figure 12 shows CF values, which are normalised by the CF value of Case 1 and $p = 0\%$, for different control strategies. As expected, the normalised CF increases when p

is increased. The impact on the p-value is larger for Case 1 but for Case 3, the p-value impact is of minor importance. For Case 3, the different CF values are mainly driven by the different control strategies and its resulting AEP. Lowest CF values are for all p values reached when using the MPC controller.

Figure 12. Comparison of Cost Factor CF between different control strategies and p-values, for (**A**) Case 1 and (**B**) Case 3. The Cost Factor is normalised by the CF resulting from P controller for Case 1 (p = 0%). The Cross Section Area data refers to the Weld 1 detail.

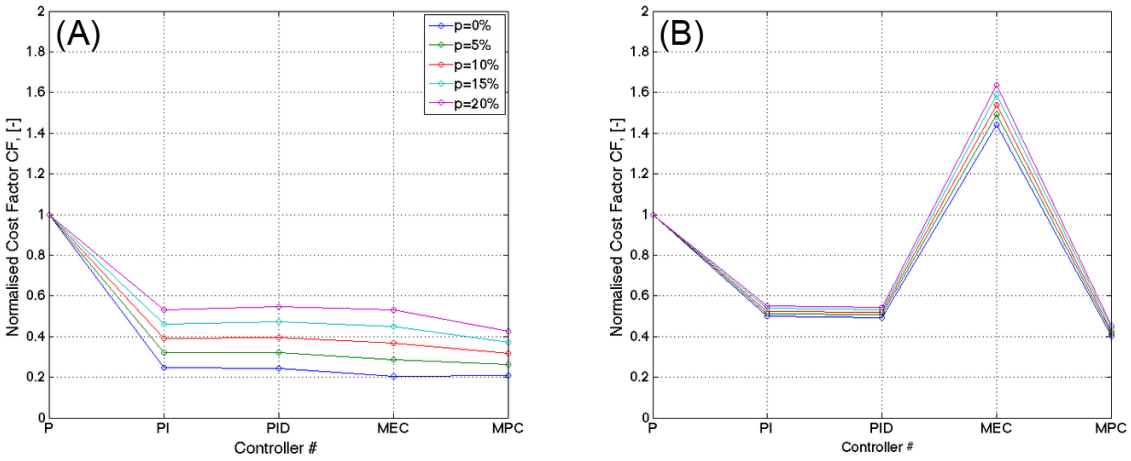

A sensitivity analysis has been carried out in order to investigate the impact of detuned control parameters on AEP and cross section area. Table 4 shows the AEP and cross section area of Weld 1 for P and PI controller, using Case 3 (constraint plus viscous drag). The P and PI power optimised gains are detuned by $\pm 20\%$ and the results are normalised by the AEP maximised case; c_c is the proportional gain and k_c is the integral gain.

Table 4. Results of the sensitivity analysis for P and PI controller. Variation of the cross section area (red text) of Weld 1 and annual energy product (blue text), normalised by the controller where AEP is maximised.

	P controller	**PI controller**		
		1.2 k_c	**k_c**	**0.8 k_c**
1.2 c_c	+5%	+1%	−3%	−10%
	−1%	−3%	−3%	−8%
c_c	0%	+4%	0%	−8%
	0%	−2%	0%	−5%
0.8 c_c	−6%	−5%	+3%	−5%
	−1%	−5%	−1%	−4%

As expected, the AEP is reduced in all cases, while the fatigue loads acting on the structure can be reduced by choosing the right detuning combination. From an economic point of view, only those cases where the reduction of power output comes along with reduced fatigue loads are of potential interest.

This is clear in the case of the P controller where the amount of damping is positively correlated to the structural load, and only the reduced damping coefficient ($0.8c_c$) can be considered. Figure 13 shows the variations of CF with respect to the p-parameter obtained from Equation (18). When the cost is assumed to be independent from the control strategy, *i.e.*, $p = 0\%$, then CF is greater than one. There is a break-even point at $p^* = 16.7\%$. That is, if the part of the cost that is influenced by the controller makes more than 16.7% of the overall costs, then it is economically wise to apply the detuned coefficient.

Figure 13. Variation of the cost factor with respect to the percentage of the cost depending on the control strategy for the P controller with reduced damping coefficient 0.8 c_c.

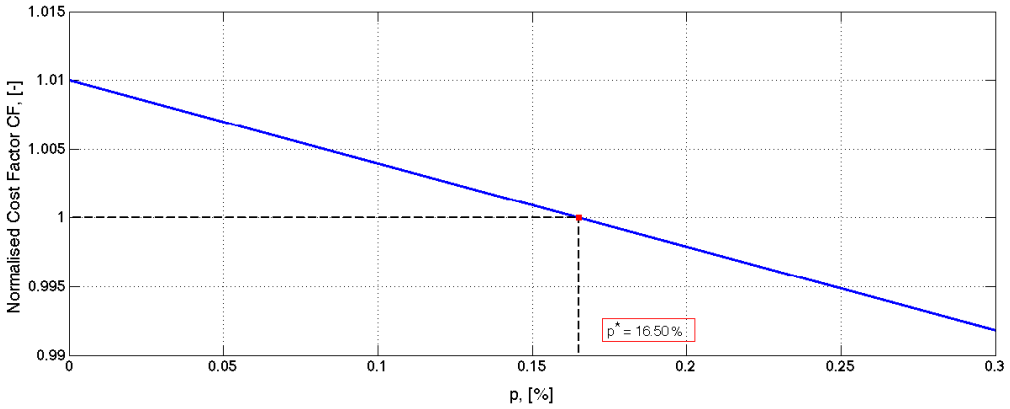

For the PI controller, Figure 14 shows the variation of the cost factor for all the cases from Table 4 and for $p = 10\%$. The contour plot indicates that for $p = 10\%$ the power-optimal controller is also economically optimal. The best detuned controller happens at 100% c_c and 80% k_c, but in this case the break-even point is $p^* = 68\%$. Up to now, only very little cost data is publicly available for WEC (see e.g., [54]). Hence, for a rough estimate of an upper bound of p, it is possible to look at the figures in the offshore wind sector. The capital expenditure varies between 50%–70% of the overall life-cycle costs of an offshore wind turbine [54–57]. The costs of the turbine itself make about one third of it [58,59]. That is, the value of p is very likely to lie well below 0.7×0.33 (23%). Transferring this p-value to the WECs, shows that only for the P controller economic improvement is realistic by detuning controller parameters. The higher break-even point of the PI controller compared to the wind turbine case leads to the conclusion that detuning the parameters does not seem to be a reasonable choice. Albeit the above parallel give some indication whether the CF is affected by the detuned control gains, it is important to bear in mind that due to the variety of WEC concepts the comparison is somehow coarse.

In addition, there is a clear lack of specificity in the wave energy sector which makes finding an economical optimum point an ill-conditioned problem.

Although the proposed methodology presents a novel and alternative description of the power optimised WEC taking into account structural fatigue several assumption has been adopted. The economical model assumes a linear dependence between structural dimensions and cost, while for a more comprehensive analysis a detailed cost model of the system should be created. Other factors as systems' complexity, operational over rated generator power, commissioning, decommissioning and operational and maintenance costs, PTO efficiency, downtime periods, components reliability, *etc*. should also be

included in the analysis. On the other hand, in relation of the actual stage of the wave energy sector what is needed is mostly a rough sieving of the available concepts rather than a detail analysis.

Figure 14. Comparison of Cost Factor CF using PI controller (Case 3) with different damping and stiffness coefficients. The CF values are normalised by the optimal P (P_{opt}) and I (I_{opt}) controller values where the power output is maximised. The value p is set equal to 10% and the Cross Section Area data refers to the Weld 1 detail.

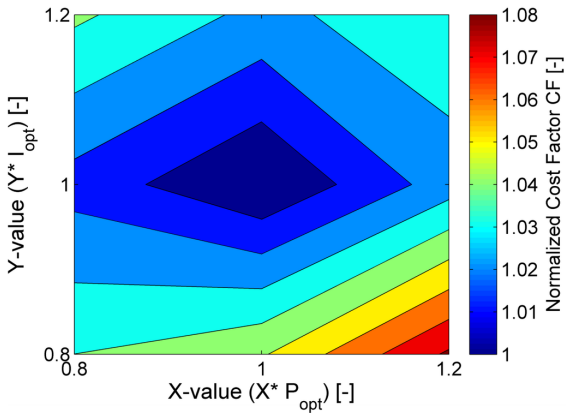

5. Conclusions

Given that the exploitation of the potential energy embedded in ocean waves can play an important role in the future energy mix, so far much effort has been put in finding the best energy configuration for a WEC. But other effects like the influence of the control strategy on the structural fatigue should not be disregarded. This might lead to designs of WECs that are not cost effective.

The methodology presented in this article aims at selecting a controller that balances energy yield and structural fatigue in an economic sense. To this end, well known control strategies, standard fatigue calculations and a simple cost model are brought together (Figure 1). The controller parameters are optimised with respect to maximum energy production. In a subsequent step, fatigue analysis and cost estimation follow.

A case study using a numerical model of the Wavestar WEC including a non-ideal PTO has been carried out to exemplarily demonstrate the method (Section 3). Even if it is applied for a specific case study, it can easily be adopted for other WEC of the wave activated body type. In contrast, the results of the case study should only very cautiously be generalised, because a specific device at a specific location has been considered.

These particular results are summarised as follows. Both energy as well as fatigue is governed by the constraint of the PTO moment for all considered controllers rather than by the position constraint or the PTO delay (Section 3.2). Two main technical conclusions can be drawn from the comparison of the passive controller (P controller) with the two active sub-optimal controllers (PI and PIDc controller) in the case with constrained PTO moment (Figure 11B). Both active controllers:

- harvest 80% of the maximum achievable energy and twice as much energy as the passive controller, and;
- need roughly 50% more material at the three considered structural details in order to reach the same life-time as the passive controller.

Feeding the proposed economic model with these results reveals that the best choice for the selected WEC is an active sub-optimal controller (Figure 12). Furthermore, the sensitivity analysis carried out with the PI controller showed that the controller parameters, which have been optimised with respect to maximum AEP, are also the cost-optimal parameters (Figure 14).

Altogether, this paper indicates the importance of balancing power output and structural fatigue for the choice of an economically optimal controller. A number of other factors such as operational *vs.* rated generator power or system complexity have not been considered here. Future work should aim to include these other factors, and more sophisticated cost models have to be developed. This would provide a basis for a certification guideline for WEC. Further steps could also be to implement the overall cost consideration already in the optimisation of the control algorithm.

Acknowledgements

The authors gratefully acknowledge the financial support from the Danish Council for Strategic Research under the Programme Commission on Sustainable Energy and Environment (Contract 09-067257, Structural Design of Wave Energy Devices) which made this work possible.

Author Contributions

The article has been planned by Francesco Ferri and Jens Peter Kofoed. The work load, in terms of numerical simulation and analysis, have been equally shared between Francesco Ferri, Boris Fischer and Simon Ambühl, who had a fundamental role in the model development too.

Conflicts of Interest

The authors declare no conflicts of interest.

References

1. Mork, G.; Barstow, S.; Kabuth, A.; Pontes, T.M. Assessing the Global Wave Energy Potential. In Proceedings of the 29th International Conference on Ocean, Offshore and Arctic Engineering, Shanghai, China, 6–11 June 2010; Volume 3, pp. 447–454.
2. Abraham, E.; Kerrigan, E.C. Optimal Active control and optimisation of a wave energy converter. *IEEE Trans. Sustain. Energy* **2013**, *4*, 324–332.
3. Ambühl, S.; Kramer, M.; Kofoed, J.P.; Sørensen, J.D.; Ferreira, C.B. Reliability Assessment of Wave Energy Devices. In *Safety, Reliability, Risk and Life-Cycle Performance of Structures and Infrastructures*; Deodatis, G., Ellingwood, B.R., Frangopol, D.M., Eds.; CRC Press LLC: Boca Raton, FL, USA, 2013.
4. Evans, D.V. Power from water waves. *Ann. Rev. Fluid Mech.* **1981**, *13*, 157–187.

5. Ringwood, J.; Butler, S. Optimisation of a Wave Energy Converter. In Proceedings of the IFAC Conference on Control Applications in Marine Systems (CAMS), Ancona, Italy, 7–9 July 2004; pp. 155–160.
6. Marquis, L.; Kramer, M.; Frigaard, P. First Power Production Figures from the Wavestar Roshage Wave Energy Converter. In Proceedings of the 3rd International Conference on Ocean Energy (ICOE), Bilbao, Spain, 6–8 October 2010; pp. 1–5.
7. Durand, M.; Babarit, A.; Pettinotti, B.; Quillard, O.; Toularastel, J.L.; Clément, A.H. Experimental Validation of the Performance SEAREV Wave Energy Converter with Real Time Latching Control. In Proceedings of the 7th European Wave and Tidal Energy Conference (EWTEC), Porto, Portugal, 11–13 September 2007.
8. Babarit, A. Optimisation Hydrodynamique et Controle Optimal d'un Recuperateur de l'Energie des Vagues. Ph.D. Thesis, Ecole Centrale de Nantes, Nantes cedex 3, France, 2005. (in French)
9. Babarit, A.; Clement, A.H. Optimal latching control of a wave energy device in regular and irregular waves. *Appl. Ocean Res.* **2006**, *28*, 77–91.
10. Hansen, R.H.; Kramer, M.M. Modelling and Control of the Wavestar Prototype. In Proceedings of the 9th European Wave and Tidal Energy Conference (EWTEC), Southampton, UK, 5–9 September 2011.
11. Nebel, P. Maximizing the efficiency of wave-energy plant using complex-conjugate control. *Proc. Inst. Mech. Eng. Part I J. Syst. Control Eng.* **1992**, *206*, 225–236.
12. Nielsen, S.R.K.; Zhou, Q.; Kramer, M.M.; Basu, B.; Zhang, Z. Optimal control of nonlinear wave energy point converters. *Ocean Eng.* **2013**, *72*, 176–187.
13. Falnes, J. *Ocean Waves and Oscillating Systems*; Cambridge University Press: Cambridge, UK, 2002.
14. Hals, J.; Falnes, J.; Moan, T. Constrained optimal control of a heaving buoy wave-energy converter. *J. Offshore Mech. Arctic Eng.* **2011**, *133*, doi:10.1115/1.4001431.
15. Richter, M.; Magana, M.E.; Sawodny, O.; Brekken, T.K.A. Nonlinear model predictive control of a point absorber wave energy converter. *IEEE Trans. Sustain. Energy* **2013**, *4*, 118–126.
16. Brekken, T.K.A. On Model Predictive Control for a Point Absorber Wave Energy Converter. In Proceedings of the IEEE Trondheim PowerTech, Trondheim, Norway, 19–23 June 2011; pp. 1–8.
17. Cretel, J.A.M.; Lighbody, G.; Thomas, G.P.; Lewis, A.W. Maximisation of Energy Capture by a Wave-Energy Point Absorber using Model Predictive Control. In Proceedings of the 18th IFAC World Congress, Milan, Italy, 28 August–2 September 2011; pp. 3714–3721.
18. Teillant, B.; Costello, R.; Weber, J.; Ringwood, J. Productivity and economic assessment of wave energy projects through operational simulations. *Renew. Energy* **2012**, *48*, 220–230.
19. *Cost Estimation Methodology: The Marine Energy Challenge Approach to Estimating the Cost of Energy Produced by Marine Energy Systems*; Commissioned by Carbon Trust; Entec, UK Ltd.: London, UK, 2006.
20. *Petroleum and Gas Industries—Fixed Steel Offshore Structures*; International Standard ISO 19902; International Organization for Standardization: Geneva, Switzerland, 2007.

21. *Wind Turbines—Part 1: Design Requirements*; International Standard IEC 61400-1; International Electrotechnical Commission: Geneva, Switzerland, 2005.
22. *Design of Offshore Wind Turbine Structures*; Offshore Standard DNV-OS-J101; Det Norske Veritas: Høvik, Norway, 2013.
23. *Guideline for the Certification of Offshore Wind Turbines*; Germanischer Lloyd Industrial Services GmbH: Hamburg, Germany, 2005.
24. *Fatigue Design of Offshore Steel Structures*; DNV-RP-C203; Det Norske Veritas: Høvik, Norway, 2010.
25. *Eurocode 3: Design of Steel Structures—Part 1-9: Fatigue*; EN 1993-1-9; European Committee for Standardisation: Brussels, Belgium, 2005.
26. Zurkinden, A.S.; Lambertsen, S.H.; Damkilde, L.; Gao, Z.; Moan, T. Fatigue Analysis of a Wave Energy Converter Taking into Account Different Control Strategies. In Proceedings of the ASME 32nd International Conference on Ocean, Offshore and Artic Engineering, Nantes, France, 10–15 June 2013.
27. *ASTM Standard for Cycle Counting Fatigue Analysis*; ASTM Standard E 1049-85; American Society for Testing and Materials (ASTM): New York, NY, USA, 2005.
28. Kramer, M. Performance Evaluation of the Wavestar Prototype. In Proceedings of the 9th European Wave and Tidal Energy Conference (EWTEC), Southampton, UK, 5–9 September 2011.
29. Ferri, F.; Kramer, M.M.; Pecher, A. Validation of a Wave-Body Interaction Model by Experimental Tests. In Proceedings of the Twenty-Third International Offshore and Polar Engineering Conference, Anchorage, AK, USA, 30 June–5 July 2013; pp. 500–507.
30. Zurkinden, A.; Ferri, F.; Beatty, S.; Kofoed, J.P.; Kramer, M.M. Non-linear numerical modelling and experimental testing of a point absorber wave energy converter. *Ocean Eng.* **2014**, *78*, 11–21.
31. Cummins, W.E. *The Impulse Response Function and Ship Motion*; Hydrodynamic Laboratory Research and Development Report; Navy Department, David Taylor Model Basin: Washington, DC, USA, 1962.
32. Perez, T.; Fossen, T.I. Time-*vs*. frequency-domain identification of parametric radiation force models for marine structures at zero speed. *Modell. Identif. Control* **2008**, *29*, 1–19.
33. Taghipour, R.; Perez, T.; Moan, T. Hybrid frequency-time domain models for dynamic response analysis of marine structures. *Ocean Eng.* **2008**, *35*, 685–705.
34. Alexander, C.K.; Sadiku, M.N.O. *Fundamentals of Electric Circuits*; McGraw-Hill: Boston, MA, USA, 2007.
35. Korde, U.A. Control System Application in Wave Energy Conversion. In Proceedings of the OCEANS MTS/IEEE Conference and Exhibition, Providence, RI, USA, 11–14 September 2000; Volume 3, pp. 1817–1824.
36. Ferri, F.; Sichani, M.T.; Frigaard P. A Case Study of Short-Term Wave Forecasting Based on FIR Filter: Optimization of the Power Production for the Wavestar Device. In Proceedings of the Twenty-second International Offshore and Polar Engineering Conference, Rhodes, Greece, 17–22 June 2012; pp. 628–635.

37. Fischer, B.; Kracht, P.; Perez-Becker, S. Online-Algortihm Using Adaptive Filters for Short-Term Wave Prediction and Its Implementation. In Proceedings of the 4th International Conference on Ocean Energy (ICOE), Dublin, Ireland, 17–19 October 2012.
38. Fusco, F.; Ringwood, J. Short-term wave forecasting for real-time control of wave energy converters. *IEEE Trans. Sustain. Energy* **2010**, *1*, 99–106.
39. Fagley, C.P.; Seidel, J.J.; Seigel, S.G. Computational Investigation of Irregular Cancelation Using a Cycloidal Wave Energy Converter. In Proceedings of the ASME 31st International Conference on Ocean, Offshore and Arctic Engineering, Rio de Janeiro, Brazil, 1–6 July 2012; Volume 7, pp. 351–358.
40. Miner, M.A. Cumulative damage in fatigue. *J. Appl. Mech.* **1945**, *12*, A159–A164.
41. Marquez-Dominguez, S.; Sørensen, J.D. Fatigue reliability and calibration of fatigue design factors for offshore wind turbines. *Energies* **2012**, *5*, 1816–1834.
42. Danish Wave Energy Center (DanWEC). Available online: http://www.danwec.com/ (accessed on 20 September 2013).
43. Andersen, T.L. WaveLab Version 3.0, 2010. Available online: http://hydrosoft.civil.aau.dk/wavelab/index.htm (accessed on 15 August 2013).
44. Hasselmann, K.; Barnett, T.P.; Bouws, E.; Carlson, H.; Cartwright, D.E.; Enke, K.; Ewing, J.A.; Gienapp, H.; Hasselmann, D.E.; Kruseman, P.; *et al*. *Measurements of Wind-Wave Growth and Swell Decay during the Joint North Sea Wave Project (JONSWAP)*; Deutches Hydrographisches Institut: Hamburg, Germany, 1973.
45. *Wamit Manual*; Chestnut Hill: Boston, MA, USA, 2012.
46. Bhinder, M.A.; Babarit, A.; Gentaz, L.; Ferrant P. Effect of Viscous Forces on the Performance of a Surging Wave Energy Converter. In Proceedings of the Twenty-second International Offshore and Polar Engineering Conference, Rhodes, Greece, 17–22 June 2012; pp. 545–549.
47. Fusco, F.; Ringwood, J. Simple and effective real-time controller for wave energy converters. *IEEE Trans. Sustain. Energy* **2013**, *4*, 21–30.
48. Ziegler, J.G.; Nichols, N.B. Optimum settings for automatic controllers. *Trans. ASME* **1942**, *64*, 759–765.
49. Hildreth, C. A quadratic programming procedure. *Nav. Res. Logist. Q.* **1957**, *4*, 79–85.
50. Lagarias, J.; Reads, J.A.; Wright, M.H.; Wright, P.E. Convergence properties of the Nelder-Mead simplex method in low dimensions. *SIAM J. Optim.* **1998**, *9*, 112–147.
51. Dixon, L.C.W.; Szeg, G.P. The Global Optimization Problem: An Introduction. In *Towards Global Optimisation 2*; North Holland: Amsterdam, The Netherlands, 1978; pp. 1–15.
52. Åström, K.; Hägglund, T. *Advanced PID Control*; The Instrumentation, Systems, and Automation Society (ISA): Research Triangle Park, NC, USA, 2005.
53. Vidal, E.; Hansen, R.H.; Kramer, M.M. Early Performance Assessment of the Electrical Output of Wavestar's Prototype. In Proceedings of the 4th International Conference on Ocean Energy (ICOE), Dublin, Ireland, 17–19 October 2012.
54. Allan, G.; Gilmartin, M.; McGregor, P.; Swales, P. Levelised costs of wave and tidal energy in the UK: Cost competitiveness and the importance of "banded" renewables obligation certificates. *Energy Policy* **2011**, *39*, 23–39.

55. Berkhout, V.; Faulstich, S.; Gorg, P.; Kuhn, P.; Linke, K.; Lyding, P.; Pfaffel, S.; Rafik, K.; Rohrig, K.; Rothkegel, R.; *et al*. *Wind Energy Report Germany*; Fraunhofer Institute for Wind Energy and Energy System Technology (IWES): Kassel, Germany, 2012.
56. Myhr, A.; Bjerkseter, C.; Agotnes, A.; Nygaard, T.A. Levelised cost of energy for offshore floating wind turbines in a life cycle perspective. *Renew. Energy* **2014**, *66*, 714–728.
57. Levitt, A.; Kempton, W.; Smith, A.; Musial, W.; Firestone, J. Pricing offshore wind power. *Energy Policy* **2011**, *39*, 6408–6421.
58. Blanco, M. The economics of wind energy. *Renew. Sustain. Energy Rev.* **2009**, *13*, 1372–1382.
59. *Value Breakdown for the Offshore Wind Sector—A Report Commissioned by the Renewables Advisory Board*; Report No. RAB (2010) 0365; Department of Energy amd Climate Change (DECC): London, UK, 2011.

Hybrid Model Representation of a TLP Including Flexible Topsides in Non-Linear Regular Waves

Wehmeyer C.[a], **Ferri F.**[b], **Andersen M.T.**[b] **and Pedersen R.R.**[a]

[a] Rambøll Offshore Wind, Esbjerg, Denmark;

[b] Department of Civil Engineering, Aalborg University, Aalborg, Denmark.

In Submitted to Energies. Date of submission May 2014.

ABSTRACT:
The rising demand for renewable energy solutions is forcing the established industries to expand and continue evolving. For the wind energy sector the vast resources in deep sea locations have encouraged the research towards the installation of turbines in deeper waters. One of the most promising technologies able to solve this challenge is the floating wind turbine foundation. For the ultimate limit state where higher order wave loads have a significant influence, a design tool that couples non-linear excitations with structural dynamics is required. To properly describe the behaviour of such a structure a numerical model is proposed and validated by physical test results. The model is applied to a case study of a tension leg platform with a flexible topside mimicking the tower and a lumped mass mimicking the rotor-nacelle assembly. The model is additionally compared to current commercial software, where the need for the coupled higher order dynamics proposed in this paper becomes evident.

KEY WORDS: Floating Wind Turbine; TLP; Non-linear Wave; Physical Model Test; Ultimate Limit State Wave Load.

Energies **2014**, *7*, 5047-5064; doi:10.3390/en7085047

OPEN ACCESS

energies

ISSN 1996-1073

www.mdpi.com/journal/energies

Article

Hybrid Model Representation of a TLP Including Flexible Topsides in Non-Linear Regular Waves

Christof Wehmeyer [1,*], Francesco Ferri [2], Morten Thøtt Andersen [2] and Ronnie Refstrup Pedersen [1]

[1] Rambøll Offshore Wind, Esbjerg 6700, Denmark; E-Mail: rrp@ramboll.com

[2] Department of Civil Engineering, Aalborg University, Sohngaardsholmsvej 57, Aalborg 9000, Denmark; E-Mails: ff@civil.aau.dk (F.F.); mta@civil.aau.dk (M.T.A.)

* Author to whom correspondence should be addressed; E-Mail: CFW@ramboll.com; Tel.: +45-516-170-36.

Received: 23 May 2014; in revised form 2 July 2014 / Accepted: 7 July 2014 / Published: 6 August 2014

Abstract: The rising demand for renewable energy solutions is forcing the established industries to expand and continue evolving. For the wind energy sector, the vast resources in deep sea locations have encouraged research towards the installation of turbines in deeper waters. One of the most promising technologies able to solve this challenge is the floating wind turbine foundation. For the ultimate limit state, where higher order wave loads have a significant influence, a design tool that couples non-linear excitations with structural dynamics is required. To properly describe the behavior of such a structure, a numerical model is proposed and validated by physical test results. The model is applied to a case study of a tension leg platform with a flexible topside mimicking the tower and a lumped mass mimicking the rotor-nacelle assembly. The model is additionally compared to current commercial software, where the need for the coupled higher order dynamics proposed in this paper becomes evident.

Keywords: floating wind turbine; TLP; non-linear wave; physical model test; ultimate limit state wave load

1. Introduction

The Horizon2020 call [1] of the EU states explicitly that innovative substructure concepts, including floating platforms, are needed for water depths beyond 50 m, in order to push the development of

competitive low carbon energy generation. One focus is to reduce the overall project risks. However, such project risks can only be accounted for or avoided if known and if their impact can be assessed by applicable tools. Conventional tools used in the oil and gas (O&G) industry for the assessment of the extreme event response of floating structures neglect two important aspects, making them non-conservative when used for floating offshore wind turbines (FOWT). Considering that the offshore wind industry intends to install floating structures at a much shallower water depth than the offshore O&G industry, *i.e.*, in the order of 50 m, a first or second order wave theory approach might not be sufficient to describe realistic wave shapes. Therefore, a higher order wave theory seems necessary. Furthermore, wind turbines are dynamically sensitive structures. Even while the floating part can be considered more or less rigid, the flexibility of the slender tower supporting a heavy rotor-nacelle assembly (RNA) influences the structure's response significantly. The significance of this is highlighted in the recently released DNVoffshore standard, J103 [2], for the design of floating wind turbine structures, which specifically addresses the importance of the flexibility of the tower for the correct simulation of pitch and roll motions. The relation between tower flexibility and response amplitude operator (RAO) shift has been pointed out by Matha [3] in recent years. A numerical model of a tension leg platform (TLP) was compared against measured responses from tests carried out within the DeepCwind framework in [4]. Besides decay tests and wind wave loading, their TLP was exposed to a number of regular waves. The software, as well as the tests considered linear waves, and a reasonable agreement was found. A numerical comparison to the physical model tests of the DeepCwind TLP was performed in [5]. An underestimation of the spectral amplitudes around the natural pitch frequency in regular waves without wind was found. It was suggested that this might be due to the harmonics in the physical wave realization coinciding with the pitch natural frequency. The current work investigates if it is possible to consider these effects by including the viscous wave excitation from higher wave harmonics for the surface-piercing, drag-dominated structural part.

In summary, the current work assesses how well a hybrid model, consisting of a linear potential theory wave excitation and viscous force non-linear wave excitation, can predict key parameters of an FOWT in intermediate water depths. Such environments are common in ultimate limit state analysis (ULS), and often, wave shapes deviate from the first or second order description. As this violates the linear theory, the hybrid model is, in the current work, compared to observations from wave-tank tests. The general problem was two-fold; the hybrid model should be able to simulate the behavior of a tethered floater exposed to non-linear waves, while also accommodating the influences of non-rigid topsides. The hybrid model is an extendable research tool forming the basis of an in-house development. Further benchmarking against available tools at a later stage is planned. It is essential to note that the work is not a design verification, but a tool validation. Even though the full tendon length could be modeled due to a deep section in the wave basin, the structure originally designed for a 100-m water depth was exposed to waves generated in approximately a 60-m water depth. This caused the waves to become non-linear and, hence, allowed the assessment of the performance of a hybrid model, including non-linear viscous wave force excitation.

2. Methods

The scope of this section is to detail the assumptions and methodologies used throughout the work. The objective of this study is to implement a numerical model of a floating wind turbine mounted on an industry-inspired TLP. The numerical model will be exposed to regular, non-linear extreme waves representing ultimate limit state (ULS) conditions. DNV J103 [2] suggests this option to assess the behavior of an offshore wind turbine structure in design conditions. The numerical model will then be validated against experimental tests. The tests were conducted in the 3D wave basin at Aalborg University on a 1:80 scale model; see Figure 1. A detailed description of the set-up and results can be found in [6].

Figure 1. (**a**) Schematic view of the floating offshore wind turbine (FOWT) tension leg platform (TLP); the marker indicates the center of gravity (CoG); (**b**) The physical model.

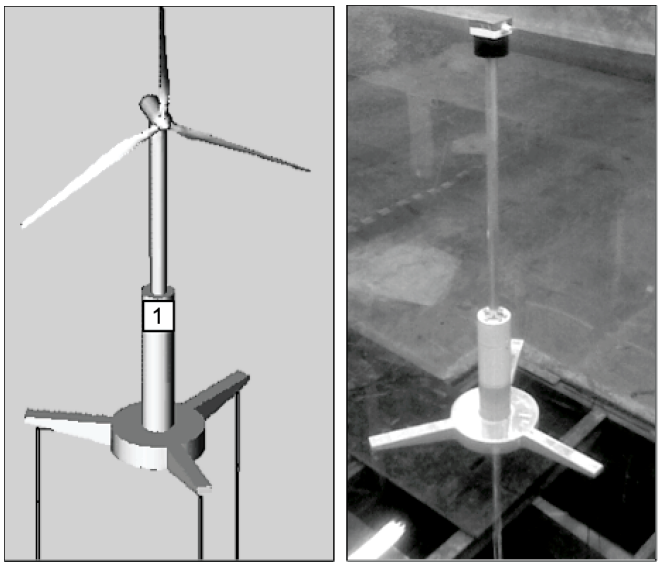

(**a**) (**b**)

Figure 2 shows a sketch of the system under investigation, where the main elements are the TLP substructure (with the associated station-keeping system), the tower and the RNA. q is the 5 degrees of freedom (DOF) displacement vector, and q_1 and q_2 are the surge and heave motion of the structure, pointing in positive x and z, respectively. TB is the tower bottom, *i.e.*, the connection point between tower and substructure. swl is the still water line. CoG is the center of gravity of the TLP. CO is the elevation of the mooring attachment point projected onto the centerline of the structure.

Figure 2. Definition of the system's DOFs and key points. RNA, rotor-nacelle assembly; TB, tower bottom; swl, still water line.

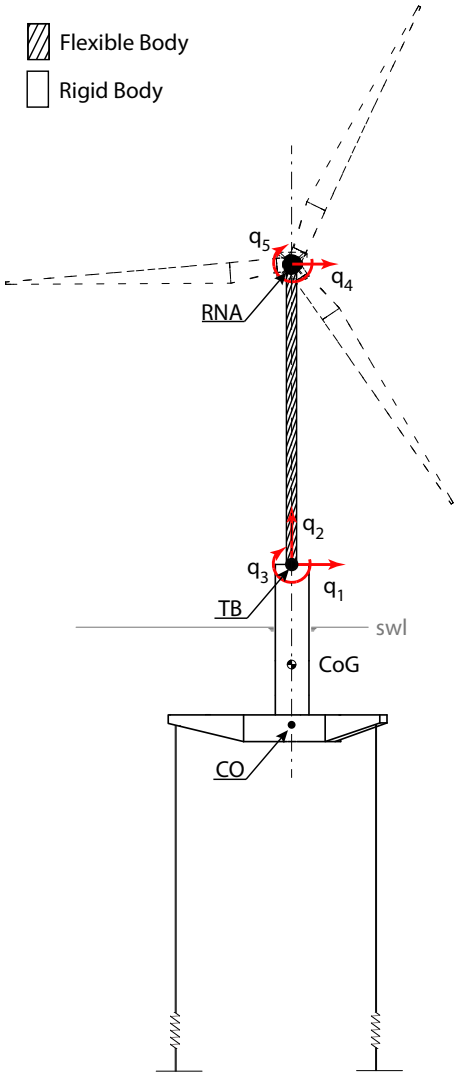

Although both wave and wind loads excite the motion of the structure, the current validation focuses on the hydrodynamic response only. It is important to note that in actual ULS conditions, the wind load on the tower, as well as on the blades can become important during fault conditions.

Considering the construction method of the floater [6], it seems sensible to assume it to be rigid. However, as already mentioned in the previous section, the influence of tower flexibility on the dynamic response of the total structure cannot be neglected [3]. Therefore, the substructure model will be coupled with a flexible beam element connecting the RNA to the rigid substructure.

The substructure has trilateral symmetry about a vertical axis passing through its center. The dynamic response is studied in long crested, *i.e.*, 2D, incident waves, as has been done in the physical model test. The simplified model and the definition of the relative coordinate system are represented in Figure 2.

2.1. Numerical Model of the Substructure

The model will be based on a boundary integral equation method (BIEM) solution with additional hydrodynamic viscous drag terms according to Morison's equation. This approach is believed to be more time efficient than complex numerical techniques, e.g., computational fluid dynamics. The need for an extra dissipative term related to viscous effects in the boundary layer is supported by the results of a non-dimensional analysis of the structure. Figure 3 shows that, based on the non-dimensional ratio between inertial and viscous loads, the flow regime changes along the vertical axis of the structure, and consequently, the use of BIEM plus a viscous drag term becomes necessary. Hence, the wave-body interaction is decomposed into four contributions:

- Wave excitation force: BIEM;
- Viscous drag forces;
- Radiation force;
- Hydrostatic force.

Figure 3. Non-dimensional ratios of inertial and viscous loads for dominating structural parts [7].

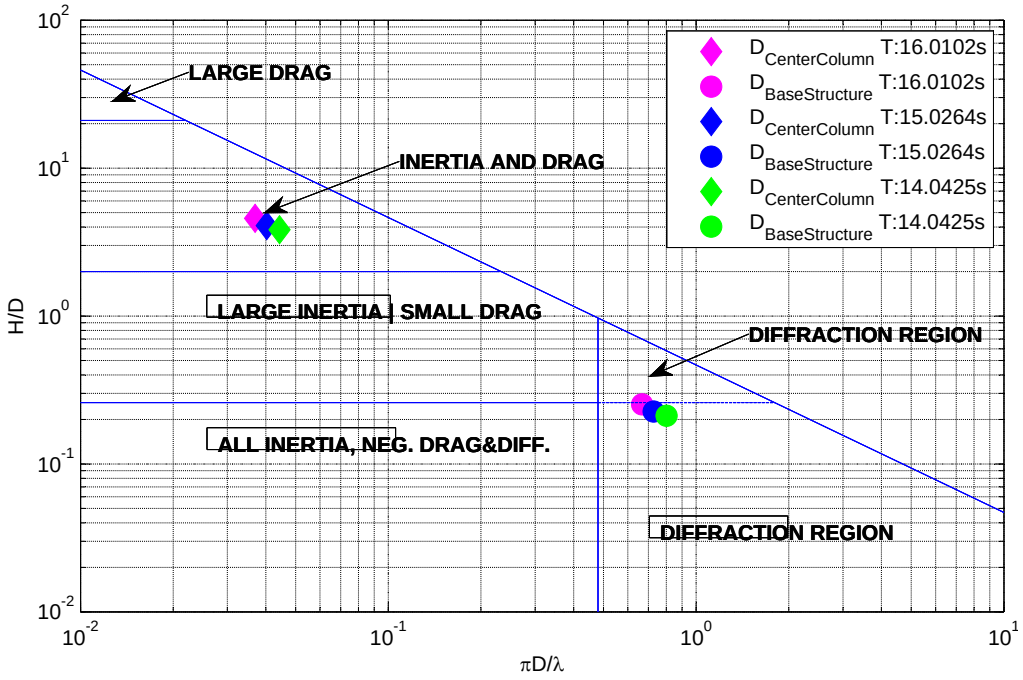

2.1.1. Wave Excitation Forces from Potential Flow

Wave excitation forces (F_{ex}) are defined as the loads exerted on a submerged structure held in equilibrium position in waves.

The total excitation forces are expressed as a summation of the Froude–Krylov forces (F_K^i) and the diffraction forces (F_D^i). The index i represents the i-th degree of freedom. The Froude–Krylov forces are due to the undisturbed incident waves, while the diffraction forces are related to the modified wave

field generated by the structure. The forces are obtained from the integration of the linearized dynamic pressure distribution over the mean wetted surface. The complex frequency coefficients, describing the summation of those two forces, are obtained from the solution of the boundary integral equation problem using the commercial software, ANSYS AQWA [8]. The wave excitation force vector (F_{ex}) is assessed in the time domain by convolution of the non-causal impulse response function (IRF) with the surface elevation time series for each DOF.

2.1.2. Viscous Drag Forces

Viscous energy dissipation, *i.e.*, flow separation, is likely to influence the motion of the system, due to the different flow regimes along the structure. This can be seen as an additional excitation force, as the wave particle velocity is likely to be higher than the body velocity, especially for the surface piercing part. The i-th viscous drag force (F_d^i) used in the model is defined in Equation (1), where i refers to the drag force component, as shown in Figure 4.

$$F_d^i = -\frac{1}{2}\rho C_D^i A^i |u^i - u_0^i|(u^i - u_0^i) \tag{1}$$

where ρ is the water density, C_D is the drag coefficient, A is the cross-sectional strip area of the body, projected in a plane perpendicular to the velocity vector, u is the body velocity and u_0 is the undisturbed particle velocity. The section-wise calculated drag force is integrated over the height and applied at the instantaneous force point of attack. As further explained in the Results section, the drag forces have been split into several contributions in order to account for the geometry changes.

Figure 4. Definition of the directions of drag coefficient application with respect to the structural cross-section.

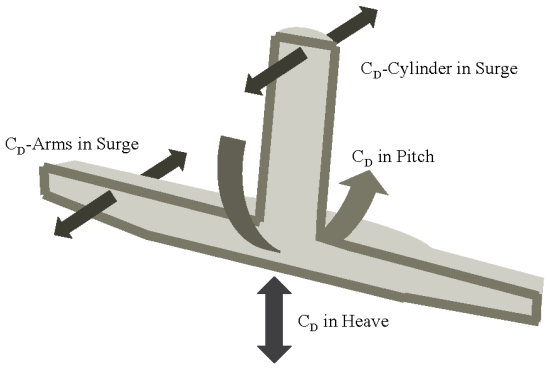

2.1.3. Radiation Forces

The radiation force is the load exerted by the moving body in otherwise calm water. The total radiation load is composed of a part proportional to the acceleration of the body (added mass) and a part proportional to the velocity (radiation damping) of it. The time domain model is represented by the so-called fluid memory terms (IRF) and the matrix of added mass at infinite frequency. This term is related to the convergence of the integral, as detailed in [9]. Although the same convolution approach

can be used to evaluate the radiation force vector (F_{rad}), it benefits the implementation to approximate the frequency response function by a system of first order ODEs. As presented in [9,10], a fifth or lower order system is enough to model a smooth response, as for the presented structure. The state space approximation of the radiation problem is obtained from a least squares fit of the radiation frequency response function. The freeware marine toolbox has been used for this purpose [10]. The selected model order is three.

2.1.4. Hydrostatic Forces

The hydrostatic stiffness matrix of the rigid body is obtained from ANSYS AQWA.

2.1.5. Numerical Model of the Station-Keeping System

A mooring system is required by every floating offshore structure for station-keeping purposes. Furthermore, for TLP-like structures, the mooring system compensates for the intrinsic instability of the system, providing a global positive restoring coefficient. For slender bodies, such as the tendons, it is possible to assume that the major load contributions come from stiffness along the axis of symmetry and from drag in the perpendicular direction. Nevertheless, due to the small cross-sectional area of the tendons used in the lab, it is possible to assume that their drag contribution is negligible, thus the mooring force reduces to a force proportional to the linear extension of the mooring cable. The mooring force F_m is detailed in the following equation:

$$F_{11} = PT + \left(\frac{3q_1}{LT}\sqrt{q_1^2 + LT^2} - LT\right)k \quad (2)$$

$$F_{22} = 3kq_2 \quad (3)$$

$$F_{33} = (kd_B^2 + 2kd_A^2)q_3 \quad (4)$$

$$F_{12} = \left(\sqrt{q_1^2 + LT^2} - LT\right)k \quad (5)$$

where F_{11}, F_{22}, F_{33} correspond to the uncoupled forces, given by a displacement in the relative DOF, while F_{12} is the heave mooring force induced by a displacement in surge. PT is the pretension at the equilibrium position; LT is the mooring cable length at the equilibrium position; k is the linear spring coefficient associated to the tendon's stiffness; d_B is the distance between bow fairlead and CO; and d_A is the distance between the port stern fairlead and CO projected in the xOzplane.

2.1.6. Numerical Model of the Tower

In order to include the dynamic influence of a flexible tower into the model, a standard linear elastic Euler–Bernoulli beam element with four degrees of freedom (q_1, q_3, q_4, q_5) has been used, where the beam top end is connected to a lumped mass representing the RNA.

Only the first mode shape for each degree of freedom is used as a consequence of the ratio between lumped mass over beam mass. The resultant model of the tower has five DOFs: the surge (q_1, q_4) plus pitch (q_3, q_5) of the bottom and top, respectively, and a shared heave motion (q_2); see Figure 2. Additionally, it is fully described by the mass and stiffness matrix. In addition to those matrices, a damping matrix is implemented to simulate the damping from the topside structure. Rayleigh damping

is used, and damping ratios are determined by decay tests. Definitions of the general mass, damping and stiffness matrices are given in [11], together with a comprehensive description of their derivation.

2.1.7. Combined Model

The above-mentioned loads are then assembled in a global system, where the equation of motion is given by:

$$M\ddot{q} = F_{rad} + F_m + F_{ex} + F_d + Kq \tag{6}$$

M is the global mass matrix, combining the substructure mass matrix, the substructure added mass matrix and the topside mass matrix. K is the global stiffness matrix, combining the substructure hydrostatic stiffness matrix and the topside structural stiffness matrix. $\ddot{q}$ is the acceleration vector and q the displacement vector.

The global mass and stiffness matrices are obtained from the summation of the sub-structure and tower matrices in the shared DOFs to ensure the dynamic coupling of the two bodies. The equation of motion is solved by the *ODE45*algorithm implemented in MATLAB [12].

2.2. Wave Model

In order to simulate ULS conditions, a proper wave model is needed. In deep water, the ULS waves can be represented with linear or non-linear waves of small order, such as first or second order Stokes waves. For severe waves in intermediate to shallow water, a higher order solution is needed. Based on the best fit with the experimentally observed wave shapes, a 30th order stream function wave theory is adopted [13]. Wave kinematics and surface elevations are obtained and subsequently applied in the hybrid model. Table 1 shows the applied regular wave parameters in the prototype scale.

Table 1. Wave parameters in the prototype scale.

Wave Parameters	Run 18	Run 17	Run 16
H_{max} (m)	17.2	15.2	14.8
T_{max} (s)	16.0	15.0	14.0

3. Results

The numerical results and their comparison with prior experimental measurements are presented in this section. In the first part, the model details are given. In the second part, the code-to-code and the code-to-experiment comparisons are presented. Three different stiffness set-ups of the hybrid model are used: very stiff, stiff and flexible; the first one is used in the code-to-code comparison and the other two in the code-to-experiment comparison. In both cases, the comparison is divided into two steps: first, the decay test response is presented, followed by the wave response in ULS conditions. The time series will have a predefined and constant color map:

- Red line: flexible model;
- Blue line: stiff model;

- Green line: very stiff/quasi-rigid model;
- Black line: reference signal (ANSYS AQWA and/or experimental results).

3.1. Parameters Definition

The prototype is a three-armed TLP structure, with an approximate total weight, including tower and turbine, of around 2,000 t, installed at a water depth of 100 m [6]. The topside mass is roughly 40% of the substructure mass. In order to include the viscous drag, it was assumed that four different viscous force contributions were sufficient. Figure 4 illustrates the idealized viscous drag contributions that are implemented in the model. These forces were included using the instantaneous relative velocities between body and water particle at specific locations. The C_D values for cylinders and for heave motions agree with common industry standards. For the heave motion, the obtained values were constant and were typical for separated flows at small KC numbers for angular parts [14]. Being a common practice in the offshore wind industry, the C_D values for the cylinder are calculated as a function of maximum undisturbed Reynolds number and maximum undisturbed KC number. More details can be found in [15].

Table 2 shows the applied drag coefficients. A KC relationship for the C_D in pitch was iteratively fitted and resulted in values similar to the ones in heave. The drag coefficient values for the projected area of the arms were iteratively fitted, as well. It is obvious that the C_D approximations for the lower part of the structure have been tailored to the structural layout and the respective assumptions. The estimated C_D value for the surface piercing cylinder in the surge direction, as well as the C_D in the heave and pitch direction agree well with values that can be found in the literature [14,16].

Table 2. Definition of applied drag coefficient values.

Direction	Structure part	C_D
Surge	Arms	1.1
Surge	Cylinder	1.8
Pitch	Base disc + arms	0.3 KC
Heave	Base disc + arms	3.3

3.2. Code-to-Code Validation

In order to validate the model, a code-to-code comparison with the commercial software, ANSYS AQWA, was carried out first. The results are presented hereafter for both the decay test and wave induced motion. The study focuses on the pitch response, being the one most affected by the tower flexibility, but results for the other DOFs are also presented in order to verify the response model. Since ANSYS AQWA models the entire structure as one rigid body, this can be used as a benchmark case to validate the hybrid model. In the hybrid model, the substructure is rigid, as well, and by applying a tower stiffness, EI, of orders of magnitude larger than the physical one, quasi-rigid body behavior is emulated.

3.2.1. Decay Test

Figure 5 shows the time series comparison between the rigid body response predicted by ANSYS AQWA and the hybrid model. The natural frequency of the rigid body motion predicted by the hybrid model is 2.05 Hz, where ANSYS AQWA predicts 2.10 Hz.

Figure 5. Code-to-code comparison between the hybrid model, including quasi-rigid topside layout pitch response and ANSYS AQWA pitch response in a decay test, normalized by the displacement in pitch at $t = 0$.

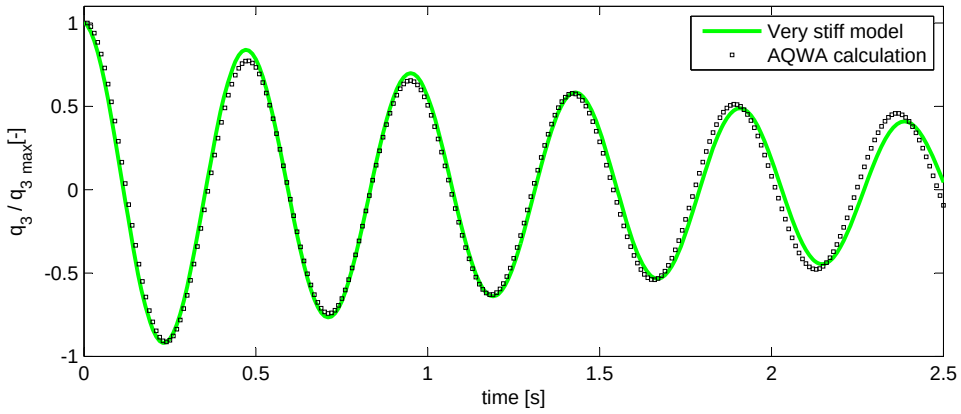

3.2.2. Regular Waves

A ULS design load case is generated with ANSYS AQWA, simulating rigid body behavior. The software generates second order regular Stoke waves. In order to mimic the physical test environment, the water depth matched the wave generation water depth in the wave tank, which, in turn, matched the water depth used in the numerical model for the generation of the stream function wave. Figure 6 shows the obtained results, and a good match is observed. The waves in the hybrid model are ramped for all cases, explaining the comparison convergence.

Figure 6. Code-to-code comparison between the hybrid model, including quasi-rigid topside layout pitch response and ANSYS AQWA pitch response under regular wave load conditions.

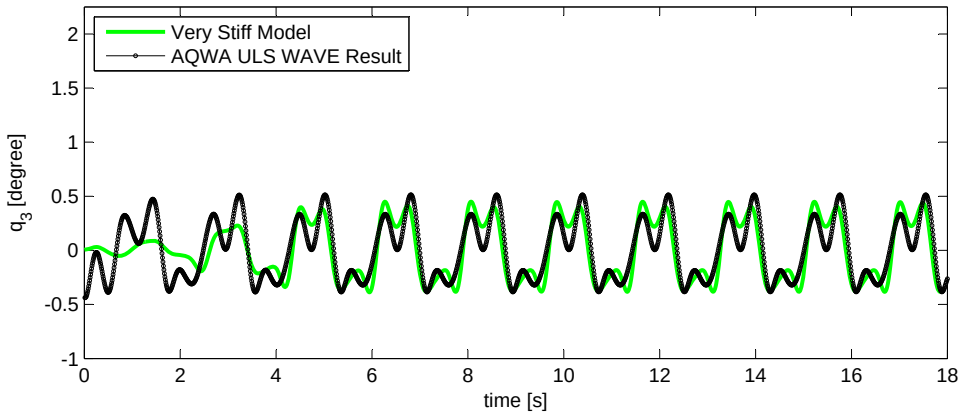

3.3. Physical Model Validation

Once a qualitative analysis of the hybrid model's capability was complete, the hybrid model was validated against experimental data. As previously mentioned, two different structural stiffness configurations form the basis of comparison, namely the stiff and flexible model [6]. The response will be evaluated in TB, as defined in Figure 2. TB has been selected as the point of comparison due to sensor location in the experimental setup. Consequently, only a single transformation from CoG to TB within the numerical model is required.

3.3.1. Decay Test

The responses in surge and heave for the flexible tower system are shown in Figures 7 and 8, respectively. Figure 9 shows the pitch response comparison between flexible and rigid tower lay-outs, for both experimental and numerical models. Only the flexible model is used for the comparison of the decay in surge and heave, since the period in surge is orders of magnitude larger than that of the natural frequency of the tower bending mode, making the two models indistinguishable. This is also the case for the heave decay, since the axial stiffness of the tower is orders of magnitude higher than the vertical stiffness of the foundation and mooring.

Figure 7. Code-to-experiment comparison between the flexible hybrid model and experimental data in a surge decay test, normalized by the displacement in surge at $t = 0$.

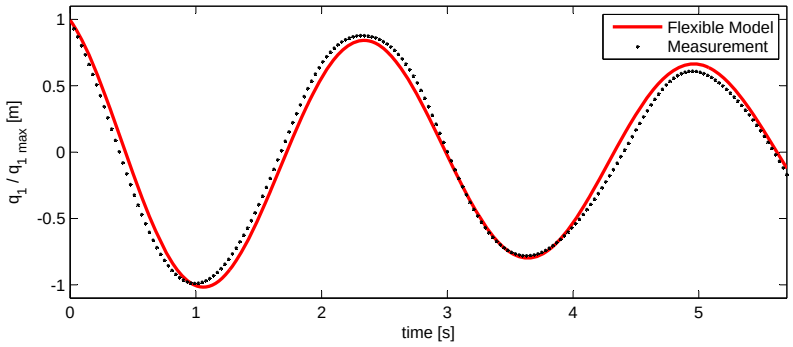

Figure 8. Code-to-experiment comparison between the flexible hybrid model and experimental data in a heave decay test, normalized by the displacement in heave at $t = 0$.

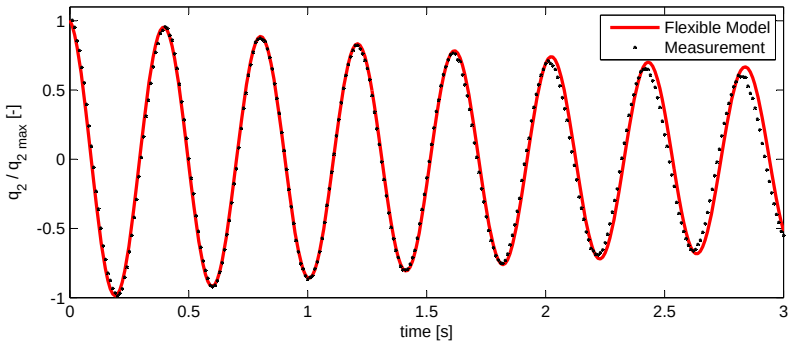

Figure 9. Code-to-experiment comparison between the flexible hybrid model and the stiff hybrid model and the experimental data in a pitch decay test, normalized by the displacement in pitch at $t = 0$.

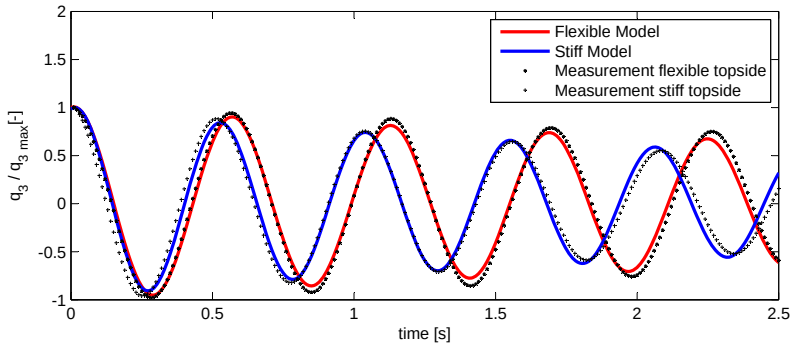

3.3.2. Regular Waves

The numerical model was subsequently applied to three different wave conditions in accordance with the three largest sea states used in the physical model tests. Example time series plots for the upper and lower bounds, *i.e.*, flexible topside response to the highest wave and stiff topside response to the lowest wave, are given in Figures 10 and 11.

Figure 10. Code-to-experiment comparison between the flexible hybrid model and experimental data under regular wave load conditions. (**a**) Pitch motion comparison; (**b**) Surface elevation comparison.

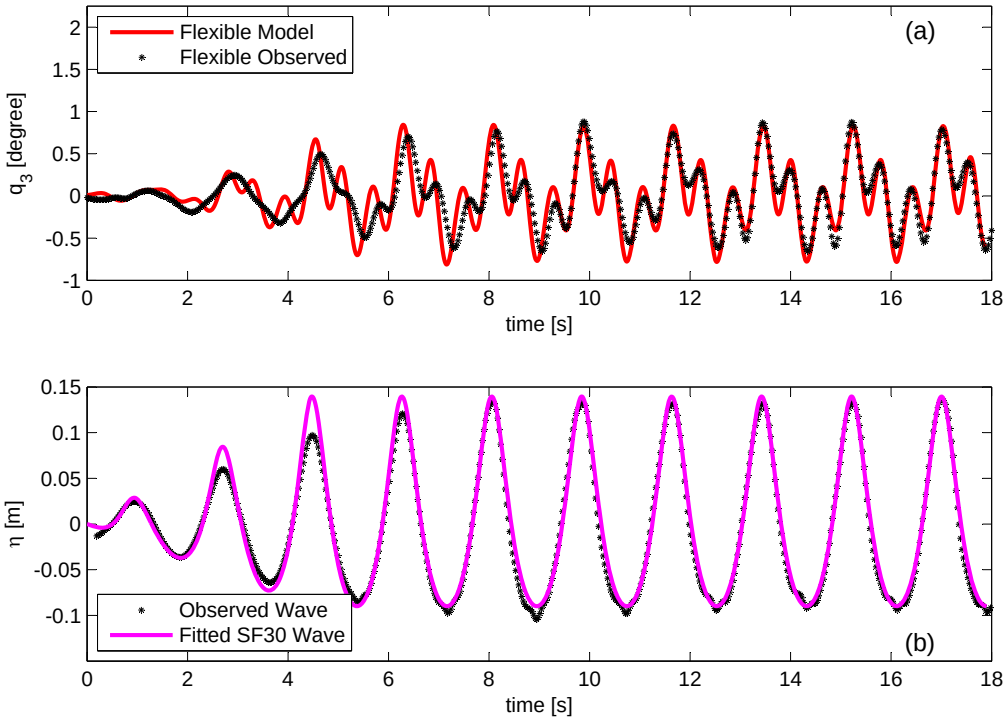

Figure 11. Code-to-experiment comparison between the stiff hybrid model and experimental data under regular wave load conditions. (**a**) Pitch motion comparison; (**b**) Surface elevation comparison.

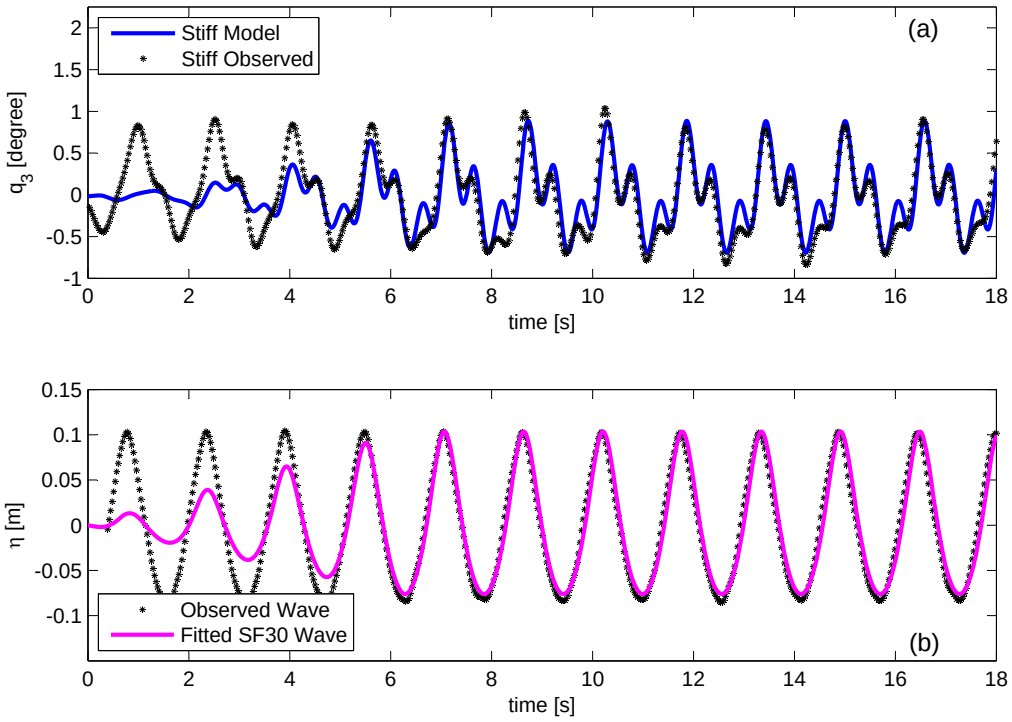

4. Discussion

In order to gain an understanding of the model quality when compared with experimental results, cross-correlation coefficients and ratios between maximum and minimum values have been obtained, excluding the initial effects from the ramping up; see Tables 3 and 4. The correlation coefficients varied between 80%–96%, with an average of 88%. The ratios between the respective predicted minimum values and observed values showed good agreement. The maximum deviation was an 18% underestimation of the numerical model. An average deviation of 8% was found.

To obtain a better understanding of the force contributions, the pitch excitation moment was split into its single components for one period; see Figure 12. It is obvious that the horizontal drag force acting on the cylinder is the dominating load, *i.e.*, the combined total moment is dominated by the kinematics above the still water level impacting on the surface piercing part. The overturning moment is much larger than the moment induced by the loads acting on the lower part of the structure. The latter is, in fact, opposite, as the horizontal velocities are acting below the point of rotation. The diffractive part of the moment dominates the negative peak when the horizontal velocity components of the wave kinematics are close to zero. Hence, neither a pure potential flow approach nor a pure viscous force approach would be able to deliver the same degree of fit.

Table 3. Comparison of key data for the pitch motion of the flexible model. Experimental (Exp.) and numerical (Num.) data.

Flexible Model	**Exp.**	**Num.**	**Exp.**	**Num.**	**Exp.**	**Num.**
Run Number	18		17		16	
H_{max} (m)	0.215		0.190		0.185	
T_{max} (s)	1.79		1.68		1.57	
Min (degree)	−0.945	−0.993	−0.890	−0.857	−0.830	−0.747
Max (degree)	0.993	1.036	0.997	0.939	0.820	0.785
Min Ratio (-)	0.95		1.04		1.11	
Max Ratio (-)	0.96		1.06		1.04	
Correlation Coeff. (%)	92		80		82	

Table 4. Comparison of key data for the pitch motion of the stiff model. Experimental (Exp.) and numerical (Num.) data.

Stiff Model	**Exp.**	**Num.**	**Exp.**	**Num.**	**Exp.**	**Num.**
Run Number	18		17		16	
H_{max} (m)	0.215		0.190		0.185	
T_{max} (s)	1.79		1.68		1.57	
Min (degree)	−0.654	−0.792	−0.797	−0.730	−0.792	−0.740
Max (degree)	0.814	0.883	0.945	0.803	0.868	0.799
Min Ratio (-)	0.83		1.09		1.07	
Max Ratio (-)	0.92		1.18		1.09	
Correlation Coeff. (%)	86		95		95	

Figure 12. Illustration of the different wave load component contributions on pitch response.

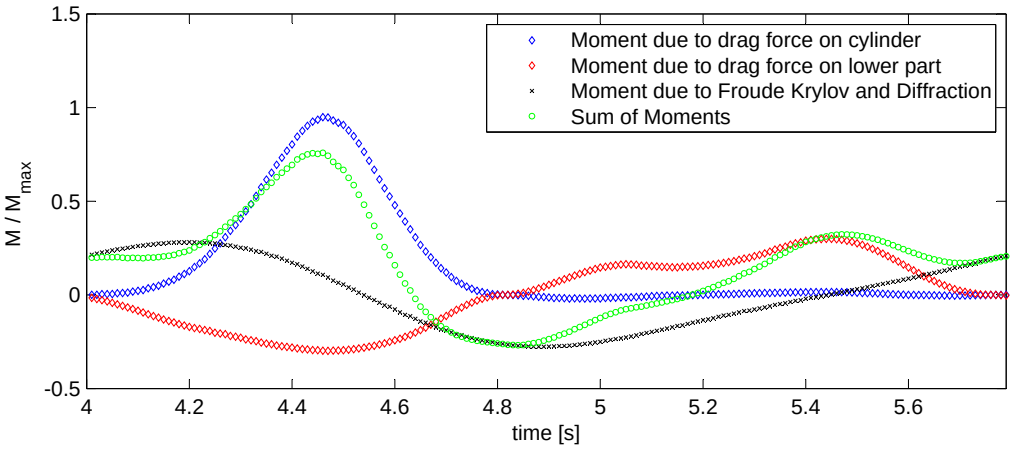

The hybrid model performs well when looking at the power spectra of the pitch decay responses; see Figure 13. Only a minor deviation is found for the very stiff model compared to the ANSYS AQWA

response. For the regular wave pitch response spectra, the results are two-fold; see Figure 14. It becomes clear that the stream function wave cannot fully reproduce the laboratory waves, and in particular, the very high frequency components are underestimated. However, the influence on the structural response is negligible. The third order component is close to the pitch eigenfrequency of all structural layouts, and consequently, the dynamic amplification due to the flexibility of the topside becomes evident. The hybrid model matches the observed pitch response, whereas the very stiff model matches the results from the ANSYS AQWA model. Room for improvement can be found at the second order component; unlike the ANSYS AQWA model, the hybrid model lacks the inclusion of the second order sum frequency excitation force, explaining why both the flexible and very stiff models underestimate the responses, while the ANSYS AQWA model shows a better match.

Figure 13. Code-to-code and code-to-experiment power spectral density comparison of the pitch motion decay response for the quasi-rigid, stiff and flexible hybrid model.

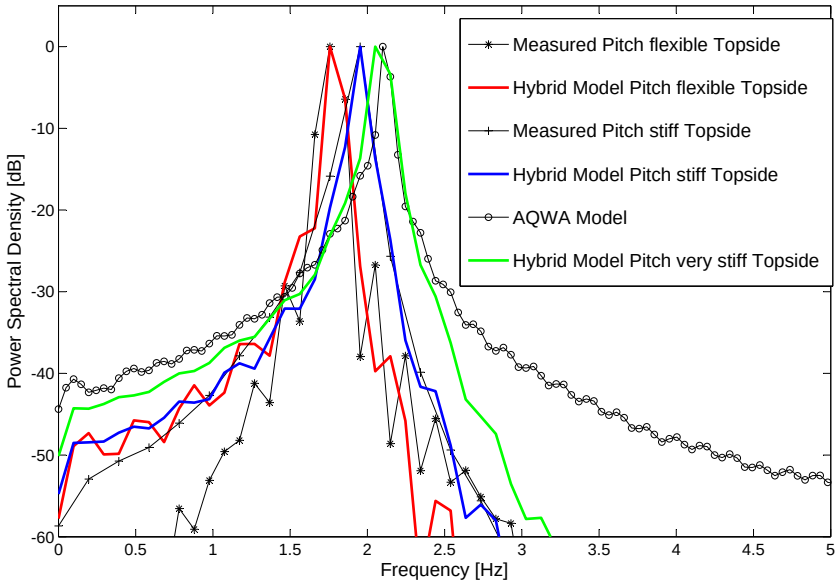

Figure 14. Code-to-code and code-to-experiment power spectral density comparison of the pitch motion response for the quasi-rigid, stiff and flexible hybrid model under regular wave load conditions.

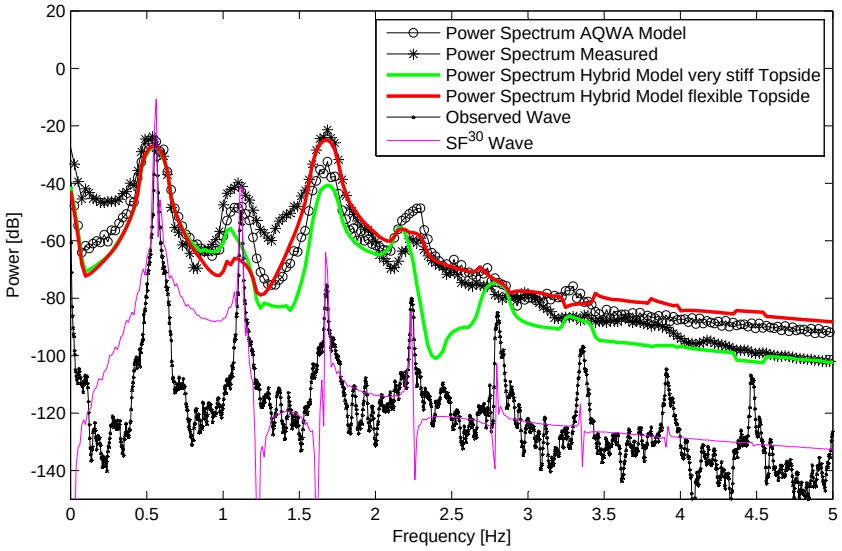

5. Conclusions

Non-linear waves are assumed to be relevant in the ULS analysis of FOWTs installed close to the minimum target water depth of ∼50 m. The intention was to set up a resource-efficient tool, able to satisfactorily approximate pitch motions of a dynamically-sensitive FOWT resulting from a nonlinear wave impact. As a numerical experiment, a hybrid model was developed, including linear potential theory forces and non-linear hydrodynamic viscous forces. The potential forces act thereby on the large volume part of the structure, whereas the viscous forces act on the cylindrical surface piercing part of the structure. Due to the violation of the potential flow approximations induced by wave non-linearity, the hybrid model needs to be validated by experimental tests. The C_D values applied in the hybrid model are used as tuning parameters. Considering that these are in sensible ranges, the overall match between the observations and the hybrid model is very good. To the authors knowledge, this is the first time a mildly-nonlinear approach has been assessed, comparing measured pitch responses to observed pitch responses excited by non-linear waves based on stream function theory. The term mildly-nonlinear describes the combination of linear radiation and wave scattering combined with additional non-linear terms, assuming small body motions. It was shown that the viscous drag contributions are an essential part of the response for the investigated structure, and it seems sensible to include those effects, as well, in subsequent irregular wave response analysis. Additionally, a code-to-code comparison was carried out and served as the performance verification for non-flexible topside configurations. It was shown that the hybrid model can be adopted to deliver more than satisfying results for different wave steepness values and different topside flexibilities. The model is thereby able to:

- Include the effects of regular, non-linear waves on an FOWT TLP structure;
- Include the effects of the dynamically-sensitive topside on the pitch response of an FOWT.

Comparing the maximum pitch values obtained by the rigid body simulation to those of the flexible topside simulation, the impact of the rigid body assumption becomes evident. Even though this appeared to be very structure specific, it underlines the importance of the correct implementation and furthermore proves that the rigid body assumption inherited from the O&G industry is not valid for FOWTs. It was not expected to obtain perfect fits, due to the complexity of the system and due to the simplifications. A higher fidelity model could be achieved by inclusion of the nonlinear Froude–Krylov force. When simulating irregular waves, second order diffraction forces might become relevant. However, the non-linear viscous contributions are expected to be of the same or higher significance, especially in severe seas for surface piercing parts, which are drag dominated. Considering the lateral extent of the structure, an integration of the instantaneous drag contribution over the wetted surface might lead to further improvement. However, the results already showed good agreement with the measured data. It is thereby concluded that the applied methodology is robust enough to be developed further. A natural next step is the assessment of key responses in irregular waves. Even though the general approach seems valid, a current limitation, and, therefore, incentive for future work, is the specific applicability of the model. Exchanging the potential flow coefficients is not a major challenge; however, the current drag coefficient implementation and the current mooring model makes the model case specific. Further development work, in order to make the model more generally applicable, *i.e.*, acceptable for different substructures and mooring configurations, is consequently planned.

Acknowledgments

The early stage PelaStar design by THE GLOSTEN ASSOCIATESwas the genesis of the subject TLP. Their contribution to the project is gratefully acknowledged. The access to the wave laboratory of Aalborg University and the support by Aalborg University's staff provided an invaluable contribution.

Author Contributions

This work was planned and drafted by the C. Wehmeyer. The key methodology and subsequently implementation of the numerical model was done by C. Wehmeyer, however with invaluable input from the co-authors. The relevant experimental tests have been shared between F. Ferri and C. Wehmeyer. The contributions and the working atmosphere during the paper development is greatly appreciated.

Conflicts of Interest

The authors declare no conflict of interest.

References

1. *Call for Competitive Low-Carbon Energy*; Technical Report H2020-LCE-2014-1; European Comission: Brussels, Belgium, 11 December 2013.
2. *Design of Floating Wind Turbine Structures*; Offshore Standard DNV-OS-J103; Det Norske Veritas AS: Hovik, Norway, June 2013.

3. Matha, D. *Model Development and Loads Analysis of an Offshore Wind Turbine on a Tension Leg Platform, With a Comparison to Other Floating Turbine Concepts*; Subcontract Report NREL/SR-500-45891; National Renewable Energy Laboratory: Golden, CO, USA, February 2010.
4. Stewart, G.M.; Lackner, M.A.; Roberton, A.; Jonkman, J.; Goupee, A.J. Calibration and validation of a FAST floating wind turbine model of the deepwind scaled tension-leg platform. In Proceedings of the 22nd International Offshore and Polar Engineering Conference (ISOPE), Rhodes, Greece, 17–22 June 2012.
5. Prowell, I.; Robertson, A.; Jonkman, J.; Stewart, G.M.; Goupee, A.J. Numerical prediction of experimentally observed behavior of a scale-model of an offshore wind turbine supported by a tension-leg platform. In Proceedings of the Offshore Technology Conference, Houston, TX, USA, 6–9 May 2013.
6. Wehmeyer, C.; Ferri, F.; Skourup, J.; Frigaard, P. Experimental Study of an Offshore Wind Turbine TLP in ULS Conditions. In Proceedings of the Twenty-third (2013) International Offshore and Polar Engineering, Anchorage, AK, USA, 30 June–5 July 2013.
7. Chakrabarti, S.K. *Hydrodynamics of Offshore Structures*; WIT Press: Southampton, UK, 1987.
8. *ANSYS AQWA*, Version 15.0; ANSYS, Inc.: Canonsburg, PA, USA November 2013.
9. Yu, Z.; Falnes, J. State-space modelling of a vertical cylinder in heave. *Appl. Ocean Res.* **1995**, *17*, 265–275.
10. Perez, T.; Fossen, T.I. A Matlab Toolbox for Parametric Identification of Radiation-Force Models of Ships and Offshore Structures. *Model. Identif. Control: Nor. Res. Bull.* **2009**, *30*, 1–15.
11. Clough, R.W.; Penzien, J. *Dynamics of Structures*; Civil Engineering Series; McGraw-Hill Education: New York, NY, USA, 1993.
12. *MATLAB*, Version 7.13.0.564 (R2011b); The MathWorks Inc.: Natick, MA, USA, 2011.
13. Dean, R.G.; Dalrymple, R.A. *Water Wave Mechanics for Engineers and Scientists*; Advanced Series on Ocean Engineering-Vol2; World Scientific: Singapore, 1991.
14. Faltinsen, O. *Sea Loads on Ships and Offshore Structures*; Cambridge Ocean Technology Series; Cambridge University Press: Cambridge, UK, 1993.
15. *Design of Offshore Wind Turbine Structures*; Offshore Standard DNV-OS-J101; Det Norske Veritas AS: Hovik, Norway, October 2007.
16. Sumer, B.M.; Fredsøe, J. *Hydrodynamics around Cylindrical Structures*; Advanced Series on Ocean Engineering, V.12; World Scientific: Singapore, 1997.

Experimental assessment of the mooring influence on the power output of floating Wave Activated Body WECs.

Angelelli E.[a], **Zanuttigh B.**[a], **Ferri F.**[b] **and Kofoed J.P.**[b]

[a] DICAM, University of Bologna, Bologna, Italy;

[b] Department of Civil Engineering, Aalborg University, Aalborg, Denmark.

In Proceeding of the 10th European Wave and Tidal Energy Conference (EWTEC), Aalborg, Denmark, 2013.

ABSTRACT:
The paper presents the preliminary results of new physical tests carried out in the directional wave basin of Aalborg University (DK). The devices under exams are two floating 7 Degrees of Freedom Wave Activated Bodies moored with a spread system composed by 4 steel chains. The devices were subject to ordinary North Sea wave climate conditions and deployed in 1:60 scale. The main purpose of this paper is to analyse the performance of a Wave Energy Converter considering the interdependencies among energy production, loads on real moorings and device movements. The mooring effects on power production and on device movements are specifically investigated by varying the chain pre-tension level. Results suggest that the power production optimization is achieved with a slack mooring system providing a quasi-static response to the ordinary wave attacks.

KEY WORDS: FLOATING WAVE ENERGY CONVERTERS; WAVE ACTIVATED BODY; EXPERIMENTS; SPREAD MOORING; CHAIN PRE-TENSION; POWER PRODUCTION.

Experimental assessment of the mooring influence on the power output of floating Wave Activated Body WECs

E. Angelelli[#1], B. Zanuttigh[#2], F. Ferri[*3], J.P. Kofoed[*4]

[#]*DICAM, University of Bologna*
Viale Risorgimento 2, 40136 Bologna (Italy)
[1]elisa.angelelli4@unibo.it
[2]barbara.zanuttigh@unibo.it

[*]*Department of Civil Engineering, University of Aalborg*
Sohngaardsholmsvej 57, 9000 Aalborg, Denmark
[3]ff@civil.aau.dk
[4] jpk@civil.aau.dk

Abstract— **The paper presents the preliminary results of new physical tests carried out in the directional wave basin of Aalborg University (DK). The devices under exams are two floating 7 Degrees of Freedom Wave Activated Bodies moored with a spread system composed by 4 steel chains. The devices were subject to ordinary North Sea wave climate conditions and deployed in 1:60 scale. The main purpose of this paper is to analyse the performance of a Wave Energy Converter considering the interdependencies among energy production, loads on real moorings and device movements. The mooring effects on power production and on device movements are specifically investigated by varying the chain pre-tension level. Results suggest that the power production optimization is achieved with a slack mooring system providing a quasi-static response to the ordinary wave attacks.**

***Keywords*— floating Wave Energy Converters, Wave Activated Body, experiments, spread mooring, chain pre-tension, power production**

Nomenclature

H_s	significant wave height (time domain)
T_p	peak period
L_P	peak wave length
l	model length
l/L_P	dimensionless model length
L_C	ratio between the length of the chain lying on the seabed and the total chain length
T_N	natural period
d	water depth
s_f	sample frequency (100 Hz)

I. Introduction

Floating Wave Energy Converters (WECs) require a mooring system in order to ensure station keeping, and more specifically to limit the drift, ensure the alignment of directional WECs with the prevailing wave conditions, avoid impact with other structures and excessive loads on the electric power umbilical. In general, the mooring system must be sufficiently rigid to allow docking for inspection and maintenance, and at the same time sufficiently flexible to minimize the forces acting on anchors, mooring lines, electricity transmission cables and on the device itself. The contemporary satisfaction of this double prerequisite usually leads also to preserve a good energy conversion efficiency. Only in exceptional cases the stiffness of the mooring lines is an active element of the conversion principle used by the device itself.

The moorings should allow large WECs motions, in order to serve their primary function, but also comply with many other requirements [1], for example interact with the body dynamic in order to increase the overall efficiency. Most designs that interact with the ocean have a natural frequency substantially larger or smaller than the frequency of the wave [2]. However, in many cases for optimum power capture WECs must operate at or near resonance: this introduces complex fatigue-based design considerations [3], [4] that also affect reliability issues. Some exceptions can be found such as the Oyster device [5].

Extreme loads, to which the device and its mooring must resist, are directly responsible for the costs of WECs [6], while the energy to be sold is produced in ordinary load conditions [7]. Currently, a relatively high rate of floating WECs have failed in their efforts due to an improper design of the mooring system (as private communication from DEXA, WaveDragon and WavePlan documented).

So far there is very limited research dedicated to verify to which extent the mooring arrangements are affecting the hydrodynamic loading on the structure, as well as the power extraction capabilities [8], [9].

The authors already analysed in [10], [11] the influence of the type of the mooring system (spread and CALM) on the power performance for a Wave Activated Body WEC. Main outcomes showed the dependence of the power production on

Optical non-contact floating object tracking using an open-source library.

Ferri F.[a], **Andreoni G..**[b], **Persic N.**[a], **Levelle J.**[a] **and Kofoed J.P.**[a]

[a] Department of Civil Engineering, Aalborg University, Aalborg, Denmark;

[b] Laboratory of Automation and Robotics of DEIS, University of Bologna, Bologna, Italy.

In Proceeding of the 10th European Wave and Tidal Energy Conference (EWTEC), Aalborg, Denmark, 2013.

ABSTRACT:
In this paper, an optical non-contact low budget method for tracking the position of multi-object is presented for marine/off-shore laboratory applications. Particular focus is given at the wave energy field and the analysis of floating wave energy converters dynamics. The measurement of the position and orientation is often a key point in this context, achieved nowadays with different standard technologies. Typically a base requirement for a measurement system is to be accurate and precise, without affecting the dynamical and statical behaviour of the system itself. Video based systems satisfy these points, but they are typically prohibitively expensive. Through the article a low budget one-camera video based system is presented and compared with other two standard methods: direct physical measurement and inertial motion unit (IMU). The system was tested both, in a dry environment and in waves. Results show an average error below 4and precision in the low frequency components but also increased high frequency noise components. Further investigation will be addressed to the implementation of a hybrid system, where the corrupted high frequency information can be replaced by the IMU signal.

KEY WORDS: IMAGE PROCESSING; PHYSICAL MODEL; FLOATING OBJECT; AUGMENTED REALITY; OPEN SOURCE.

Optical non-contact floating object tracking using an open-source library

Francesco Ferri*[1], Gildo Andreoni†[2], Neven Perisic*[3], John Lavelle*[4] and Jens Peter Kofoed*[5]
*Civil Engineering Department
Aalborg University, Aalborg, Denmark
E-mail: [1]ff@civil.aau.dk
[3]np@civil.aau.dk
[4]jlav@civil.aau.dk
[5]jpk@civil.aau.dk
†Laboratory of Automation and Robotics of D.E.I.S,, University of Bologna, Italy
E-mail: [2]andgildo@gmail.com

***Abstract*—In this paper, an optical non-contact low budget method for tracking the position of multi-object is presented for marine/off-shore laboratory applications. Particular focus is given at the wave energy field and the analysis of floating wave energy converters dynamics. The measurement of the position and orientation is often a key point in this context, achieved nowadays with different standard technologies. Typically a base requirement for a measurement system is to be accurate and precise, without affecting the dynamical and statical behaviour of the system itself. Video based systems satisfy these points, but they are typically prohibitively expensive. Through the article a low budget one-camera video based system is presented and compared with other two standard methods: direct physical measurement and inertial motion unit (IMU). The system was tested both, in a dry environment and in waves. Results show an average error below 4%, with increased high signal accuracy and precision in the low frequency components but also increased high frequency noise components. Further investigation will be addressed to the implementation of a hybrid system, where the corrupted high frequency information can be replaced by the IMU signal.**

***Index Terms*—Image processing, Physical Model, Floating Object, Augmented Reality, Open Source**

I. Introduction

The first part of this article will be used to introduce the audience to the general problem of measuring objects position in marine/off-shore laboratory applications, while the specific system will be presented in Section II. Within the ocean engineering fields, the performance or the dynamic behaviour of any floating structure can be obtained in two different ways:

1) Numerical Simulation
2) Physical Test

Numerical simulations are a standard method for analysing wave energy converters (WECs) due to the relatively high accuracy, flexibility and low price, when compared with physical tests. On the other hand, since any numerical model is always a simplified description of a real system, a validation procedure, based on experiments, is needed. This last point is especially true for the case of modelling a wave energy converter, due to the non-linearities, which arise from seeking large body excursions. With physical tests, one of the measured quantities is often the body's position and orientation, useful for example to calculate force displacement curves or to describe the system dynamics. The pose (position and orientation) is a 6x1 vector containing three translations and three rotations varying with time. This information is sufficient to describe six degree of freedom (DOF), i.e. the exact position of each point of the single rigid body. In marine applications those quantities are commonly called:
surge, sway, heave: Translations in x, y and z axis respectively
roll, pitch, yaw: Rotations around x, y and z axis respectively.
A fundamental requirement for any measurement system is that it delivers an accurate and precise position signal, without affecting and modifying the system dynamics. The accuracy and precision will be quantified in this work using the measurement error offset, and the normalized mean square error (NMSE), respectively.
In order not to affect the measured value, the measuring system should be weightless and not physically connected to any other reference system. Currently, the position of a rigid body in a wave basin can be adequately measured in several different ways, examples of which are listed below:

Direct physical measurement: the body is connected to an external reference system, and the changes in a measured variable are related to the changes in position. For example, the variable voltage output given by a potentiometer is related to the number of turn of a shaft, where a cable is rolled, defining a relation between voltage and unrolled cable length.

Inertial measurement unit (IMU): information from accelerometers, gyroscopes and optionally magnetometers are combined to obtain acceleration and orientation in the six DOFs. The position can be assessed from the accelerations signals, when the orientation of the system with respect to the global coordinate system is known.

Proximity sensor: the position of the body is determined from changes in the field (electrical or magnetic) or in the return signals (ultrasonic, laser, radar, etc.). These rates of change are associated with the position of the body.

Video Based system: the position of the body or points on it is obtained from each video frame. The relation between the

Wavestar WEC

B

The objective of this appendix is to give details for the physical model of the Wavestar WEC single floater developed at Aalborg University, Civil Engineering Department by Morten Kramer. The Wavestar WEC (Wavestar, 2014) is a multi point absorber that extracts the wave energy potential from the motion of floaters induced by the passing waves. The floaters are attached to a fixed platform by arms. The hinge between the floater arm and the platform restrains the motion of the floater except for the rotation around the hinge axis, resulting in one rotational DoF for each floater. The platform is held stationary by four bottom fixed piles. Fig. B.1 shows the large-scale prototype installed near Hanstholm (DK). The machine is composed by four bottom fixed piles and two floaters, each of them 5 m in diameter, and represents a section of the prospected complete machine with 20 floaters. The length of the floater arms is ∼10 m.

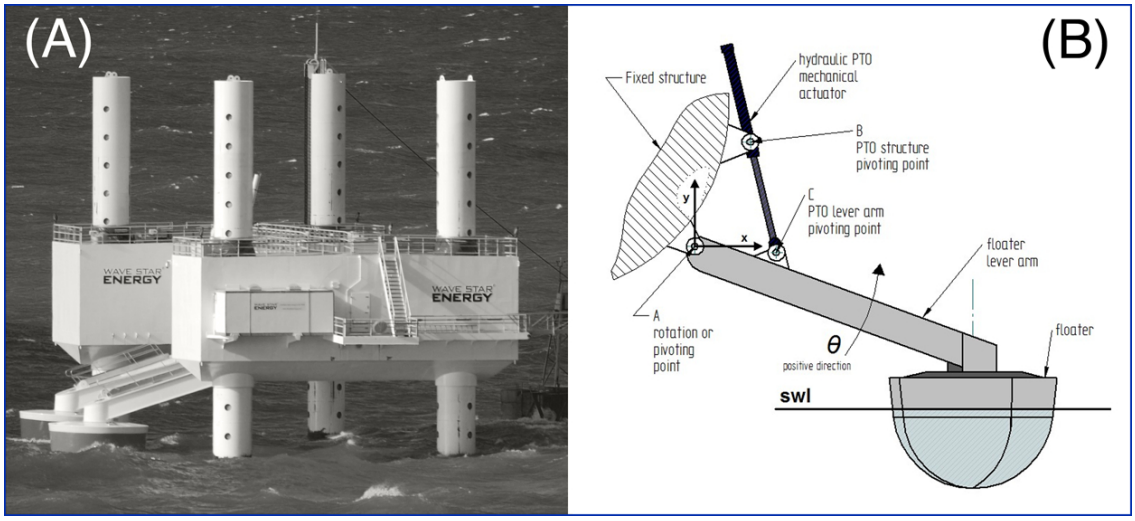

Fig. B.1. (A) - Large-scale prototype installed in 2009 near Hanstholm (DK). The machine fed electricity into the grid until it was moved to the harbour for reconfiguration in September 2013. (B) - Schematic representation of a single floater of the Wavestar WEC. θ represent the rotational DoF and A identifies the pivoting point of the floater. The power is extracted by means of an hydraulic PTO system, represented on the figure by its actuator only.

Fig. B.1 (B) shows a schematic representation of a single floater of the Wavestar WEC. The pivoting point is represented by the point A. The rotational degree of freedom and its relative positive direction are represented with the greek letter θ.

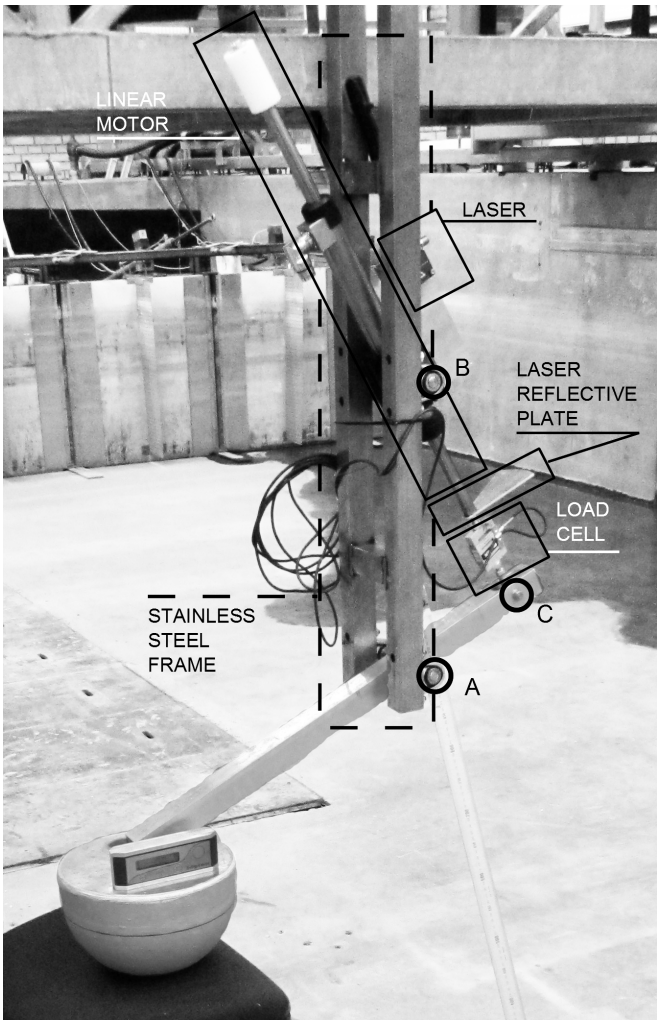

Fig. B.2. Small-scale (1:20) physical model of the Wavestar WEC single floater. Points A, B and C correspond to the ones sketched in Fig. B.1.

Fig. B.2 shows the small-scale physical model of the Wavestar WEC single floater. The selected scale is 1:20 with a resulting floater diameter of 0.25 m. The floater is equipped with a laser, to measure the motor stroke and therefore the floater rotation, with a load cell, to measure the load acting on the PTO arm, and with a linear servo electrical motor acting like and active PTO system. The connection point C is moved on the rear of point A with respect to the large scale prototype. The floater is made hollow accounting for the usage of ballast material.

The electrical motor is fully controlled by a xPC connection. The connection is built in the Matlab/Simulink environment, see Fig. B.3. Briefly, the requested operations, such as the control law, the data calibration, etc., are defined in a Simulink block diagram in the host computer. The information is compiled in c-code and sent to the target computer where a real time operating system (xPC) applies the custom operations. The xPC communicates with a I/O board where the data from the load cell and laser is collected. The raw data is

treated and used to defined the set-point, either the position of, or the force acting on the floater. The set point is sent to the motor controller (low level controller) which tracks the set-point using a feed-back scheme (PID controller).

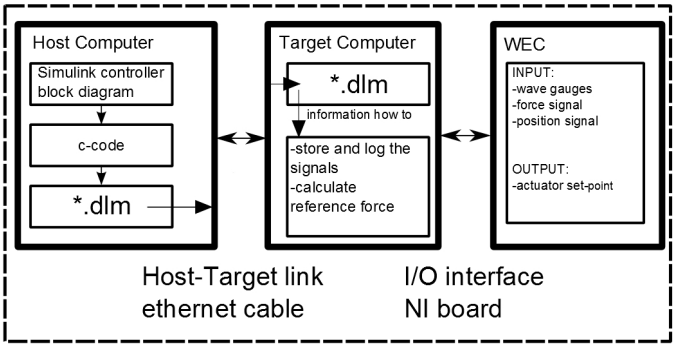

Fig. B.3. Communication flow diagram between host computer, target computer and WEC.

An example of the capability of the physical model is given in Fig. B.4. The figure shows the comparison between the numerical calculated (full line) and the measured (dots) mean absorbed power for two different sea states, IRB1 and IRB2, in function of the damping coefficient (C_c). The sea states are defined as:

- **IRB1**: H_{m0} = 0.051 m and T_p = 1 s
- **IRB2**: H_{m0} = 0.08 m and T_p = 1.25 s.

The JONSWAP wave spectrum with $\gamma = 1$ and the random noise technique were used for the wave generation.

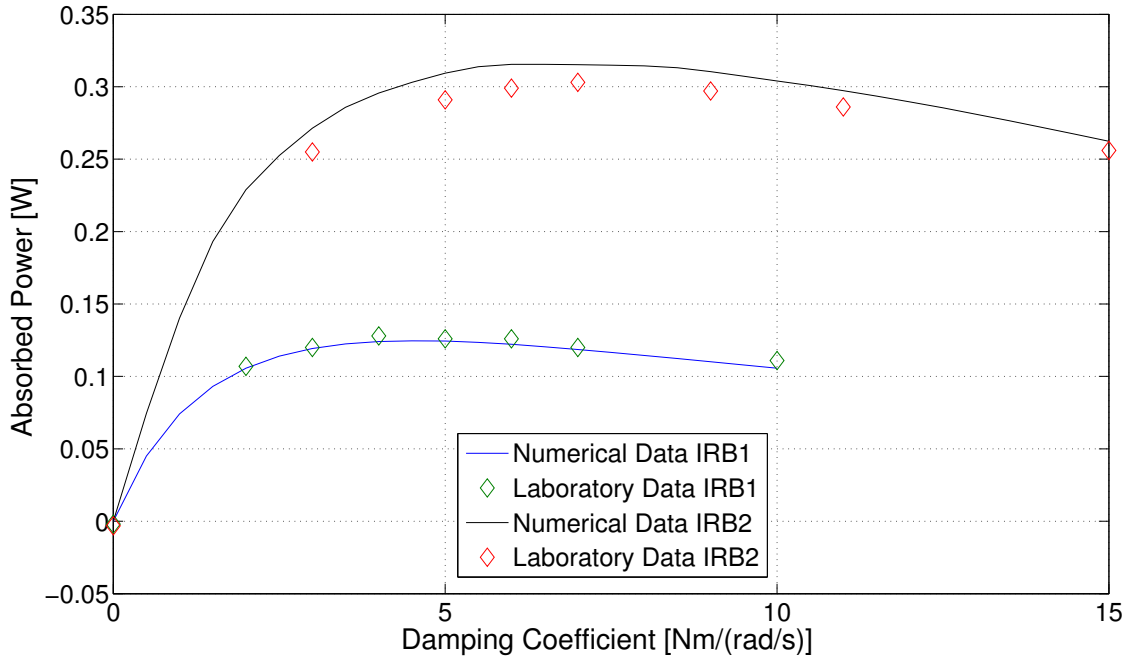

Fig. B.4. Absorbed power in function of the damping coefficients (C_c) for two different sea states. IRB1: $H_{m0} = 0.051$ m and $T_p = 1$ s. IRB1: $H_{m0} = 0.08$ m and $T_p = 1.25$ s. In both cases the wave steepness is near 3.5 %. A JONSWAP spectrum with $\gamma = 1$ is used for the wave generation. The sample time of each test is five minutes.

The adopted controller is a simple passive scheme proportional to the velocity of the floater. Fig. B.5 shows the comparison between the measured and requested linear relation between floater angular velocity and exerted PTO moment. The signal variance around the red line is ascribable to both measurement noise, inner control latency, and friction in the hinge (bearing).

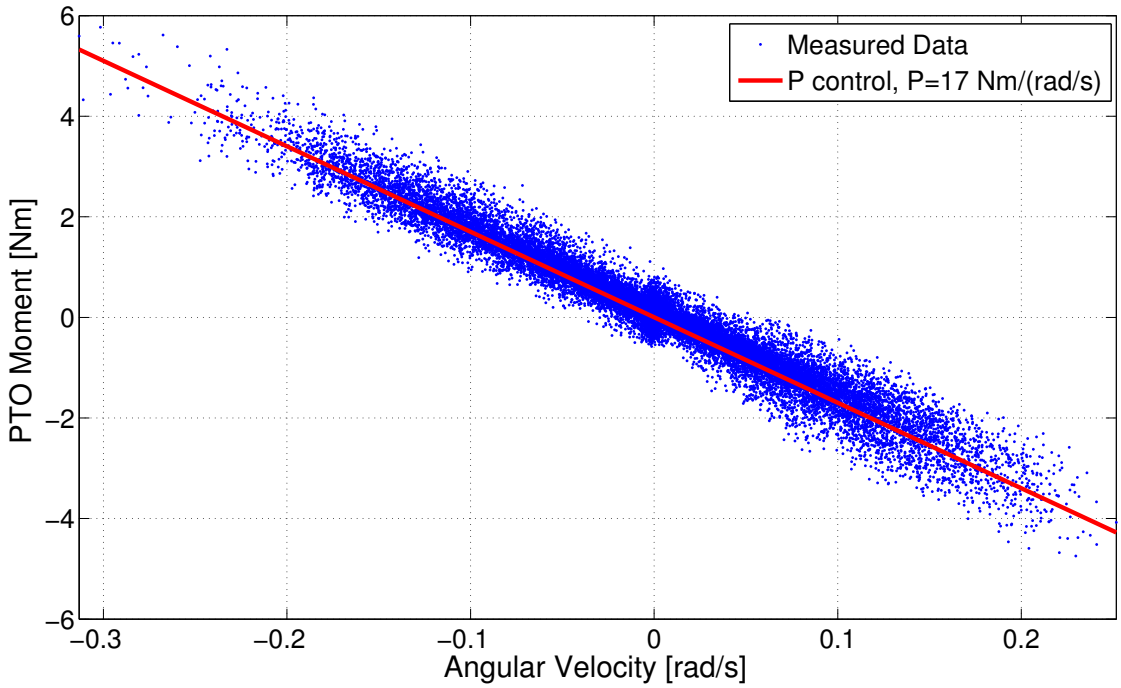

Fig. B.5. Angular velocity versus PTO moment, measured (dots) and requested (full line)

Weptos WEC

C

The objective of this appendix is to describe the implementation of a wave-to-wire model for the Weptos WEC, in extension of the methodology given in Ch. 3. The Weptos WEC (Weptos, 2014) is a multi-body system that extracts the wave energy potential from the motion of floaters induced by the passing waves. The floaters are connected to a main floating platform. The platform is composed by two legs arranged in an A-shaped configuration with variable opening angle. The A-apex defines the bow of the system. The floaters are evenly distributed along two axes, one for each sides of the platform (port and starboard). These axes are parallel to the axes defined by the platform legs. Each floater (rotor) is hinged to the platform, and the connection leaves only one rotational DoF between platform and rotor. The rotor shape is based on the well-known Salter's duck (Salter, 1974), where the tip of the duck is pointing outwards.

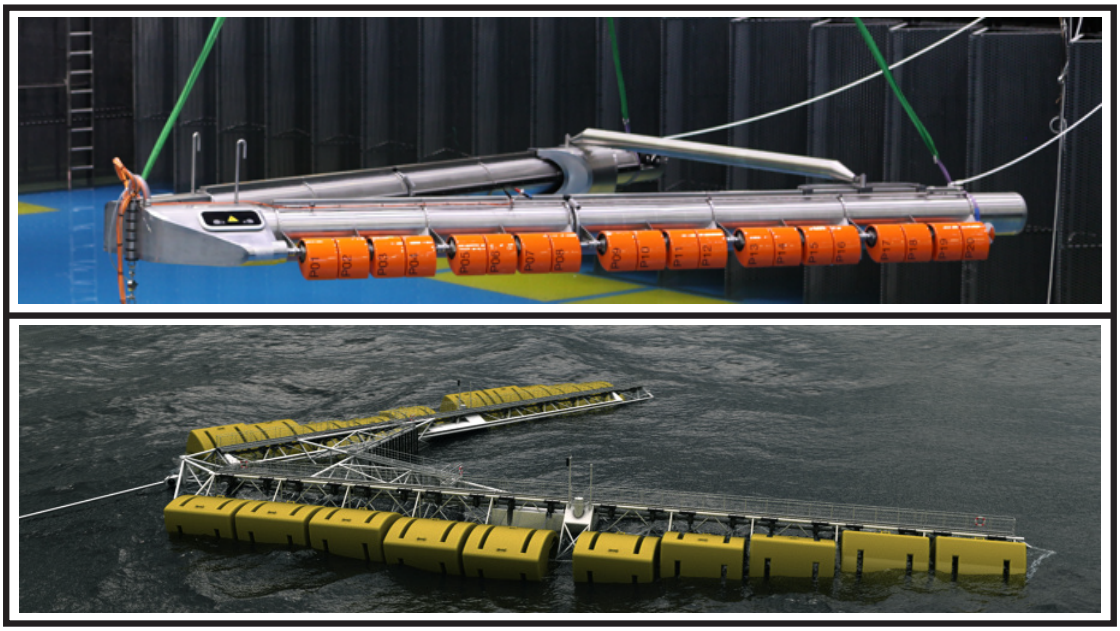

Fig. C.1. Old (top) and newest (bottom) configurations of the Weptos WEC. The A-shaped platform is the grey (metal) coloured body and the rotors are the orange and yellow coloured bodies. Images' source: (Weptos, 2014)

Fig. C.1 shows two different configurations: the top one is the old configuration, which was tested in the CCOB facility in Santander, Spain (Pecher et al., 2012b), while the bottom one is the newest configuration under development. They only differ in the design of the platform, and in the number of rotors for each axis, e.g 20 vs 10. The device is moored and the mooring system allows the orientation of the WEC in 360^o.

Numerical Model

The proposed numerical model of the Weptos WEC is based on the old configuration, due to the presence of experimental data for the validation procedure, but the methodology is generally applicable to multi-body WECs. Due to the complexity of the system, the first stage of analysis uses a fully linear numerical model based on the solution of the Diffraction/Radiation problems, i.e. gyroscopic, viscous drag and non-linear hydrostatic contributions are considered negligible. The last two terms are expected to have an important share in the force summation for each rotor, and their implementation is part of the future works list.

Due to the presence of a floating platform, the motion of each element of the WEC affects the motion of the rest of the system, and for this reason the system needs to be modelled as a multi-body system. The constrained motion between platform and rotor can be modelled either explicitly or implicitly. The former solution makes use of additional springs or algebraic equations to bound the motion of the constrained DoFs: the system is firstly formulated as a loose cluster of bodies and the constraints are applied afterwards. The utilisation of additional springs with high stiffness coefficient should be discouraged, because the resulting system of equations is stiff and slow to solve thus. In contrast, the implicit method re-maps the total number of DoFs of the loose system into the so called generalised DoFs, discarding all the unavailable DoFs. For the case of the Weptos with 40 rotors (old configuration) the explicit approach leads to a system with 246 (6*40+6) DoFs, while the implicit approach leads to 46 (40+6) generalised DoFs. It is important to bear in mind that, the position of a rigid body in the 3D space is completely determined by 6 DoFs. Due to the important reduction of the system's order, the implicit approach is considered hereafter. It is important to highlight that similar methods have been proposed in recent years (Taghipour, 2008; Ruehl et al., 2014; Ó'Catháin et al., 2008), and the overall methodology is not new as such, but its application in wave energy conversion systems is an important topic of research.

Fig. C.2 shows the meshed geometry relative to the Weptos WEC and the coordinate systems used. The black arrows define the inertial coordinate system, while the local coordinate systems are represented by the x-axis (red arrow) and y-axis (green arrow). The vertical axis is pointing upwards and it is not represented for graphical reasons. The main differences with the model shown in Fig. C.1 are:

- Simplified platform, the legs are made of two cylinders, and the transversal beam is absent.
- The space between the rotors is set to zero, in order to remove the error of the linear solution for those small gaps.

- The platform can only move in three DoFs, x-direction, z-direction and rotation around y-axis. This approximation is possible because only 2D long crested waves travelling in the direction parallel to the x-axis of the WEC are used.

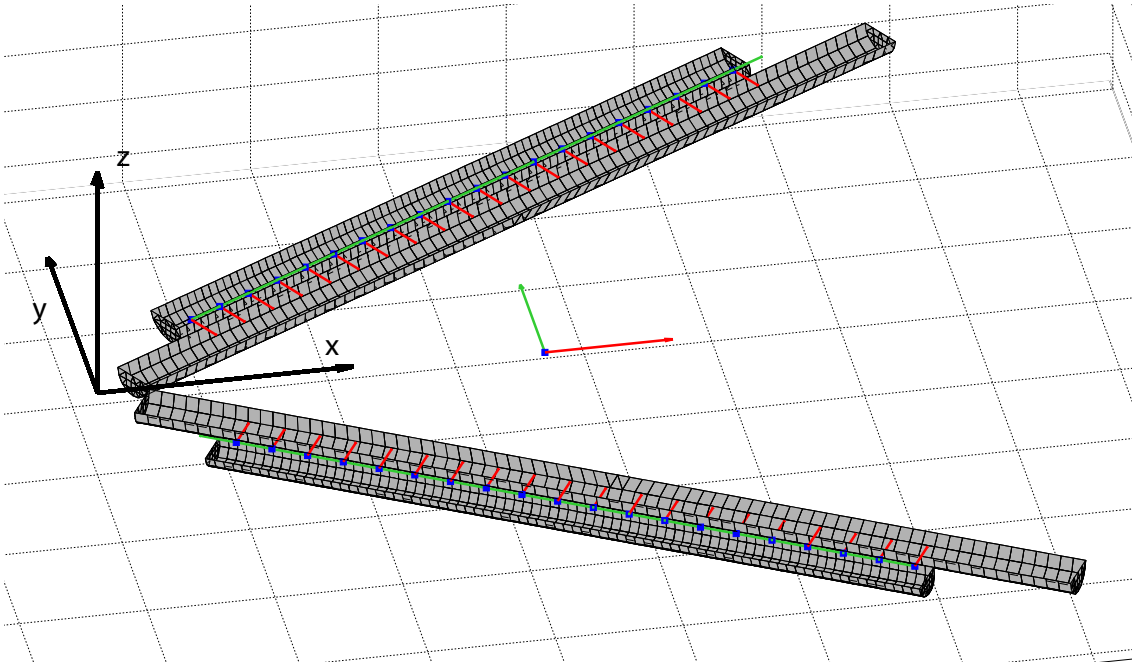

Fig. C.2. Meshed Weptos WEC. The black arrows define the inertial coordinate system, while the local coordinate systems are represented by the x-axis (red arrow) and y-axis (green arrow).

The EoM of the multi-body WEC with generalised DoFs does not differ from the EoM of a single rigid body WEC (3.15,3.18).

Both WAMIT and Nemoh softwares can calculated the linearised solution of the Diffraction/Radiation problems for a system with generalised DoFs. In contrast, ANSYS Aqwa does not use generalised DoFs and the EoM is solved with the explicit formulation of the constraint. The software Nemoh has been used for the purpose.

Three main steps are needed to formulated the EoM of the Weptos WEC, given the geometry description and the Nemoh solutions.

1. Define the mass matrix in the generalised base;
2. Map the Nemoh output into the generalised base;
3. Map the hydrostatic stiffness matrixes into the generalised base.

Mass Matrix

The mass matrix is formulated using an energy based approach as partially described in (3.19,3.20). Briefly, the Lagrangian (L) is defined as the summation of the kinetic (T_i) and potential (P_i) energy for each body of the system. T_i is defined as:

$$T_i = \frac{1}{2} m_i \overline{v}_i^T \overline{v}_i + \frac{1}{2} \overline{w}_i^T I_i \overline{w}_i \tag{C.1}$$

Here, m_i and I_i are the mass and the inertia matrix, and $\overline{v}_i$ and $\overline{w}_i$ are the linear velocity vector and the angular velocity vector of the CoG. All the variable are related to the i-th body. It is possible to introduce the the geometric Jacobian matrix ($\mathbf{J}$), which relates the generalised velocity vector ($\dot{\overline{q}}$) to the velocity — linear and angular — of the point of interest (p_i),

$$\begin{bmatrix} \overline{v}_{p_i} \\ \overline{w}_{p_i} \end{bmatrix} = \mathbf{J}\dot{\overline{q}} = \begin{bmatrix} \mathbf{J_v} \\ \mathbf{J_w} \end{bmatrix} \dot{\overline{q}} \tag{C.2}$$

The Jacobian matrix is decomposed into a linear velocity term ($\mathbf{J_v}$) and a angular velocity term ($\mathbf{J_w}$). Substituting (C.2) into (C.1) brings to:

$$T_i = \frac{1}{2}\dot{\overline{q}}^T \left(m_i \mathbf{J_v}_i^T \mathbf{J_v}_i + \mathbf{J_w}_i^T I_i \mathbf{J_w}_i \right) \dot{\overline{q}} \tag{C.3}$$

The summation of the i-th contributions over the number of bodies brings to:

$$T_i = \frac{1}{2}\dot{\overline{q}}^T \left[\sum_i \left(m_i \mathbf{J_v}_i^T \mathbf{J_v}_i + \mathbf{J_w}_i^T I_i \mathbf{J_w}_i \right) \right] \dot{\overline{q}} = \frac{1}{2}\dot{\overline{q}}^T \mathbf{M}(\overline{q})\dot{\overline{q}} \tag{C.4}$$

$\mathbf{M}(\overline{q})$ can be linearised by assuming small rotations — $\cos(\theta)=1$ and $\sin(\theta)=\theta$ — , and deleting all the second or higher order terms.

The Jacobian matrix can be formulated using the constraint (joint) information. $\mathbf{J}_i$ is further decomposed as:

$$\mathbf{J}_i = \left[\overline{J}_1 \; \overline{J}_2 \; \ldots \; \overline{J}_{Ndof} \right] = \left[\overline{J}_j \right] \tag{C.5}$$

where $\overline{J}_j$ is a column vector of dimension 6x1 describing the connectivity between the bodies and j identifies the j-th generalised degree of freedom. $\overline{J}_j$ is defined as:

$$\overline{J}_j = \begin{cases} \begin{bmatrix} \overline{k}_j \\ \overline{0} \end{bmatrix} & \text{if joint j is prismatic} \\ \begin{bmatrix} \overline{k}_j \times \overline{r}_j \\ \overline{k}_j \end{bmatrix} & \text{if joint j is revolute} \end{cases} \tag{C.6}$$

Here, $\overline{k}_j$ is the vector defining the generalised DoF in the inertial coordinate system, i.e. for the vertical displacement $\overline{k}_j = [0, 0, 1]$, and $\overline{r}_j$ is the position vector between the CoG of the i-th body and p_i, defined in the inertial coordinate system.

Nemoh mapping

The need of a matrix to map from the Nemoh output to the generalised base is linked to the way how Nemoh generates the output file. The mapping matrix is merely a summation matrix. The hydrodynamic coefficients of the platform are defined at its own CoG. Each of the rotors will have the same DoF of the platform, in this case surge, heave and pitch, plus the additional rotation about its own axis. The summation matrix needs to sum the rotors

surge, heave and pitch to the ones of the platform. For the case study the summation matrix $\mathbf{T_r}$ is shaped as:

$$\mathbf{T_r} = \begin{pmatrix} 1 & 0 & 0 & 1 & 0 & 0 & 0 & 1 & 0 & 0 & 0 \\ 0 & 1 & 0 & 0 & 1 & 0 & 0 & 0 & 1 & 0 & 0 \\ 0 & 0 & 1 & 0 & 0 & 1 & 0 & 0 & 0 & 1 & 0 \\ 0 & 0 & 0 & 0 & 0 & 0 & \boxed{1} & 0 & 0 & 0 & 0 \\ 0 & 0 & 0 & 0 & 0 & 0 & 0 & 0 & 0 & 0 & \boxed{1} \end{pmatrix} \tag{C.7}$$

The matrix is exemplified for a simplified system with only two rotors (Ndof=5) for graphical reasons, where Ndof is the number of generalised DoFs. The red and orange boxes represent the rotors rotational DoFs, while the first three rows of the matrix define the summation of each body in the platform DoFs.

Hydrostatic mapping

The hydrostatic stiffness matrixes are evaluated for the platform and one rotor at their CoG in the local coordinate system. The stiffness matrix is a 6x6 matrix defined for the canonical 6 DoFs of a rigid body. The mapping rule from the generalised DoFs to the generalised hydrostatic force vector is defined as:

$$\overline{F}_{hy} = \mathbb{T}\,\overline{q} = \mathbb{A}^{-1}\,\mathbb{K}\,\mathbb{A}\,\overline{q} \tag{C.8}$$

Here, $\mathbb{A}$ is the matrix ([Ndof x (6*Nb)]) to map from the generalised DoFs to the canonical 6 DoFs for each independent body, expressed in the body local coordinate system, and $\mathbb{K}$ is a matrix ([(6*Nb)x(6*Nb)]) obtained from the concatenation of the hydrostatic stiffness matrix for each body, e.g $\mathbb{K} = [\mathbf{K_p}\mathbf{K_r}\mathbf{K_r}\ldots\mathbf{K_r}]^T$ where the rotor matrix is repeated Nb-1 times. Nb is the number of bodies of the WEC, in this case 41, 40 rotors plus 1 platform. $\mathbb{A}$ is obtained from the linearised transformation matrixes between the different point of the structure, expressed in the inertial coordinate system. The hydrostatic stiffness matrix for the platform ($\mathbf{K_p}$) and for the rotor ($\mathbf{K_r}$) are calculated in Nemoh.

Preliminary results

In order to define the Weptos numerical model, the information about mooring and PTO models are needed. First, the mooring system is modelled as a linear spring, acting on the surge DoF only. Therefore, the stiffness matrix is a zeros matrix with the entry (1,1) equal to the stiffness coefficient. The latter is obtained from the interpolation of the force/displacement plot as presented in (Pecher et al., 2012b). The PTO model is based on an ideal actuator model, i.e. unitary transfer function, and on a P-control law, resistive controller where the PTO force is proportional to the body velocity. The damping coefficient (C_c) of the controller was selected based on an energy maximisation principle, using the simplex method, (Lagarias et al., 1998).

For the system specification see (Pecher et al., 2012b).

The results reported below are given for the Hanstholm SD. The SD is scaled using the Froude scaling law with a scale ration 1:20. Fig. C.3 shows the capture with ratio (CWr) in function of T_p. CWr is defined as the ratio between the mean absorbed power at the WEC and the wave power per unit of wave front multiplied by the absorption length of the

WEC. The blue line represents the solution of the system presented in Fig. C.2, and the red line is the same curve but scaled by a factor 0.24/0.29. The latter represents the ratio between the real rotor width and the approximated rotor width used to remove the gap between rotors.

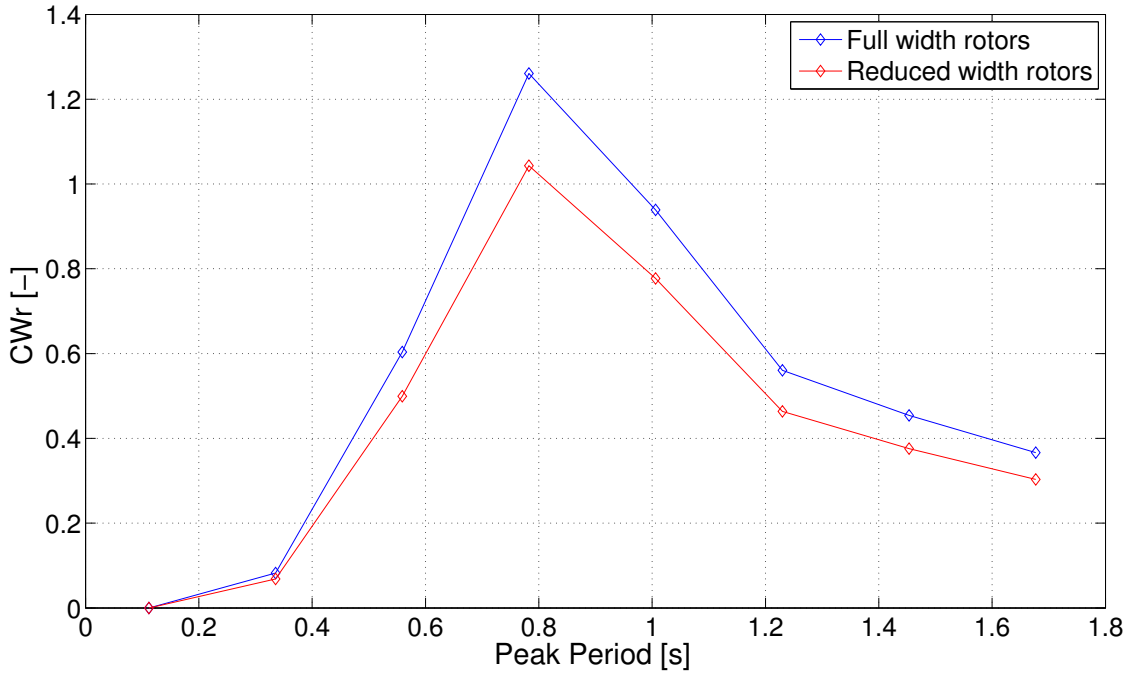

Fig. C.3. Capture width ratio in function of T_p for the Hanstholm SD at the scale 1:20. The blue line represents the solution of the model depicted in Fig. C.2, and the red line represents the same results with the application of a correction factor to account for the gap between rotors.

The results presented in Fig. C.3 are in line with the results published in (Pecher et al., 2012b). The trend of CWr in function of T_p has a similar shape, even though the numerical model overestimate the maximum CWr of about 40 %. This error comes from a summation of different approximations, the most important being listed hereafter:

- PTO model: The PTO model of the physical WEC is based on the overrunning clutch mechanism, which entails energy extraction in one direction only (upstroke) and torque transfer only if the rotor velocity is higher then the PTO axle velocity. The numerical model of the PTO considers the mono-directional power absorption by dividing the absorbed power by a factor two, but does not consider any other non-linearity or frictions. The torque is constantly transferred from rotor to ideal generator.

- Hydrodynamic model: The hydrodynamic model does not include any viscous drag dissipation, neither quadratic nor linearised, but the KC number of the rotors goes from 5 to > 10. Therefore, the viscous drag contribution should have a significant impact in the force summation

- Due to the large number of DoFs it has not been possible to run a mesh convergency study.